TECHNISCHE UNIVERSITÄT MÜNCHEN
Fakultät Wissenschaftszentrum Weihenstephan für
Ernährung, Landnutzung und Umwelt

The role of primary cilia in skeletal muscle

Lisann Heyner

Vollständiger Abdruck der von der Fakultät Wissenschaftszentrum Weihenstephan für Ernährung, Landnutzung und Umwelt der Technischen Universität München zur Erlangung des akademischen Grades

Doktors der Naturwissenschaften

genehmigten Dissertation.

Vorsitzende: Prof. Dr. Nina H. Uhlenhaut

Prüfer der Dissertation:

1. Prof. Dr. Martin Hrabé de Angelis

2. Prof. Dr. Gunnar Schotta

Die Dissertation wurde am 17.10.2019 bei der Technischen Universität München eingereicht und durch die Fakultät Wissenschaftszentrum Weihenstephan für Ernährung, Landnutzung und Umwelt am 05.05.2020 angenommen.

Table of Contents

1 List of Abbreviations

µg	microgram
µl	microliter
AAV	adeno-associated virus
Aph1b	anterior pharynx defective 1 homolog B
APS	ammonium persulfate
Arl13b	ADP ribosylation factor like GTPase 13B
Arp2/3	actin-related protein 2/3
ATP	adenosine triphosphate
Bbs	Bardet-Biedl Syndrome
BLOC-1	biogenesis of lysosome-related organelles complex-1
BSA	bovine serum albumin
BW	body weight
Cdc42	cell division cycle 42
cDNA	complementary DNA
CME	clathrin-mediated endocytosis
Cre	cyclization recombination
CSL	CBF1, suppressor of hairless, Lag-1
d	day
DAPI	4′,6-Diamidin-2-phenylindol
DGC	dystrophin-glycoprotein complex
Dll4	delta like canonical Notch ligand 4
DMD	Duchenne Muscular Dystrophy
DMEM	Dulbecco's modified Eagle's medium
DNA	deoxyribonucleic acid
DPBS	Dulbecco's phosphate-buffered saline

E12.5	embryonic day 12.5
ECL	enhanced chemiluminescence
e.g.	for example
EDL	*extensor digitorum longus*
EDTA	ethylenediaminetetraacetic acid
EdU	5-Ethylnyl-2'-deoxyuridine
FACS	fluorescence activated cell sorting
F-actin	filamentous actin
FBS	fetal bovine serum
Fbx-32	F-box protein 32
FCS	fetal calf serum
g	gram
Gapdh	glyceraldehyde-3-phosphate dehydrogenase
GDP	guanosine diphosphate
GEF	guanosine exchange factor
GFP	green fluorescent protein
Gli1	glioma-associated oncogene homolog 1
Glut4	glucose transporter type 4
gRNA	guide ribonulceic acid
GTP	guanosine triphosphate
GTT	glucose tolerance test
h	hour
HeyL	hairy/enhancer-of-split related with YRPW motif-like protein
Hes1	hairy/enhancer of split-1
Hh	hedgehog
Hipk2	homeodomain interacting protein kinase 2

HSA	human α-skeletal actin
Hsp90	heat shock protein 90
IFT	intraflagellar transport
Ift88	intraflagellar transport protein 88
IgG	immunoglobulin G
IgY	immunoglobulin Y
IR	insulin receptor
kb	kilobase
kg	kilogram
KO	knock-out
l	liter
LGMD2H	Limb-Girdle Muscular Dystrophy type 2H
loxP	locus of crossover in P1
LRb	leptin receptor b
MCM	mutated estrogen receptor – Cre - mutated estrogen receptor
Meg3	maternally expressed 3
mg	milligram
MHC	myosin heavy chain
min	minute
ml	milliliter
MLC	myosin light chain
M.O.M.	mouse on mouse blocking buffer
mRNA	messenger ribonulceic acid
MTJ	myotendinous junction
mTmG	membranous Tomato membranous GFP
Murf-1	muscle RING-finger protein-1

Myf5	myogenic factor 5
Myf6	myogenic factor 6
MyoD	myogenic differentiation
n	number
N_2	liquid nitrogen
NICD	notch intracellular domain
NMJ	neuromuscular junction
NMR	nuclear magnetic resonance spectroscopy
OCT	optimal cutting temperature
p	probability
Pax3	paired box protein 3
Pax7	paired box protein 7
PBS	phosphate-buffered saline
PBST	phosphate-buffered saline with Tween-20
PCR	polymerase chain reaction
PFA	paraformaldehyde
Prdm16	PR domain zinc finger protein 16
Rac1	Rac family small GTPase 1
RBP-Jκ	recombination signal binding protein for immunoglobulin kappa J
Rcan1	regulator of calcineurin 1
RFP	red fluorescent protein
RING	really interesting new gene
RNAseq	RNA sequencing
RT	room temperature
rt qPCR	real-time quantitative PCR
SC	satellite cell

SDCCAG3	serologically defined colon cancer antigen 3
SDS	sodium dodecyl sulfate
Shh	sonic hedgehog
TAE	tris-acetate-EDTA buffer
TBST	tris-buffered saline with Tween-20
TEMED	Tetramethylethylenediamine
Tiam1	T-lymphoma invasion and metastasis-inducing protein 1
Tln2	talin-2
TAM	tamoxifen

2 Abstract

Primary cilia have been shown to be important signaling integrators during development and adult tissue homeostasis. However, their role in skeletal muscle is not very well known. Primary cilia are, among others, present on muscle satellite cells, fibro/adipogenic precursors, myoblasts and freshly formed myotubes (but disassemble after time). I performed *in vivo* magnetic resonance imaging to determine body composition of male *Bbs4*$^{-/-}$ mice at a time point when body weight is not significantly different from littermate *Bbs4*$^{+/+}$ animals. I tested grip strength as a read-out for muscle function independent of body weight and analyzed skeletal muscle tissues, neuro-muscular junctions and fiber type composition to characterize the muscle phenotype of *Bbs4*$^{-/-}$ mice. To better understand underlying mechanisms, I combined immunohistochemical and immunoblotting as well as luciferase-based Notch1 signaling assays in a myoblast cell line. In male *Bbs4*$^{-/-}$ mice, lean to fat mass ratio and grip strength are significantly reduced compared to *Bbs4*$^{+/+}$ animals. I did not observe atrophy or defects in neuronal input, morphology of neuro-muscular junctions or composition of metabolic fiber types. Altered expression levels of dedifferentiation markers in *Bbs4*$^{-/-}$ mice muscles indicated a phenotype in muscle regeneration. Further, Notch signaling activity and signaling components are upregulated when ciliary/ basal body composition is impaired in muscle progenitors inhibiting myotube formation. Several lines of evidence suggest that ciliary/ basal body integrity is required for skeletal muscle differentiation and the modulation of Notch1 signaling in muscle progenitor cells. This could have important implications for the treatment and management of ciliopathy patients but also potentially for those suffering from sarcopenic obesity that is more common in elderly patients.

3 Zusammenfassung

Es konnte bereits gezeigt werden, dass Primärzilien eine essentielle Rolle bei der Entwicklung und Homöostase ausdifferenzierter Zellen und Gewebe einnehmen. Ihre Rolle im Skelettmuskel ist jedoch bis heute noch nicht vollständig geklärt. Unter anderem kommen Zilien in folgenden Zellen vor: muskuläre Satellitenzellen, Vorläuferzellen der Fibroblasten und Adipozyten, Myoblasten sowie neu gebildeten Muskelfasern (wo sie nach deren Entstehung wieder abgebaut werden). In der vorliegenden Arbeit habe ich mit Hilfe von *in vivo* Kernspintomografie den Körperbau von *Bbs4*$^{-/-}$ Mäusen zu einem Zeitpunkt gemessen, an dem sie hinsichtlich des Körpergewichtes keinen signifikanten Unterschied zu *Bbs4*$^{+/+}$ Mäusen aufwiesen. Als Test für gewichtsunabhängige Muskelfunktion wurde der Grip-Strenght Test durchgeführt. Weiterhin wurden Skelettmuskel, neuromuskuläre Verbindungen sowie die Muskelfaserkomposition analysiert um den Muskelphänotyp der *Bbs4*$^{-/-}$ Mäuse zu untersuchen. Für weiterführende Untersuchungen der zugrundeliegenden Mechanismen wurden immunohistochemische Assays, Immunoblots sowie Luziferase-basierte Notch1 Signalweg Assays in einer Myoblastenzelllinie durchgeführt. In männlichen *Bbs4*$^{-/-}$ Mäusen ist sowohl die lean to fat ratio, wie auch die Muskelstärke anhand des Grip Strenght Tests signifikant reduziert im Vergleich zu *Bbs4*$^{+/+}$ Mäusen. Eine muskuläre Atrophie, Defekte im neuronalen Input, Veränderungen der Morphologie neuromuskulärer Verbindungen oder der Muskelfaserkomposition wurden nicht nachgewiesen. Veränderte Expressionslevel von Dedifferenzierungsmarkern in *Bbs4*$^{-/-}$ Muskeln deuteten auf einen Phänotyp in der muskulären Regeneration hin. Des Weiteren sind die Notch Signalweg Aktivität sowie Komponenten des Signalwegs erhöht in Myoblasten mit verringerter ziliärer/Basalkörper-Funktion durch Reduktion der Expression des anterograden Transportproteins Ift88. Diese Myoblasten weißen auch eine verringerte Differenzierungsrate zu Muskelfasern auf. Die Ergebnisse deuten darauf hin, dass die Funktionalität der Zilien/Basalkörper eine Voraussetzung für die Differenzierung der Myoblasten des Skelettmuskels sowie die Modulation des Notch1-Signalweges darstellt. Diese Ergebnisse können einen wichtigen Einfluss auf die Behandlung und Therapie von Patienten mit einer Ziliopathie haben, oder auch auf Patienten mit Sarkopenischer Adipositas, die vermehrt in älteren Patienten auftritt.

4 Introduction

4.1 Diabetes mellitus and glucose homeostasis

In 2014, approximately 422 Mio people worldwide suffered from diabetes and the number of patients nearly doubled since 1980. In 2012, diabetes caused approximately 1.5 million deaths and is associated with various complications like stroke, cardiovascular disease, leg amputation, blindness and kidney failure (World Health Organization 2016). Therefore, diabetes is challenging health care systems in countries all over the world. For example, the German health system spends 1.7-fold more money on patients with diabetes than on patients without (Jacobs et al. 2017). The causes and molecular mechanisms behind the development of diabetes and associated complications are not fully understood.

The name *diabetes mellitus* is related to the “sweet tasting” urine of the patients. Besides polyuria, diabetes is characterized by chronical high blood glucose (hyperglycemia) and increased thirst. We distinguish mainly between three kinds of diabetes: type 1 diabetes, type 2 diabetes and gestational diabetes. The last form is temporally restricted to pregnancy and it increases disease risk for the child and the mother later in life. Type 1 diabetes is an autoimmune disease targeting pancreatic insulin producing β-cells. The most common form affecting ~90% of diabetics is type 2 diabetes, caused by a combination of diminished insulin release of pancreatic β-cells and reduced response to insulin action (insulin resistance) of peripheral tissues like skeletal muscle, smooth muscle or liver. Over the last years, closer insights into the development and characteristics of diabetes type 1 and type 2 led to the discovery of diabetes forms with characteristics of both, type 1 and type 2. Examples are adult patients diagnosed with type 1 diabetes (latent autoimmune diabetes in adults/LADA), or pediatric type 2 diabetes patients as well as patients demonstrating characteristics of both diabetes forms. These discoveries yield in the generation of new terms, for example “autoimmune phenotypic type 2 diabetes” or “type 1 diabetes adult onset” (Brooks-Worrell and Palmer 2011; Juneja et al. 2001; Libman et al. 2008; Lohmann et al. 1997; Mayer-Davis et al. 2017). Further, a recent publication used data from newly diagnosed adult type 2 diabetes patients from five cohorts for a data-driven cluster analysis with six variables. This study identified five subgroups of patients with different characteristics and progression/risk of diabetic complications. These new subgroups were named severe autoimmune diabetes (SAID), severe insulin-deficient diabetes (SIDD), severe insulin-resistant diabetes (SIRD), mild obesity-related diabetes (MOD) and mild age-related diabetes (MARD). This clustering may provide a base for better and earlier patients´ treatment (Ahlqvist et al. 2018).

4.2 Glucose metabolism and skeletal muscle

Healthy fasting humans have blood glucose levels below 5.5 mmol/l, but diabetic patients show fasting blood glucose levels of at least 7.0 mmol/l. It has been shown, that around 70-75% glucose is taken up by skeletal muscle related to insulin stimulation within hyperinsulinemic clamp studies (DeFronzo et al. 1981; Shulman et al. 1990). Consequently, this organ plays an important role in glucose homeostasis and the etiology of diabetes. The modern lifestyle is characterized by high caloric food intake and reduced physical activity, thereby promoting obesity which leads to elevated risk of cardiovascular and metabolic diseases as well as enhanced cancer risk (Ballestri et al. 2016; Eheman et al. 2012; Grover et al. 2015; Larsson, Mantzoros, and Wolk 2007; Larsson, Orsini, and Wolk 2005). Obese patients were shown to have increased blood levels of insulin and free-fatty acids (FFA). Both features induce insulin resistance (inability to respond to normal insulin levels) and accelerate the progression to type 2 diabetes (Kim, Reaven, and Kim 2017; Petersen et al. 1998; Roden et al. 1996; Shanik et al. 2008; Spiller, Blüher, and Hoffmann 2018; Tabák et al. 2009). In healthy conditions, postprandial elevated blood sugar induces pancreatic β-cells to secrete insulin into the blood stream, which binds and activates insulin receptors of peripheral tissues. The activated signaling cascade triggers the translocation of the vesicular glucose transporters (Glut4 most prominent in skeletal muscle) to the membrane of peripheral tissues, which leads to increased glucose transport and disposal (Birnbaum 1989; Charron et al. 1989; James, Strube, and Muecdler 1989; Klip and Pâquet 1990). Therefore, glucose homeostasis depends on the sensitivity of peripheral tissues to insulin. Besides insulin-dependent glucose uptake, skeletal muscle showed increased glucose uptake due to Glut4 translocation to the sarcolemma depending on contraction/exercise, by a mechanism distinct from insulin-induced Glut4 translocation (Goodyear et al. 1995; Goodyear et al. 1990; Lee, Hansen, and Holloszy 1995; Lund et al. 1995). Insulin resistant muscle of normoglycemic women has been shown to internalize glucose during exercise in normal levels (Braun et al. 2004). Further, exercise can increase skeletal muscle insulin sensitivity and decrease the risk for development of type 2 diabetes (Heath et al. 1983; Mikines et al. 1988). Internalized glucose of both, insulin- and exercise-induced glucose uptake, is used for glycogen synthesis. Glycogen is a polysaccharide utilized for energy storage. In humans, skeletal muscle has been shown to store ~80% of whole body glycogen (Hawley et al. 1997; Ivy et al. 1988; Jensen et al. 2011). During exercise/contraction, glycogen released glucose is a major source of energy in skeletal muscle. Therefore, high-intense exercise diminishes glycogen content in muscles (Bergström, Hultman, and Roch-Norlund 1972; Kochan et al. 1979). Further, the muscular glycogen content is associated with muscular endurance capacity and exercise increases the muscular glycogen storage capacity (Bergström, Hultman, and Roch-Norlund 1972; Kochan et al. 1979).

Besides skeletal muscle, adipose tissue and the liver are the main tissues showing insulin-stimulated glucose uptake. The concentration of glycogen in the liver is higher compared to skeletal muscle, but since the organ is much smaller, it stores only a fraction of whole-body glycogen. Livers of obese patients generate and secrete increased amounts of very-low-density lipoproteins, which serve as a source of FFA to other organs (Chan et al. 2014). Therefore, obese patients accumulate FFA in non-fat storage tissues like skeletal muscle. Further, FFA enrichment in muscle induced the accumulation of intramuscular ceramide, synthesis of diacylglycerol and activation of Protein Kinase C. These changes lead to impaired insulin receptor signaling and therefore reduced postprandial glucose uptake, triggering the establishment of type 2 diabetes (Dresner et al. 1999; Szendroedi et al. 2014; Yu et al. 2002). Besides the accumulation of FFA, skeletal muscle of type 2 diabetes patients shows altered metabolism by reduced mitochondria content and reduced oxidative fibers (Marin et al. 1994; Nielsen et al. 2010; Nyholm et al. 1997), accumulation of intramuscular fat (Hilton et al. 2008), decreased capillary density (Prior et al. 2009) and reduced muscle strength (Andersen, Gjerstad, and Jakobsen 2004; Park et al. 2006). Studies done in *ob/ob* and *db/db* mice also show reduced regeneration capacity of muscle progenitor cells in a hyperglycemic environment (Nguyen, Cheng, and Koh 2011). Therefore, both skeletal muscle metabolism and regeneration capacity are affected in type 2 diabetes.

4.3 Primary cilia are signaling hubs of the cell

Primary cilia are specialized organelles which were identified 1898 in human tissue (Zimmermann 1898). Since then, primary cilia were found in numerous organism and mammalian tissues, where they extrude from the cell into the lumen of the tissue. The main body of the cilium is called axoneme, which in primary, non-motile cilia consists of 9 microtubule doublets. Assembly and maintenance of these microtubules is regulated by an active transport mechanism named intraflagellar transport (IFT), which is well studied in the model organisms *Chlamydomonas reinhardtii* and *Caenorhabditis elegans*. IFT is divided into IFTB/anterograde (towards the ciliary tip) and IFTA/retrograde (towards the ciliary base) transport processes. For each transport process a protein complex needs to be established. IFT-A complex consists of 6 subunits: IFT144, 140, 139, 122, 121, 43; and IFT-B complex is assembled from 16 subunits: IFT172, 88, 81, 80, 74, 70, 57, 56, 54, 52, 46, 38, 27, 25, 22, 20 (Cole et al. 1998; Fan et al. 2010; Ishikawa et al. 2014; Piperno and Mead 1997; Piperno et al. 1998; Wang et al. 2009). The IFT complexes are associated with cargo and a specialized motor protein for movement along the axoneme. For the transport along the cilium, cargos are loaded on IFT complexes at the ciliary base and IFT enables the selective transport across

the transition zone and against a concentration gradient (Berbari, Johnson, et al. 2008; Craft et al. 2015; Craige et al. 2010; Williams et al. 2011). Cargo usually are axonemal building units, signaling molecules or IFT components, since IFT-A has to be transported to the ciliary tip and IFT-B particles also have to be transported out of the cilium. At the ciliary tip, IFT-B complexes disassemble and release cargo. For retrograde transport of cargo from the cilium, IFT-A complexes assemble at the ciliary tip and release cargo at the ciliary base (Buisson et al. 2013; Liang et al. 2014; Pedersen, Geimer, and Rosenbaum 2006). The movement of cargo associated to IFT complexes is depending on motor proteins. The cilia-specific Kinesin-2 is the motor protein for anterograde cargo movements towards the ciliary tip and is needed for the establishment of primary cilia (Johnson and Rosenbaum 1992). Dynein 1b is needed for retrograde transport towards the ciliary base, therefore needed for moving cargo out of the cilium. Contrary to Kinesin-2, Dynein 1b is not cilia-specific. Dysfunctional IFT is linked to a number of cellular processes like differentiation (Ezratty et al. 2011; Fu et al. 2014; Tsujikawa and Malicki 2004), division and cancer (Jonassen et al. 2008; Menzl et al. 2014; Seeley et al. 2009), signaling (Beales et al. 2007; Schneider et al. 2005) and diseases (ciliopathies, see below). Further, knock-out of *Ift88*, a well-studied anterograde transport protein, abolishes the assembly of primary cilium axoneme completely and leads to embryonic lethality (Huangfu et al. 2003; Liu 2005; Pazour et al. 2000).

Besides cilia-related functions, IFT proteins have been found to have non-cilia related functions often within cell cycle regulation and cell division. In *chlamydomonas*, ift27 acts during cell division at the cleavage furrow and as a cell-cycle regulator (Qin et al. 2007; Wood et al. 2012). *Ift88* knock-out has been shown to inhibit centrosome maturation, which induces spindle mis-positioning and defective cell division (Delaval et al. 2011). Further, depletion of *Ift88* from human, mouse and zebrafish cells was shown to induce mitotic delay (Delaval et al. 2011; Robert et al. 2007). Contrary, mutation of *Ift88* in mouse liver progenitor cells induced an overproliferative phenotype (You et al. 2012). These results suggest a cell type specific role of Ift88 in cell cycle regulation apart from its role of a ciliary transport protein. Ift20 is expressed in non-ciliated lymphoid cells where it is involved in clustering and recycling of protein complexes at the immune synapse (Finetti et al. 2009, 2014). Moreover, Ift20 was found at the *cis*-Golgi in ciliated IMCD3 and RPE cells, suggesting a role in intracellular vesicle trafficking of proteins designated for the ciliary membrane (Follit et al. 2006, 2008).

The ciliary axoneme is anchored to the cell at the basal body (**Schematic 1**), which is derived from the mother centriole (older centriole with distal and subdistal appendages contrary to the younger daughter centriole) and associated with the plasma membrane of the cell by transition fibers. The basal body is spatially and functionally associated with the BBSome. This complex consists of 7 Bardet-Biedl Syndrome proteins (BBS1, BBS2, BBS4, BBS5, BBS7, BBS8,

BBS9). The protein names are derived from the disease they are associated with: mutations in BBS proteins lead to Bardet-Biedl Syndrome (BBS), a genetic disease which is generated due to genetic mutations in cilia-related genes and belongs to the group of ciliopathies (see below). So far, 21 BBS proteins have been identified. It has to be stated that not all BBS proteins are components of the BBSome. BBS6 and BBS12 for example are chaperonins, helping during the BBSome assembly (Seo et al. 2010). BBS11 (TRIM32) is a E3 ubiquitin ligase, related to protein degradation and mentioned to be involved in BBS2 degradation (Zhang et al. 2012). The BBSome can recognize cilia targeting sequences of cilia-designated proteins (Jin et al. 2010; Seo et al. 2011). Activation of BBS3 (ARL6) by GTP binding induces the assembly of a BBSome/BBS3 coat on the surface of membranes designated for transport to the cilium (Berbari et al. 2008; Jin et al. 2010; Nachury et al. 2007). BBS proteins can remodel IFT complexes at the ciliary tip and base (Wei et al. 2012). Within the cilium, the BBSome and cargo move along the axoneme associated to the IFT machinery (Lechtreck et al. 2009; Ou et al. 2005). Further, IFT27 has been shown to interact with BBS3 and loss of IFT27 induces accumulation of the BBSome and cargo on the cilium (Liew et al. 2014). Therefore, IFT27 and BBS proteins play a role in regulated protein removal from the cilium. Besides cilia-related roles, some BBS proteins have been shown to have non-ciliary functions, as described above for IFT proteins. For example bbs1 and bbs4 were shown to be involved in the Notch-receptor recycling from the plasma membrane in zebrafish (Leitch et al. 2014). BBS8 was found at focal adhesion sites, colocalized with vinculin in IMCD3 cells and involved in actin polymerization (Hernandez-Hernandez et al. 2013).

The ciliary membrane is a specialized part of the cell membrane covering the cilium. Compared to the plasma membrane, it is characterized by a different lipid composition, such as enrichment of sphingolipids (Janich and Corbeil 2007; Tyler et al. 2009) as well as accumulation of receptors and mechano-/ chemosensors. The kind of lipids or receptors concentrated on the cilium strongly depends on the cell type. Ciliary extracts of rat olfactory sensory neurons have been shown to accumulate 50-fold more cyclic nucleotide gated channels and adenylate cyclase III compared to total cell extracts (Mayer et al. 2008). Both proteins are components of the olfactory transduction cascade. A diffusion barrier at the base of the cilium restricts the entry of vesicles and proteins into the cilium and keeps the characteristics of ciliary and plasma membrane stable. This transition zone, also called ciliary gate, is characterized by Y-shaped linkers, connecting axonemal microtubules with the ciliary membrane. Another structure of the transition zone is the ciliary pocket, which is an invagination of the plasma membrane around the primary cilium. The ciliary pocket functions as a common site of endocytosis in certain organisms (Molla-Herman et al. 2010; Rattner et al. 2010). In *Trypanosoma brucei,* the flagellar pocket is the main site of endocytosis and lack

of functional BBSome drastically diminishes endocytosis, leading to diminished virulence of *Trypanosoma* (Langousis et al. 2016).

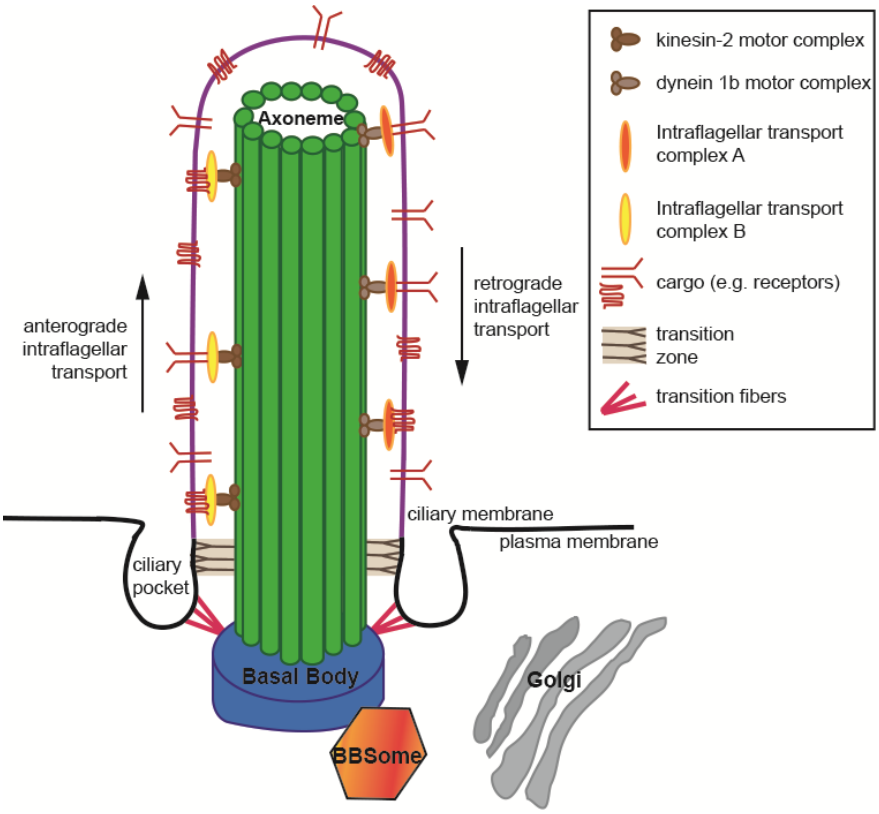

Schematic 1: Illustration of the primary cilium. The primary cilium is established by anterograde intraflagellar transport based on the Kinesin-2 motor complex along the microtubules of the axoneme towards the ciliary tip. Transport from the cilium is associated with Dynein 1b complexes in a retrograde intraflagellar transport movement. The basal body is associated with the BBSome, which coordinates sorting and trafficking of vesicular and membranous IFT cargo (e.g. receptors and ion channels) to and from the cilium. The ciliary membrane differs from the plasma membrane and is separated by the transition zone and the ciliary pocket. Further, within the transition zone microtubular triplets from the basal body reduce to microtubular doublets.

Primary cilia emerge from the mother centriole of not proliferating cells at the cell cycle phase G1/G0. Initially, the mother centriole migrates to the plasma membrane as an initial step of ciliogenesis. The mother centriole docking to the membrane is mediated by distal appendage proteins (DAP) (Schmidt et al. 2012; Tanos et al. 2013). One well studied marker of DAP is the chromosomal protein 164 (Cep164), which associates to the centrosome in a cell cycle dependent manner. A peak of accumulation at the centrosome was detected during G1/G0 phase, where Cep164 acts in the docking of vesicles at the mother centriole (Schmidt et al. 2012). During the initial phase of cell cycle progression from G1- to S-phase, cilia are disassembled to release the centriole for establishment of the mitotic spindle. Loss of ciliary

function is in close relation to the development of cancer, since ciliation seems to be a critical regulator of cell cycle progression (Jonassen et al. 2008; Li et al. 2011; Menzl et al. 2014; Seeley et al. 2009). However, certain forms of cancer show ciliated cells. For example, primary cilia mediate Hedgehog signaling in human urothelial carcinoma cell lines, which induces proliferation and tumor growth (Fei et al. 2012).

Primary cilia play an important role during development. But also cells in adult tissue can be ciliated. Examples are fibroblasts, epithelial cells of renal tubes, cholangiocytes, as well as astrocytes, neurons and neuronal progenitors. In general, stem-cell like progenitor cells in adult tissue are frequently ciliated and cilia are shown to regulate differentiation (Fu et al. 2014; He et al. 2014; Tummala, Arnsdorf, and Jacobs 2010). The stem-cell like progenitor cell within the skeletal muscle tissue is named satellite cell (SC). SCs are quiescent cells and keepers of the regenerative capacity of the tissue. Once activated, SCs are called myoblasts. SCs and myoblasts are ciliated and abolishment of the cilium was shown to diminish differentiation efficiency into myotubes (Fu et al. 2014). Further, cilia were suggested as an essential organelle for SC self-renewal, since asymmetric division led to one ciliated daughter stem cell that sustained quiescent (Marican, Cruz-Migoni, and Borycki 2016). How the primary cilium keeps the SC in quiescence is not known. There might be differences in signal reception between ciliated and not ciliated cells. But the specific function of the cell signaling hub in this process needs further investigation.

4.4 Ciliopathies

As stated above, primary cilia are involved in main cellular functions like cell cycle, cell polarity and signaling. Ciliary dysfunctions cause a wide spectrum of phenotypes in various tissues and organs. Therefore, a disease related to ciliary function is called ciliopathy. This group of genetic pleiotropic disorders shares common phenotypes like polydactyly, renal failure, kidney cysts, cognitive impairment, retinal degeneration or obesity. **Schematic 2** gives an overview of ciliary proteins and related ciliopathies in humans.

The most common genetic cause for dialysis and kidney transplants is Autosomal Dominant Polycystic Kidney Disease (ADPKD) with around 12.5 Mio patients worldwide, which affects the genes polycystic kidney disease 1 or 2 (PKD1 or PKD2). It is usually diagnosed between the ages of 30 to 50 years old and characterized by the development of liquid filled cysts in the kidneys. Affected kidneys can be 20-fold larger than unaffected organs. Besides the kidneys, also the liver, pancreas and spleen are affected and appear to develop cysts in ADPKD. One of 20.000 live births presents with Autosomal Recessive PKD (ARPKD), which is characterized by early onset and a mortality rate of 30-50% during birth or shortly after.

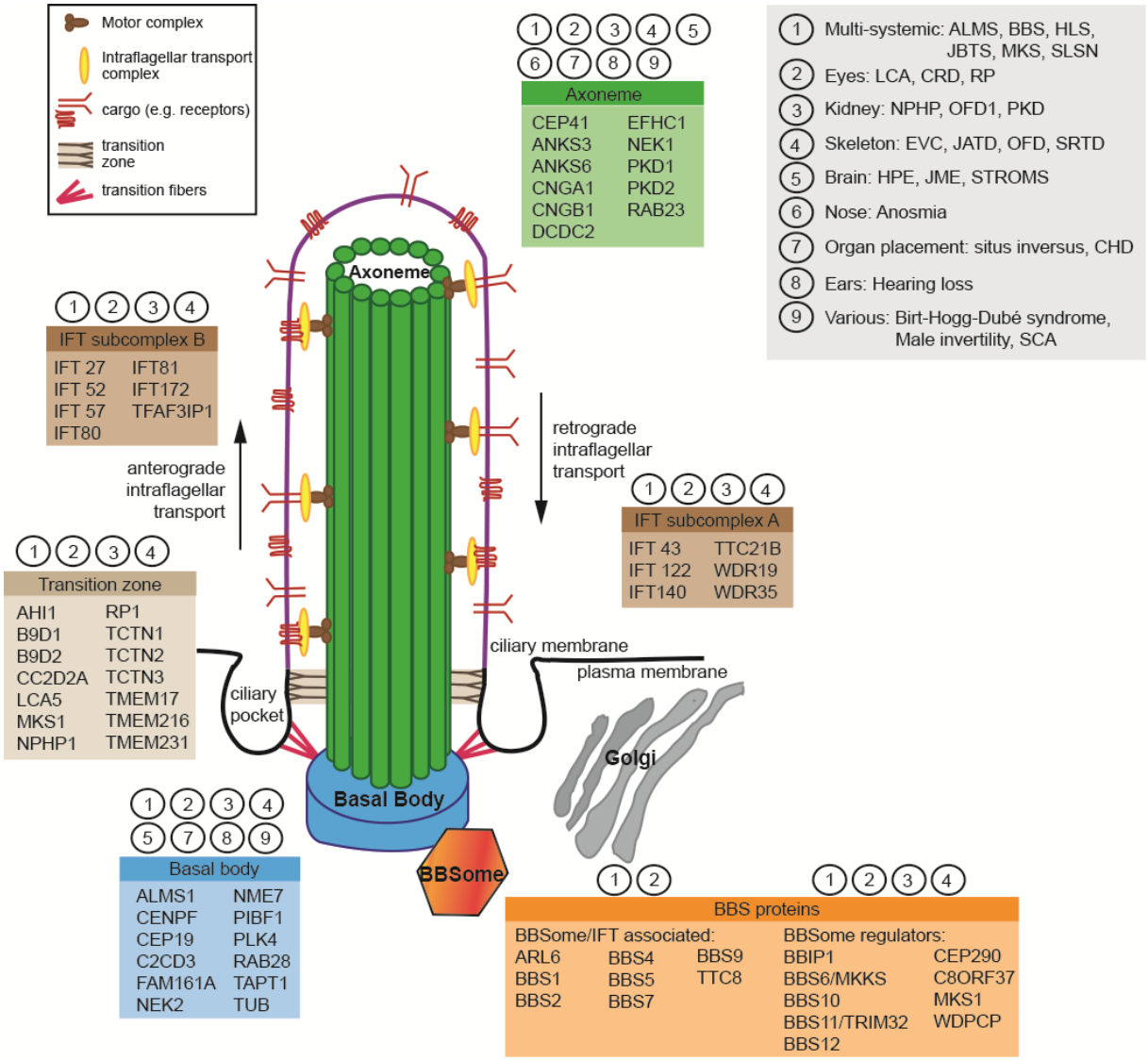

Schematic 2: Links between ciliary proteins and ciliopathies. Schematical illustration of important ciliary compartments with selected ciliopathy related genes in humans. Numbers are illustrating groups of ciliopathies, that can be induced by mutation of the corresponding genes. ALMS: Alström syndrome, BBS: Bardet-Biedl Syndrome, HLS: Hydrolethalus syndrome, JBTS: Joubert syndrome, MKS: Meckel syndrome, SLSN: Senior-Løken syndrome, LCA: Leber congenital amaurosis, CRD: Cone-rod dystrophy, RP: Retinitis pigmentosa, NPHP: Nephronophtisis, OFD1: Orofaciodigital syndrome 1, PKD: Polycistic kidney disease, EVC: Ellis-van Crefeld syndrome, JATD: Jeune asphyxiating thoracic dystrophy, OFD: Orofaciodigital syndrome, SRTD: Short-rib thoracic dysplasia, HPE: Holoprosencephaly, JME: Juvenile myoclonic epilepsy, STROMS: Strømme syndrome, CDH: Congenital heart diesease, SCA: Spinocerebrellar ataxia.

Two ciliopathy families show skeletal muscle insulin resistance and the development of diabetes. One is a rare recessively inherited ciliopathy named Alström Syndrome (ALMS), induced by mutation of the gene *ALMS1*. The phenotypic spectrum between patients is broad, which makes diagnosis and early onset of treatment difficult. Primary features of ALMS are

obesity, insulin resistance as well as loss of vision and hearing. Secondary features are type 2 diabetes, cardiomyopathy, hypertriglyceridaemia as well as renal and hepatic dysfunction (Marshall et al. 2005).

The second ciliopathy showing skeletal muscle insulin resistance and development of diabetes is Bardet-Biedl Syndrome (BBS). Investigations of this thesis were done on BBS4, a Bardet-Biedl Syndrome disease gene attributing to approximately 2.3% of the BBS cases (Katsanis 2004). The most abundant pathogenic variants are BBS1 and BBS10, which are mutated each in approximately 20% of BBS patients (Katsanis 2004; Stoetzel et al. 2006). BBS is a rare genetic disease and characterized in humans by multisystemic phenotypes. Beales and colleagues published a population survey of 109 BBS patients. This publication demonstrated rod-cone dystrophy as a common phenotype of BBS. On the average of 8 years, patients were described for night-blindness with ongoing loss of vision. Further, almost 70% of the BBS patients within the cohort study showed polydactyly. Another 62% of BBS patients showed learning difficulties and half of the cohorts' patients appeared with developmental delay and attended a special school. Almost 50% of the patients were diagnosed for renal malformations. Hereby, common abnormalities are the formation of kidney cysts. Hypogonadism affects almost every male patient and males usually are infertile. However, females can have irregular menstrual cycles and give birth to healthy children (Beales et al. 1999). Other cohort studies showed obesity in approximately 90% of the BBS patients (Bell and Penrose 1958; Klein and Ammann 1969) and loss of lean mass in male BBS patients compared to weight-matched controls (Grace et al. 2003). Besides these characteristics, common complications in patients with BBS4 are congenital heart disease (7%), hypertension (8%) and diabetes mellitus (45%) (Beales et al. 1999; Green et al. 1989; M'Hamdi, Ouertani, and Chaabouni-Bouhamed 2014).

To investigate the impact of ciliary function in the development of diabetes and other phenotypes of the disease, BBS mouse models were generated. Bbs4 knock-out (*Bbs4*$^{-/-}$) mouse models were used to get insights into the function of Bbs4 by investigation of knock-out related phenotypes. Abolishment of Bbs4 from the cells does not affect ciliary structure, but ciliary function and assembly of flagella. Therefore *Bbs4*$^{-/-}$ mouse sperms are immotile, which makes males infertile (Mykytyn et al. 2004). Further, *Bbs4*$^{-/-}$ mice undergo retinal degeneration by apoptosis of photoreceptor cells, inducing loss of vision (Mykytyn et al. 2004). Although *Bbs4*$^{-/-}$ mice are born smaller than wildtype littermates, they become obese during adulthood. Compared to other Bbs mouse models like *Bbs2*$^{-/-}$ or *Bbs6*$^{-/-}$, *Bbs4*$^{-/-}$ mice show highest body weight (Rahmouni et al. 2008). Increased weight gain in Bbs mice is related to hyperphagia caused by involvement of neuronal cilia in satiety regulation (Davenport et al. 2007; Eichers et al. 2006; Rahmouni et al. 2008). Further, as described for human patients,

also *Bbs4*$^{-/-}$ mice show anomalies of kidney structure and function (Guo et al. 2011). Summing up, the mouse model nicely reproduces the human phenotype and therefore can be used as a model to investigate the molecular mechanisms behind the disease.

Blood tests showed abnormal lipid composition as well as increased levels of insulin and leptin in the blood of *Bbs4* knock-out mice, indicating aberrant metabolism (Eichers et al. 2006; Mykytyn et al. 2004). Interestingly, *Bbs4*$^{-/-}$ mice have difficulties in glucose handling already before onset of obesity which is related to diminished first phase insulin secretion by pancreatic β-cells (Gerdes et al. 2014). This study showed that the development of diabetes is not a secondary effect of obesity. Instead, diabetes is a direct effect of ciliary dysfunction in metabolically active organs. This would also explain why BBS patients exhibit higher risk for the development of diabetes than control obese patients (Mujahid et al. 2018). Going deeper into the role of cilia in diabetes, the insulin receptor (IR) has been shown localized on the cilia of ß-cells (Gerdes et al. 2014). Moreover, the membranous expression of the IR in peripheral tissue of not obese mice is affected by loss of Bbs proteins (Starks et al. 2015), indicating another pathway involved in aberrant glucose metabolism in Bardet-Biedl Syndrome. Reduced membranous expression of the IR in peripheral tissue (like adipose tissue, liver and skeletal muscle) leads to decreased insulin signaling and inhibits the uptake of postprandial blood glucose which promotes the onset of diabetes (Starks et al. 2015). Due to altered metabolism, patients with diabetes develop a characteristic skeletal muscle phenotype (see above), including a reduced number of mitochondria, reduced muscle strength and accumulation of intramuscular fat. The study presented here was carried out to shed light on the importance of ciliary proteins for skeletal muscle function and metabolism before the onset of hyperglycemia.

4.5 Myopathies: skeletal muscle atrophy and dystrophy

Around 70-75% of postprandial glucose is taken up by skeletal muscle related to insulin stimulation (Shulman et al. 1990). Therefore, it is the main organ for post-prandial glucose metabolism. As shown before, skeletal muscle fiber precursors are ciliated and abolishment of primary cilia by Ift88 knock-down affects Shh signaling and differentiation efficiency into myofibers (Fu et al. 2014). So far, the skeletal muscle phenotype in the *Bbs4*$^{-/-}$ mouse model has not been characterized.

On average, 38.4% of the body mass in men are skeletal muscle mass. In women the portion is 30.6% (Janssen et al. 2000). Skeletal muscle therefore is the major muscle type besides cardiac and smooth muscle. During skeletal muscle myogenesis, single myoblasts fuse to form cylindrical, syncytical myofibers. Single myofibers are separated from each other by a

cell membrane, called sarcolemma. Within the muscle, bundles of fibers are formed, called fascicles. Layers of connective tissue (fasciae) encircle the fascicles. Within the muscle fiber, myofibrils of repeating actin and myosin filaments, termed sarcomers give the striated appearance. The skeletal muscle action is voluntary controlled by the nervous system. In contrast to skeletal muscle, cardiac and smooth muscle perform involuntary movements. The heart muscle is composed of individual, single nucleated cardiomyocytes. The cardiomyocytes form long fibers through intercalated disks, which join the cells at their distal ends. The intercalated disks are adhering structures that enable the formation of an electrochemical syncytium. Cardiomyocytes also contain sarcomeres, therefore they also belong to the group of striated muscles. Smooth muscles appear in vessels, the wall of hollow organs and respiratory passageways and are not striated. Those cells are spindle shaped and unbranched. Like cardiomyocytes and in contrast to myofibers, smooth muscle cells do not fatigue.

For the generation of force, two processes are coupled: excitation and contraction. Distal motor neuron endings contain a high number of vesicles filled with the neurotransmitter acetylcholine (ACh). Once an action potential reaches the presynaptic membrane of the neuromuscular junction (NMJ), voltage-gated Ca^{2+}-channels open to increase intracellular calcium concentration. Intracellular signaling cascades promote the translocation of ACh-filled vesicles towards the presynaptic membrane and to release ACh into the cleft separating nerve and muscle. Binding of ACh activates nicotinic acetylcholine receptors (nAChR) at the postsynaptic membrane of the myofiber. Intracellular signaling cascades trigger opening of Na^+ channels along the muscle to propagate the signal. Na^+ influx leads to depolarization of the muscle and the release of Ca^{2+} from the sarcoplasmic reticulum into the cytoplasma. Ca^{2+} binds troponin, which therefore undergoes a conformational change and helps to translocate tropomyosin (Lehman, Craig, and Vibert 1994). In not activated muscles, tropomyosin is bound to myosin and blocks the interaction to actin. The myosin complex is composed of 2 myosin heavy chains (MHC) twisted around each other. At the head end of the MHC, two myosin light chains (MLC) are associated with each MHC. MLC stabilize the myosin complex and in striated muscle determine the speed of ATPase activity. In the absence of tropomyosin, the MHC head of the myosin complex can reach forward and bind actin to form a cross bridge. Under the consumption of ATP myosin contracts in the neck region of MHC, releases actin and reaches forward to bind the next actin molecule. This process is repeated in a series of replicated events for muscle contraction and called myosin-actin cycling. Since muscles contain repeated filaments of actin and myosin, actin-myosin cycling induces the filaments to slide over one another (Huxley and Niedergerke 1954; Huxley and Hanson 1954). Movement is generated, when the force of myosin-actin cycling reaches myotendinous junctions (MTJ).

Force strength can depend on a variety of effectors, e.g. muscle length, efficiency of activation by nervous system, muscle architecture and velocity of movement.

Based on their metabolism, skeletal muscle can be divided into glycolytic and oxidative muscles according to their main fiber type. Glycolytic fibers are also called Type II or fast twitch, because of their ability to contract quickly. These fibers fatigue quickly, because they produce energy by glycolysis, which cannot be restored during the exercise. One example for fast twitch muscle in mouse is the *extensor digitorum longus* (EDL), which mainly consists of Type IIb fibers. The EDL is localized at the front site of the mouse hind leg. Oxidative fibers are also called Type I or slow twitch, because their maximum shortening velocity is much slower compared to fast twitch fibers. Furthermore, they utilize also free fatty acids and triglycerides using aerobic metabolism pathways. Therefore, these kind of fibers are needed for energy production over long time duration like jogging or walking. One example for slow twitch muscle in mouse is the *soleus* (Soleus), which mainly consists of Type I and Type IIa fibers (intermediate metabolism between Type I and IIb). The Soleus is localized in the back side of the mouse hind leg, underneath the glycolytic *gastrocnemius* (Gastrocnemius). Fiber types can be immunohistochemically stained based on differentially expressed myosin heavy chains that are associated with the fiber type. Using this method fiber type shifts can be detected. Fiber type shift is a common phenomenon of the skeletal muscle in the adaption to stimuli like exercise, nutrient restriction or hyperglycemia (Pette and Staron 2000; Sher and Cardasis 1976). Skeletal muscle from patients with diabetes for example shows a shift from oxidative Type I to glycolytic Type II fibers (Gaster et al. 2001; Hickey et al. 1995; Oberbach et al. 2006).

A common phenotype regarding skeletal muscle is muscle wasting. Possible explanations for this phenotype can be sarcopenia, atrophy or dystrophy. The first one, sarcopenia, is an age-dependent form of muscle mass loss and associated with fibrosis, accumulation of intramuscular fat, fiber type shift and degeneration of NMJ (Cruz-Jentoft et al. 2010; Ryall, Schertzer, and Lynch 2008). Skeletal muscle atrophy can be associated with muscle disuse (e.g. long time bed rest, peripheral nerve damage or spinal cord injury), starvation, aging or disease and is based on an imbalance of muscular protein homeostasis shifted to proteasomal degradation causing loss of muscle mass. Specific characteristics of atrophic muscle are decreased fiber diameter, force production, protein content and fatigue resistance. Two common markers for muscle atrophy are the muscle specific E3 ubiquitin ligases Murf-1 (muscle RING-finger protein-1) and Fbx-32 (F-box protein 32) (Bodine et al. 2001; Gomes et al. 2001), which have been found upregulated e.g. in spinal muscular atrophy or diabetes (Bricceno et al. 2012; Lecker 2004; Wang et al. 2006). E3 ubiquitin ligases are involved in the last step of substrate ubiquitination. First, E1 (ubiquitin activating enzymes) activates ubiquitin

in an ATP-dependent reaction. Activated ubiquitin is then transferred to E2 (ubiquitin conjugating enzyme). In the last step ubiquitin is transferred from E2 to a substrate lysine by E3 (ubiquitin protein ligase). Unlike other E3 ligases, Murf-1 and Fbx-32 are belonging to the RING (really interesting new gene) finger ubiquitin ligases and do not contain a catalytic region for ubiquitination of the substrate. RING finger proteins serve as a scaffold between E2 bound ubiquitin and the substrate by bringing them in close proximity (Ozkan, Yu, and Deisenhofer 2005). Substrates can be monoubiquitinated at one lysine as a single molecule, as an ubiquitin chain or multiubiqutinated at several lysines. Ubiquitinated substrates are degraded by the 26S proteasome.

Another form of muscle wasting is dystrophy, which is characterized by muscle weakness and degeneration. The most common form of dystrophy is Duchenne muscular dystrophy, which in humans shows first signs of disease at approximately 3 years of age. Progressive muscle degeneration leads to death between 20 to 30 years of age. Dystrophy is caused by dysfunctionality of proteins of the dystrophin-glycoprotein complex (DGC, also called dystroglycan complex) (Ervasti et al. 1990). The complex is critical for linking the cytoskeleton to the extracellular matrix in MTJ and therefore needed for force generation. The complex consists out of two different subcomplexes, as they are the glycoprotein complex and the cytoplasmic complex as well as associated proteins (Yoshida et al. 1994; Yoshida and Ozawa 1990). The glycoprotein complex further divides into the membrane spanning sarcoglycan complex and the extracellular associated dystroglycan complex of the sarcolemma, which is connected to the tendinous extracellular matrix by laminins. Associated proteins are, among others, sarcoglycan associated transmembrane sarcospan as well as intracellular dystrophin and dystrobrevins. The function of dystrophin is the anchoring of sarcolemmal F-actin and myofiber microtubule to the dystroglycan complex. The DGC is one of two linkage systems between the muscle cytoskeleton and the tendon, also known as MTJ. The second form is an α7β1Integrin based system of integrins anchoring intracellular actin to laminin of the extracellular matrix. Intracellular proteins to strengthen the membrane spanning integrins are associated, e.g. tensin, paxillin or vinculin. Like the DGC based linkage system, also the integrin linkage system is crucial for the connection of muscular cytoskeleton and tendon, together representing the primary site of muscle force transmission. Although integrins are found all over the sarcolemma, they are significantly enriched in MTJ (Bao et al. 1993; Miosge et al. 1999). β1Integrins are, in addition to MTJ, also crucial for the functionality of NMJ (Martin et al. 1996). These structures are sites of cholinergic neurotransmission to control muscle contraction. In adult individuals, skeletal muscle fibers are monoinnervated, which means one fiber is connected to one motorneuron only. On the other hand, one motorneuron innervates several fibers. As a common complication in dystrophy, changes in NMJ morphology like

aberrant acetylcholine fragmentation in the presynaptic membrane or clustering of the acetylcholine receptor in the postsynaptic membrane (Lyons and Slater 1991) have been detected.

As stated above, dystrobrevins are associated with the DGC. Further, dysbindin is linked to α-dystrobrevin at the NMJ and the DGC of striated muscle (Grady et al. 1999, 2000). Dysbindin is part of BLOC-1 (biogenesis of the lysosome-related organelles complex-1), which is involved in lysosomal-endosomal trafficking (Delevoye et al. 2016; Peter et al. 2013; Setty et al. 2007, 2008). Moreover, ubiquitinated dysbindin was shown to be a target of the E3 ubiquitin ligase Trim32 (Tripartite Motif Containing 32, BBS11) (Locke et al. 2009). Mutations of Trim32 induce Limb girdle muscular dystrophy type 2H (LGMD2H), Bardet-Biedl Syndrome 11 and cancer (Albor et al. 2006; Chiang et al. 2006; Frosk et al. 2002; Kano et al. 2008). The mutation related to BBS11 has been detected in the BBox domain of *Trim32*, whereas mutations related to LGMD2H were found in the C-terminal region of the gene (Locke et al. 2009). Besides the link of dysbindin to the ciliopathy BBS11, BLOC-1 has been shown to interact with Ift20 and is required for the transport of polycystin-2 to primary cilia (Monis, Faundez, and Pazour 2017). Although skeletal muscle dystrophy has not been reported in BBS patients, loss of lean mass has been described (Grace et al. 2003). Moreover, reduced grip strength of *Bbs5*$^{-/-}$ mice has been reported (Dickinson et al. 2016). These findings lead to the question, if there is a functional muscle phenotype also in *Bbs4*$^{-/-}$ and if atrophy or dystrophy plays a role.

4.6 Skeletal muscle regeneration

Embryonic skeletal muscle differentiation occurs in two phases. During the mouse primary or embryonic phase (E10.5-E12.5), Paired box protein 3 (Pax3) positive muscle progenitor cells derived from dermomyotomal progenitors migrate into the limb buds and fuse to form primary myofibers (Horst et al. 2006; Hutcheson et al. 2009; Otto, Schmidt, and Patel 2006). These primary fibers are characterized by the expression of slow myosin heavy chains (MHC) as well as myosin light chain 1 (MyLC1) and provide the base for the formation of early myotomes and limb muscles (Kelly et al. 1997). Within the secondary or fetal phase (E14.5-17.5) of muscle generation, Pax3 expression is reduced and Paired box protein 7 (Pax7) expression is upregulated in a subpopulation of Pax3 positive myoblasts. Pax7 (a marker for muscle progenitor cells in adult tissue) positive cells fuse to primary fibers and with themselves to form secondary fibers and push muscle growth (Biressi, Molinaro, and Cossu 2007; Horst et al. 2006; Jostes, Walther, and Gruss 1990). Characteristics for secondary fibers are expression of β-enolase, MyLC3 (myosin light chain 3) or fast MHC isoforms (Fougerousse et al. 2001; Van Horn and Crow 1989; Keller et al. 1992).

In mice, SC are localized between the basement membrane and the sarcolemma of fibers around 2 days before birth. Up to four weeks after birth, SC keep proliferating to establish a pool of cells with regenerative capacity (Tajbakhsh 2009; White et al. 2010). During homeostasis, these cells stay quiescent in G0 phase, expressing high levels of Pax7. This transcription factor is crucial to maintain the SC pool and is therefore necessary for the regenerative capacity of the muscle, as evidenced by the *Pax7* Null mice which failed to regenerate skeletal muscle (von Maltzahn et al. 2013; Seale et al. 2000). Activated and proliferating myoblasts are characterized by expression of MyoD (myogenic differentiation). Impairment of MyoD has been shown to inhibit regeneration (Megeney et al. 1996; White et al. 2000). MyoD expression is increased in newly formed myotubes, and lost in adult myofibers. Markers for myofibers are for instance the fiber type specific myosin heavy chain (MHC) types or Myf6 (**Schematic 3**). The immortal myoblast cell line C2C12 is a common tool within *in-vitro* studies of regeneration (Blau et al. 1985; Yaffe and Saxel 1977). The advantages of this cell line are: (1) C2C12 cells are easy to culture and fast to expand, (2) easy to transfect/transduce, (3) avoidance of systemic whole-body factors inducing secondary phenotypes and (4) reduction of animal experiments.

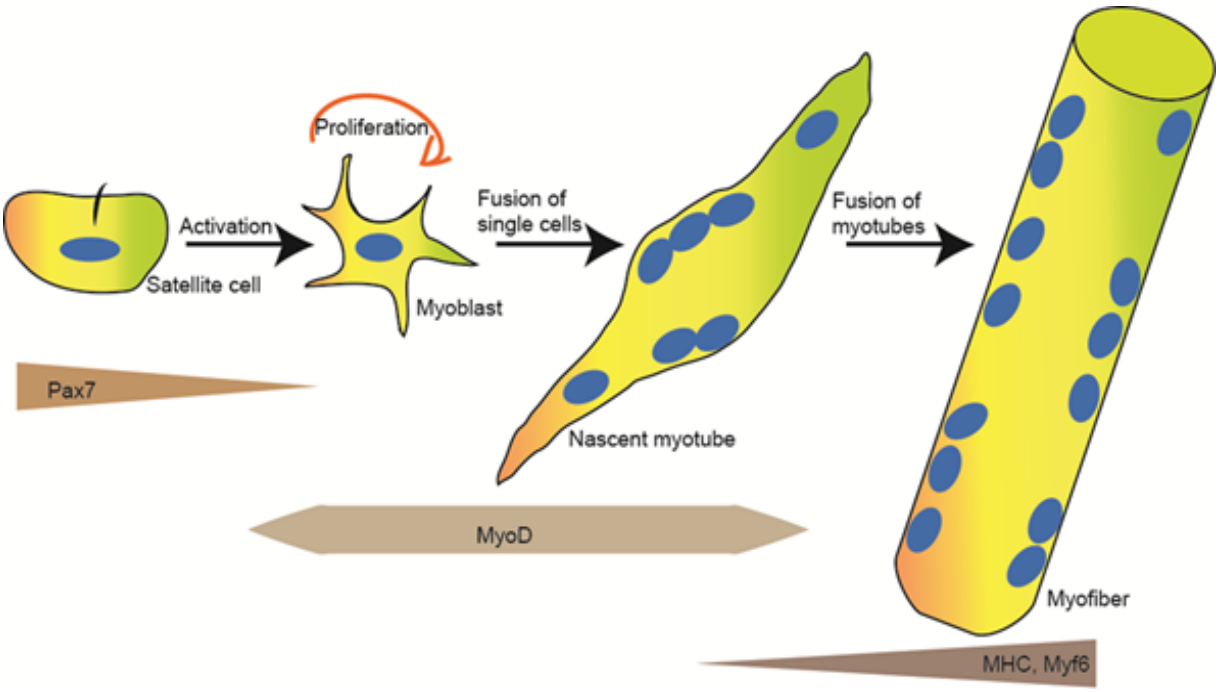

Schematic 3: Stages of skeletal muscle differentiation and marker expression. Quiescent satellite cells are ciliated and express high levels of Pax7. After activation, Pax7 expression is decreased and MyoD expression is activated in proliferating myoblasts. Myoblasts fuse to form myotubes, which are characterized by high expression of MyoD. For the formation of myofibers, myotubes fuse among each other accompanied by further myoblast incorporation. Adult myofibers are characterized by the expression of MHC and Myf6.

Notch signaling is known as an important driver for SC quiescence and self-renewal. Five Notch receptor ligands in mammals (Delta-like (Dll) 1, 3 and 4 as well as Jagged 1 and 2) are known so far and provided by the myofiber. After activation, Notch receptor (four Notch receptors reported, 1-3 described in SC) is cleaved intracellularly by the γ-secretase complex and extracellularly by tumor necrosis factor-alpha-converting enzyme (TACE/ADAM). TACE is a metalloprotease with a protease domain for regulation of transmembrane proteins by cleavage reactions. γ-secretase is a complex with minimum presenilin (Ps), nicastrin, anterior pharynx defective 1 (Aph) and presenilin enhancer 2 (Pen-2), that cleaves transmembrane proteins like E-cadherin, ephrin-B2 or Notch receptor. After Notch receptor cleavage, the Notch intracellular domain (NICD) is released and transported into the nucleus, where it binds the CSL (CBF1, suppressor of hairless, Lag-1) transcription factor (also known as recombination signal binding protein for immunoglobulin kappa J (RBP-Jκ)) and activates expression of Notch target genes like HeyL (hairy/enhancer-of-split related with YRPW motif-like protein) or Hes1 (hairy/enhancer-of-split1) (**Schematic 4**, Castel et al. 2013; Jarriault et al. 1995). The remaining transmembrane and extracellular domain of the receptor got internalized to early endosomes and further sorted to endocytic compartments like late endosomes, recycling endosomes or lysosomes. Asymmetric SC division is controlled by the asymmetric distribution of the Notch antagonist Numb. The cytoplasmic adaptor protein mediates the binding of an E3 ubiquitin ligase to Notch, leading to reduction of Notch signaling in one daughter cell. This cell undergoes differentiation, whereas the daughter cell with high Notch signaling remains proliferative (Bjornson et al. 2012; Conboy and Rando 2002).

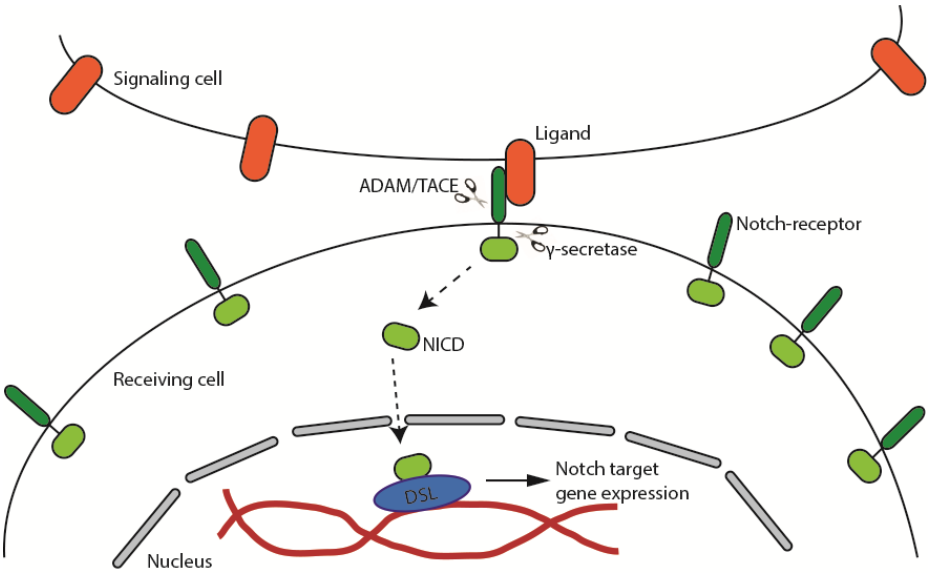

Schematic 4: Illustration of Notch signal pathway. Notch signal pathway gets activated by ligand binding to the Notch receptor and proteolytic cleavage of the receptor by ADAM/TACE and γ-secretase to release Notch intracellular domain (NICD). NICD translocates into the nucleus where it binds the Notch-specific transcription factor DSL to induce expression of Notch target genes.

Depending on the tissue as well as the cell type and its biological role, Notch-signaling has different functions. In mammals, these functions are thought to be regulated by the combination of the four different Notch receptors and their five ligands. For example, Notch1 seems to have a critical role within the transition of activated SC to quiescence *in vivo* (Wen et al. 2012). On the other hand, Notch3 was shown to be a negative regulator for SC proliferation, since Notch3 deficient mice showed increased SC self-renewal and therefore increased SC number (Kitamoto and Hanaoka 2010). In adult skeletal muscles, quiescent SC express Notch receptors 1, 2 and 3 and show high Notch signaling activity which keeps the SC in a quiescent state. Notch3 activity was shown to be activated in SC by nascent muscle fibers expressing Dll4. This Dll4-Notch3 signaling combination during differentiation was shown to keep not activated SC in the quiescent state to maintain the SC pool and further regenerative capacity (Low et al. 2018). On the other hand, Notch1 and Notch2 cooperate during SC quiescence and activity, thereby maintaining the SC pool during quiescence and regulating cell-fate decisions in differentiating myoblasts (Fujimaki et al. 2018). Further, overexpression of Jagged1 diminished the phenotype severity in Golden Retrievers affected by Duchenne muscular dystrophy, implementing Jagged1 as a target for the therapy of muscular dystrophies (Vieira et al. 2015). These data illustrate the importance of regulated Notch signaling activity in skeletal muscle differentiation and regeneration (**Schematic 5**). To the best of my knowledge, no link between the primary cilium and Notch signaling during myoblast differentiation has been reported. However, in other cell types a link between Notch signaling and cilia has been described. Wildtype epidermal cells showed colocalization of Notch3 and Presenilin-2 (a subunit of γ-secretase) with the cilium (Ezratty et al. 2011), suggesting a role of the cilium in Notch signaling. Further, loss of cilia during embryonic skin development caused abnormal proliferation and differentiation effects by deregulated Notch signaling (Ezratty et al. 2011). Mouse corneal epithelial cells lacking cilia also showed increased proliferation and diminished Notch signaling activity caused by reduced NICD1 expression (Grisanti et al. 2016).

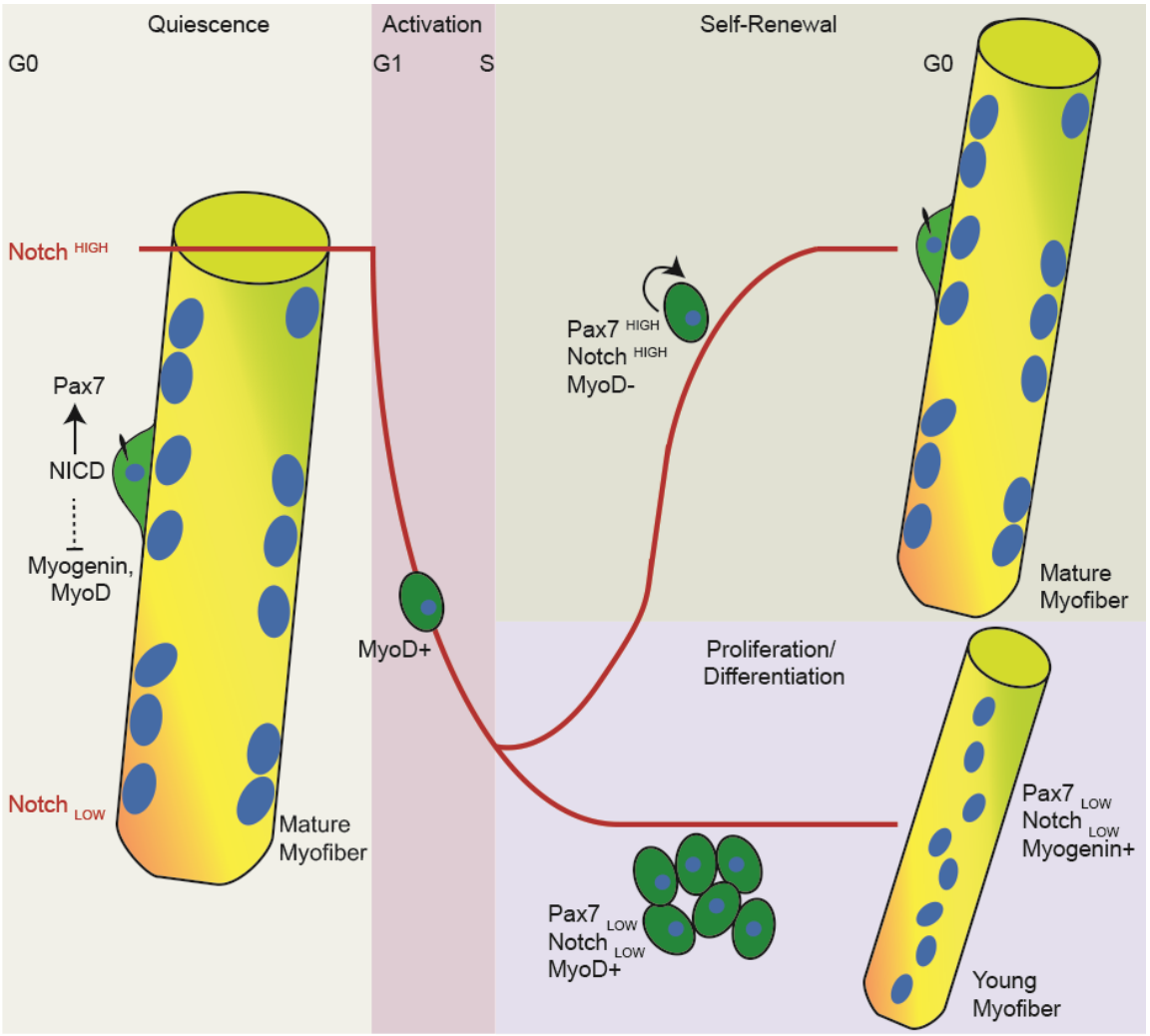

Schematic 5: Notch signaling during myogenesis. Quiescent ciliated satellite cells attached to mature myofibers in adult skeletal muscle tissue show high Notch signaling activity. Notch intracellular domain (NICD) regulated gene transcription prevents expression of differentiation markers and keeps *Pax7* expression high. During activation, Notch signaling and thereby *Pax7* expression are downregulated, allowing expression of *MyoD* in activated and proliferating cells. Myoblasts differentiate, thereby fusing into multinucleated myofibers for skeletal muscle regeneration. A subset of activated myoblasts gains back high levels of Notch signaling and therefore Pax7 expression. These cells return to a quiescent state for further regeneration.

As mentioned above, the abundance of signaling molecules is increased on the ciliary membrane compared to the plasma membrane. The kind of molecules accumulated are depending on the cell type and function. A well-studied cilia-dependent signaling pathway is hedgehog (Hh) signaling (**Schematic 6**), which has been shown deregulated in rhabdomyosarcoma (Fu et al. 2014). In the absence of the ligands sonic hedgehog (Shh), desert hedgehog (Dhh) and indian hedgehog (Ihh), the receptor Patched 1 (Ptc1) is located at the ciliary membrane and around the ciliary base, suppressing the accumulation of Smoothened (Smo) in the ciliary membrane (Rohatgi, Milenkovic, and Scott 2007). On the

other hand, Ptc1 keeps the zink-finger protein GLI (Gli) transcription factors at the ciliary tip, where it is bound to the repressor suppressor of fused (Sufu). After binding of the Hh ligand to Ptc1, the receptor is excluded from the cilium, Smo enters and accumulates in the ciliary membrane, as well as Gli proteins that are released from Sufu, exit the cilium and enter the nucleus, thereby activating Hh signal pathway related gene expression (Corbit et al. 2005; Haycraft et al. 2005; Zeng, Jia, and Liu 2010). Besides Hh and Notch signaling, the impact of ciliary dysfunction on canonical Wnt signaling is still controversial (Abdelhamed et al. 2013; Huang and Schier 2009; Sugiyama et al. 2011).

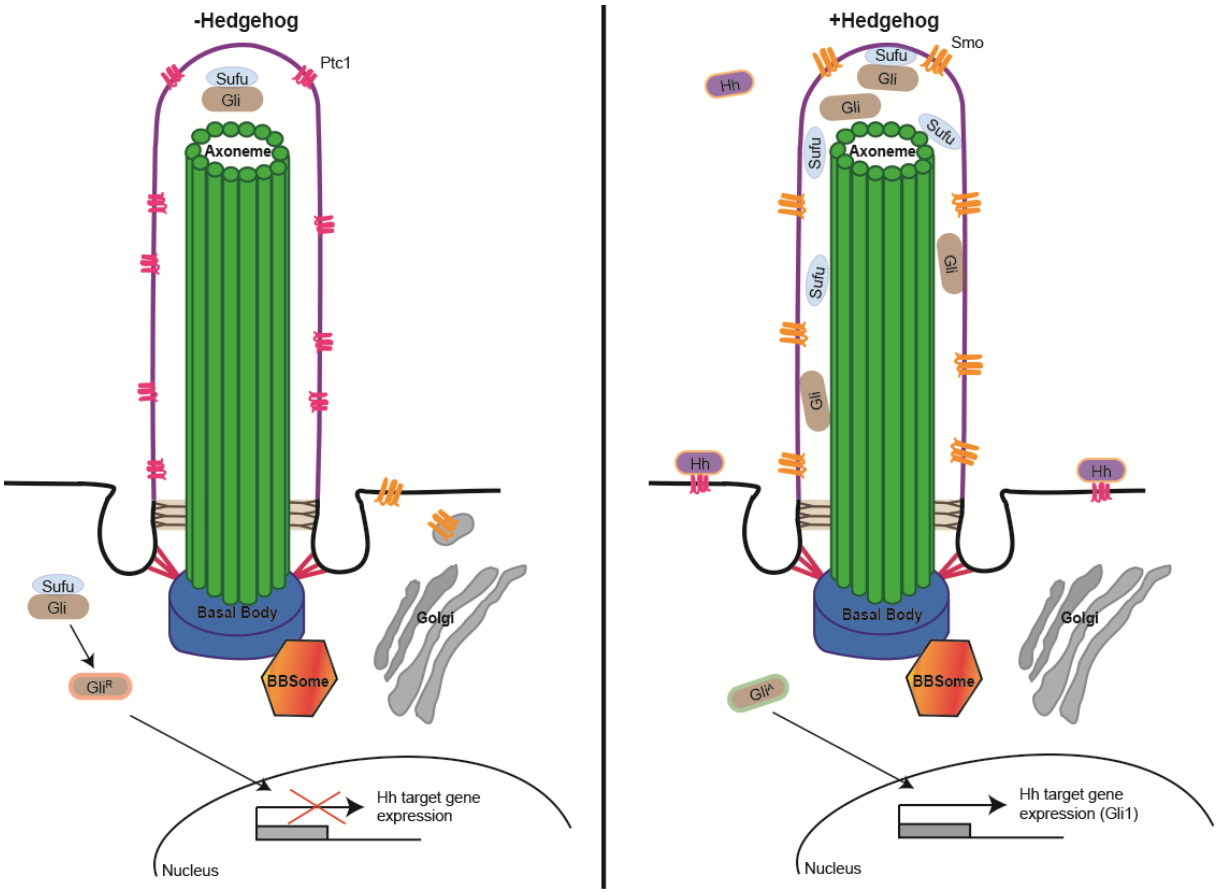

Schematic 6: Hedgehog signaling regulation. Without the Hedgehog ligand, Ptc1 accumulates in the cilium and suppresses ciliary location of Smo. Gli is repressed by Sufu and cannot translocate into the nucleus (Gli^R). Hedgehog-bound Ptc1 exits the cilium and enables Smo to accumulate there. Gli gets released (Gli^A) and can enter the nucleus to induce Hh target gene expression.

4.7 Actin remodeling and endocytosis

Endocytosis is a process of internalizing extracellular or transmembrane material by invagination of the cell membrane and the formation of intracellular vesicles. The internalized material can be proteins, macromolecules, fluids or electrolytes. Three different kinds of endocytosis exist: (1) phagocytosis is the process used by macrophages for the internalization

of bacteria or the mechanism amoeba use for food internalization (Aggeler and Werb 1982; Christiansen and Marshall 1965). (2) pinocytosis is divided in macropinocytosis of large molecules (e.g. nutrients or antigens) and caveolae-mediated micropinocytosis. In most cells types, transmembrane caveolin-1 or -2 have been shown associated with complexes of proteins called cavins-1, -2 or -3 (Hill et al. 2008; Pelkmans et al. 2004; Pelkmans and Zerial 2005; Scherer et al. 1996). Muscle cells use specifically caveolin-3 and cavin-4/MURC for endocytosis (Bastiani et al. 2009; Tagawa et al. 2008). (3) receptor-mediated endocytosis is a selective form of endocytosis for clathrin-dependent internalization of specific molecules. Clathrin-mediated endocytosis (CME) is associated with iron-saturated transferrin uptake as well as turnover of plasma-membrane lipids and proteins. The first step of CME is the formation of clathrin coated pits. Therefore, intramembranous phosphatidyl-inositol(4,5)bisphosphate (PtdIns(4,5)P_2) recruits adaptor proteins like huntingtin interacting protein 1 (HIP1), clathrin-assembly lymphoid myeloid leukaemia protein (CALM/AP180), autosomal recessive hypercholesterolemia (ARH) or the clathrin adaptor complex AP-2 to the membrane. Trimers of clathrin heavy chains, called triskelion, bind the membranous adaptor proteins and assemble a clathrin coat at the site of endocytosis. In the second step of CME, triskelia were shown to recruit further proteins that help during the formation of curved membrane vesicles and invagination. For further scission of the vesicle from the cell membrane, oligomers of dynamin form a ring around the invagination neck. A domain of dynamin has been shown to bind cortactin, that activates the Arp2/3 complex (actin-related protein 2/3) and further stimulates the formation of filamentous actin (F-actin). Preventing actin assembly is known to inhibit scission of vesicles from the membrane (Merrifield, Perrais, and Zenisek 2005). Further, intracellular clathrin-coated vesicles are uncoated in a HSC70 dependent, ATP consuming reaction.

The control of actin polymerization is connected to intracellular membrane trafficking and endocytosis. Important factors for the activation of G-actin polymerization are members of the Ras homologue (Rho) family of small GTPases, like cell division cycle 42 (Cdc42) and Rac family small GTPase 1 (Rac1). Cdc42 takes part in many vesicle-transport steps in the cell, for example in the regulation of endo- and exocytosis, transport of molecules between endoplasmatic reticulum and Golgi-appartus as well as post-Golgi transport (Egorov et al. 2009; Hehnly et al. 2009; Luna et al. 2002). Rac1, on the other hand, was found to act only during clathrin-dependent endo- and exocytosis (Lamaze et al. 1996; Matas et al. 2005). Both proteins were shown to inhibit transport after overexpression (Lamaze et al. 1996; Luna et al. 2002). The main overlapping function of Rac1 and Cdc42 is the regulation of endocytosis by actin polymerization. These small GTPases have to be activated through binding of GTP, which is catalyzed by specific guanine nucleotide exchange factors (GEFs). Tiam1 (T-

lymphoma invasion and metastasis-inducing protein 1) is the Rac1 specific GEF and activates Rac1 by catalyzing the exchange of GDP for GTP (Schmidt and Hall 2002). Further, Rac1 as well as Cdc42 were shown to activate Arp2/3, which is the actin nucleator for the formation of filamentous actin (F-actin), (**Schematic 7**).

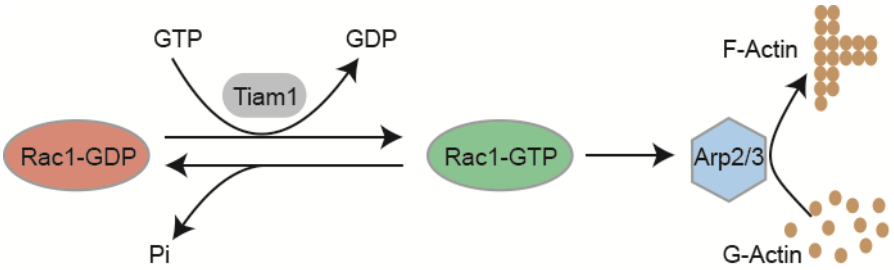

Schematic 7: Model of Rac1 activation for induction of actin polymerization. The Rac1 specific GEF Tiam1 catalyzes Rac1 activation by exchange of GDP with GTP. Active Rac1-GTP cascade activates Arp2/3 at the cell cortex for actin polymerization.

In cultured muscle cells as well as murine and human skeletal muscle, Rac1 has been shown to regulate insulin stimulated Glut4 translocation and glucose transport (JeBailey et al. 2007; Nozaki et al. 2012; Sylow et al. 2013; Ueda, Kataoka, and Satoh 2008). The insulin signaling cascade activates Rac1, which in turn initiates the autophosphorylation of p21-activated kinase (PAK) on threonine 423 (JeBailey et al. 2004). Interestingly, the activity of Rac1 and PAK were shown impaired in insulin resistant skeletal muscles of mouse and human (Sylow et al. 2013). The activated PAK pathway has been shown to induce the reorganization of the cortical actin cytoskeleton by Arp2/3 activation. In addition to the metabolic function of Rac1 in adult fibers, both Rac1 and Cdc42 have been shown to be involved in the fusion efficiency of mouse myoblasts. Rac1 and Cdc42 mutant myoblasts showed normal migration, and α- as well as β-catenin accumulation at the contact sites of two myoblasts. However, the accumulation of vinculin and actin polymerization has been found to be reduced at contact sites. Moreover, Rac1 but not Cdc42 mutant myoblasts showed reduced recruitment of Arp2/3 at the contact sites. Nevertheless, fusion efficiency of Rac1 and Cdc42 mutant myoblasts had been found significantly reduced (Vasyutina et al. 2009). Besides Rac1 and Cdc42, additional cytoskeletal actin regulatory proteins have been found to be involved in myoblast fusion, like N-Wasp (Neural Wiskott-Aldrich Syndrome protein), Dock1 (Dedicator of cytokinesis protein 1) and Nap1 (nucleosome assembly protein 1) (Gruenbaum-Cohen et al. 2012; Laurin et al. 2008; Nowak et al. 2009). Further, the recently described master regulator of myoblast fusion, myomaker (Tmem26), also depends on cytoskeletal remodeling (Bi et al. 2017; Millay et al. 2013; Quinn et al. 2017). Shisa2, a transmembrane protein of the endoplasmatic reticulum

has been found repressed by high Notch signaling activity in quiescent SC. Upon SC activation and Notch depression, Shisa2 expression has been shown to be upregulated in myoblasts. Based on Rac1 and Cdc42 F-actin assembly, Shisa2 promotes polarized F-actin aggregation and myoblast fusion. Besides the positive regulation of fusion, Shisa2 was not shown to affect myoblast differentiation based on MHC expression (Liu et al. 2018).

4.8 Aim of the thesis

Bbs4$^{-/-}$ mice were shown to have metabolic complications like obesity, insulin resistance of peripheral organs and an increased risk for the development of diabetes. Further, impacts of cilia on kidney and liver cyst formation as well as retinal degradation are well investigated. The role of primary cilia in skeletal muscle development and function are poorly understood. Therefore, the aim of the thesis was (1) the characterization of the skeletal muscle phenotype in *Bbs4*$^{-/-}$ mice and (2) the identification of underlying mechanisms.

5 Results

5.1 Muscle phenotype of the Bbs4 mouse model

For the following study I took advantage of an established *Bbs4*$^{-/-}$ mouse line (Kulaga et al. 2004). *Bbs4*$^{-/-}$ mice were generated by insertion of a gene-trapping cassette between exon 1 and exon 2 of the *Bbs4* gene (**Schematic 8**), inducing an alternative mRNA splice isoform leading to a premature stop codon and thus nonsense-mediated degradation of the *Bbs4* mRNA. *Bbs4*$^{+/+}$ mice do not carry the trapping cassette in their genome, whereas knock-out mice (*Bbs4*$^{-/-}$) carry the trapping cassettes in both alleles and heterozygous mice in one allele (*Bbs4*$^{+/-}$).

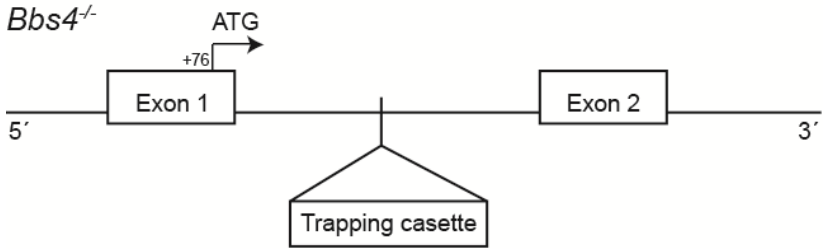

Schematic 8: Trapping cassette in the *Bbs4* gene between the exons 1 and 2. (Taken and modified from Kulaga et al. 2004)

Bbs4$^{-/-}$ are runted compared to their *Bbs4*$^{+/+}$ littermates within the first weeks of life. However, after birth they show increased weight gain compared to *Bbs4*$^{+/+}$ littermates and become obese and hyperglycemic at 4 to 6 month of age (Eichers et al. 2006; Mykytyn et al. 2004). In order to characterize our *Bbs4*$^{-/-}$ cohort, I compared size and body weight of male mice. Female *Bbs4*$^{-/-}$ mice were excluded, since onset of obesity and severity have been shown gender specific; females show a stronger phenotype (Eichers et al. 2006). Further, using only male mice excludes hormonal side-effects of females like the estrous cycle. As described in previous reports, also *Bbs4*$^{-/-}$ mice used for this study were smaller after birth compared to *Bbs4*$^{+/+}$ littermates (**Figure 1A**). However, they showed increased weight gain between 4 and 14 weeks after birth. Therefore, 14 weeks old mice of our cohort had the same size and body weight (*Bbs4*$^{+/+}$=28.62 g, *Bbs4*$^{-/-}$=28.25 g, **Figure 1A and B**).

Even before onset of obesity, *Bbs4*$^{-/-}$ mice show impaired glucose handling when challenged with glucose. Knock-out of *Bbs4* has been shown to induce blunted first-phase insulin secretion in mouse pancreatic β-cells (Gerdes et al. 2014). Since the *Bbs4*$^{-/-}$ mouse model is a global knock-out, it is possible that the lack of *Bbs4* in other organs and tissues also leads

to phenotypes that interfere with glucose handling and metabolism. In humans, around 70-75% glucose is taken up by skeletal muscle related to insulin stimulation within hyperinsulinemic clamp studies (DeFronzo et al. 1981; Shulman et al. 1990). Therefore, this organ is responsible for the majority of glucose absorption and glucose storage as muscle glycogen (Kelley et al. 1988). In diabetes patients, skeletal muscle shows several phenotypes including fiber type shift, atrophy, reduced strength, accumulation of fat and reduced capillarization. This combination of characteristics is referred to as “diabetic muscle” (Andersen, Gjerstad, and Jakobsen 2004; Hilton et al. 2008; Marin et al. 1994; Nielsen et al. 2010; Park et al. 2006; Prior et al. 2009). In this context, reduced skeletal muscle differentiation efficiency has been described for diabetic *ob/ob* and *db/db* mice (Nguyen, Cheng, and Koh 2011). Skeletal muscle fiber precursors (called satellite cells, SC) are ciliated and ablation of primary cilia affects differentiation efficiency into multinucleated myofibers (Fu et al. 2014). Based on this evidence, I aimed to investigate the role of the BBSome protein Bbs4 and the anterograde transport protein Ift88 in skeletal muscle function.

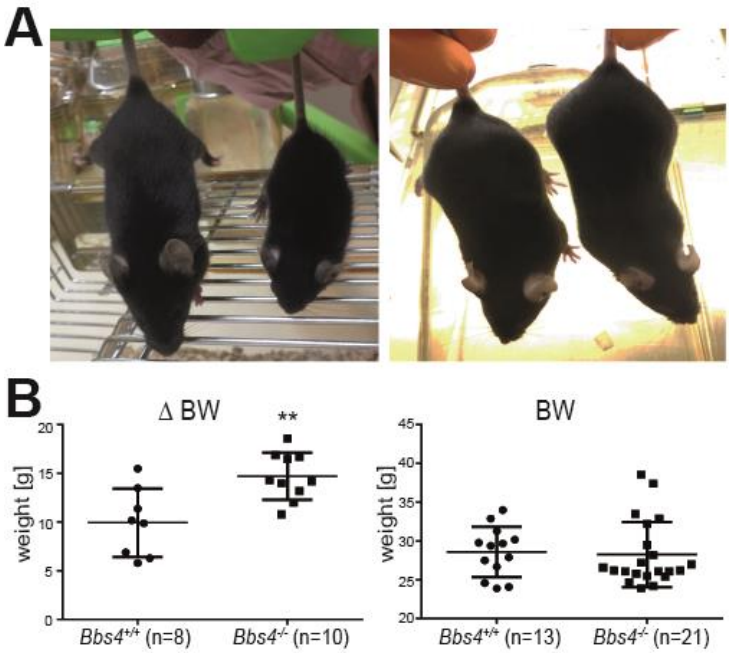

Figure 1: Mouse line characterization showed increased body weight gain of *Bbs4*$^{-/-}$ mice after birth. (A) *Bbs4*$^{+/+}$ (left mouse on both pictures) and *Bbs4*$^{-/-}$ (right mouse on both pictures) littermates. Same mice 3 weeks old (left image) and 14 weeks old (right image). (B) Body weight (BW) gain between 4 and 14 weeks showed increased weight gain of *Bbs4*$^{-/-}$ mice (p=0.003). In comparison, 14 weeks old animals exhibited the same body weight.

5.1.1 *Bbs4*$^{-/-}$ mice showed decreased skeletal muscle strength

In order to characterize skeletal muscle of *Bbs4*$^{-/-}$ mice compared to *Bbs4*$^{+/+}$ controls, I

measured lean mass and fat mass of these animals using NMR analysis. Aberrant results could indicate muscle mass loss or fat accumulation in these mice. Comparable results were obtained by comparing the body composition of 14 weeks old mice having the same body weight, since *Bbs4*$^{-/-}$ are runted after birth and become obese during adulthood. The absolute fat mass of *Bbs4*$^{-/-}$ mice was significantly enhanced compared to *Bbs4*$^{+/+}$ mice (*Bbs4*$^{+/+}$=2.09 g, *Bbs4*$^{-/-}$=5.32 g), whereas lean mass was significantly decreased (*Bbs4*$^{+/+}$=24.52 g, *Bbs4*$^{-/-}$ =21.45 g). Consequently, the ratio of lean to fat mass was significantly decreased in *Bbs4*$^{-/-}$ mice (*Bbs4*$^{+/+}$=14.27, *Bbs4*$^{-/-}$=4.76). Relative to the body weight, *Bbs4*$^{-/-}$ mice showed increased fat mass (*Bbs4*$^{+/+}$=0.07, *Bbs4*$^{-/-}$=0.18) and significantly decreased lean mass (*Bbs4*$^{+/+}$=0.86; *Bbs4*$^{-/-}$=0.77) (**Figure 2**).

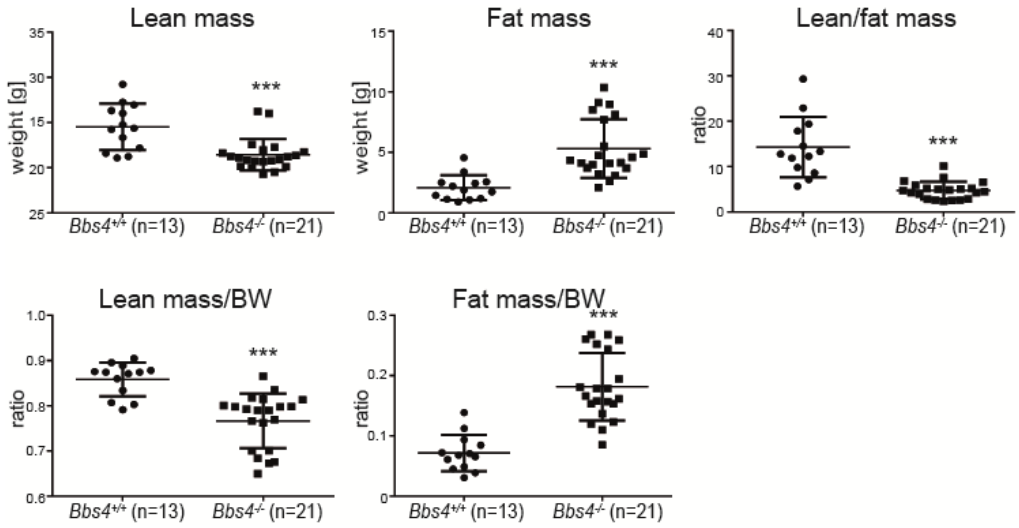

Figure 2: Absolute body composition measurements and ratios of 14-week-old *Bbs4*$^{-/-}$ mice by NMR analysis. Significant decrease of absolute lean mass (p≤0.001) and increase of absolute fat mass in *Bbs4*$^{-/-}$ compared to *Bbs4*$^{+/+}$ controls. Ratio of lean/fat mass (p≤0.001) and lean mass to body weight (p≤0.001) are significantly decreased (p≤0.001), whereas fat mass to body weight ratio is increased (p≤0.001) in *Bbs4*$^{-/-}$ animals.

To investigate whether skeletal muscle function is affected, I measured grip strength of the front legs of 14-week-old *Bbs4*$^{-/-}$ mice using a grip strength meter. Mice were placed with their front legs above a metal grid attached to the grip strength meter and were allowed to hold the grid. In a fast-horizontal movement, mice were pulled away from the grid. The maximum force exerted before the mice released the grip was measured and recorded as absolute grip strength. Absolute grip strength was normalized to body weight and is presented as relative grip strength. *Bbs4*$^{-/-}$ mice had significantly reduced relative grip strength compared to *Bbs4*$^{+/+}$ controls (*Bbs4*$^{+/+}$=5.6, *Bbs4*$^{-/-}$=4.6) (**Figure 3**). Within the cohort of 20 *Bbs4*$^{-/-}$ mice for this

experiment, 5 animals revealed a stronger phenotype, which demonstrated in body weight of at least 35 g. Extrapolation of this group from the cohort showed an even stronger reduction of grip strength in *Bbs4*$^{-/-}$ mice (*Bbs4*$^{+/+}$=5.6, *Bbs4*$^{-/-}$=3.4) with a more prominent phenotype (**Figure 3**). This data shows the first evidence of a skeletal muscle phenotype in *Bbs4*$^{-/-}$ mice.

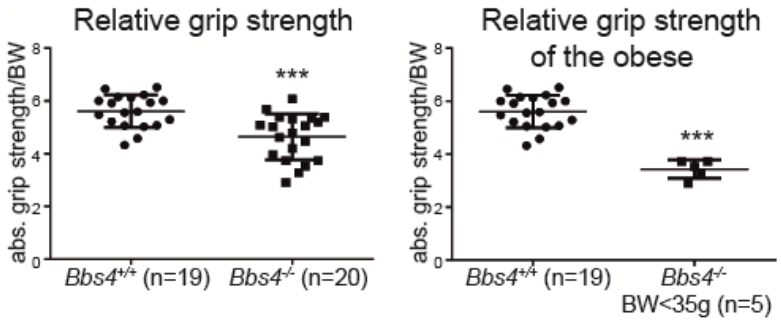

Figure 3: Grip strength measurement of 14-week-old *Bbs4*$^{-/-}$ mice. Relative grip strength of *Bbs4*$^{-/-}$ mice is significantly decreased compared to *Bbs4*$^{+/+}$ controls (p≤0.001). Stratifying by severity of obesity, the effect is greater (p≤0.001).

5.1.2 Generation of an inducible, muscle-specific Ift88 knock-out mouse line

As stated previously, Bbs4 is a basal body-related protein. Because of the finding that Bbs4 loss-of-function is linked to grip strength in mice, I wanted to investigate the role of the primary cilium itself in adult skeletal muscle. Knock-out of the intraflagellar transport protein Ift88 abolishes axonemal assembly. Transport machineries are needed for the translocation of cargo to the cilium or export from the cilium in a retrograde transport process. In order to generate a skeletal muscle specific knock-out mouse line, I used a *HSA-MCM* mouse line generated previously (McCarthy et al. 2012). Here, the promoter of the human α-skeletal actin (*ACTA1*) gene is used to drive skeletal muscle specific expression of a chimeric Cre recombinase. This specific Cre is flanked by mutated estrogen receptor (Mer) binding domains, forming a Mer-Cre-Mer complex (MCM). Further, incorporation of ß-globin intron II (BGI) and poly(A) tail (A) ensures proper splicing and transcript stability. In this mouse model, Cre is constitutively expressed in skeletal muscle. However, restricted to tamoxifen administration, tamoxifen binds Mer and enables its translocation into the nucleus where it mediates site-specific recombination.

I used the *ROSA26*$^{mTmG/mTmG}$ mouse line (Muzumdar et al. 2007) to test efficiency and specificity of Cre induction and Cre-mediated recombination after tamoxifen administration. Therefore, I crossed the *ROSA26*$^{mTmG/mTmG}$ reporter mouse line with *HSA-MCM* mice to obtain an inducible *HSA-MCM;ROSA26*$^{mTmG/mTmG}$ mouse line (**Schematic 9A)**. Without induction, the fluorescent protein *membranous Tomato* is expressed. Tamoxifen binds the recombinant Mer

proteins, which initiates the transport of the MCM complex into the nucleus, where Cre acts as a recombinase (**Schematic 9B**). Recombination between the LoxP sites deletes the *membranous Tomato* signal and allows expression of *membranous GFP* (green fluorescent protein). Between postnatal day 25 and 35 mice of both lines were induced with tamoxifen or corn oil as a control, through oral gavage for 5 consecutive days.

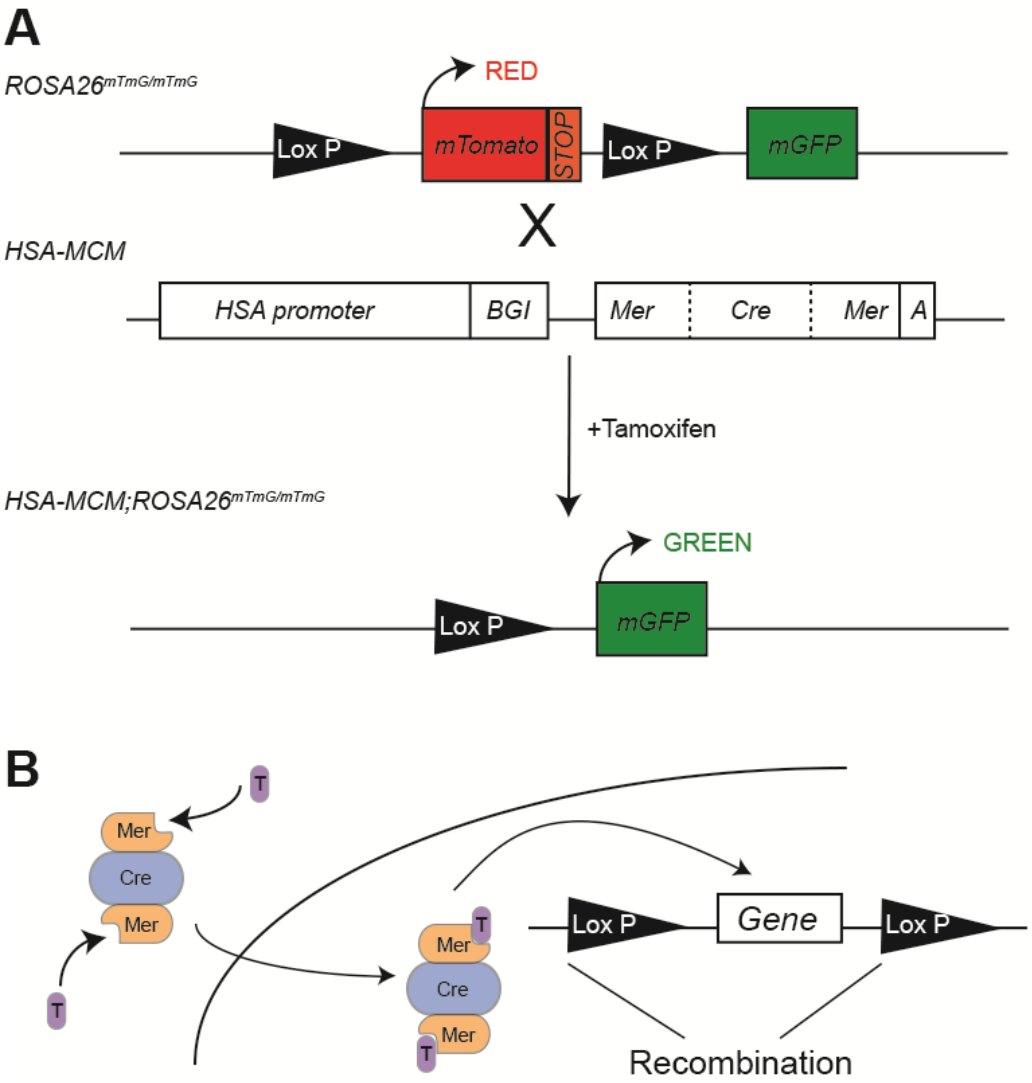

Schematic 9: *HSA-MCM;ROSA26*$^{mTmG/mTmG}$ reporter mouse line breeding and induction. (A) Crossing of the *ROSA26*$^{mTmG/mTmG}$ line with the *HSA-MCM* mouse line. All cells of *HSA-MCM;ROSA26*$^{mTmG/mTmG}$ line express membranous Tomato (red signal). After tamoxifen induction and skeletal-muscle-specific Cre-mediated recombination of mTomato the expression of membranous GFP (green signal) is induced. HSA=human α-skeletal actin, Mer=mutated estrogen receptor, BGI=beta globin intron II. (B) Illustration showing tamoxifen-induced translocation of the Mer-Cre-Mer complex into the nucleus. Nuclear Cre induces recombination between the LoxP sites.

Four weeks after induction of *HSA-MCM;ROSA26*$^{mTmG/mTmG}$ mice, I could detect green signal of membranous GFP restricted to skeletal muscle of tamoxifen induced mice. Membranous Tomato signal, but no GFP signal could be detected in skeletal muscle, cardiac muscle and two examples for smooth muscle tissue of control mice, as well as cardiac and smooth muscle of tamoxifen-treated mice (**Figure 4**). This observation leads to the conclusion that Cre is not active without induction and the *HSA-MCM* promoter activity is restricted to skeletal muscle. Moreover, since no red (mTomato) muscle fibers could be detected within the tamoxifen induced group, induction efficiency was high.

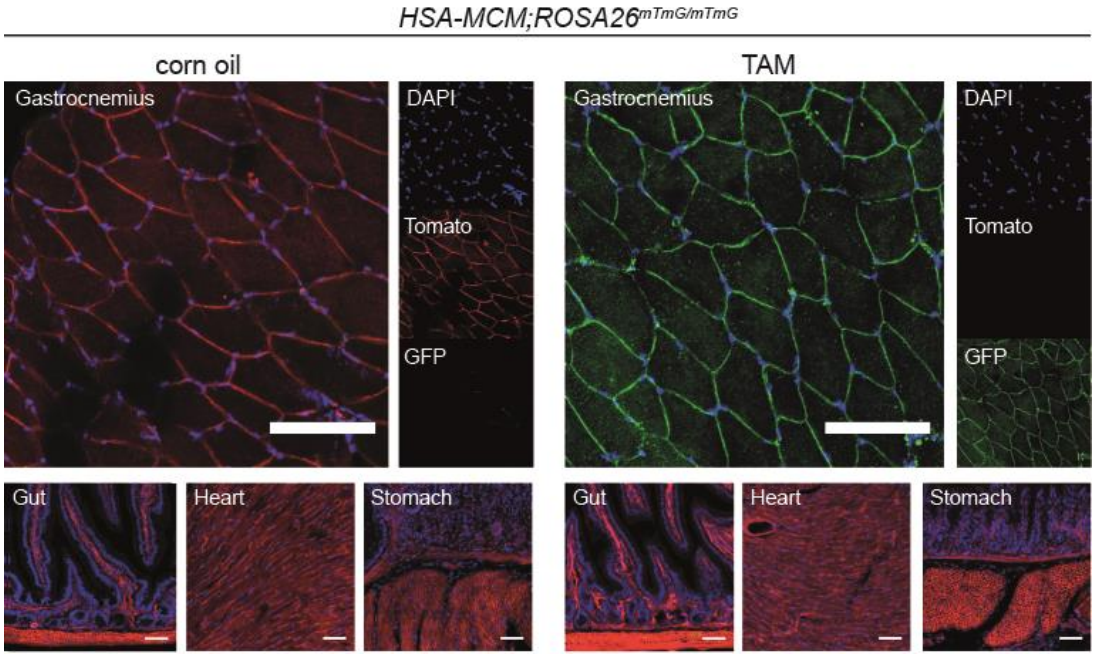

Figure 4: Tamoxifen induced Cre expression and tissue-restriction of *HSA-MCM;ROSA26*$^{mTmG/mTmG}$ reporter mice. Representative immunostaining images of Gastrocnemius muscle (up), cardiac and smooth muscle tissue (down: gut, heart and stomach) cryosections of *HSA-MCM;ROSA26*$^{mTmG/mTmG}$ mice four weeks after induction with tamoxifen (TAM) or corn oil as control. n=3. Scale bar=100 µm.

To investigate the role of cilia-related Ift88 protein in differentiated skeletal muscle fibers, I generated a skeletal-muscle-specific (McCarthy et al. 2012), inducible *Ift88*$^{flox/flox}$ (Haycraft et al. 2007) knock-out mouse line, named *HSA-MCM;Ift88*$^{flox/flox}$ (**Schematic 10**). Two and four weeks after induction, *HSA-MCM;Ift88*$^{flox/flox}$ mice were weighed in order to compare body weight gain of the tamoxifen-induced and control group. Four weeks after induction, body composition was determined and grip strength was tested as described before for *Bbs4*$^{-/-}$ mice (**Figure 5A**). To confirm tissue-specific and inducible Cre-mediated recombination of *Ift88*$^{flox/flox}$, samples of Gastrocnemius and heart muscle were lysed and DNA was extracted.

Using the genotyping-PCR protocol for *Ift88*$^{flox/flox}$, signals specific for floxed-alleles (370 bp) were detected in tissues induced with tamoxifen or corn oil. After administration of tamoxifen and Cre-mediated *Ift88*$^{flox/flox}$ recombination a Δ-signal (270 bp, *Ift88*$^{\Delta/\Delta}$) was exclusively detected in skeletal muscle (**Figure 5B**). Signal strength was reduced, because skeletal muscle lysates also include immune-cells, vessels and a variety of other cells than muscle cells that are present in skeletal muscle tissue. These cells do not respond to the tamoxifen induced recombination of *Ift88*$^{flox/flox}$, therefore giving an *Ift88*$^{flox/flox}$ background signal.

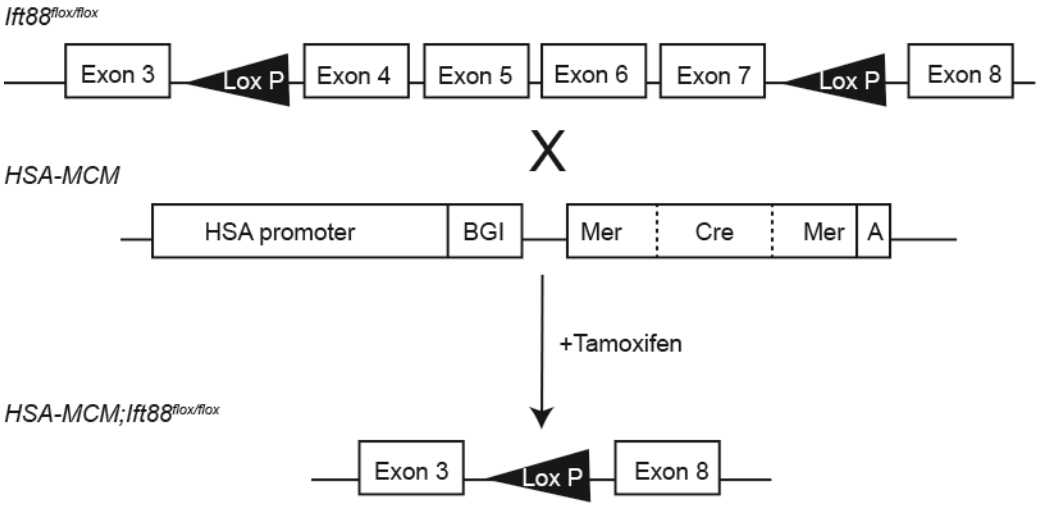

Schematic 10: Illustration of generating the *HSA-MCM;Ift88*$^{flox/flox}$ mouse line. *Ift88*$^{flox/flox}$ mice with LoxP flanking Exons 4 to 7 were crossed with *HSA-MCM* mice, which express Cre under the human α-skeletal actin (HSA) skeletal-muscle-specific promoter. Tamoxifen administration induces Cre-mediated recombination between the LoxP sites in the *HSA-MCM;Ift88*$^{flox/flox}$ mouse line. Mer=mutated estrogen receptor, BGI=beta globin intron II, A=poly (A) tail.

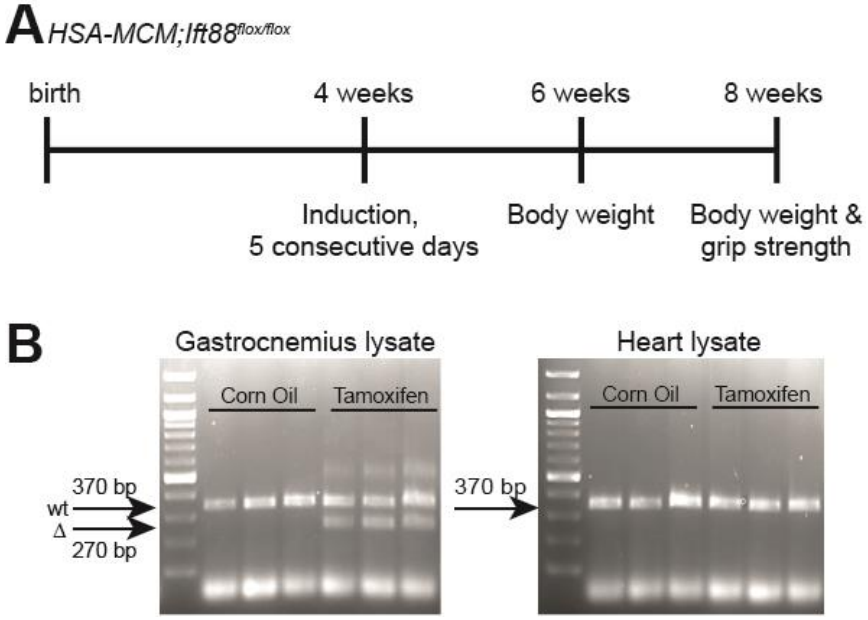

Figure 5: Time line and skeletal muscle-specific induction of *HSA-MCM;Ift88*$^{flox/flox}$ mice. (A) Timeline of experiment. (B) Gastrocnemius and heart muscle lysate showing floxed wildtype (wt) alleles in both tissues (370 bp), but tamoxifen-specific induction of recombination is restricted to skeletal muscle by detection of Δ-signal (270 bp). n=3.

5.1.3 Ciliary impairment does not induce intramuscular fat accumulation

I did not detect altered body weight gain or absolute body weight between the control (corn oil) and tamoxifen-treated group within four weeks after induction. Tamoxifen induced *HSA-MCM;Ift88*$^{flox/flox}$ mice had significantly increased absolute fat mass (corn oil=1.47 g, TAM=1.82 g), as well as fat to body weight ratio (corn oil=0.0602, TAM=0.0752). Lean to fat mass ratio was significantly increased (corn oil=15.98, TAM=11.89), but I did not detect a difference in absolute lean mass between the two groups (**Figure 6A**). I tested grip strength as described for *Bbs4*$^{-/-}$ mice 4 weeks after *HSA-MCM;Ift88*$^{flox/flox}$ mice induction. There was no difference in relative grip strength (**Figure 6B**) and therefore I concluded that there is no skeletal muscle phenotype in tamoxifen-induced *HSA-MCM;Ift88*$^{flox/flox}$, as detected in *Bbs4*$^{-/-}$ mice.

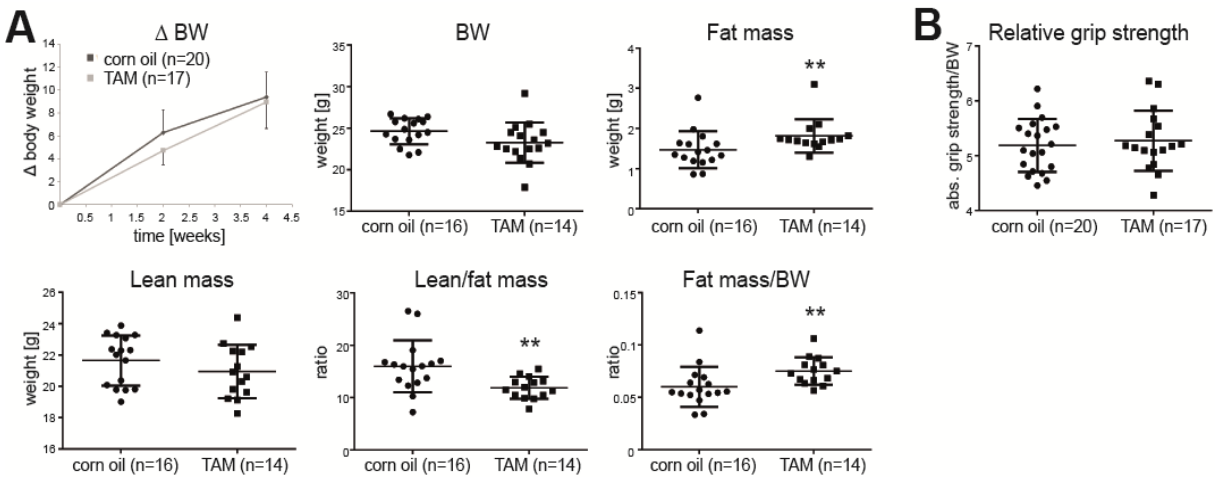

Figure 6: Body composition and grip strength phenotype does not indicate alterations in skeletal muscle of *HSA-MCM;Ift88*$^{flox/flox}$ mice 4 weeks after induction. (A) Absolute body composition measurements by NMR analysis and ratios. No significant difference in body weight gain, absolute body weight and absolute lean mass of the induced or control group. Absolute fat mass (p=0.006), lean/fat mass ratio (p=0.005) and fat/body mass ratio (p=0.004) differ significantly from control group. (B) Relative grip strength does not differ significantly.

I detected an increased fat mass in both cilia-related knock-out mouse lines (*Bbs4*$^{-/-}$ and *HSA-MCM;Ift88*$^{flox/flox}$). Since NMR analysis does not give information about the distribution of fat in the body, I used Oil Red-O staining to test for an accumulation of intramuscular fat. Therefore, cryosections of fresh frozen Gastrocnemius were histochemically treated with fresh dissolved Oil Red-O, which stains triglycerides and lipids. Comparing the intensity and distribution of Oil Red-O staining, there is no accumulation of fat in tamoxifen induced *HSA-MCM;Ift88*$^{flox/flox}$ or *Bbs4*$^{-/-}$ compared to control groups (**Figure 7A and B**).

Skeletal muscle progenitor cells have been shown to differentiate into brown adipocytes during embryogenesis and adulthood (Yin et al. 2013). A critical transcriptional cofactor for differentiation of SC into brown adipocytes is Prdm16 (PR domain containing 16). I compared mRNA levels of *Prdm16* in EDL and Soleus of 14-week-old *Bbs4*$^{-/-}$ and *Bbs4*$^{+/+}$ mice to check if *Bbs4* loss-of-function leads to brown adipogenesis in skeletal muscle. I could not detect aberrant browning marker expression in both muscles (**Figure 7C**). Taking together data of Oil Red-O staining and *Prdm16* expression, I concluded that there is no accumulation of adipocytes in *Bbs4*$^{-/-}$ and induced *HSA-MCM;Ift88*$^{flox/flox}$ skeletal muscle or brown fat in *Bbs4*$^{-/-}$ skeletal muscle before onset of obesity. The increased mass of fat, therefore, has to be localized somewhere else in the body, e.g. subcutaneous, abdominal or in the liver and has to be further investigated.

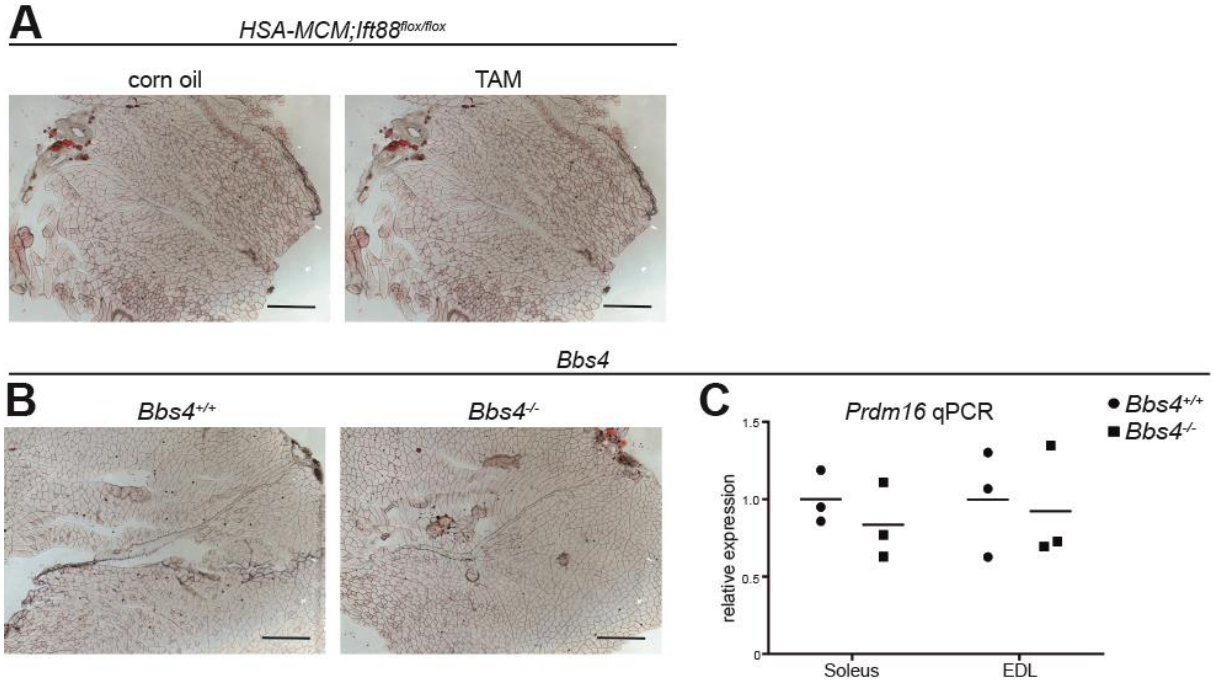

Figure 7: Loss of ciliary function does not initiate intramuscular adipogenesis. Histochemical Oil Red-O staining of Gastrocnemius muscle from (A) *HSA-MCM;Ift88*$^{flox/flox}$ and (B) *Bbs4*$^{-/-}$ mice. n=3. (C) EDL and Soleus muscle of *Bbs4*$^{+/+}$ and *Bbs4*$^{-/-}$ do not show difference in *Prdm16* mRNA levels. n=3.

5.1.4 *Bbs4*$^{-/-}$ skeletal muscle does not exhibit changes in fiber type composition, atrophy or dystrophy

Bbs4$^{-/-}$ mice showed decreased lean mass and grip strength performance than *Bbs4*$^{+/+}$ controls. One possible reason for muscle weakness could be due to shifts in fiber type composition. Skeletal muscle fibers can be divided into fast and slow twitch, based on the differential expression of myosin heavy chains, which goes in hand with differences in fiber metabolism. Slow twitch muscles use free fatty acids and triglycerides for oxidative ATP generation. On the other hand, fast twitch fibers utilize glucose for ATP synthesis. Based on the myosin heavy chain staining we can differentiate four kinds of fibers. (1) Type I fibers are slow twitch and rich in mitochondria. (2) Type IIa fibers are called intermediate, because they show characteristics in-between Type I and (3) Type IIb / IIx, which are the glycolytic fast twitch fibers. (4) Hybrid fibers express at least two types of myosin heavy chain. These hybrids can either be a normal phenotype of the muscle or an indication for fiber type transition, which occurs when fibers change from one type to another one. This occurs in order to adapt to new environmental and metabolic conditions (Pette and Staron 2000; Sher and Cardasis 1976). For example, insulin resistant skeletal muscle of diabetic patients is characterized by shift to fewer Type I and more Type II fibers (Gaster et al. 2001; Hickey et al. 1995; Oberbach et al. 2006). To characterize fiber type composition of oxidative Soleus and glycolytic EDL muscle

of *Bbs4*$^{-/-}$ and control mice, I stained fresh frozen cryosections of 14-week-old male mice for myosin heavy chain types I, IIa and IIb. Remaining unstained fibers were considered as IIx (**Figure 8A**). Based on immunostainings, I counted the number of fiber types per muscle section. I did not detect changes in fiber type composition in these muscles (**Figure 8B**). Therefore, there is no indication that reduced grip strength in *Bbs4*$^{-/-}$ mice is linked to a shift in fiber type composition.

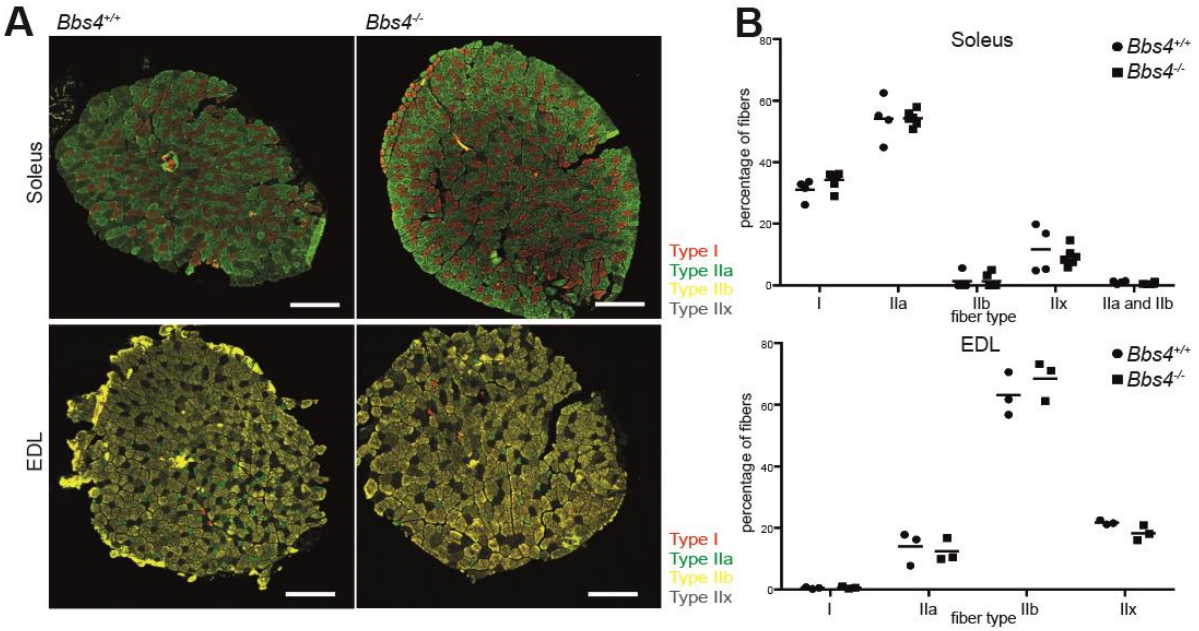

Figure 8: Soleus and EDL fiber type composition of *Bbs4*$^{-/-}$ mice. (A) Representative image of Soleus and EDL cross sections. Fiber types were detected based on immunostaining of differentially expressed myosin heavy chains (slow fibers (Type I, red) intermediate fibers (Type IIa, green) and fast fibers (Type IIb, yellow and Type IIx, not stained)). Scale bar=300 µm. (B) Fiber types were counted and illustrated as percentage of all fibers.

The observed reduction in lean muscle mass in *Bbs4*$^{-/-}$ mice could be caused by a lack of proper muscle development or loss of muscle mass. Two common markers for muscle atrophy are the muscle specific E3 ubiquitin ligases Murf-1 and Fbx-32. I investigated the abundance of both proteins in Soleus and EDL muscle lysates using Western Blot analysis. There was no significant increase in the E3 ubiquitin ligases compared to control, that could indicate skeletal muscle atrophy (**Figure 9A and B**).

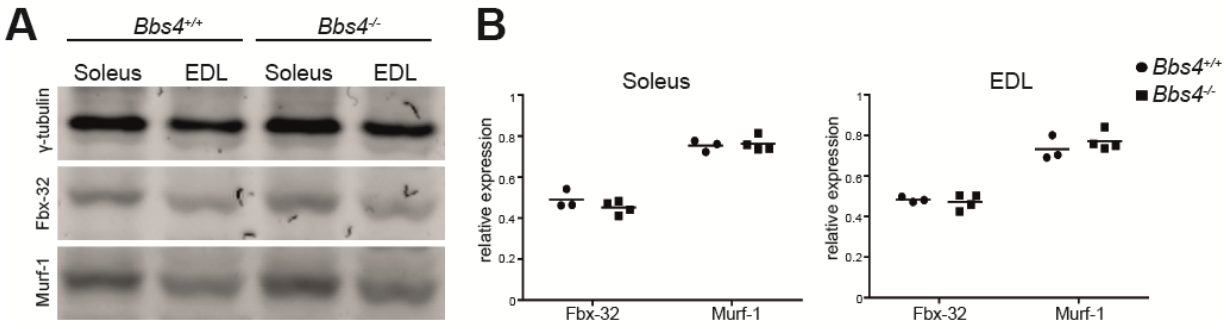

Figure 9: Western Blot and quantification of atrophy marker in *Bbs4*$^{-/-}$ mice. (A) Western Blot of Fbx-32 and Murf-1 in *Bbs4*$^{-/-}$ and *Bbs4*$^{+/+}$ Soleus and EDL. (B) Quantification of Western Blot results.

Besides atrophy, another form of muscle mass wasting is dystrophy, which is based on dysfunctionality of dystrophin or proteins of the dystroglycan complex (DGC). Changes in NMJ morphology have been considered as a common complication in dystrophy. Such changes are aberrant acetylcholine fragmentation in the presynaptic membrane or clustering of the acetylcholine receptor in the postsynaptic membrane (Lyons and Slater 1991). To characterize NMJ of *Bbs4*$^{-/-}$ mice, I used fluorescently labelled α-bungarotoxin, which has high affinity to nicotinic acetylcholine receptor on floating skeletal muscle sections (Balass, Katchalski-Katzir, and Fuchs 1997). Further, I used antibodies against neurofilament and synaptophysin to visualize neurons and acetylcholine vesicles in the presynaptic membrane. Using IMARIS software I calculated and compared the volume of bungarotoxin staining as well as the number of branch points and terminal points of the structure based on immunostainings. I could not detect a significant change in the criteria for dystrophy-related NMJ morphology (**Figure 10A**). Moreover, I compared paxillin abundance, a protein associated with the integrin α7β1 based myotendinous junction (MTJ) complex, which was found upregulated in skeletal muscle of the dystrophy mouse lines *mdx* and *γ*SG$^{-/-}$ (Sen et al. 2011). Therefore, paxillin abundance was compared in *Bbs4*$^{-/-}$ and *Bbs4*$^{+/+}$ Soleus and EDL muscle. Western Blot quantification gave no evidence for upregulation of paxillin (**Figure 10B**). Taken together with data from NMJ analysis, there is no evidence for dystrophy in *Bbs4*$^{-/-}$ mice.

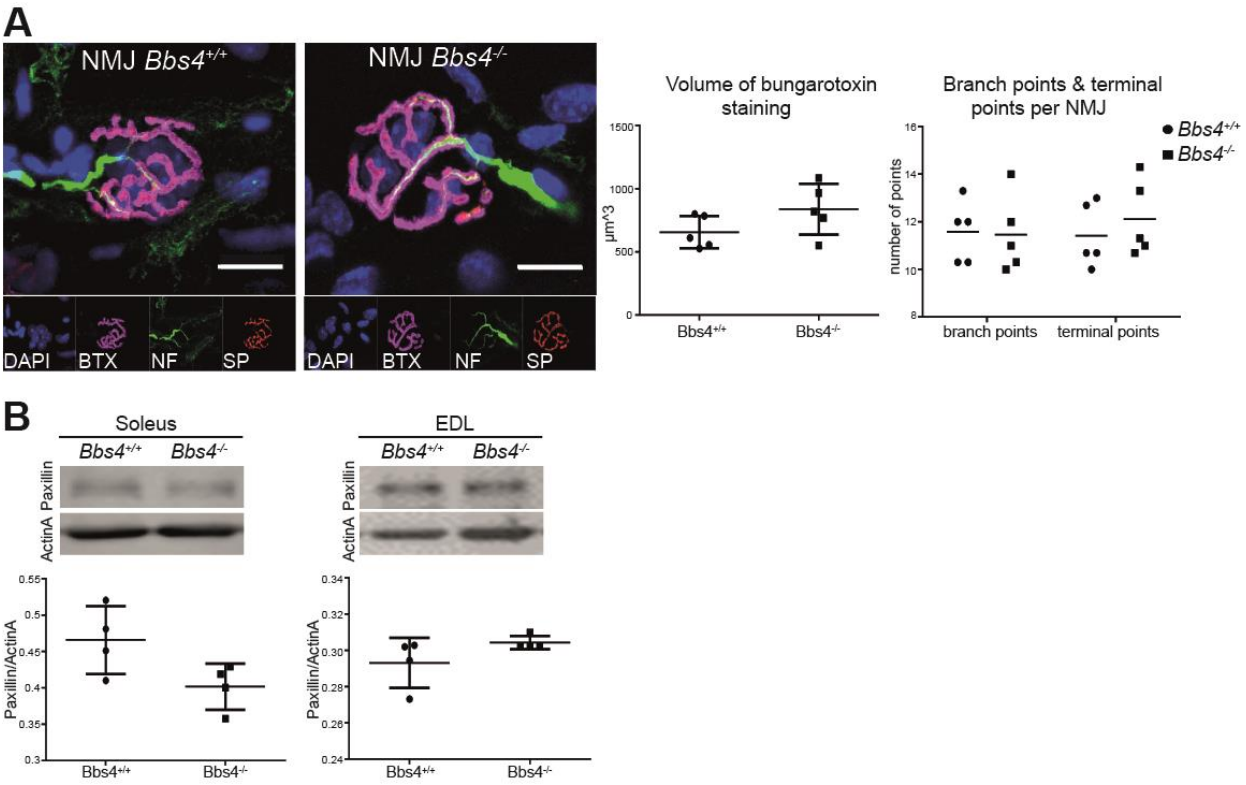

Figure 10: NMJ and MTJ in *Bbs4*$^{-/-}$ mice. (A) Representative confocal maximum projections of NMJ. Immunochemical staining for DAPI (blue), neurofilament (green, NF), synaptophysin (red, SP, presynaptic vesicular acetylcholine) and fluorescently labelled α-bungarotoxin (pink, BTX) are indicated. Scale bar=10 µm. Quantification of α-bungarotoxin volume, branch points and terminal points. (B) Paxillin protein abundance and quantification in Soleus and EDL muscles.

5.2 Differential gene expression in *Bbs4*$^{-/-}$ and *Bbs4*$^{+/+}$ mice

As stated in the introduction, Bbs4 is involved in protein trafficking (Leitch et al. 2014; Starks et al. 2015). Therefore, abolishment of Bbs4 from the cell can interfere with activation and signal transduction of signaling pathways. For example, loss of *Bbs4* has been shown to reduce leptin receptor signaling in the hypothalamus (Seo et al. 2009). Further, reduced expression of follistatin-like 1 (FSTL1) in 3T3-L1 adipocytes lacking Bbs4 has been detected (Prieto-Echagüe et al. 2017), indicating an involvement in gene expression. Here, I wanted to investigate the effect of *Bbs4* abolishment on the gene expression in skeletal muscles. **Figure 11** illustrates the principal component analysis of EDL and Soleus muscle from RNA-Seq results. Within these two examples for glycolytic and oxidative skeletal muscle, 88% of genes are expressed differentially (PC1). Within the further sections, I took a closer look on the genes differentially expressed between *Bbs4*$^{-/-}$ and *Bbs4*$^{+/+}$ muscles.

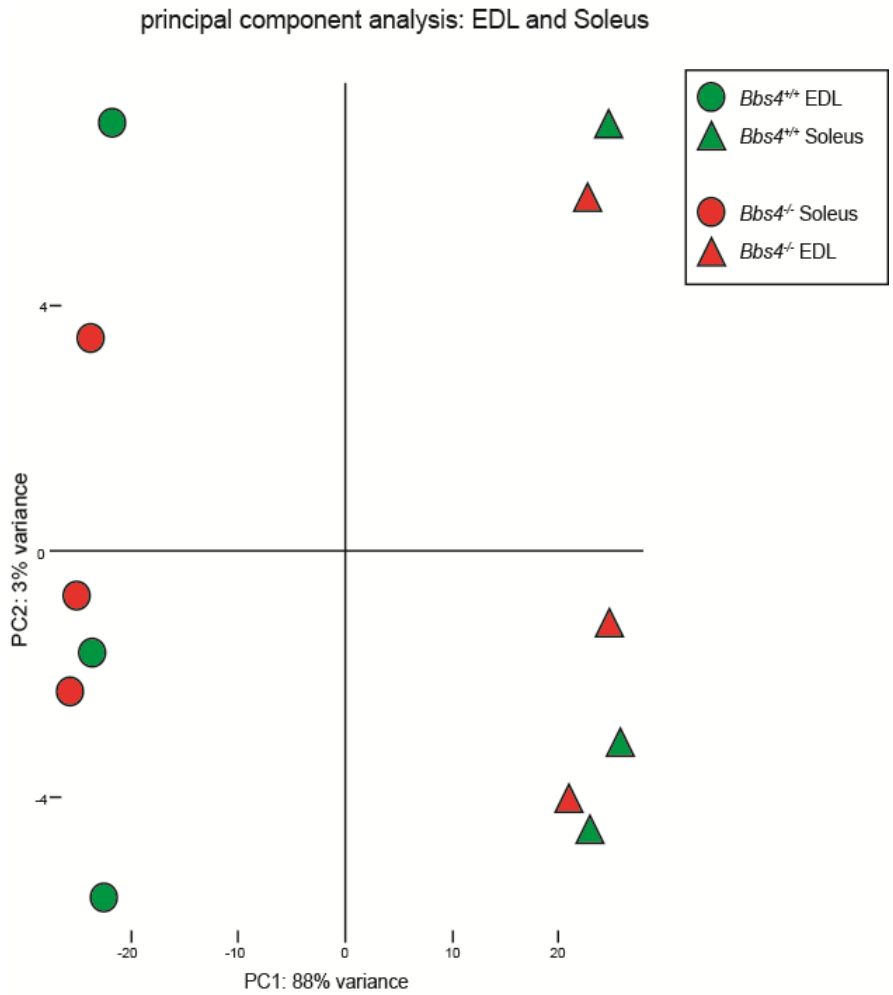

Figure 11: Principal component analysis of EDL and Soleus RNA-Seq results. PC1 illustrates 88% variance in gene expression between glycolytic EDL and oxidative Soleus muscles.

5.2.1 Characterization of *Bbs4*$^{-/-}$ Soleus based on RNA-Seq candidate genes

I performed RNA-Seq analysis on oxidative Soleus muscles to characterize skeletal muscle gene expression of *Bbs4*$^{-/-}$ and control mice. I did not observe genotype-dependent effects in PCA (**Figure 12**). Most of the variance was explained by batch effects so that litter mates cluster together. I cannot exclude a contribution of sample preparation at this point, but all samples were processed at the same time. **Figure 13** illustrates the top 30 deregulated genes in Soleus muscle of *Bbs4*$^{-/-}$ mice.

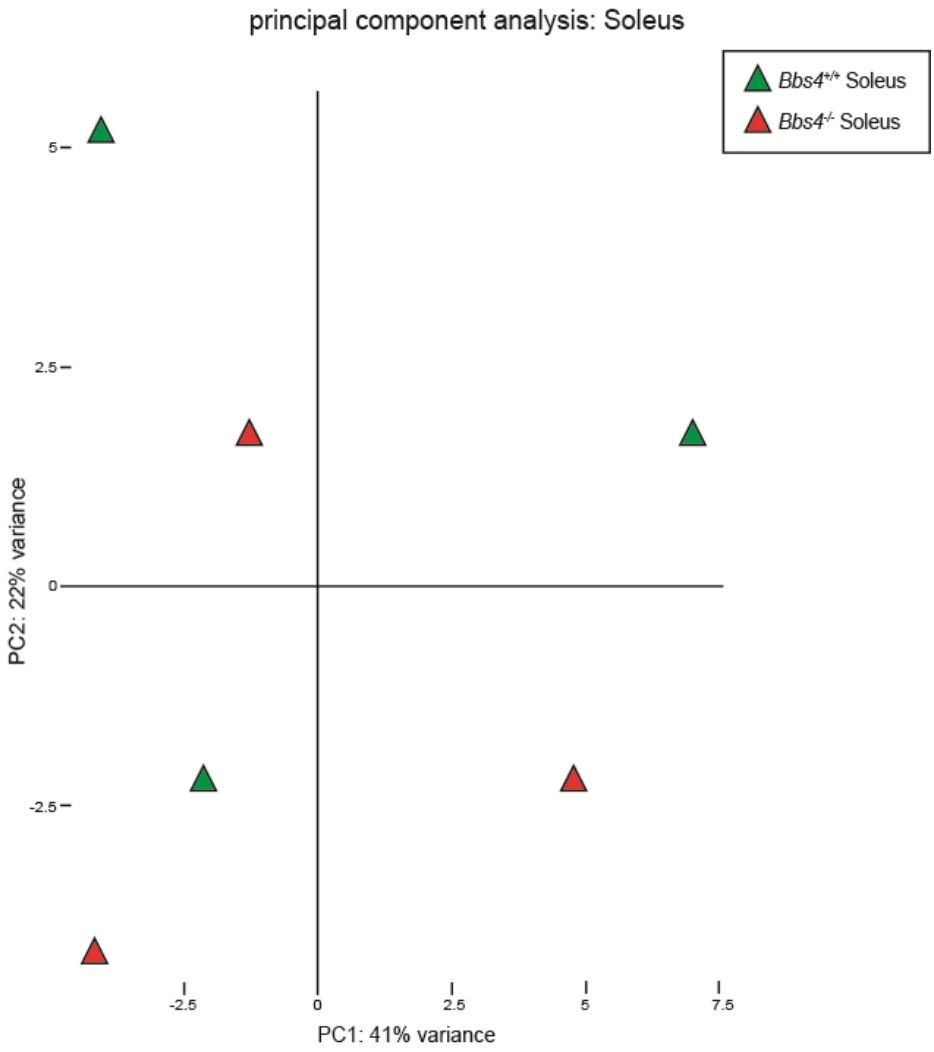

Figure 12: Principal component analysis of *Bbs4*$^{-/-}$ and *Bbs4*$^{+/+}$ Soleus. PC1 and PC2 illustrate no clusters of *Bbs4*$^{-/-}$ and *Bbs4*$^{+/+}$ muscles. n=3.

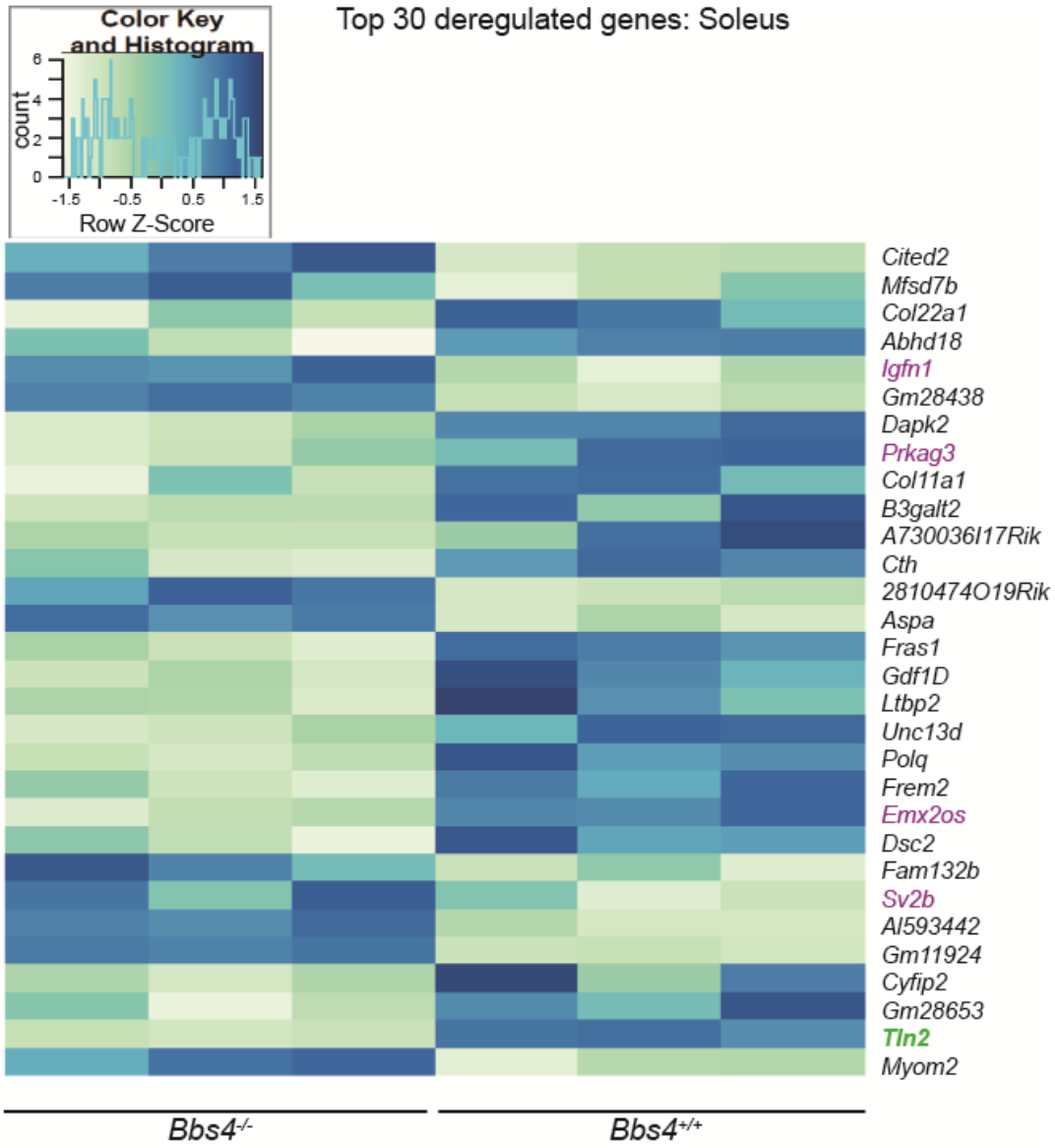

Figure 13: Top 30 deregulated genes of Soleus in 14-week-old *Bbs4*$^{-/-}$ mice. Indicated by colors: Tln2 (green) and structural as well as regeneration-related proteins (purple). n=3.

I tried to confirm deregulated expression of interesting candidate genes by real-time qPCR. *Igfn1* (*Immunoglobulin-like and fibronectin type III domain containing 1*) and *Tln2* (*Talin2*) are skeletal muscle structural proteins. *Prkag3* (*Protein kinase AMP-regulated gamma 3*) is involved in the regulation of energy metabolism. Further, *Emx2* (*Empty-spiracles homeobox 2*) and *Sv2b* (*Synaptic vesicle protein 2b*) have been shown involved in the regeneration of skeletal muscle. *Emx2* has been shown upregulated after muscle injury (Musaro et al. 2004), and *Sv2b* expression has been shown upregulated in *Mrf4* (*Muscle regulatory factor 4*, a myogenic marker) deficient mice (Clark, Law and Hong 2015).

Real-time qPCR using a Bbs4 probe showed efficient *Bbs4* knock-out in Soleus (99.8% reduction). However, I could not confirm deregulation of RNA-Seq candidate genes, except *Tln2* (**Figure 14**). This structural protein is shown downregulated in RNA-Seq and real-time qPCR (30% reduction). Tln2 has been shown to play also an important role in myoblast fusion (Conti et al. 2009), indicating a regenerative defect of *Bbs4*$^{-/-}$ Soleus. Most of the qPCR candidates show a big deviation of expression within the *Bbs4*$^{-/-}$ or *Bbs4*$^{+/+}$ groups. Specificity of the used qPCR probes could influence the result. Certain splice isoforms of the transcript might not be recognized by the qPCR probe, leading to aberrant data to RNA-Seq results.

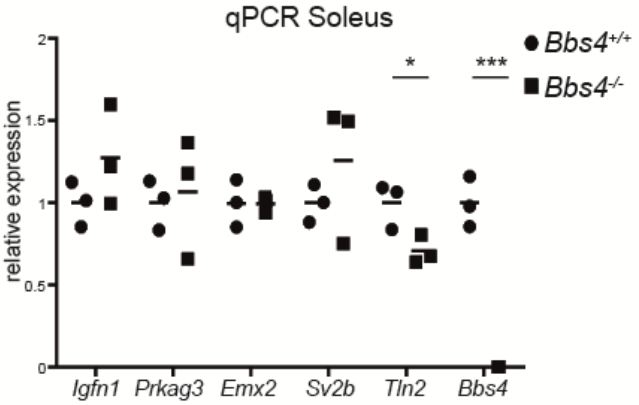

Figure 14: Real time qPCR results of candidate genes in *Bbs4*$^{-/-}$ Soleus. No significant difference in the expression of *Igfn1*, *Prkag3*, *Emx2* and *Sv2b* was detected. *Tln2* (p=0.037) and *Bbs4* (p<0.001) expression is significantly reduced in *Bbs4*$^{-/-}$ Soleus.

5.2.2 Characterization of *Bbs4*$^{-/-}$ EDL based on RNA-Seq candidate genes

As described for Soleus muscle, RNA-Seq was performed with EDL muscle of *Bbs4*$^{-/-}$ and *Bbs4*$^{+/+}$ mice. Principal component analysis of the RNA-Seq data in EDL showed less batch effect and therefore variation between the samples than Soleus muscle (**Figure 15**). Here, a separation between the genotypes is possible and the difference in the genotype explains 28% of the variation between *Bbs4*$^{-/-}$ and *Bbs4*$^{+/+}$ mice (PC2). Within the Top 30 deregulated genes, mRNA levels of Notch-signaling-related proteins (*Rcan1* (*Regulator of calcineurin 1), Hipk2* (*Homeodomain interacting protein kinase 2*), *Aph1B* (*Anterior pharynx defective 1 homolog*), *Meg3* (*Maternally expressed 3*) and *Kcng4* (*Potassium voltage-gated channel subfamily 4 member*)) as well as *Tiam1* (*T-lymphoma invasion and metastasis-inducing protein 1*) showed upregulation in glycolytic EDL muscles. Like Soleus, also EDL muscle showed reduced expression of *Tln2* (*Talin-2*) in *Bbs4*$^{-/-}$ compared to *Bbs4*$^{+/+}$ mice (**Figure 16**).

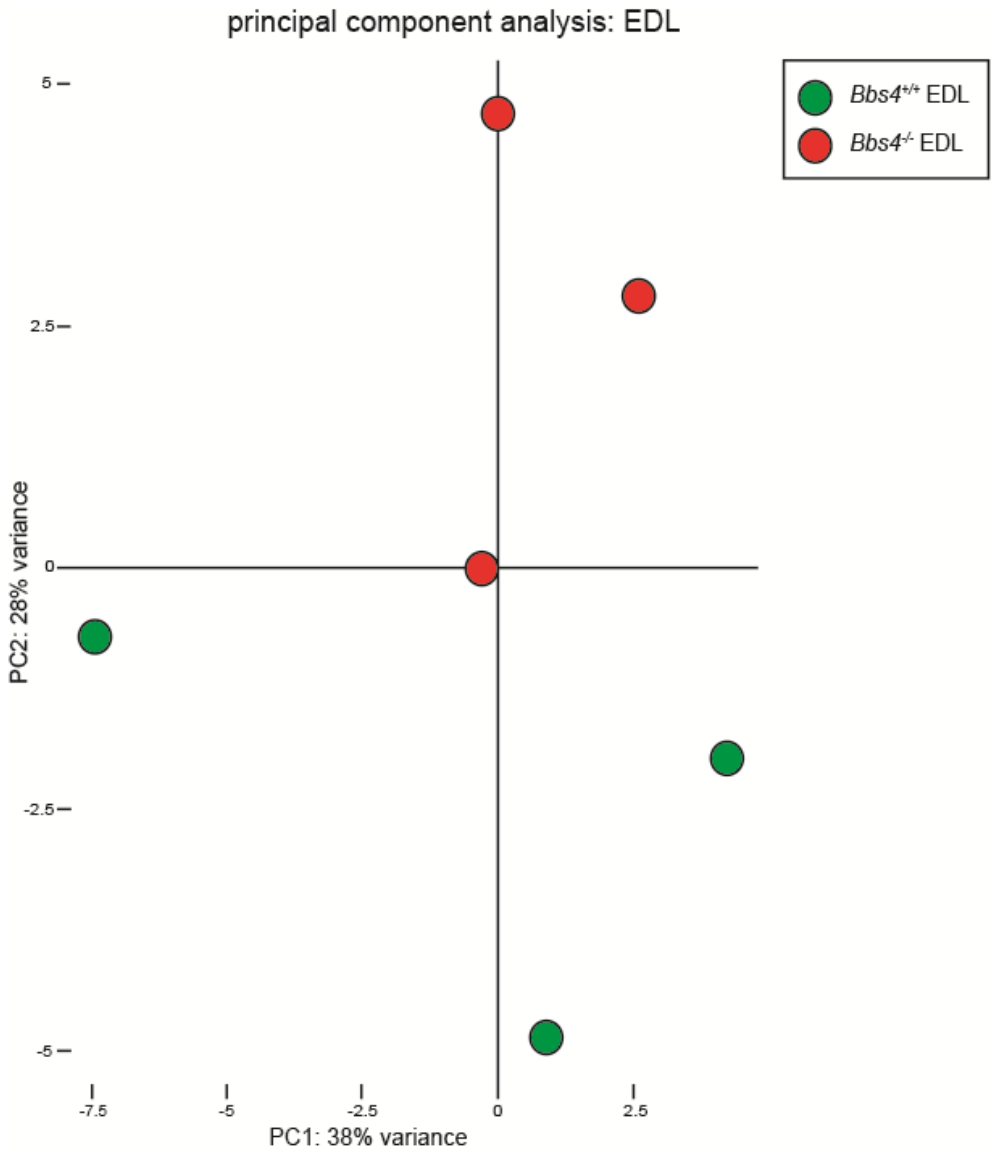

Figure 15: Principal component analysis of *Bbs4*$^{-/-}$ and *Bbs4*$^{+/+}$ EDL RNA-Seq data. Clusters of the genotype illustrate differential gene expression between the genotypes. PC2 demonstrates 28% variance in genes expression of *Bbs4*$^{-/-}$ and control EDL. n=3.

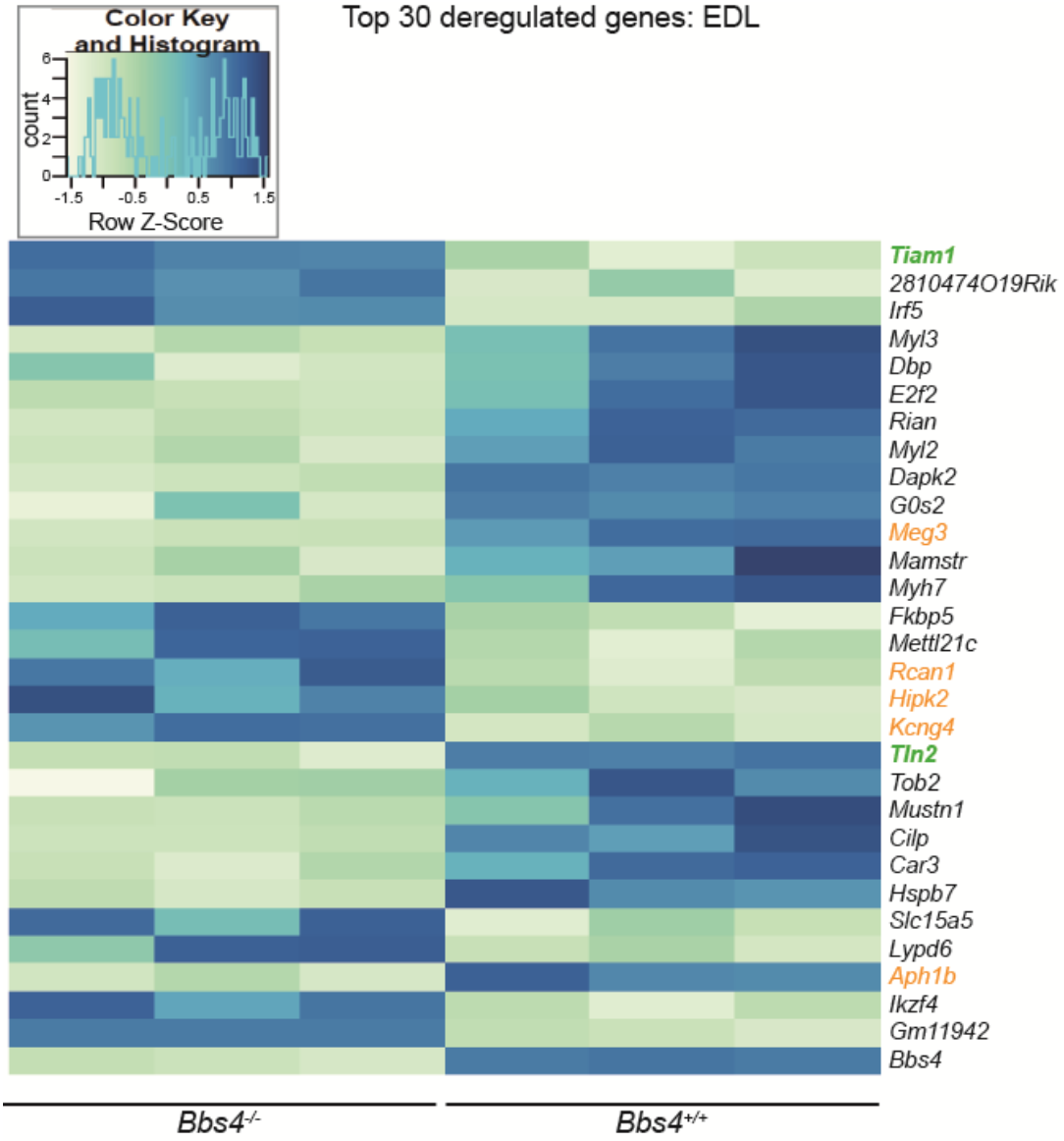

Figure 16: Top 30 deregulated genes of EDL in 14-week-old *Bbs4*$^{-/-}$ mice. Indicated by colors: Tln2 and Tiam1 (green) and genes affected by deregulated Notch signaling (orange). n=3.

To confirm RNA-Seq data, I performed real-time qPCR on mRNA obtained from EDL muscle. Real-time qPCR using a Bbs4 probe showed efficient loss of *Bbs4* mRNA in *Bbs4*$^{-/-}$ EDL (99.9% reduction). Confirming RNA-Seq data, *Tln2* was downregulated also in real-time qPCR (approximately 38% downregulation, **Figure 17A**). Tln2 is involved in muscle differentiation and was found upregulated in C2C12 and primary human myoblasts during myotube formation (Senetar, Moncman, and McCann 2007). In Soleus RNA-Seq and real time qPCR I also could detect downregulation of *Tln2* expression. Therefore, muscle mass loss in *Bbs4*$^{-/-}$ might be a regenerative phenotype. However, by comparing Tln2 expression at the protein levels, I could not detect a significant difference (**Figure 17B**), which could be caused by low specificity of

the antibody (Gilda et al. 2015). In general, Western Blot analysis of skeletal muscle is difficult, since the tissue is hard to lysate, which can keep protein yield low. In addition, since the most abundant muscular proteins are myosin and actin, a high amount of protein lysate has to be loaded and a strongly binding antibody has to be applied to detect the protein of interest.

RNA-Seq data indicated upregulation of *Tiam1* transcripts in EDL muscle. Tiam1 functions as the guanine nucleotide exchange factor (GEF) of Rac1, which is besides Cdc42 and RhoA a member of the Rho-family GTPases. In skeletal muscle, insulin signaling activates Rac1, which promotes actin polymerization that is required for transport of Glut4 vesicles to the membrane (Chiu et al. 2011). Therefore, *Tiam1* deregulation could have effects on muscle glucose metabolism. However, real-time qPCR data indicated significant reduction of approximately 48% *Tiam1* mRNA in *Bbs4*$^{-/-}$ compared to *Bbs4*$^{+/+}$ EDL (**Figure 17A**). Specificity of the used probe could influence the result of real-time qPCR data. Certain splice isoforms of the transcript might not be recognized by the qPCR probe, inducing aberrant data to RNA-Seq results. I could not detect differences of Tiam1 abundance in EDL on the protein level (**Figure 17B**). Discrepancies between gene expression and protein level could be explained by post-transcriptional regulation of the gene of interest. As mentioned above, also the specificity and efficiency of the antibody can alter the readout of protein abundance (Gilda et al. 2015). Taken together, I could not confirm RNA-Seq data of upregulated Tiam1 expression in *Bbs4*$^{-/-}$ mice.

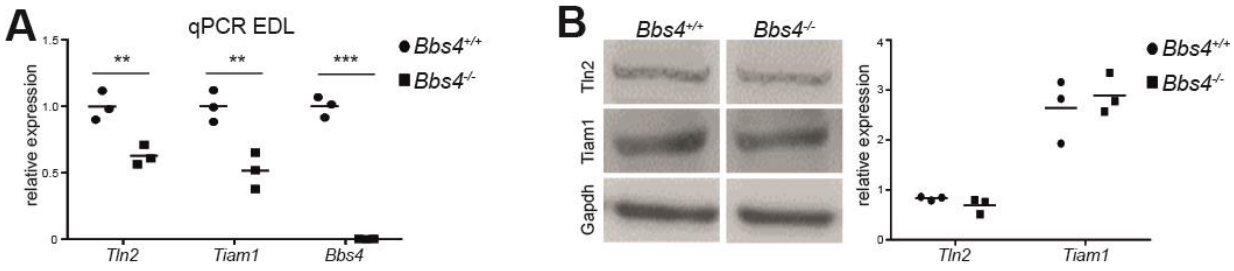

Figure 17: Expression level and protein abundance of Tln2 and Tiam1 in *Bbs4*$^{-/-}$ EDL. (A) relative gene and (B) protein expression experiments on EDL of 14-week-old mice. Significant reduction of Tln2 ($p=0.0085$), Tiam1 ($p=0.01$) and Bbs4 ($p\leq0.001$) mRNA was detected.

Notch signaling regulation is important for proper skeletal muscle differentiation, as described in the introduction. Therefore, detection of differentially expressed Notch-related genes in the RNA-Seq of EDL muscle could indicate a regenerative phenotype, leading to muscle weakness. To confirm RNA-Seq data, real-time qPCR was conducted. Notch-related candidates *Aph1b* and *Hipk2* do not appear expressed differentially between *Bbs4*$^{-/-}$ and

Bbs4$^{+/+}$ EDL. Also results of *Meg3*, *Rcan1*, and *Kcng4* expression does not show statistically significant difference by real-time qPCR analysis (**Figure 18**). Here, as mentioned before, mice within one group show big differences in expression levels. One could assume, that the *Bbs4*$^{+/+}$ outlier with high expression in *Meg3*, *Rcan1*, and *Kcng4* is the same mouse and the sample got contaminated or destroyed. However, the outliers with high *Rcan1* and *Kcng4* expression is the same mouse, while the data point with high *Meg3* expression illustrates another mouse.

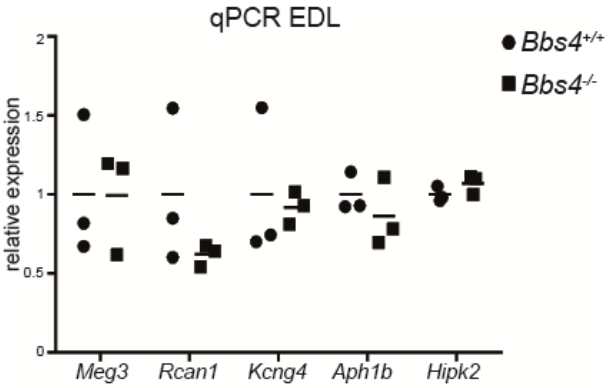

Figure 18: Real time qPCR analysis of *Bbs4*$^{-/-}$ EDL. Expression of Notch-related candidate genes is not significantly different between *Bbs4*$^{-/-}$ and *Bbs4*$^{+/+}$ muscles.

I detected broad deviation in gene expression within the *Bbs4* cohort groups. Therefore, I wanted to investigate if stochastical effects in pathway activation of early embryonal development are altered in *Bbs4*$^{-/-}$ mice. If stochastical effects play a role within this observation, muscles at the end of primary phase (E10.5-E12.5) of muscle generation would show aberrant Notch signaling. During the primary phase, Pax3-positive muscle progenitor cells migrate into the limb buds and fuse to myotubes. Afterwards, a population of Pax3-positive myoblasts starts expressing *Pax7* and downregulates expression of *Pax3*. This is the step towards the secondary phase (E14.5-17.5) of skeletal muscle formation in which Pax7-positive cells fuse to primary fibers and among each other to form secondary fibers (Biressi, Molinaro, and Cossu 2007; Horst et al. 2006; Jostes, Walther, and Gruss 1990). As shown in **Figure 1**, *Bbs4*$^{-/-}$ mice clearly have a phenotype in body size in the first weeks after birth, but I could not see an obvious difference in size at E12.5 (**Figure 19**). The 4 limb buds per embryo at stage E12.5 were removed, pooled and mRNA as well as protein was extracted. I performed real-time qPCR to test expression of Notch signaling related candidate genes and detected significant downregulation (50%) of *Aph1b* mRNA in *Bbs4*$^{-/-}$ limb buds as well efficient downregulation of *Bbs4* (99.96% reduced, **Figure 20A**). Aph1b is one component of the γ-

secretase complex that cleaves the activated Notch-receptor to release Notch-intracellular-domain for further signal transduction. Notch-signaling plays an important role in satellite cell activation and myoblast differentiation. During embryogenesis, high Notch signaling keeps Pax7-positive cells proliferative to expand the cell mass and generate muscle tissue (Mourikis et al. 2012). In contrast, high levels of Notch signaling prevents SC in adult tissue from differentiation (Bjornson et al. 2012; Mourikis, Sambasivan, et al. 2012) to keep a population of cells in a quiescent state (Fujimaki et al. 2018). Myoblast differentiation goes in hand with downregulation of Notch signaling (Conboy and Rando 2002). Therefore, reduction of *Aph1b* could affect the signal transduction after Notch pathway activation. However, I could not detect deregulation of Aph1B protein levels at E12.5 limb buds (**Figure 20B**).

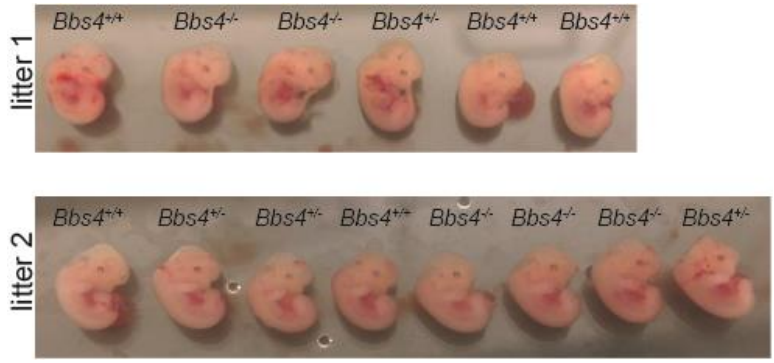

Figure 19: No visible difference in body size at E12.5 between the genotypes. Pictures showing litters from *Bbs4*$^{+/-}$ matings.

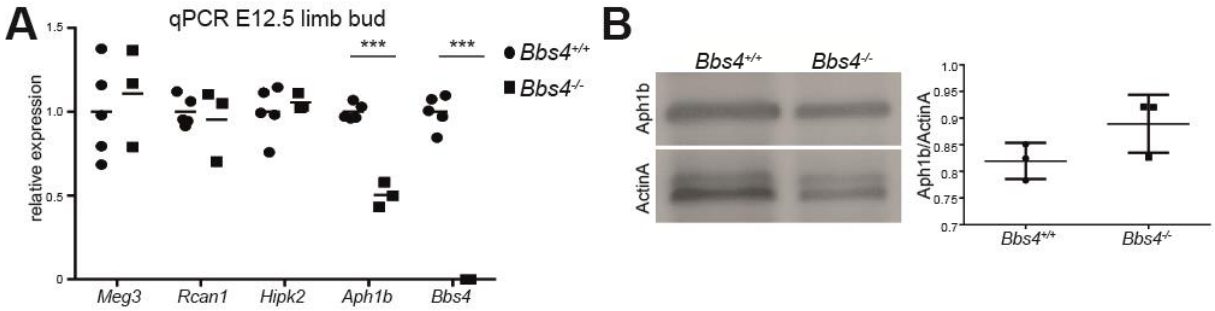

Figure 20: Comparison of mRNA and protein abundance in E12.5 *Bbs4*$^{-/-}$ limb buds. (A) Expression levels of Notch-candidate genes *Meg3*, *Rcan1* or *Hipk2* are similar between the genotypes. *Aph1b* was significantly downregulated (p≤0.001) in *Bbs4*$^{-/-}$ limb buds. Bbs4 TaqMan real-time qPCR for *Bbs4* added as a control (p≤0.001). (B) Protein levels of Aph1b do not indicate aberrant protein abundance.

Taken these data together, I discovered lean mass reduction and reduced skeletal muscle

strength of *Bbs4*$^{-/-}$ mice. However, I could not detect the same phenotype in an inducible, skeletal muscle-specific *Ift88*$^{-/-}$ mouse line (*HSA-MCM;Ift88*$^{flox/flox}$), although these mice showed increased fat mass. So far, for the *Bbs4*$^{-/-}$ mouse line I could exclude dedifferentiation of myoblasts to adipocytes, changes in fiber types, atrophy or dystrophy as a cause of muscle mass loss and muscle weakness. Data of mRNA expression from RNA-Seq experiments indicated aberrant *Tiam1* expression as well as differences in the expression of Notch and differentiation-related genes (*Tln2*, Emx2, Sv2b, *Meg3*, *Rcan1*, *Hipk2*, *Aph1b*). However, I was not able to completely confirm this data on mRNA or protein expression level. Nevertheless, RNA-Seq data points to an effect in muscle differentiation/regeneration. *In vitro* experiments using the mouse myoblast cell line C2C12, as described below, gave more insight into cilia-related phenotypes on Notch signaling in myoblasts and its implication in muscle regeneration.

5.3 Ift88 knock-down myoblasts show reduced differentiation efficiency

Skeletal muscle tissue consists of multinucleated myofibers. Satellite cells (SC) are attached to the fibers. These ciliated stem-like cells provide a heterogeneous progenitor pool for muscle regeneration. Until activation, they are in a quiescent state with a very low rate of proliferation. During muscle regeneration, SC get activated and show increased proliferation. Activated SC are called myoblasts and characterized by expression of MyoD. A myoblast can divide asymmetrically and give rise to a quiescent cell and an activated cell (Troy et al. 2012), which will fuse with other myoblasts to form new myofibers. The activated daughter cell is characterized by a higher Numb content, a Notch signaling inhibitor. Downregulation of Notch signaling in the daughter cell initiates further expression of myogenic markers and fusion of myoblasts within myofiber regeneration (Conboy and Rando 2002; Shinin et al. 2006). Additionally, a SC can divide symmetrically into two equal cells for muscle regeneration (Bentzinger et al. 2013; Le Grand et al. 2009). Results of experiments described above in skeletal muscle tissue of adult 14-week-old mice and E12.5 limb buds pointed to a cilia-related regenerative defect. Further, to avoid limitations of tissue availability and to better understand the role of primary cilia in myoblast differentiation, I established an *in vitro* system.

5.3.1 Characterization of *shIft88*-expressing C2C12 myoblasts

I performed the following experiments with the mouse myoblast cell line C2C12. Using a lentiviral delivery system, I induced knock-down of *Ift88*, which plays a major role in the establishment and maintenance of primary cilia. Knock-out of *Ift88* was shown to completely abolish the primary cilium from the cells (Pazour et al. 2000). Before characterization of effects

on myoblast signaling and differentiation, I wanted to investigate the knock-down efficiency and proliferative capacity of the cells. Therefore, I first investigated the *shIft88*-knockdown efficiency regarding primary cilia appearance as well as protein abundance. I stained C2C12 cells for primary cilia using acetylated tubulin and Arl-13B. The number of cells was counted based on DAPI staining. I detected reduced percentage of ciliated cells (25% ciliated *LacZ*-expressing C2C12, 11% ciliated *shIft88*-expressing C2C12). Remaining cilia in the *shIft88*-expressing cells appeared shorter compared to cilia of the control cells (**Figure 21A and B**). Further, C2C12 transfected with pLENTI *shIft88* showed 46% reduction of Ift88 protein in whole-cell lysates compared to control (**Figure 21C**).

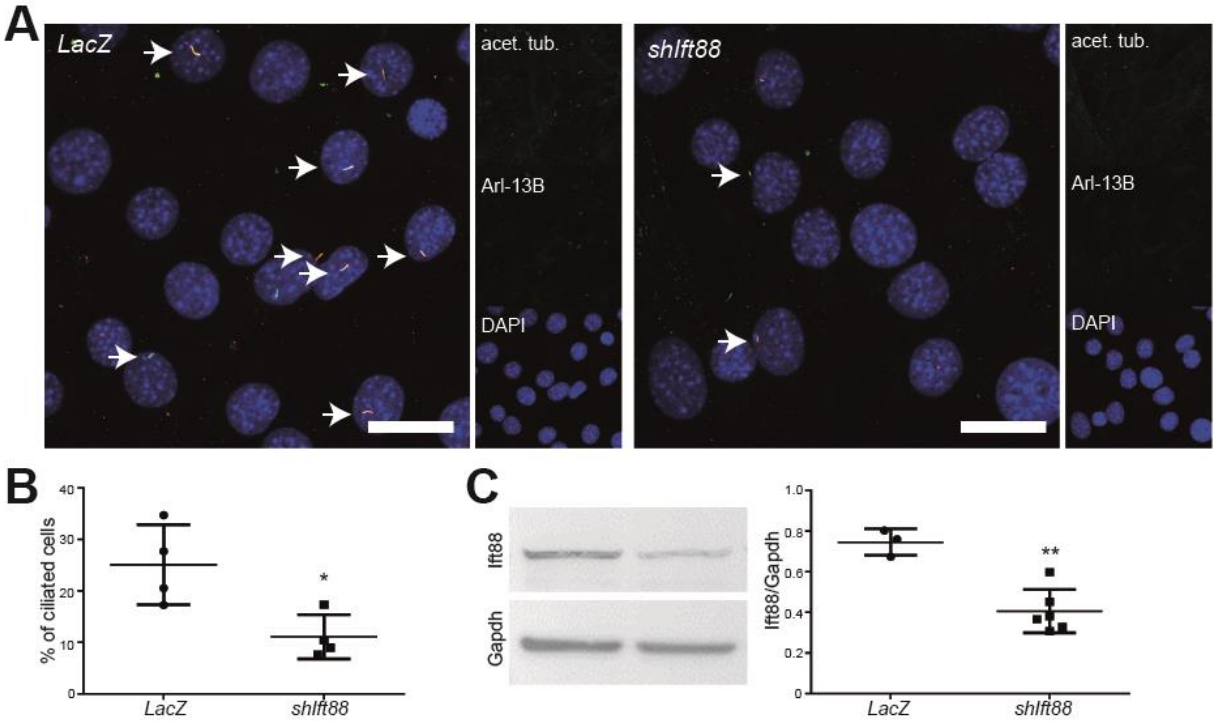

Figure 21: Characterization of the *shIft88*-expressing C2C12 cell line. (A) Staining of acetylated tubulin (green) and Arl-13B (red) to illustrate primary cilia (indicated with arrows). DAPI shown in blue. Scale bar=10 µm (B) Quantification of percentage of ciliated cells based on immunostainings. Significant reduction of cilia number in *shIft88*-expressing cells (p=0.02). (C) Western Blot analysis of Ift88 abundance. Significant Ift88 down-regulation (p=0.002) in *shIft88*-expressing C2C12 cells.

Since the primary cilium functions as a signaling hub for different pathways in the cell, ablation or dysfunction of primary cilia can cause changes in cell polarity and cell cycle. However, lack of *Ift88* does not always result in increased proliferation (Jonassen et al. 2008; Menzl et al. 2014; Seeley et al. 2009). One study showed mitotic delay induced by spindle-misorientation of HeLa cells, primary mouse kidney cells and zebrafish embryos lacking *Ift88* (Delaval et al.

2011). The ciliary axoneme extends from the mother centriole of the cell. During the initial phase of cell cycle progression from G1- to S-phase, cilia are disassembled to release the centriole, the nucleation point of the mitotic spindle. Therefore, cilia cannot be present in cycling cells and disrupted cilia disassembly blocks cell cycle progression. After passing S- and M-phase, cilia are re-assembled in G1- or G0-phase. To characterize the role of cilia in the C2C12 cell cycle, I analyzed the cell cycle of *shIft88*-expressing C2C12 myoblasts with help of propidium iodide-stained DNA content using FACS analysis. The histograms of *LacZ*-expressing and *shIft88*-expressing C2C12 show a high number of proliferating cells. Based on the histogram I could not differentiate between S-phase and G2-/M-phase (**Figure 22A**). However, calculating the percentage of cells in resting G0-/G1-phase against active S-/G2-/M-phase, *shIft88*-expressing C2C12 myoblasts show significant higher percentage of resting (G0-/G1) cells (44.6% *Ift88*-depleted C2C12 and 37.5% control cells) and a reduced percentage of actively proliferating (S-/G2-/M) cells (35.0% *Ift88*-depleted C2C12 and 39.4% control cells, **Figure 22B**).

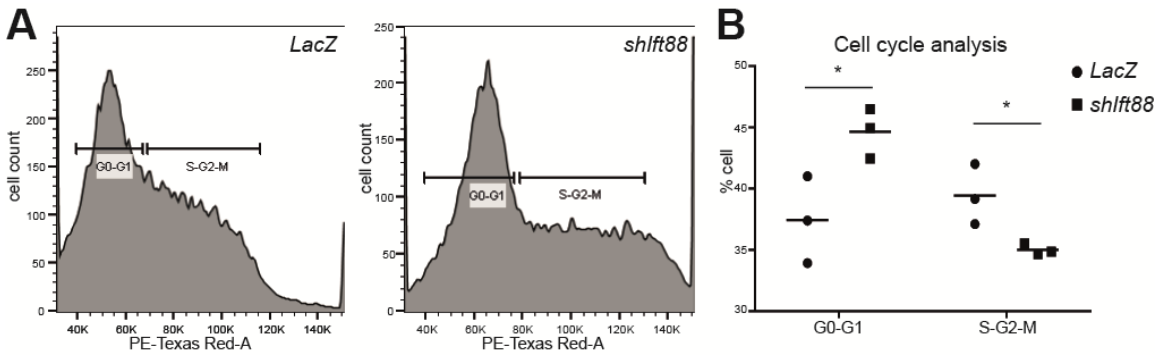

Figure 22: Cell cycle and proliferation analysis of *Ift88*-depleted C2C12 cells. (A) Propidium iodide-stained C2C12 cell cycle analysis. Representative histograms illustrate gating of the counted events. (B) Percentage of cells in G0-/G1-phase and S-/G2-/M-phase based on histogram gating. Significant increase of *shIft88*-expressing C2C12 in resting phase (p=0.03) and decrease in proliferating phase (p=0.038).

5.3.2 Altered Rac1 and Cdc42 activity in Ift88-depleted C2C12 myoblasts

I detected significant downregulation of *Tiam1* mRNA in adult EDL muscles by real-time qPCR analysis. As stated above, Tiam1 is the Rac1-specific GEF and activates Rac1 by catalyzing the exchange of GDP for GTP (Schmidt and Hall 2002). I confirmed 50% downregulation of *Tiam1* mRNA in *shIft88*-expressing C2C12 compared to *LacZ*-expressing control cells (**Figure 23A**). To test if *Tiam1* misregulation has an effect on Rac1 and Cdc42 (another member of Rho-family GTPase) activity, I used commercially available kits. Total Rac1 and Cdc42 protein levels are enhanced in *Ift88*-depleted myoblasts. However, the active GTP-bound forms

(Rac1-GTP and Cdc42-GTP) are equal between *Ift88*-knockdown and *LacZ*-expressing cells (**Figure 23**). Normalized to total Rac1 and Cdc42 protein levels, the active GTP bound form was significantly increased in *shIft88*-expressing C2C12 cells (126% increased active Rac1, 56% increased active Cdc42). High levels of activated protein does not necessarily indicate higher protein activity. Since both proteins are involved in endocytic processes, further investigations on endocytosis in *Ift88*-depleted myoblasts will give more information about Rac1 and Cdc42 activity.

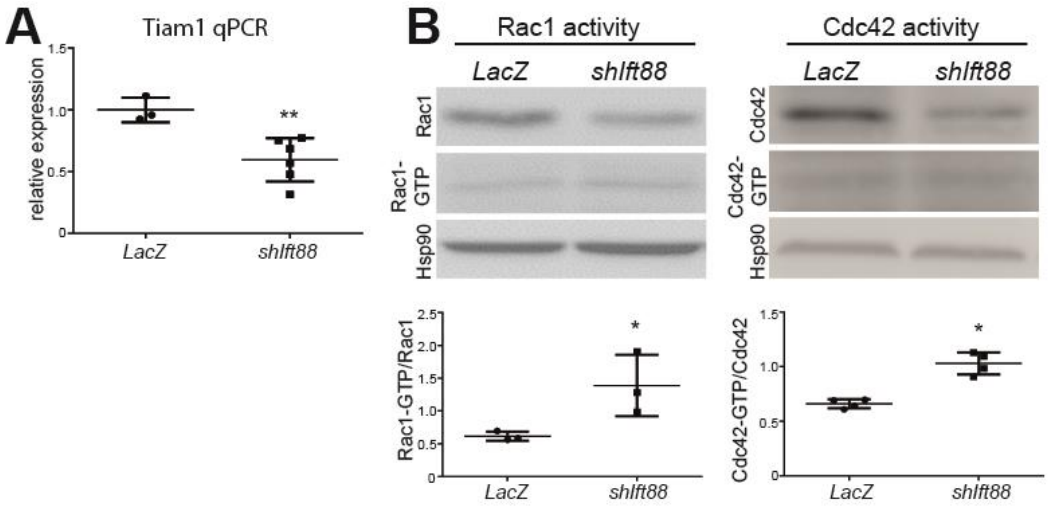

Figure 23: Decreased gene expression of *Tiam1* mRNA and increased Rho-family GTPases protein activation in *Ift88*-depleted C2C12 cells. (A) TaqMan real-time qPCR showing significant downregulation of *Tiam1* mRNA in *shIft88*-expressing C2C12 cells compared to *LacZ*-expressing control. (p=0.014). (B) Western Blot analysis of pull-down of GTP-bound Rac1/Cdc42 to total Rac1/Cdc42 showing significant upregulation of active form in *shIft88*-expressing cells compared to control. (Rac1: p=0.048), (Cdc42: p=0.029).

Cdc42 participates in intracellular vesicle-transport, regulating different processes like endo-/exocytosis, transport of molecules between endoplasmatic reticulum and Golgi-apparatus as well as post-Golgi transport (Egorov et al. 2009; Hehnly et al. 2009; Luna et al. 2002). Whereas Rac1 was found only to act during clathrin-dependent endocytosis and exocytosis (Lamaze et al. 1996; Matas et al. 2005). The main overlapping function of Rac1 and Cdc42 is regulation of endocytosis by actin polymerization (Lamaze et al. 1996; Luna et al. 2002). To investigate the endocytic capacity of *shIft88*- and *LacZ*-expressing myoblasts, I performed a transferrin uptake assay, which is known as the “gold standard” for the investigation of endocytotic recycling. To see time-dependent uptake of transferrin, I treated *Ift88*-knockdown and control cells with 0.01 mg/ml fluorescently-labelled transferrin for up to one hour. Images of cells were taken at the confocal microscope and fluorescence intensity of single cells in the obtained images was measured using Fiji software. The uptake of transferrin over time was not

significantly altered in *shIft88*-expressing compared to *LacZ*-expressing myoblasts (**Figure 24A**). Therefore, I did not detect an endocytosis-related phenotype in these cells.

Further, I performed a Dll4 internalization assay. Therefore, I treated myoblasts lacking *Ift88* and control cells for 75 min with 2.0 µg/ml His-tagged Dll4, one of five Notch-receptor ligands. After Notch-activation, the receptor together with tagged Dll4 is internalized, inactivated and recycled. This process was visualized and quantified by staining against His-tag and analysis of fluorescence intensity of single cells using Fiji software. Within 75 min, I could not detect a significant difference in uptake of His-tagged Dll4 between *LacZ*- and *shIft88*-expressing cells (**Figure 24B**). Although Rac1 and Cdc42 are overexpressed and the level of active GEF forms is increased, I could not find an evidence for alterations in endocytosis of myoblasts lacking *Ift88*.

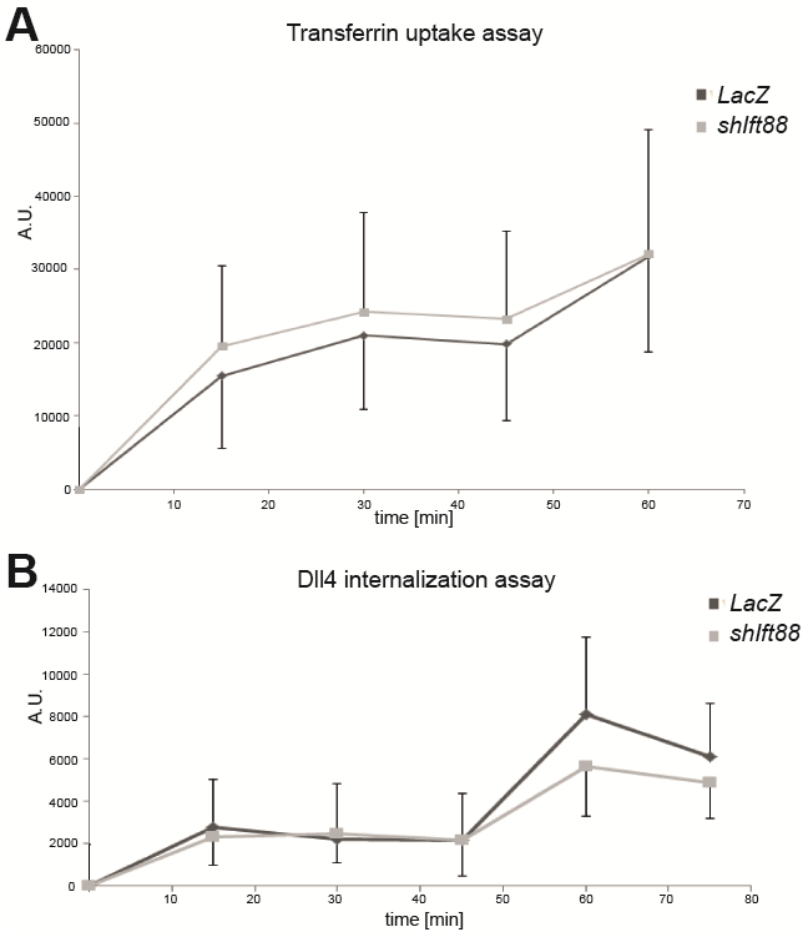

Figure 24: Transferrin and Dll4 internalization are not affected in *Ift88*-knockdown myoblasts. (A) Representative histogram showing internalization of transferrin by relative fluorescence intensity over time. (n=4). (B) Representative histogram showing internalization of His-tagged Dll4 by relative fluorescence intensity over time. (n=3).

5.3.3 Increased Notch1 signaling in *Ift88*-knockdown C2C12 myoblasts

RNA-Seq data of adult *Bbs4*$^{-/-}$ EDL muscles showed Notch signaling-related genes deregulated (**Figure 16**). To get a better understanding about Notch signaling in *Ift88*-depleted myoblasts, I characterized this signal pathway in *shIft88*- and *LacZ*-expressing C2C12 cells. I used a Luciferase Notch1-pathway responsive reporter assay to monitor pathway activity. Four different constructs were electroporated into the cells in different combinations. The main readout about Notch activity was generated by combining a CSL Firefly luciferase reporter vector constitutively expressing *Renilla* luciferase vector (CSL reporter) with a Notch1 NICD1 expression vector (Notch1ΔE). Importantly, the entire extracellular domain is deleted. The Notch1ΔE vector encodes the NICD1 domain, which still has to get cleaved by the cell to become active. Then NICD1 domain can interact with cellular CSL and bind to CSL responsive elements of the CSL reporter vector to induce firefly luciferase gene expression. Independent from Notch1 activity, this plasmid expresses a *Renilla* luciferase as an internal control to monitor the transfection efficiency. Further, the kit contains a control non-inducible luciferase vector consistently expressing *Renilla* luciferase (neg. ctrl. reporter) to measure background luciferase activity. Further, a negative control expression vector (ctrl. vector) is necessary to monitor Notch1 pathway specific expression of Firefly luciferase. Two days after the transfection, cell lysates were used to determine Firefly and *Renilla* luciferase activity. Therefore, a substrate is added to the lysate which is oxidized by the luciferase. This process produces bioluminescence, which is quantified in a plate reader. Normalized to *Renilla* luciferase expression, I detected increased Firefly luciferase activity in *shIft88*-expressing myoblasts compared to *LacZ*-expressing control. The increase of luciferase activity between the single experiments was ranging from 1.8- to 3.0-folds. **Figure 25A** shows a representative result of almost 2-fold increased luciferase activity in *shIft88*-expressing C2C12 cells. These results indicate an increased Notch1 activity in *Ift88*-knockdown cells compared to control.

To test if Notch signaling was misregulated on the transcriptional level, I performed real-time qPCR analysis to compare mRNA levels of Notch signaling-related genes *Jagged1*, *Notch1* and *Aph1b*. Ift88 probe was added to the experimental setup to quantify knock-down efficiency also on the mRNA level, which was 71% compared to the control (aberrant data to Western Blot results might be induced by weak antibody binding to Ift88). I could not detect significant differences in mRNA abundance of *Jagged1* and *Aph1b* in *Ift88*-knockdown cells, but I detected significant *Notch1* upregulation of about 58% compared to control (**Figure 25B**). Comparing the protein abundance of Notch1, I could confirm a significant upregulation about 138% compared to *LacZ*-expressing myoblasts. Aph1b is not deregulated on the protein levels, as shown before on the mRNA level. Surprisingly, Jagged1 protein is 48% upregulated but mRNA expression was not significantly changed in *Ift88*-depleted myoblasts (**Figure 25C**).

Differences between protein and mRNA level readout could be induced by low binding efficiency of the qPCR probe. This data suggests that ciliary impairment leads to aberrant Notch1 signaling in C2C12 cells. Notch signaling regulation is crucial for myoblast differentiation into myotubes. Therefore, I wanted to investigate the impact of ciliary impairment on myoblast differentiation in further experiments.

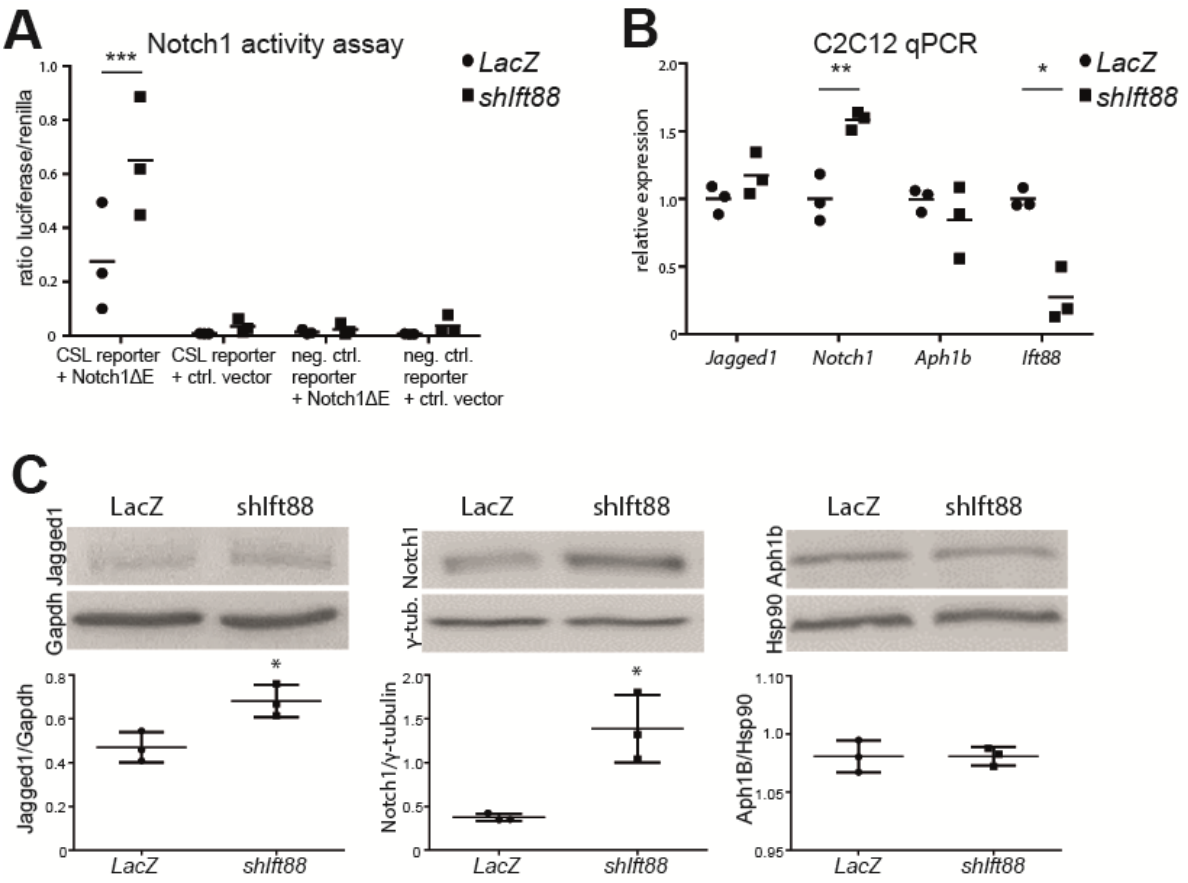

Figure 25: Notch1 luciferase activity assay, real-time qPCR analysis and Western Blot indicate increased Notch1 signaling in *Ift88*-depleted C2C12 myoblasts. (A) Representative result of luciferase activity assay illustrating Notch1 signaling activity in C2C12 cells. *Ift88*-depleted C2C12 cells show about twice the signaling activity of control cells. (p≤0.001). (B) Real-time qPCR result showing increased *Notch1* mRNA abundance (p=0.006) and efficiency of *Ift88* knockdown (p=0.017). No aberrant expression of *Jagged1* and *Aph1b*. (C) Confirmation of the upregulation of Notch1 (p=0.02), and upregulation of Jagged1 (p=0.022) on protein level compared to *LacZ*-expressing control. Protein levels of Aph1b are not changed.

5.3.4 Differentiation and MyoD expression of C2C12 myoblasts

Notch signaling is a known driver for satellite cell (SC) quiescence and self-renewal. Several studies showed a critical role of Notch signaling in keeping these cells quiescent to sustain

SC population. Further, Notch signaling induces the expression of the SC marker Pax7 (Bjornson et al. 2012; Mourikis et al. 2012). In proliferating myoblasts, Notch signaling is downregulated when expression of *MyoD* starts (Liu et al. 2013; Wen et al. 2012). Proliferating cells start to express myogenin and either fuse with each other to form new myotubes, or fuse with existing myofibers in regenerating skeletal muscle. A small population of *MyoD* expressing cells is able to return to the quiescent state by upregulating Notch (Wen et al. 2012). As shown above, *shIft88*-expressing C2C12 cells show increased Notch signaling. Since Notch downregulation is crucial for SC activation, proliferation and differentiation, I expected a defect in differentiation efficiency of *Ift88*-knockdown C2C12 cells.

I established a differentiation protocol using *LacZ*-expressing C2C12 cells. For this purpose, I let the cells grow to confluence (**Figure 26A**) and induced differentiation by changing the medium to differentiation medium. Myoblasts start to elongate and fuse to myofibers, which can be detected as early as 2 d after induction. In cultures of 5 d differentiated cells, I detected multinucleated myofibers (**Figure 26A**). Protein levels of MyoD in *LacZ*- and *shIft88*-expressing C2C12 cells are similar before induction. All samples show increased MyoD expression 2 d after induction of differentiation. Within the first 2 d after induction, an increase of 71% in MyoD protein expression was detected in *LacZ*-expressing C2C12 cells, whereas *Ift88*-depleted C2C12 cells showed significantly reduced MyoD protein expression induction ((1)43% and (2) 35%) compared to control (**Figure 26B**). Diminished MyoD expression indicates reduced induction of differentiation in *Ift88* knock-down cells.

5.3.5 Fusion and differentiation index of *Ift88*-depleted myoblasts

The *LacZ*-expressing control C2C12 cells used for the experiments above show a high potential for differentiation. Because I detected upregulation of Notch1 signaling using a Notch pathway responsive luciferase reporter kit in *Ift88* knock-down myoblasts, I characterized their differentiation efficiency. Phalloidin-labelling of F-actin in 5 d differentiated cells outlined myotubes (**Figure 27A**). In order to characterize the fusion index of *LacZ*- and *shIft88*-expressing C2C12 cells, I counted the number of nuclei per myotube, illustrating the number of fused cells. For all three clonal cell lines investigated, I detected significant loss of fusion efficiency ranging from approximately 3% to 7% in *shIft88*-expressing C2C12 cells compared to control (**Figure 27B**). To verify this observation, I calculated the differentiation index as percentual fraction of nuclei that are part of a myofiber. Also here, I found significant reduction of differentiation index from 5% to 10%, depending on the clonal cell line (**Figure 27C**). These results support the hypothesis of *Ift88*-dependent regulation of Notch signaling and therefore alteration in C2C12 cell differentiation efficiency.

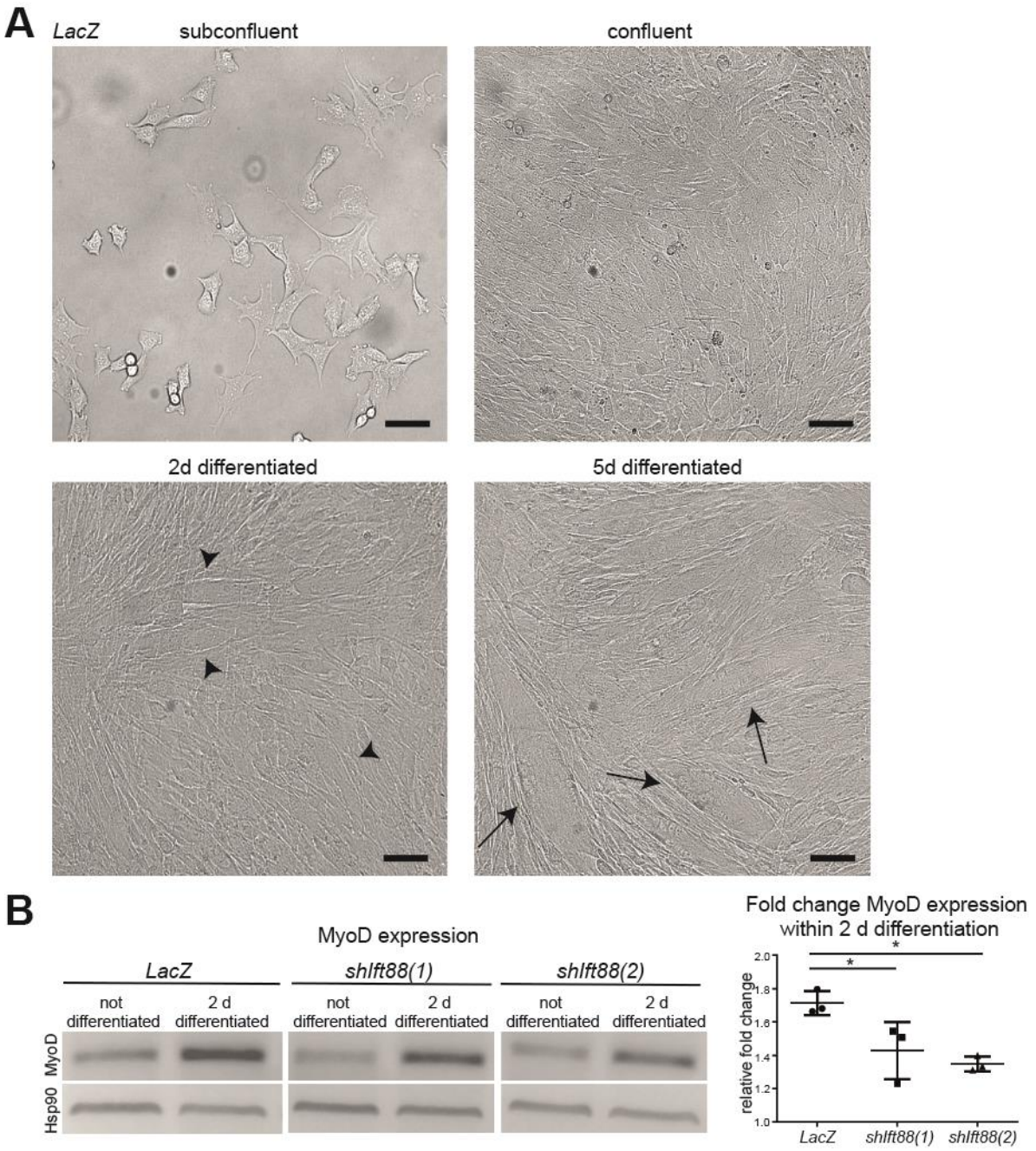

Figure 26: Myotube formation and MyoD protein expression showing differentiation capacity of *LacZ*-expressing C2C12 cells. (A) Light microscopic images of subconfluent, confluent as well as 2 d and 5 d differentiated *LacZ*-expressing C2C12 cells showing induction of differentiation by formation of myofibers (2 d, indicated by arrowheads) and multinucleated myotubes (5 d, indicated with arrows). Scale bar=100 µm. (B) Western Blot analysis of MyoD expression in not differentiated and 2 d differentiated *LacZ*- and *shlft88*-expressing C2C12 cells. Significant reduction in fold-change MyoD expression between *LacZ*- and *shlft88*(1)-(p=0.039) / *shlft88*(2)-expressing cells (p=0.020).

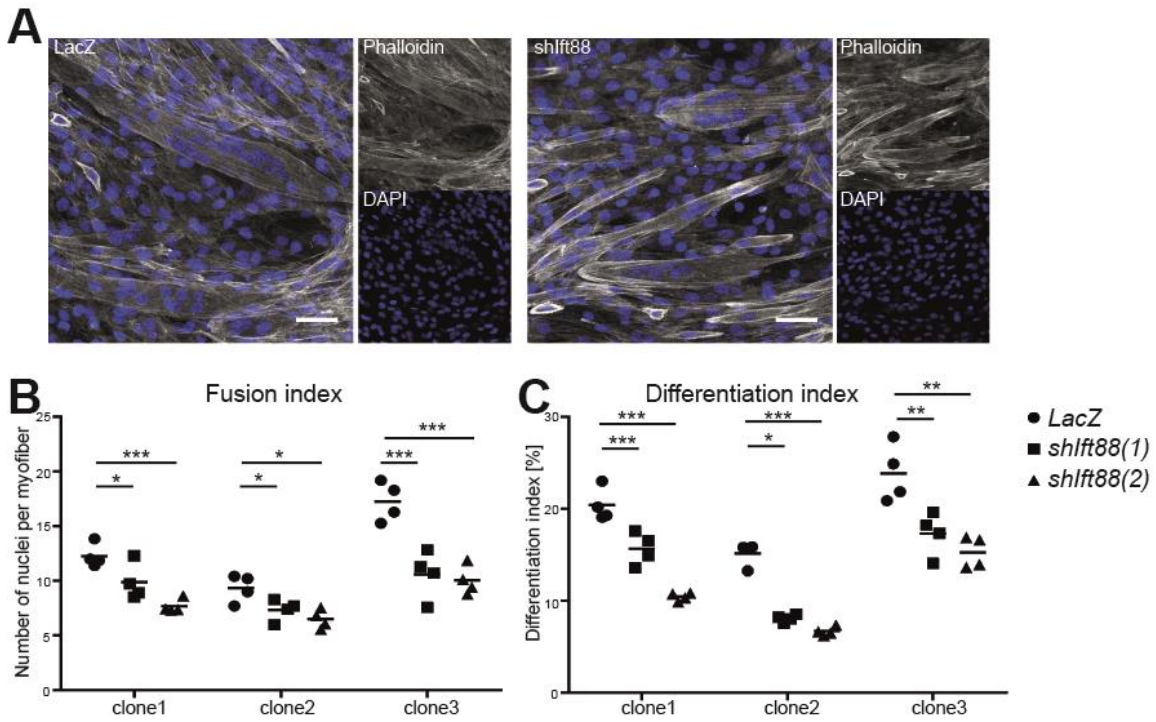

Figure 27: The differentiation efficiency of *shIft88*-expressing C2C12 myoblasts is reduced. (A) Representative immunostaining images illustrating multinucleated myotubes 5 d after differentiation in *LacZ*- and *shIft88*-expressing C2C12 cells. Grey: phalloidin, blue: DAPI. Scale bar050 µm. (B) Fusion index indicating reduced fusion of cells in all three *Ift88* knock-down clonal cell lines. (clone 1: p(*LacZ*/*shIft88*(1))=0.041; p(*LacZ/shIft88*(2)=≤0.001; clone 2: p(*LacZ/shIft88*(1))=0.049; p(*LacZ/shIft88*(2))=0.012; clone 3: p(*LacZ/shIft88*(1))≤0.001; p(*LacZ/shIft88*(2))=0.001). (C) Differentiation index confirming reduced differentiation efficiency of *shIft88*-expressing C2C12 myoblasts. (clone 1: p(*LacZ/shIft88*(1))=0.001; p(*LacZ/shIft88*(2))≤0.001; clone 2: p(*LacZ/shIft88*(1))=0.029; p(*LacZ/shIft88*(2))≤0.001; clone 3: p(*LacZ/shIft88*(1))=0.009; p(*LacZ/shIft88*(2)=0.002).

Taken together, I showed that control C2C12 myoblasts can upregulate MyoD expression to induce differentiation and myotube formation. Contrarily, *Ift88*-depleted C2C12 cells appeared to have deregulated Notch signaling, as well as reduced MyoD expression after induction of differentiation and therefore reduced differentiation efficiency. This data strongly points to a function of primary cilia in proper myoblast Notch signaling regulation and myotube formation. Therefore, impaired muscle regeneration of adult tissue could cause muscle mass loss in ciliopathies, such as Bbs4.

5.3.6 Confirmation of Hh signaling regulation in differentiating myoblasts

The primary cilium is a signaling hub, therefore ablation of cilia does not only affect one signaling pathway. One well investigated cilia-dependent signaling pathway is Hh. Fu and colleagues showed that ciliary disassembly in primary mouse myoblasts goes in hand with

reduced Hh signaling during differentiation (Fu et al. 2014). Further, they detected reduced differentiation efficiency and Hh signaling of *Ift88*-depleted myoblasts. I wanted to investigate Hh signaling during differentiation also in my *Ift88* knock-out clonal cell lines. As shown in the paper, I detected downregulation of the Hh response gene *Gli1* during differentiation by comparing expression levels of not differentiated and 5 d differentiated *shIft88*- and *LacZ*-expressing C2C12 cells. Contrary to previous observations, I could not detect reduction of *Gli1* in myoblasts lacking *Ift88*. However, I detected a significant upregulation of *Gli1* expression (51%) in not differentiated *shIft88*-expressing C2C12 myoblasts compared to *LacZ*-expressing control. After 5 d differentiation, I detected similar *Gli1* mRNA expression levels (**Figure 28**), suggesting a downregulation of Hh signaling during differentiation as stated by Fu and colleagues. The overexpression of *Gli1* in *Ift88*-expressing myoblasts could indicate a compensational mechanism of the cells lacking properly functional cilia. A similar mechanism might also induce enhanced Notch1 activity in these cells.

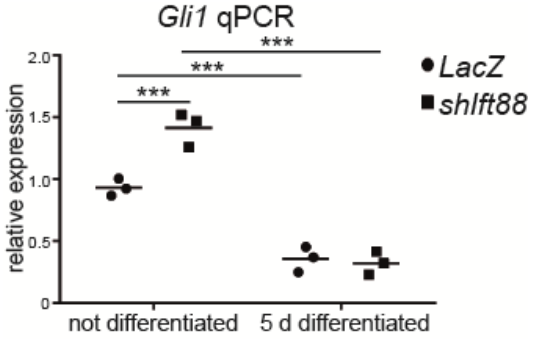

Figure 28: Regulation of *Gli1* mRNA expression during differentiation. Not differentiated *shIft88*-expressing C2C12 cells express significantly more *Gli1* mRNA compared to control. (p≤0.001). *Ift88*-depleted and *LacZ*-expressing C2C12 significantly downregulate *Gli1* during differentiation (p(*LacZ*)≤0.001; p(*shIft88*)≤0.001). Therefore, no difference in Gli1 expression after 5 d differentiation was detected.

Taken together, the data of this study shows the importance of cilia for proper Notch and Hh signaling in myoblasts. For the first time, this study reveals a connection between upregulation of Notch signaling activity due to myoblast ciliary impairment. The data indicates a regenerative phenotype of skeletal muscle in a ciliopathy model, which could explain *Bbs4*$^{-/-}$ mouse lean mass and grip strength reduction.

6 Discussion

6.1 The role of ciliary proteins in skeletal muscle

6.1.1 Lean mass and grip strength in *Bbs4*$^{-/-}$ mice

Bardet-Biedl Syndrome is a genetic, pleiotropic disorder with multisystemic phenotypes induced by mutated proteins of the BBS family. A common feature of Bardet-Biedl Syndrome is the development of impaired glucose tolerance and diabetes type 2 mellitus (Moore et al. 2005). Skeletal muscle plays an important role for glucose homeostasis, since it takes up around 80% of postprandial blood glucose (DeFronzo et al. 1981). Therefore, I set out to investigate the skeletal muscle phenotype in *Bbs4*$^{-/-}$ mice. Nuclear Magnetic Resonance Spectroscopy of 14-week-old male mice with the same body weight showed decreased lean mass in *Bbs4*$^{-/-}$ compared to wildtype mice, as shown before by other groups for mice and human BBS patients (Eichers et al. 2006; Grace et al. 2003). Since lean mass consists of organ, skeleton and muscle mass, this result does not conclusively indicate loss of muscle mass. Therefore, I subsequently performed a grip strength test (Bioseb) of the front legs using a grip strength meter. The results showed that reduced lean mass of *Bbs4*$^{-/-}$ mice was accompanied by reduced relative grip strength compared to *Bbs4*$^{+/+}$ mice. Within the grip strength test cohort, 5 out of 20 *Bbs4*$^{-/-}$ mice have been shown to have a strong phenotype indicated by body weight >35 g at 14 weeks. These mice showed more severe grip strength reduction, indicating a correlation between severity of the phenotype and reduction of skeletal muscle function. Since high-fat diet induced obesity has not been shown to affect muscle mass (DeNies et al. 2014), the observed reduction in lean mass and grip strength in *Bbs4*$^{-/-}$ mice might indicate a function of Bbs4 in skeletal muscle, rather than a secondary effect caused by increased fat mass. Grip strength and lean mass of tamoxifen induced and control *HSA-MCM;Ift88*$^{flox/flox}$ mice does not indicate a significant difference. This observation points on a role of Bbs4 in differentiated skeletal muscle besides its role in the primary cilium.

The relative grip strength was calculated by absolute measurement of strength in grams relative to the body mass as described before (Altamirano et al. 2014; Ge et al. 2016). Normalization to lean mass is not used in the field. Reduced lean mass and grip strength have also been reported for *Bbs5*$^{-/-}$ mice by the International Mouse Phenotyping Consortium (Dickinson et al. 2016). The Bioseb grip strength test and other methods for *in vivo* muscle strength measurements rely on the natural behavior of mice to grasp. One example is the weight test, where the ability of mice to lift weights can be tested. For this test, steel wire is connected to different weights, for example steel chain links. The mouse is held on its tail base above the steel wire and allowed to grasp it. Then the mouse is lifted and time is measured

until it releases the weight. If the mouse can hold the weight 3 seconds, the mouse is lowered to the bench and the test is repeated with a higher weight (Deacon 2013). Both the grip strength and the weight test, are based on force generation of the legs only. A third method, called Kondziellas inverted screen test, demands whole body musculature. In this experimental set up, mice are placed on a wire mesh. The mesh is turned by 180° and the time until the mouse releases the mesh and falls down is measured (Kondziella 1964). The three described methods can be influenced by anatomical, behavioral or neurological factors of the mouse. For example, mice with a hyperactive phenotype would maybe move more on the Kondziellas inverted screen and get exhausted faster than control mice. Another phenotype influencing all three test methods are changes in the neuronal input by motor neurons. Therefore, another possibility for muscle strength evaluation are *ex vivo* force measurements after electrical stimulation. The advantage of this method is the exclusion of non-muscle-related phenotypes, that can influence *in vivo* measurements (Park et al. 2012). Within this study, I used the grip strength test, partially because the other two described *in vivo* tests measure time to release. Repeated measurements can train the mouse to release the weights before getting exhausted. Further, Kondziellas inverted screen test is more dependent on the body weight than the other two described methods. The Bioseb grip strength test measures directly the maximum force exerted until the mice release the grip, independent of body weight or exhaustion and is a standardized test by the German Mouse Clinic. Systemic effects of muscle weakness in the *Bbs4*$^{-/-}$ mouse model were excluded by the investigation of NMJ and MTJ markers. Further, *Bbs4*$^{-/-}$ muscles were tested for the two most common atrophy markers, which were expressed at the same levels as in control mice.

Both Bbs4 and Bbs5 proteins are components of the BBSome and have been shown to have functional redundancy in cilia of *C. elegans.* In this study, single mutation of *bbs4* or *bbs5* did not induce ciliary dysfunction, but double *bbs4;bbs5* mutation induced deregulated removal of sensory receptors from the cilium leading to accumulation of receptors on the cilium (Xu et al. 2015). Moreover, mutation of *BBS4* or *BBS5* in human and mouse have been found to induce similar multisystemic phenotypes, e.g. obesity, impaired glucose handling and retinitis pigmentosa (Green et al. 1989; Iannaccone et al. 2005; Meehan et al. 2017; Mykytyn et al. 2001). Therefore, it could be possible that both forms of BBS also exhibit a muscular phenotype. Furthermore, *Bbs11*$^{-/-}$ (*Trim32*) is associated with Limb girdle muscular dystrophy. Within one family, four siblings have been reported to have *BBS*, which was induced by a point mutation in the *TRIM32* gene (Chiang et al. 2006). Trim32 is a ubiquitin ligase of actin and dysbindin among others, and associated to skeletal muscle myopathy (Kudryashova et al. 2005; Locke et al. 2009). The result of *Bbs5*$^{-/-}$ and *Bbs4*$^{-/-}$ lean mass and grip strength reduction indicate an implication of myopathy in Bardet-Biedl Syndrome. Whether myopathy is a primary

phenotype of BBS, according to its muscular function, or a secondary phenotype due to impaired glucose handling and muscle metabolism is not clear. I performed a fiber typing analysis of the glycolytic EDL and oxidative Soleus muscle from 14-week-old *Bbs4*$^{-/-}$ and control mice and did not observe any indications for fiber type shift similar to what is observed in type 2 diabetes. However, at the same age, mice already showed a reduced lean mass and grip strength, indicating a primary phenotype of *Bbs4*$^{-/-}$ mice in skeletal muscle function. The pathway through which Bbs4 interferes with muscular functionality has to be investigated in further experiments. Within this thesis, I show impaired myoblast differentiation of *Ift88* knock-down cells. Unlike *Bbs4*, ablation of *Ift88* does not only induce ciliary dysfunction, it also blocks ciliary assembly. Decreased *Tln2* mRNA expression in Soleus and EDL muscle of *Bbs4*$^{-/-}$ mice indicated a differentiation phenotype, which could be investigated more in detail using *Bbs4*-depleted C2C12 cells. Further, an inducible skeletal muscle or SC specific *Bbs4*$^{-/-}$ mouse line will indicate the function of Bbs4 in adult muscle and SC. To obtain *in vivo* data of differentiation in *Bbs4*$^{-/-}$ muscle progenitor cells, skeletal muscle regeneration in the mouse could be induced by cardiotoxin injection and observation of the regenerative capacity. Although there is still work to be done, this study for the first time showed a skeletal muscle phenotype of *Bbs4*$^{-/-}$ mice, providing a basement for future research.

6.1.2 Fat mass and obesity in *Bbs4*$^{-/-}$ mice

Bbs mouse models are known to develop obesity (Green et al. 1989). Nuclear Magnetic Resonance Spectroscopy of 14-week-old male *Bbs4*$^{-/-}$ mice of this study showed increased fat mass compared to control mice. Also *HSA-MCM;Ift88*$^{flox/flox}$ mice showed increased fat mass compared to controls 4 weeks after induction. Although obesity is a common phenotype in ciliopathies, this study shows for the first time increase in fat mass after skeletal muscle specific *Ift88* depletion. To date, the obesity phenotype in Bbs mice has been limited to hyperphagia and a hypothalamic defect in feeding behavior (Rahmouni et al. 2008; Sherafat-Kazemzadeh et al. 2013). Postnatal knockout of *Bbs1*, a protein of the BBSome complex like Bbs4 and Bbs5, in neuronal cells indicated reduced trafficking of the leptin receptor b (LRb) to the membrane, ultimately leading to leptin resistance. Dysregulation of LRb in the hypothalamus is thought to induce obesity (Davenport et al. 2007; D. F. Guo et al. 2016). Tamoxifen-induced cilia reduction in adult mice has been shown to increase food intake and body weight, which underlines an implication of the hypothalamus in this phenotype. Further, these mice showed increased fat mass as well as increased serum leptin, insulin and glucose levels. However, mice lacking cilia only in POMC (proopoimelanocortin) neurons also become obese, but delayed compared to global cilia-impaired mice. These results indicate additional roles for primary cilia in energy homeostasis beside the hypothalamus (Davenport et al. 2007).

Contrary to the hypothesis that obesity is induced by defective leptin signaling induced hyperphagia, preobese ciliary impaired mice have been shown to respond to the administration of leptin by reduction of food intake. This study indicates leptin resistance as a secondary effect of obesity (Berbari et al. 2013). A study using *Bbs12*$^{-/-}$ mice suggested adipocyte hyperplasia as a result of aberrant mesenchymal stem cell differentiation towards adipocytes as a reason for increased fat mass (Marion et al. 2012).

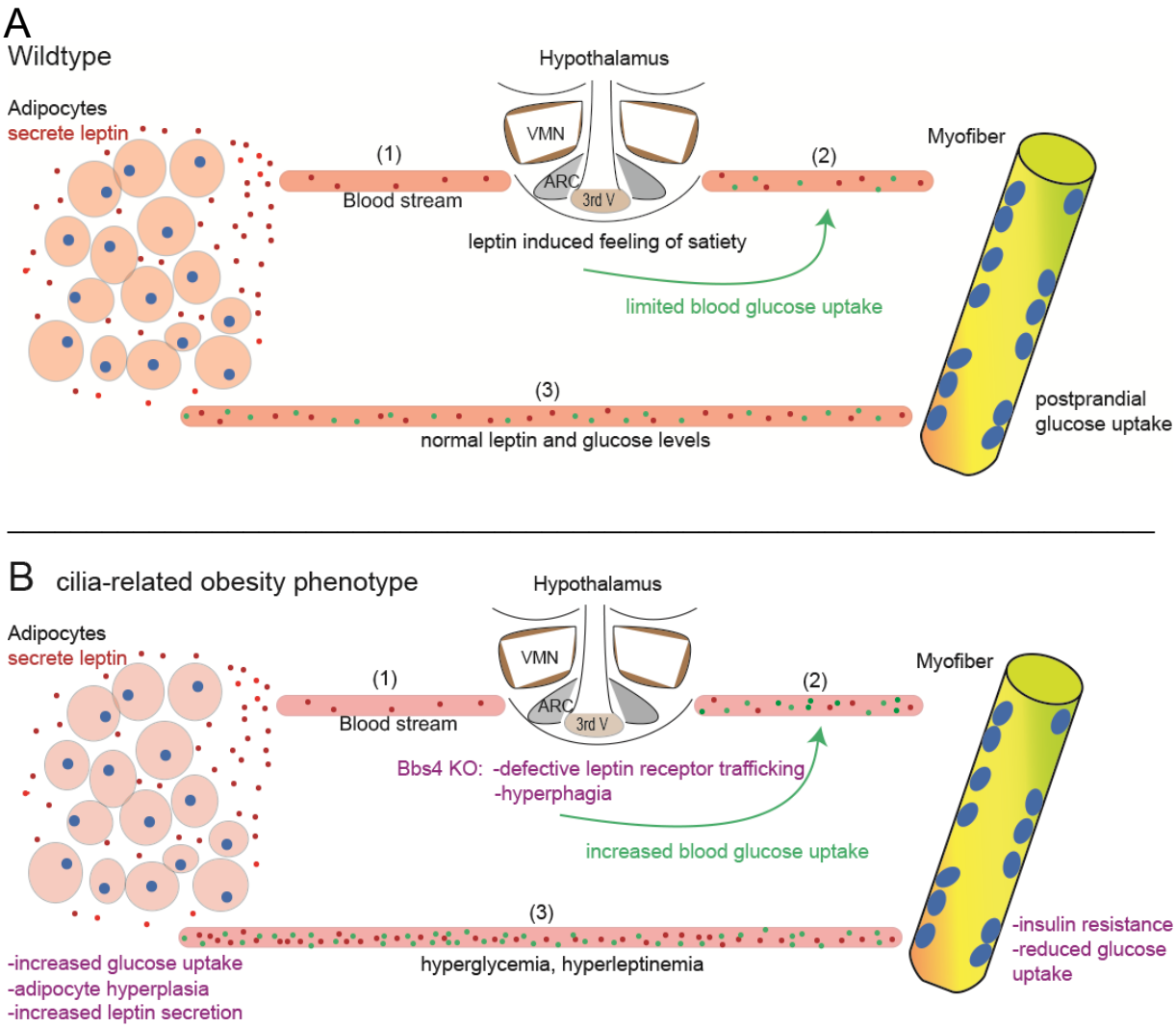

Schematic 11: Model, describing the cilia-related obesity phenotype in *Bbs4*$^{-/-}$ and tamoxifen induced *HSA-MCM;Ift88*$^{flox/flox}$ mice. The upper panel A illustrates the wildtype situation, where adipogenic leptin signals satiety regulation to the hypothalamus through the blood-brain barrier (VMN: ventromedial nuclei, ARC: arcuate nucleus, 3rd V: third ventricle) (1). The feeling of satiety reduces feeding and prostprandial blood glucose is mainly taken up by skeletal muscle to keep homeostasis (2). Leptin and blood glucose levels are within standard ranges (3). The lower panel B illustrates the situation in obese cilia-related knock-out mice. Adipogenic leptin signals do not reach the hypothalamus (1) due to diminished membranous leptin exposure. Therefore, feeding continues keeping glucose intake high (2). Glucose cannot be taken up by skeletal muscle due to diminished insulin receptor exposure, but adipogenic uptake increases, leading to hyperplasia. Increased leptin and glucose levels in the blood can be detected (3).

Oil Red-O staining of Gastrocnemius from tamoxifen-treated *HSA-MCM;Ift88*$^{flox/flox}$ mice and *Bbs4*$^{-/-}$ mice did not show intramuscular fat accumulation. Therefore, depletion of *Ift88* or *Bbs4* from skeletal muscle seems to induce fat accumulation in organs other than skeletal muscle. Skeletal muscle specific insulin-receptor (IR) knock-out mice showed adipose tissue hyperplasia. Since blood-glucose levels in this mice were in the normal range, adipose tissue compensated the diminished muscular glucose uptake, triggering fat pad growth (Brüning et al. 1998; Cariou et al. 2004; Kim et al. 2000). The same mechanism might occur in *Bbs4*$^{-/-}$ and tamoxifen-induced *HSA-MCM;Ift88*$^{flox/flox}$ mice, inducing adipocyte hyperplasia. These data indicate the involvement of Bbs4 and Ift88 in skeletal muscle metabolism by affecting insulin resistance. Bbs proteins in fibroblasts have been shown to interact with IR and are related to IR trafficking to the membrane (Starks et al. 2015). In pancreatic β-cells, the insulin-receptor is localized at the primary cilium and ciliary dysfunction diminishes first-phase insulin secretion (Gerdes et al. 2014). Moreover, Ift88 has been proposed to interact with SDCCAG3, which is involved in endosomal trafficking and therefore might also play a role in IR recycling or Glut4 translocation (McGough et al. 2014; Yu et al. 2016). This studies show that *Bbs4* and *Ift88* knock-out in adult muscle might impair skeletal muscle insulin signaling and glucose uptake and induce adipose hyperplasia independent of leptin signaling or obesity. Adipose hyperplasia in this study was detected by the increased fat mass in *Bbs4*$^{-/-}$ and tamoxifen-induced *HSA-MCM;Ift88*$^{flox/flox}$ mice. Results of this study, together with other studies of non-cilia related phenotypes of Bbs proteins (Hernandez-Hernandez et al. 2013; Langousis et al. 2016; Leitch et al. 2014) further explain the multisystemic characteristic of Bardet-Biedl Syndrome (**Schematic 11**).

6.1.3 Genotype/phenotype correlations of *Bbs4*$^{-/-}$ mutations

The development of certain Bbs4-specific phenotypes does not affect all *Bbs4*$^{-/-}$ mice. For example, the obesity phenotype has a penetrance of 40% in male *Bbs4*$^{-/-}$ mice, retinal dystrophy has a penetrance of 80% in male and female *Bbs4*$^{-/-}$ mice (Eichers et al. 2006). However, also patients with BBS and ALMS were shown to have big ranges in severity and onset of disease-related phenotypes as well as associated complications (Cox et al. 2012; Harnett et al. 1988; Marshall et al. 2005). Therefore, observed deviations within the *Bbs4*$^{-/-}$ cohort might be caused by differences in the penetrance of the phenotype and is a normal characteristic of the disease. This suggestion is supported by a study of Norwegian *BBS4*$^{-/-}$ mutation carriers. All patients developed severe retinitis pigmentosa early in life, but the obesity phenotype varied from mild to severe between families. Also cognitive impairment

showed a big range, some individuals even showed cognitive ability in a normal range (Riise et al. 2002). It has to be stated that studies on Bbs4 in mouse and cell culture are often working with *Bbs4* knock-out or knock-down mediated by shRNA (Mykytyn et al. 2004; Prieto-Echagüe et al. 2017; Su et al. 2014; Swiderski et al. 2007). BBS in humans is a consequence of mutations in at least one of the *BBS* genes leading to a dysfunctional protein. Several mutations are described for the *BBS4* gene, like a heterogeneous 2 bp insertion in exon 8 or homozygous transversions in exon 7 (A → C) or 4 (G → C) (Iannaccone et al. 2005; Mykytyn et al. 2001; Riise et al. 2002). One mutation leading to BBS4 loss-of-function has been found in a Chinese family (Li et al. 2014). It has been proposed, that BBS is a oligogenic disease, which means the phenotype is only present if more than one gene presents a pathogenic variant. Katsanis and colleagues described individuals showing triallelism. These patients appeared with a homozygous mutation in one BBS locus and an additional heterozygous mutation in another BBS locus for the presence of the full BBS phenotype (Katsanis et al. 2001). Since then, different studies contradicted or supported the finding of oligogenicity in BBS (Badano et al. 2003; Beales et al. 2003; Mykytyn et al. 2002, 2003).

6.1.4 Postnatal body size in mouse and human *Bbs4*$^{-/-}$

A dominant phenotype of *Bbs4*$^{-/-}$ mice is the runted body size at weaning age. One of the novel findings of this study is that *Bbs4*$^{-/-}$ embryos had the same size at E12.5, indicating normal embryonic growth. Therefore, the runted phenotype seems to present after birth, at a time when pups are sucking milk from the mother teat. This hypothesis is supported by the increased weight gain of *Bbs4*$^{-/-}$ mice after weaning when they eat pelleted food. Therefore, at 10-14 weeks, they have the same size and body weight as wildtype littermates (Eichers et al. 2006). Since BBS human patients and *Bbs4*$^{-/-}$ mice have been shown to be anosmic (Kulaga et al. 2004), affected mice maybe cannot find the maternal teat and receive less milk than their littermates before weaning. Starting from the time of feeding on chow pelleted food, *Bbs4*$^{-/-}$ mice gain weight faster than their *Bbs4*$^{+/+}$ littermates and reach the same body weight at 14 weeks. The fast gain in body weight, as well as the increased fat mass could be explained by the hyperphagic phenotype of *Bbs4*$^{-/-}$ mice (Rahmouni et al. 2008). Further, loss of sense of smell might be replaced by the ability of the mice to see the food pellets.

The hypothesis of reduced growth due to amosmia related difficulty to find the maternal teat is supported by data of olfactory bulbectomized mouse and rat pups, which have been found to fail feeding and show growth retardation (Cooper and Cowley 1976; Singh and Tobach 1975; Singh, Tucker, and Hofer 1976). Further, a growth retardation phenotype of BBS patients has not been described, but about one third of BBS patients developed obesity within

the first year of life (Beales et al. 1999; Putoux et al. 2012). Therefore, the runted body size is a phenotype restricted to rodents and might not be a primary effect of ciliary impairment. This hypothesis could be tested by feeding newborn *Bbs4*$^{-/-}$ mice by hand. If the shortened phenotype is restricted to anosmia related failure in finding the teat, hand-fed *Bbs4*$^{-/-}$ and hand-fed *Bbs4*$^{+/+}$ mice would gain weight evenly. Taken together, this study pointed out a difference between the mouse and human phenotype of BBS.

6.2 *Ift88* knock-down effects myoblast cell cycle

Knock-down of *Ift88* protein induced significant reduction of cilia number (25% ciliated *LacZ*-expressing C2C12, 11% ciliated *shIft88*-expressing C2C12) in C2C12 myoblasts. So far, publications show contradictory functions of cilia and Ift88 in cell cycle progression. For example, loss of cilia correlates with overproliferation in cancerous tissue (Egeberg et al. 2012; Seeley et al. 2009; You et al. 2012). Are cilia not established because of continuous proliferation or does loss of cilia induce proliferation? The depletion of *Ift88* from non-ciliated HeLa cells induced cell cycle progression, whereas overexpression of *Ift88* blocked transition from G1- to S-phase, therefore inhibited cell cycle progression and induced apoptosis (Robert et al. 2007). Further, the establishment of primary cilia has been shown to block cell cycle progression to S-phase in RPE-1 cells (Li et al. 2011) and ciliary length has been correlated with cell cycle length in zebrafish embryos (Kim et al. 2011). Contrary, lack of *Ift88* has been associated with mitotic delay in zebrafish embryos as well as HeLa and primary mouse kidney cells (Delaval et al. 2011). HeLa cells lacking Ift88 showed defective establishment of astral mitotic microtubule arrays and spindle misorientation (Delaval et al. 2011). This data contradicts the finding, that loss of Ift88 induces cell cycle progression. The impact of ciliation on cell cycle progression might be cell type specific.

Within this study, I showed increased number of *shIft88*-expressing myoblasts in not-cycling G0-/G1-phase and decreased number of actively cycling cells (S-/G2-/M-phase) using FACS cell cycle analysis, indicating an arrest in G0-/G1-phase of cells lacking *Ift88*. The observed increased number of cells in G0-/G1-phase underpins the observation of Delaval and colleagues (Delaval et al. 2011), who described mitotic delay in *Ift88* knock-down of human and mouse cells as well as zebrafish embryos. This study uncovered a non-ciliary function of Ift88 within the establishment of mitotic microtubule arrays. During cell cycle, Ift88 seems to have different functions, as it blocks cell cycle transition in G1-phase by the establishment of the cilium, and progresses the cell cycle by establishment of mitotic microtubule arrays. Further, mutation of *Ift88* did not interfere with proliferation in *C. elegans*, *Chlamydomonas* and *Trypanosoma brucei*, suggesting organism-specific functions of Ift88 (Haycraft et al. 2001;

Kohl, Robinson, and Bastin 2003; Pazour et al. 2000).

6.3 Implication of ciliary impairment on actin remodeling in skeletal muscle

Membrane receptors are delivered to the cell membrane in intracellular vesicles. After activation, endocytic internalization of membranous receptors and their further endosomal processing play a critical role in cell signaling. I showed 50% reduced *Tiam1* mRNA expression levels in *shIft88*-expressing C2C12 compared to control C2C12 myoblasts. Since Tiam1 is the GEF for Rac1, I tested presence of active, GTP-bound Rac1 in *shIft88*-expressing C2C12 myoblasts compared to control cells. The expression of total Rac1 protein is reduced in *Ift88* knock-down C2C12 myoblasts. The abundance of active Rac1-GTP remains unchanged, indicating that reduced *Tiam1* expression did not affect Rac1 activation. One reason could be that remaining *Tiam1* mRNA amount is sufficient for the translation of a critical level of Tiam1 protein to keep Rac1 activation constant. Similarly, analysis of GTP-bound and total CdC42, another small GTPase and regulator of endocytosis, revealed slight decrease in total Cdc42 but constant levels of GTP-bound Cdc42. These results indicate a normal activation of the GTPases, but reduced total protein expression. So far, transcriptional regulation of Rac1 and Cdc42 is not well understood. Investigation of transcriptional regulators and their connection to Ift88 and the cilium would help to understand these results. However, since I could not detect a significant difference in Dll4 or transferrin internalization, also actin polymerization and endocytosis seemed not affected in *shIft88*-expressing C2C12 myoblasts. A possible explanation could be, that actin modulation and endocytosis in myoblasts is not dependent on Ift88 itself. Taken together, although total Rac1 and Cdc42 expression is reduced in *shIft88*-expressing C2C12 myoblasts, I could not find an indication for altered endocytosis or actin remodeling.

6.4 Primary cilia involvement in myoblast function

6.4.1 Primary cilia involvement in myoblast Notch signaling

Epidermal cells showed colocalization of Notch3 and Presenilin-2 (a subunit of γ-secretase) with the cilium, suggesting a role for primary cilia in Notch signaling and skin development (Ezratty et al. 2011). To date, loss of *Ift88* has been shown to diminish Notch signaling in mouse corneal epithelial and epidermal cells, leading to defects in differentiation and proliferation. Therefore, the primary cilium is suggested to regulate cell fate and homeostasis by the regulation of Notch signaling (Ezratty et al. 2011; Grisanti et al. 2016). Regulation of Notch signaling in SC is crucial for proper muscle regeneration and SC maintenance. The link

between primary cilia in myoblasts and Notch signaling is poorly understood so far. I have shown that knock-down of *Ift88* in C2C12 myoblasts results in a decreased percentage of ciliated cells (25% ciliated *LacZ*-expressing C2C12, 11% ciliated *shIft88*-expressing C2C12). Concomitantly, NICD1 signaling was approximately 2-fold increased in this cells. Further, I detected enhanced Notch1 and Jagged1 protein expression in *Ift88*-depleted myoblasts.

Increased Notch signaling activity has been associated with differentiation of the cell. For example, epidermal cells of the interfollicular epidermis and hair follicles that have committed to differentiation or undergo differentiation show increased Notch signaling activity compared to not differentiating cells (Favier et al. 2000; Kopan and Weintraub 1993; Pan et al. 2004; Powell et al. 1998). In contrast, ciliated SC exhibit high levels of Notch signaling during quiescence and Notch signaling is downregulated during differentiation (Bjornson et al. 2012; Liu et al. 2013; Mourikis, Sambasivan, et al. 2012; Wen et al. 2012). These results show cell type specific differences in Notch pathway activity. However, the precise nature of the molecular interaction between Notch and the primary cilia machinery remains elusive. Immunofluorescent staining of Notch components could help to characterize the spatial relationship between the ciliary and plasma membrane in myoblasts. So far, investigations of suprabasal epidermal cells showed accumulation of Notch3 at the primary cilium (Ezratty et al. 2011). Notch signaling in *Ift88*-depleted C2C12 cells is elevated, which could indicate the loss of deactivating feedback mechanisms repressing *Notch1*, *Jagged1* and NICD1. In zebrafish, cilia-related proteins bbs1 and bbs4 have been shown involved in primary-cilia independent Notch receptor endosomal trafficking and sorting after activation. *Bbs1* and *bbs4* morphants showed accumulation of Notch receptors in late endosomes, due to aberrant endosomal sorting (Leitch et al. 2014). The observed overabundance of Notch1 and Jagged1 in *shIft88*-expressing C2C12 cells does not indicate the subcellular localization of the protein, an accumulation in vesicles caused by defective vesicular trafficking cannot be excluded. However, transferrin and Dll4 internalization experiments did not indicate defective endocytosis in *shIft88*-expressing C2C12 myoblasts. Further, I could not detect an indication for alterations in actin remodeling. Therefore, there is no indication for the same mechanism in myoblasts, as described for zebrafish.

Increased NICD1 signaling activity could be caused by defective negative regulation mechanisms. Notch is regulated by Numb, a cytoplasmic adaptor protein mediating the binding of Notch1 receptor and NICD1 to the E3 ubiquitin ligase Itch during myogenesis (Beres et al. 2011; McGill et al. 2009; McGill and McGlade 2003; Qiu et al. 2000). In 50% of human breast cancer, increased cell proliferation was linked to increased Notch signaling due to alterations in Numb mediated proteasomal degradation (Pece et al. 2004). In addition to *Notch1*, *Gli1* mRNA is significantly upregulated in *shIft88*-expressing C2C12 myoblasts, which

is commonly associated with increased Shh signaling. Since Numb also regulates Gli1 proteasomal degradation by Itch (Di Marcotullio et al. 2007, 2011), these results strongly point on a deregulation of Numb functionality in *Ift88*-depleted myoblasts. Defective feedback mechanisms might induce continuous expression of *Notch1*, *Jagged1* and *Gli1*. Due to the need of Notch regulation during SC activation and myoblast differentiation, Numb has been shown to be involved in muscle regeneration. Numb-deficient C2C12 myoblasts and SC have been shown to have defective differentiation and proliferation, thereby inhibiting normal skeletal muscle regeneration (George et al. 2013; Kuang et al. 2009). Several ciliary proteins are involved in the regulation of proteasomal activity (Gerdes et al. 2007; Gerhardt et al. 2015; Liu et al. 2014) and the “cilia-regulated proteasome” is associated with different ciliopathies. Taken together, the results of this thesis for the first time showed a connection between the primary cilium and Notch signaling activity in muscle progenitor cells. Further, it gives a first indication for the involvement of aberrant proteasomal degradation as an underlying mechanism for enhanced Notch signaling activity.

6.4.2 Primary cilia involvement in myoblast differentiation

Increased Notch signaling activity is needed to keep SC in a quiescent state. *shIft88*-expressing C2C12 myoblasts show increased Notch1 expression and NICD1 activity compared to control. During differentiation, *Ift88* knock-down cells showed decreased *MyoD* expression as well as diminished regeneration efficiency, as determined by differentiation and fusion index. These results indicate a role of Ift88 in myoblast differentiation. Previous studies described effects of cilia-related Notch signaling deficiency on the differentiation processes in different cell types. Unlike satellite cells, where Notch signaling is required for quiescence, activation of Notch signaling drives differentiation in many other cell types. Cilia were ablated by knock-down of *Ift88* in keratinocytes or a conditional knock-out of *Ift88* during mouse embryogenesis. Consistently, Notch signaling was impaired, suggesting a role for the primary cilium per se. Reduced Notch signaling triggered defects in the differentiation and cell-fate decision during epidermal development before onset of Shh signaling (Ezratty et al. 2011). Defective Notch signaling in skin development has been described to be caused by reduced cleavage of the Notch receptor and NICD release at the ciliary base. Cells lacking cilia by conditional *Ift88* knock-out showed reduced Notch signal transduction which triggered defective epidermal differentiation (Ezratty et al. 2011; Ezratty, Pasolli, and Fuchs 2016). Moreover, Notch signaling was shown to be involved in the regulation of proliferation and vertical migration of basal corneal epithelial cells during differentiation (Grisanti et al. 2016). Therefore, the primary cilium has been implicated in Notch signaling and differentiation in a number of cell types.

Reduced differentiation efficiency of *shIft88*-expressing C2C12 cells has already been described. That study showed deregulated Shh signaling after the loss of cilia, which has been correlated to reduced differentiation efficiency of the cells (Fu et al. 2014). The authors did not describe the effect of cilia ablation on Notch signaling, which would have been important, since Notch is known as an indispensable regulator of SC quiescence, proliferation and differentiation. Results of this thesis filled this gap, showing increased NICD1 signaling and deficiency in differentiation of *shIft88*-expressing C2C12 myoblasts. In agreement with Fu and colleagues (Fu et al. 2014), I found reduced *Gli1* mRNA expression during C2C12 myoblast differentiation. In contrast, I detected increased *Gli1* expression in non-differentiated *shIft88*-expressing myoblasts compared to control cells. Increased Shh signaling has been described to reduce differentiation in rhabdomyosarcoma by repression of *MyoD* expression and the differentiation of embryonal myoblasts (Bren-Mattison and Olwin 2002; Gerber et al. 2007). I detected the same observations of reduced MyoD expression and differentiation efficiency in myoblasts with impaired ciliary function.

Zebrafish bbs1 and bbs7 knockout models showed expanded expression of the *shh* ligand in the pectoral fin/limb bud. However, *shh* expression in the neural tube was not affected (Tayeh et al. 2008). Shh signaling plays an important role in limb and fin patterning (Biesecker 2011; Riddle et al. 1993). Defective fin patterning is characterized by changes in fin skeletal elements, similar to defective limb patterning. Therefore, the upregulation of shh in the fin/limb bud of bbs1/bbs7 knock-out embryos could induce polydactyly, a common characteristic of Bbs. Further, MEF cells from *Bbs7*$^{-/-}$ mice showed an accumulation of Patched1 and Smoothened in cilia compared to wildtype control, going in hand with decreased response to Shh ligand (Zhang, Seo, et al. 2012). These results suggest a role of Bbs proteins in the exit of proteins from the cilium and in the regulation of signal transduction. Taken together, I showed deregulation of Notch and Shh signaling activity in non-differentiated C2C12 myoblasts with ciliary impairment. This observation strengthens the idea, that several pathways are affected in cells lacking cilia, the signaling hub of the cell. Most likely, Bbs phenotypes are linked to a combination of diverse deregulated signaling pathways with ciliary involvement.

Notch activity is critical for SC quiescence and is dramatically reduced after SC activation (Bjornson et al. 2012; Liu et al. 2013; Mourikis et al. 2012). Continuously active Notch1 signaling in SC keep this cells in quiescence, which could explain reduced differentiation of *shIft88*-expressing C2C12 cells in this study. It has been shown that Notch signaling is sufficient for *Pax7* expression of the cells and inhibition of myogenic markers, like MyoD (Kondoh, Sunadome, and Nishida 2007; Mourikis et al. 2012; Wen et al. 2012). Notch-related transcriptional activity is initiated by diffusion of NICD into the nucleus, subsequent binding of

NICD to CSL (CBF1, suppressor of hairless, Lag-1) transcription factor and induction of Notch-target gene expression like *Hey-1*, *Hes-1* and *Pax7* that inhibit the myogenic program (Buas, Kabak, and Kadesch 2010; Jarriault et al. 1995; Olguin and Olwin 2004; Sasai et al. 1992; Wen et al. 2012). Moreover, the NICD/CSL complex inhibits the expression of myogenic markers like *MyoD*. Consequently, Notch signaling inhibits myogenic differentiation (Kopan, Nye, and Weintraub 1994; Lindsell et al. 1995). In *Ift88*-depleted myoblasts, high NICD1 activity inhibits proper *MyoD* induction and myoblast activation, as shown in this study. Diminished fusion of myoblasts could be explained by reduced Shisa2 (Shisa family member 2) activity. Shisa2 is an adaptor for the modulation of transmembrane proteins and is repressed by high Notch signaling activity (Pei and Grishin 2012). Further, knock-down of *Shisa2* has been shown to reduce myoblast fusion efficiency due to modulations in the F-actin distribution (Liu et al. 2018). Therefore, Notch-regulated expression of *Shisa2* might explain reduced fusion of C2C12 myoblasts.

Based on previously published data and my own findings, a new model of cilia-related Notch signaling in the regulation of muscle regeneration can be drawn (**Schematic 12**). Here, *Ift88* knock-down and loss of ciliation in muscle progenitor cells leads to increased Notch1 signaling for example via reduced NICD1 degradation at cilia-related proteasomes. Elevated Notch signaling prevents the cells from proper activation and keeps the progenitor cells in a quiescent state. In addition, increased NICD1 activity represses myogenic markers and factors for efficient myoblast fusion. Therefore, *Ift88* knock-down results in reduced myogenic differentiation efficiency, as detected in this study. This model would explain cilia-related muscle mass loss in *Bbs4*$^{-/-}$ mice due to reduced regenerative capacity of the skeletal muscle.

Bbs4 loss-of-function does not abolish ciliogenesis, but affects ciliary functionality (Mykytyn et al. 2004). For example, mutations of *Bbs4* in cells and zebrafish have been shown to interfere with the regulation of signaling pathways by selective proteolysis by the cilia-related proteasome (Gerdes et al. 2007; Liu et al. 2014). Therefore, as described above for *shIft88*-expressing myoblasts, affecting ciliary function by *Bbs4* ablation could cause defective Notch signaling and increased NICD1 activity by decreased proteasomal degradation. High Notch signaling in *Bbs4*$^{-/-}$ SC could induce a similar effect of reduced skeletal muscle regeneration as suggested for *Ift88* knock-out myoblasts. Reduced *Tln2* expression in *Bbs4*$^{-/-}$ Soleus and EDL as well as differential expression of Notch-related candidate genes in *Bbs4*$^{-/-}$ EDL support this hypothesis. Tln2 has been shown to play an important role in myoblast fusion (Conti et al. 2009) and has been found upregulated in C2C12 and primary human myoblasts during myotube formation (Senetar, Moncman, and McCann 2007). Reduced regenerative capacities of skeletal muscle could cause muscle mass loss and grip strength reduction in *Bbs4*$^{-/-}$ mice, as described within this study. *In vitro* differentiation experiments on Bbs4-deficient C2C12

myoblasts could validate this hypothesis. Moreover, expression patterns of Notch signaling components in isolated muscle progenitor cells from *Bbs4*$^{-/-}$ and wildtype mice will show levels of Notch signaling activity. Based on our present understanding, I predict increased Notch signaling activity in *Bbs4*$^{-/-}$ myoblasts.

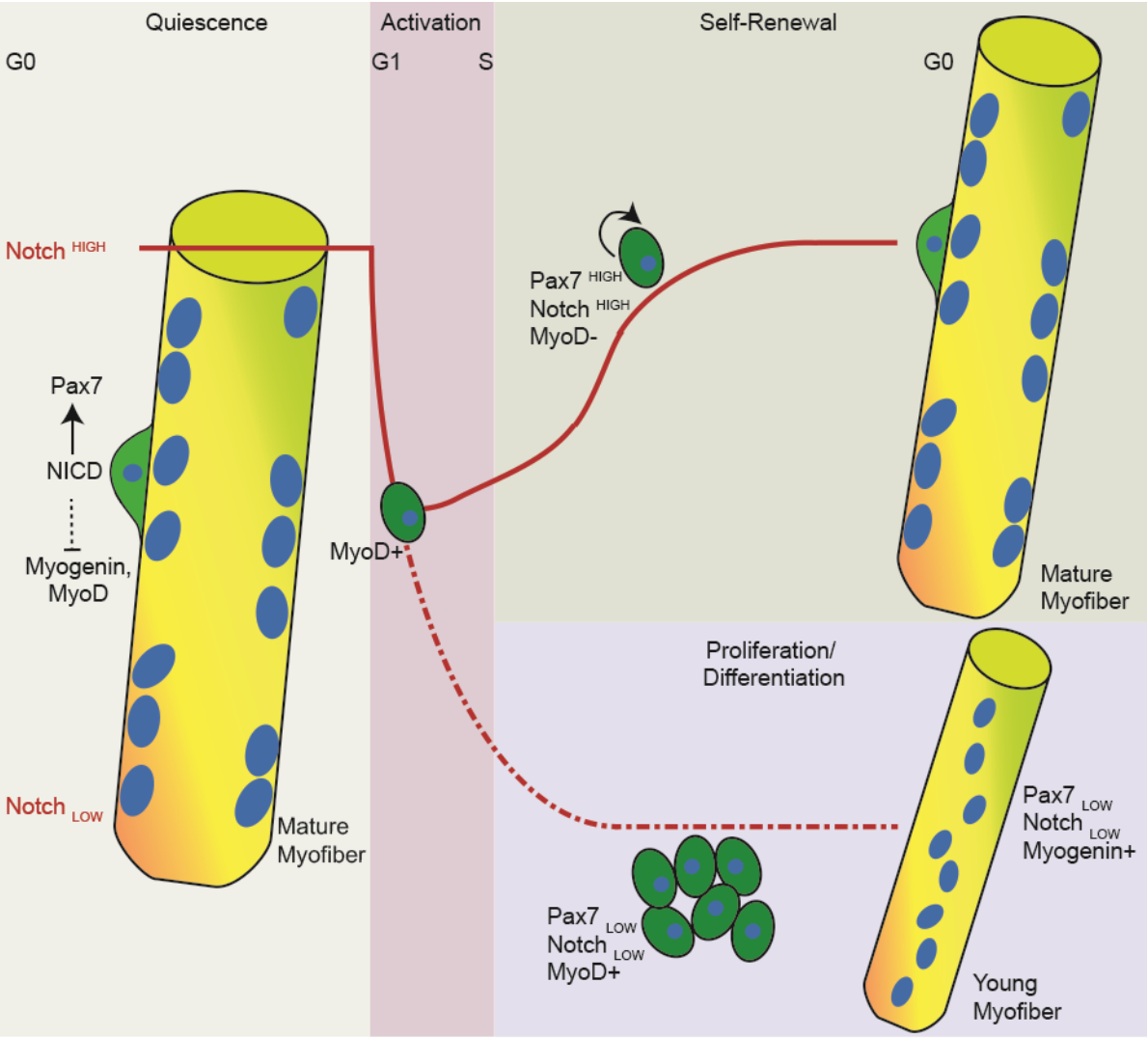

Schematic 12: Skeletal muscle regeneration model of myoblast with increased Notch signaling. Elevated Notch signaling activity in quiescent muscle progenitor cells prevents the cell from entering the myogenic program by continuous *Pax7* expression and *MyoD* repression. Insufficient Notch signaling downregulation during the activation phase inhibits proper *MyoD* expression and keeps the cells in an inactive state. Proliferation and differentiation are inhibited, causing reduced skeletal muscle regeneration.

Taken together, this study for the first time shows a skeletal muscle phenotype in *Bbs4*$^{-/-}$ mice before onset of obesity or hyperglycemia, indicated by lean mass and grip strength reduction. Further investigations of *Bbs4*$^{-/-}$ muscles and ciliary-impaired myoblasts indicated a role of

primary cilia in Notch signaling activity regulation and differentiation of skeletal muscle progenitor cells.

6.5 Gene editing as a potential treatment of muscle mass loss in ciliopathies

Preventing muscle mass loss is crucial for the motility of ciliopathy patients, but also patients of other muscular diseases. For the particular phenotype of diminished regeneration, muscle progenitor cells and not adult skeletal muscle can be addressed by gene editing of *Bbs4*. So far, SC targeting has been investigated in Duchenne muscular dystropthy (DMD). This disease is characterized by postnatal loss of muscle mass induced by mutations in the gene encoding Dystrophin, an essential structural protein in cardiac and skeletal muscle (Ervasti and Campbell 1991). Further, during the progression of DMD, satellite cells lose their ability to form new myofibers (Dumont et al. 2015; Sacco et al. 2010). Using the gene editing strategy CRISPR-Cas9, *mdx* mice (mutated *dystrophin* gene, model organism for DMD) have been shown to express functional dystrophin in cardiac muscle, skeletal muscle and SC. Therefore, an adapted CRISPR-Cas9 system has been used. One adaptation was the use of Cas9 from Staphylococcus aureus (SaCas9), which is a smaller ortholog of Cas9. Further, using the muscle-tropic serotype 9, SaCas9 was packed into recombinant AAV (adeno-associated virus) particles. A dual delivery system named “AAV-*Dmd*-CRISPR” could improve functional and structural aspects of skeletal muscle (Tabebordbar et al. 2016; Zincarelli et al. 2008). Unfortunately, the AAV-mediated delivery of CRISPR-Cas9 to SC is very low in the mouse model (<5%) (Tabebordbar et al. 2016). Similar studies using the CRISPR-Cas9 system with different AAV serotypes, gRNAs, routes of administration, regulatory elements and Cas9 proteins showed similar improvement of the skeletal muscle phenotype, but affected only differentiated striated muscle and not SC (Long et al. 2016; Nelson et al. 2016). Further adaptations of this technic have to be done to increase the delivery rate to SC. Instead of AAVs, also lipid-nanoparticle mediated delivery or cell penetrating peptides combined with muscle-homing peptides could be used to deliver Cas9 and gRNAs and might help to enhance efficiency of the system (Gao et al. 2014; Kim et al. 2014; Ramakrishna et al. 2014; Yin et al. 2016; Zuris et al. 2015). Besides *in vivo* therapy, extraction of muscle stem cells, *ex vivo* gene editing and transplantation to the patient could be another therapy approach, which is difficult to realize because SC are rare and difficult to expand. Further, they have to be delivered via intramuscular injection. However, this limitations might overcome by further adaptations of the method (Zhu et al. 2017). Once an efficient delivery system is discovered, it can be adapted to target mutations in *Bbs4* or *Ift88* for the treatment of muscle mass loss and proper SC differentiation in ciliopathies.

So far, ciliopathies cannot be cured because of its embryonal onset and multisystemic character. Present treatments rely on the treatment of single symptoms like diabetes, obesity, loss of vision, hypertension and renal failure, because a mechanism of whole-body gene editing is not investigated so far. Examples for treatments to prevent photoreceptor-loss are injection of Bbs4-AAV into the retina of *Bbs4*$^{-/-}$ mice or Dfnb21-AAV into the retina of *whirlin*$^{-/-}$ mice affected by Usher-syndrome 2d, another ciliopathy (Simons et al. 2011; Zou et al. 2011). Further, treatments against obesity comprise special diets, biatric surgery or antiobesity medication. Work on melanocortin receptor agonists seems to provide a promising tool against obesity (Seo et al. 2009). Other studies show that the cilium itself can be addressed. Here, ciliary beating of airway cells of patients affected by primary ciliary dyskinesia (PCD) was rescued by *ex vivo* gene editing (Lai et al. 2016). This work shows promising results for further studies concerning ciliary function. Present *in utero* gene editing experiments have been shown to cure heritable liver diseases in mice (Rossidis et al. 2018). *In vitro* fertilization experiments on human zygotes showed that gene editing at a very early stage is possible (Ma et al. 2017). To treat ciliopathies, gene editing of the zygote would be necessary. Although we have the technical possibilities to treat zygotes, this is long before diagnosis of the disease can be made. Further, the number of genes causing ciliopathies is high and even within a single family specific mutations can occur. Therefore, individual therapy and whole-exon sequencing or whole-genome sequencing is a pivotal tool to detect the kind of mutation for further gene editing.

However, investigations on muscular diseases like DMD will provide basic techniques which can be used in the therapy of skeletal muscle in ciliopathy and other diseases with a muscular phenotype. Until a new technique is found for whole-body gene editing, it will be only possible to treat single symptoms of ciliopathies. Therefore, further investigations have to be done to understand the molecular mechanisms underlying the disease. This new insights might can be used to find new forms of treatment. Within my thesis work, I discovered a muscular phenotype of *Bbs4*$^{-/-}$ mice and showed the importance of Ift88 for proper myoblast differentiation. I hope these investigations will support the understanding of ciliopathy phenotypes and the search for a therapy to improve patients' life quality.

7 Material and Methods

7.1 Material

7.1.1 Equipment

Agarose gel chamber	Mini (neolab)
	Midi (neolab)
Balances	ABS (Kern & Sohn GmbH)
	EWB (Kern & Sohn GmbH)
Cameras	AxioCam MRc (Zeiss)
Centrifuges	5804R (Eppendorf)
	5430C (Eppendorf)
	Ministar Microcentrifuge (VWR)
Cell counter	TC20™ Automated cell counter (Biorad)
Cryostat	Ag Protect (Leica)
ddH_2O	QPod (Millipore)
Electroporation system	Neon (Invitrogen)
Developer	ChemStudio SA^2 (Analytic Jena)
FACS	FACS Aria III (BD Biosciences)
Freezers	-20°C Medline, premium nofrost (Liebherr)
	-80°C (Thermo Scientific)
Fridge	4°C comfort (Liebherr)
Gel documentation system	UVsolo TS Imaging System (Biometra)
Glassware	Schott-Duran (Schott)
Grip strength meter	Bio GS-3 (Bioseb)
Ice machine	AF103 (Scotsman)
Incubation systems/ovens	Thermomixer Thermostat plus (Eppendorf)
	Oven (Thermo Scientific)
Incubators	BBD6220 (Thermo Scientific)
	Incubator C16 (Labortect)
	Innova42 (New Brunswick Scientific)
Magnetic resonance analyzer	EchoMRI 100 (EchoMRI)
Microscopes	Axiovert 200M (Carl Zeiss AG)
	AxioScope.A1 (Carl Zeiss AG)

	SP5 II (Leica)
Microwave	700W (Severin)
N_2 tank	Biostore systems (Cryo Anlagenbau GmbH)
PCR machines	Personal Thermocycler (Biometra)
	Professional Trio Thermocycler (Biometra)
	BioER GeneTouch (Biozym)
pH meter	Mettler Toledo FiveEasy (Hanna Instruments)
Photometer	NanoDrop 2000c (Thermo Fisher Scientific)
Pipettes	1000 µl / 200 µl / 20 µl / 10 µl / 2.5 µl Eppendorf Research (Eppendorf)
Pipetboys	Accu-jet pro (Brand GmbH)
	Pipetgirl (Integra)
Plate reader	Varioskan Lux (Thermo Scientific)
Polyacrylamid gel chamber	Biometra EcoMini (Analytic Jena)
Polyacrylamid blot chamber	Biometra EcoMini (Analytic Jena)
Power supply (gel chambers)	Power Source 300V (VWR)
qPCR cycler	ViiA7 Real-time PCR system (Life Technologies)
Roller/Mixers	VSR 23 (VWR international)
	Shaker DOS-10L (neolab)
	RMS (Assistent)
	Rocker 247 (Everlast)
Sterile hood	MSC Advantage (Thermo Scientific)
Stirrer	D-6011 (neolab)
Tissue Lyser	Tissue Lyser II (Quiagen)
Ultrasonic bath	Ultrasonic cleaner (VWR)
Vortexers	IKA Vortex 1 (IKA)
	Vortex-Genie 2 (Scientific Industries)
Water bath	WB10 (P-D Industriegesellschaft mbH)
	Aqualine 5 (Lauda)

7.1.2 Consumables, size standards and serum

50 ml/ 15 ml tubes	Falcon
2 ml/ 1.5 ml / 0.2 ml eppis	Eppendorf (safe-lock reaction tubes)
15 cm/ 10 cm/ 6 cm dishes	Thermo Scientific Fisher (nunc)

10 cm bacterial plates	Becton Dickinson GmbH (BD Falcon™)
6-,12-, 24-well plates	Thermo Scientific Fisher (nunc) (straight/conical)
96-well plate	Thermo Scientific Fisher (Nunclon Delta Surface, white bottom)
8-well chambers	IBIDI (IBIDI-treat 8-well imaging plates)
24-well plates	IBIDI (µ-Plate 24-well)
50 ml/ 25 ml plastic pipettes	Greiner bio-one
10 ml/ 5 ml/ 2 ml plastic pipettes	Greiner bio-one
10 µl/ 200 µl tips	Sarstedt
1000 µl tips	Biosphere
0.1 µl/ 0.5 µl/ 2 µl filter tips	Biosphere
10 µl/ 200 µl/ 1000 µl filter tips	Biosphere
Adhesive covers	Life Technologies (optical adhesive covers)
Blotting paper	GE Healthcare Buchler GmbH & Co (Whatman paper)
Cell strainer	Falcon (Nylon cell strainer 70 µm)
Cell culture inserts, netwell	VWR (Membrane Ø 15 mm, mesh size 74 µm)
Counting chambers	Biorad (counting slides dual chamber for cell counter)
Coverslips	Thermo Scientific (Menzel round, Ø 13 mm, #1)
	Thermo Scientific (Menzel, 24 mm x 50 mm, #1)
Cryovials	Sarstedt (2 ml)
Cuvettes	Brand (1.5 ml semi-micro)
DNA ladder	New England BioLabs (100 bp)
Donkey serum	Millipore
Embedding molds	Sigma (Peel-a-way embedding molds, S-22)
FACS tubes	Falcon (5 ml polypropene round bottom tube)
Glass slides	Thermo Scientific (45°)
	Thermo Scientific (Menzel Gläser SuperFrost Plus)
Goat serum	Biozol
Needles	Sterican 30G x ½ ``
Nitrocellulose membrane	Biorad
Parafilm	Pechiney Plastic Packaging
Pasteur pipettes, plastic	Carl Roth GmbH & Co. KG
PCR-stripes	Kisker Biotech
Protein ladder	Life Technologies (PageRuler Plus Pre-Stained)

qPCR 96-well plates	Life Technologies (MicroAmp Fast optical 96-well reaction plate)
qPCR 384-well plate	Thermo Scientific
Scalpels	Aesculap AG & Co
Syringes	Braun (Omnifix 30 ml / 3 ml)
Syringe filter	Millex-GP (Filter unit fast flow and low binding 0.22 µm)

7.1.3 Kits and Mastermix

Active Cdc42 Detection Kit (Cell Signaling Technology)

Active Rac1 Detection Kit (Cell Signaling Technology)

BLOCK.iT U6 RNAi Entry vector kit (Thermo Fisher Scientific)

Dual-Glo Luciferase Assay System (Promega)

ECL Detection Kit (Millipore)

Gene JET Plasmid Miniprep Kit (Thermo Fisher Scientific)

Gene JET Plasmid Maxiprep Kit (Thermo Fisher Scientific)

Gene JET Gel Extraction Kit (Thermo Fisher Scientific)

Maxima First Strand cDNA Synthesis Kit (Thermo Fisher Scientific)

Notch1/CSL Reporter Kit (Notch Signaling Pathway) (BPS Biosciences)

PCR Mycoplasma Test Kit (AppliChem)

Primer (Eurofins MWG Operon)

Pwo-Master (Roche)

QIAquick PCR Purification Kit (Qiagen)

RNeasy Mini Kit, RNeasy Micro Kit, miRNA Micro Kit (Qiagen)

SuperSignal West femto maximum sensitivity substrate (Life Technologies)

TaqMan Fast Advanced Master Mix (Life Technologies)

7.1.4 Chemicals

(If not indicated chemicals were purchased from Sigma-Aldrich, Merck or Carl Roth)

A Acetic acid

Acrylamide/bisacrylamide (Rotiphorese)

Agarose (Biozym Scientific)

APS

B BCA

BSA

Bromine phenol blue

C Calcium chloride

Chloroform, 99+%

Copper(II) sulfate

D DAPI

1,4-Diazabicyclo[2.2.2]octane (Dapco)

2,5-Dimethoxy-4-chloroamphetamine (DOC)

Dimethylsulfoxide (DMSO), >99,9%

Dithiothreitol (DTT)

DNAZap (Thermo Fisher Scientific)

dNTPs (Fermentas)

E EDTA

Ethanol, 96%

Ethidiumbromide

F Folin Phenol Reagent

G Glycerol

Glycine

H 10N HCl

HEPES (powder)

I Isopentane

Isopropanol, 100%

M Magnesium chloride

Methanol, 100%

Milk powder (Becton Dickinson)

M.O.M. (Vector)

Mounting medium – Jung Tissue Freezing medium (Leica)

MOPS

β-mercaptoethanol

N Nitrogen(l) (Linde AG, München)

NP40 (Life Technologies)

Oil Red-O

Opti-MEM I Reduced Serum Medium (Life Technologies)

P Paraformaldehyde

Penicillin/Streptomycin

Polyacrylamide

Polyvinyl-alcohol

Potassium chloride (KCl)

Potassium hydrogenphosphate (KH_2PO_4)

Propidium iodide

R RNaseZAP

S Sodium carbonate

Sodium chloride

Sodium desoxycholate

Sodium dodecyl sulphate (SDS)

Sodium hydrogenic phosphate (Na_2HPO_4)

Sodium hydroxide

Sodium potasium tartrate ($NaKC_4H_4O_6.4H_20$)

Sodium tetraborate ($Na_2B_2O_7$)

SuperBlock (PBS) blocking buffer (Thermo Fisher Scientific)

T Tamoxifen

TEMED

Triethylphosphate

Tris-base

Tris-HCl

Triton X-100

Trizol (Invitrogen)

Tween-20

7.1.5 Buffers and solutions

Western Blot

RIPA buffer:	150 mM NaCl, 1 mM EDTA, 0.1% DOC, 1% NP40, 50 mM Tris-HCl pH 7.4
Lowry A:	2% Na_2CO_3 in 0,1 M NaOH
Lowry B:	1% $CuSO_4$ in diH_20
Lowry C:	2% Sodium Potassium Tartrate ($NaKC_4H_4O_6.4H_20$) in H_2O
APS:	10% APS (in dH_2O)
4x Tris/SDS:	1.5 M Tris, 0.4% SDS (adjust to pH 8.8)
4x Tris/SDS:	0.5 M Tris, 0.4% SDS (adjust to pH 6.8)

4x SDS-loading buffer:	200 mM Tris/HCl, pH 6.8, 8% SDS, 40% Glycerol 0.4% bromine phenol blue (add freshly 400 mM DTT)
10x Running buffer:	25 mM Tris, 192 mM glycine, 0.1% SDS
10x Transfer buffer:	25 mM Tris, 192 mM glycine, 10% Methanol (add fresh)
10x TBST:	100 mM Tris/HCl, 1.5 M NaCl, 2% Tween-20 (adjust to pH 7.4)
Blocking solution:	5% milk powder in 1x TBST
(Femto-) ECL-solution:	Solution A and B mix: 1:1 (mix shortly before usage)

Immunostainings

10x PBS:	1.37 M NaCl, 26.8 mM KCl, 0.101 M Na_2HPO_4, 17.6 mM KH_2PO_4
PBST:	1x PBS + 0.1% Tween-20 (adjust to pH 7.4)
4% PFA:	1.3 M PFA in 1x PBS (adjust to pH 7.2 - 7.4)
Permeabilization buffer:	0.1% TritonX-100, 5% FBS in dH_2O
Blocking buffer:	0.1% Tween-20, 10% FBS, 3% serum (goat or donkey) in PBS
DAPI:	5 mg DAPI in 25 ml PBS
Elvanol (embedding):	0.015 mM Polyvinyl-alcohol, 24 mM Tris pH 6.0, 2 g DABCO in 90 ml H_2O and 37.8 ml Glycerol
M.O.M.:	2 drops M.O.M. (mouse on mouse blocking) in 2.5 ml PBS

DNA-Isolation

Lysis buffer:	100 mM Tris/HCl pH 8.5, 5 mM EDTA, 0.2% SDS, 200 mM NaCl
50x TAE:	50 mM EDTA, 2 M Tris, 1M acetic acid

7.1.6 Solutions for cell culture

DPBS (-Ca/-Mg)	Gibco
0.005% Trypsin-EDTA	Gibco
DMEM (4.5 g/l glucose)	Gibco
Penicillin/Streptomycin (100x)	Gibco
FCS	Sigma Aldrich
Bovine Calf Serum	Sigma Aldrich
Horse serum	Sigma Aldrich

7.1.7 Enzymes and inhibitors

DNA-Polymerase	Thermo Fisher Scientific (Taq DNA Polymerase, recombinant)
RNase-free DNase I	Qiagen
Phosphatase & Proteinase inhibitors	Thermo Fisher Scientific
Proteinase K	Roche

7.1.8 Antibodies

Table 1: List of primary antibodies for Western Blot analysis

Primary Antibody	Catalog number	Manufacturer
Fbx-32	ab74023	Abcam
Murf-1	AF5366	R&D Systems
Tiam1	ABN1488	Millipore
Tln2	ab105458	Abcam
Jagged1	2620S	Cell Signaling
Notch1	3608S	Cell Signaling
Aph1b	PA5-69997	Thermo Fisher Scientific
MyoD	MA-12902	Thermo Fisher Scientific
Rac1	8631S	Cell Signaling
Cdc42	8747	Cell Signaling
Ift88	13967-1-AP	Proteintech
Gapdh	CB1001	Merck Biosciences
Hsp90	4874	Cell Signaling
Gamma-tubulin	T5326	Sigma
ActinA	612656	BD Biosciences
Paxillin	AHO0492	Invitrogen

Table 2: List of secondary antibodies for Western Blot analysis

Secondary Antibody	Label	Catalog number	Manufacturer
Anti-mouse IgG	HRP	115-036-062	Dianova
Anti-rabbit IgG	HRP	12-348	Millipore
Anti-mouse IgG (H+L)	680LT	926-68022	Licor
Anti-rabbit IgG	680LT	926-68021	Licor
Anti-goat IgG	800CW	926-32214	Licor

Table 3: Primary antibodies for immunofluorescence

Primary Antibody	Catalog number	Manufacturer
Type I MHC	BA-D5	Developmental Studies Hybridoma Bank
Type IIa MHC	SC-71	Developmental Studies Hybridoma Bank
Type IIb MHC	BF-F3	Developmental Studies Hybridoma Bank
Neurofilament	2H3	Developmental Studies Hybridoma Bank
Synaptotagmin	ab32127	Abcam
GFP	GFP-1020	Aves Labs
RFP	ORD003515	Chromotek
Acetylated tubulin	T6793	Sigma-Aldrich
Arl13B	17711-1-AP	Proteintech
His-tag labeled with Alexa Fluor 647	4E3D10H2/E3	Thermo Fisher Scientific

Table 4: Secondary antibodies for immunofluorescence

Secondary Antibody	Label	Catalog number	Manufacturer
Anti-chicken IgY	Cy2	703-225-155	Dianova
Anti-rat IgG (H+L)	Cy3	712-165-153	Dianova
Anti-mouse IgG1 (γ1)	488	A21121	Invitrogen
Anti-mouse IgM (µ chain)	546	A-21045	Life Technologies
Anti-mouse IgG2b (γ2b)	405	SAB4600477	Sigma
Anti-rabbit IgG	647	A31573	Invitrogen
Anti-mouse IgG2b (γ2b)	647	A-21242	Life technologies
Phalloidin	546	A22283	Invitrogen
Bungarotoxin	555	B35451	Life Technologies

7.1.9 TaqMan primer

Table 5: TaqMan probes used for quantitative rtPCR

Probe	Catalog number	Manufacturer
Tln2	Mm00659397_m1	Thermo Fisher Scientific
Tiam1	Mm00437079_m1	Thermo Fisher Scientific

Bbs4	Mm00614565_m1	Thermo Fisher Scientific
Meg3	Mm00522599_m1	Thermo Fisher Scientific
Rcan1	Mm01213406_m1	Thermo Fisher Scientific
Hip2k	Mm00439329_m1	Thermo Fisher Scientific
Aph1b	Mm00781167_s1	Thermo Fisher Scientific
Jagged1	Mm00496902_m1	Thermo Fisher Scientific
Notch1	Mm00627185_m1	Thermo Fisher Scientific
Prdm16	Mm00712556_m1	Thermo Fisher Scientific
Ift88	Mm01313467_m1	Thermo Fisher Scientific
Gli1	Mm00494654_m1	Thermo Fisher Scientific

7.1.10 Cell line and culture medium

C2C12	immortal myoblast cell line derived from a C3H mouse donor (Blau et al. 1985; Yaffe and Saxel 1977)
Growth medium	DMEM (4.5 g/l glucose,) supplemented with 1x P/S (Gibco) and 10% FCS
Differentiation medium	DMEM (4.5 g/l glucose,) supplemented with 1x P/S (Gibco) and 2% HS

7.1.11 Mouse lines

Bbs4$^{-/-}$	Genetrap between exon 1 and 2 (Kulaga et al. 2004)
Ift88$^{flox/flox}$	floxed Ift88 (flox flanking exons 4 to 6; B6.129P2-Ift88$^{tm1Bky/J}$ (Haycraft et al. 2007))
HSA-MCM	Tamoxifen inducible Cre under control of human skeletal actin promoter (McCarthy et al. 2012)
ROSA26$^{mTmG/mTmG}$	Expression of membranous Tomato before, and membranous GFP after induction of Cre-mediated recombination (Muzumdar et al. 2007)

7.2 Methods

7.2.1 Ethical approval

Lentiviral treatments regarding to biosafety level 2 were registered at the Regierung von Oberbayern (55.2-1-54-2532-187-2015). Procedures with live animals were carried out

according to current animal welfare regulations with the approval of Regierung von Oberbayern (50-8791-8.1005.2021) and in compliance with the German Animal Protection Act, the guidelines of the Society of Laboratory Animals (GV-SOLAS) and Federation of Laboratory Animal Science Associations (FELASA).

7.2.2 Genotyping of mouse lines

DNA isolation

Genomic DNA was obtained from mouse ear punches. Therefore, tissue samples were lysed in 500 µl lysis buffer supplemented with 100 µg/ml proteinase K (fresh) overnight at 55°C. The next day samples were vortexed and remaining hair and cell fragments were pelleted by centrifugation (10 min, 14.000 rpm). DNA in the supernatant was precipitated with 500 µl isopropanol, mixed well and centrifuged (10 min, 14.000 rpm, 4°C). The DNA pellet was washed with 70% Ethanol (10 min, 14.000 rpm, 4°C), air-dried and resuspended in 60 µl nuclease-free water. To dissolve DNA better, sample was headed up to 60°C for 10 min.

Genotyping PCRs

Bbs4:

Primer: 5'-GTAACTGGCTTTTTGCATCACTCAT-3' / 5'-TCAGTTGGGGATACACAAATAAACC-3' / 5'-AAATGGCGTTACTTAAGCTAGCTTGC-3'

95°C 5 min - (95°C 30 s - 65°C 30s – 72°C 1 min) x9, each cycle 1 °C reduced annealing temperature – (95 °C 30 s – 55°C 30 s – 72°C 1 min) x24 – 72°C 10 min – 16°C pause

500 bp=wildtype allele, 300 bp=genetrapp allele

HSA-MCM:

Primer: 5´-CAC CAG CCA GCT ATC AAC TCG-3´ / 5´- TTA CAT TGG TCC AGC CAC CAG -3´

94°C 3 min - (94°C 45 s - 61°C 30s – 72°C 1 min) x40 – 72°C 3 min – 16°C pause

200 bp=positive for Cre

Ift88^{flox}:

Primer: 5´- GCCTCCTGTTTCTTGACAACAGTG-3´ / 5´-GGTCCTAACAAGTAAGCCCAGTGTT-3´ / 5´-CTGCACCAGCCATTTCCTCTAAGTCATGTA-3´

94°C 5 min - (94°C 30 s - 60°C 40s – 72°C 1 min) x35 – 72°C 10 min – 16°C pause

370 bp=floxed allele, 350 bp=wildtype allele, 270 bp=delta allele

***ROSA26$^{mTmG/mTmG}$*:**

Primer: 5´- CTCTGCTGCCTCCTGGCTTCT -3´ / 5´- CGAGGCGGATCACAAGCAATA -3´ / 5´- TCAATGGGCGGGGGTCGTT -3´

94°C 30 s - (94°C 30 s - 58°C 40s – 72°C 40 s) x35 – 72°C 10 min – 16°C pause

330 bp=wildtype allele, 250 bp=mTmG allele

Electrophoresis

Orange G (5 µl/sample) was added to the PCR product. 1.5% agarose gels were prepared in 1x TAE buffer, after cooling down Ethidiumbromide (1:20.000) was added and the gel was poured into agarose gel chambers. Gel running chambers were filled with 1x TAE buffer and sample was loaded on the gel. By applying voltage, the DNA fragments were separated by size. After running completed the PCR products were detected using the UV Solo gel documentation system.

7.2.3 Mouse line phenotyping

Tamoxifen induction

To induce Cre-mediated recombination of *HSA-MCM;Ift88$^{flox/flox}$* and *HSA-MCM;ROSA26$^{mTmG/mTmG}$*, mice between post-natal day 25 and day 35 were treated with 100 mg/kg bodyweight tamoxifen dissolved in corn oil by sonication for 2 h in the dark. Corn Oil was used as a control. The oral gavage was conducted once per day on 5 consecutive days.

Body composition and grip strength measurements

Body composition measurement by magnetic resonance analyzer (EchoMRI) and grip strength test were performed on 14 weeks old Bbs4 mice or 4 weeks after induction on *HSA-MCM;Ift88$^{flox/flox}$* mice. Before each of the two procedures, body weight of the mice was obtained with a standard balance. Absolute body composition values (lean and fat mass in grams) were used to calculate relative values with respect to the body weight. Absolute grip strength tests were performed with BIOSEB´s grip strength meter in grams in three measurements in a row per mouse. For this test it was crucial to let the mouse hold the grip

only with the two front legs parallel on the grid and to pull the mouse in a fast, homogene horizontal movement. The relative grip strength was calculated by dividing the absolute grip strength by the body weight.

Plug matings

For the investigation of E12.5 embryos of Bbs4 mice, timed pregnancies by plug matings were performed. Therefore, a female Bbs4$^{+/-}$ and a male Bbs4$^{+/-}$ were mated overnight. In the morning the female was separated from the male and checked for a vaginal plug, which consists of coagulated secretions from the male and lasts up to 12 h after breeding. Plug positive females were dissected 12 days after breeding for embryonic limb bud experiments.

7.2.4 Tissue dissection

Tissue isolation and processing

To prepare lysate of adult skeletal muscle (EDL, Soleus or Gastrocnemius) or E12.5 limb buds, tissue was carefully dissected and snap-frozen in liquid N_2-cooled isopentane. Afterwards muscles/limb buds were transferred in an eppi and stored at -80°C.

Post processing for RNA and protein

In order to lysate adult skeletal muscle tissue the frozen samples were transferred in a 2 ml eppi containing a stainless metal ball and 500 µl Trizol (RNA extraction) or Ripa buffer (protein extraction) supplemented with protease- and phosphatase inhibitor. Tissue was lysed in a tissue lyser for 45 s at 30 Hz.

Limb buds are a very soft tissue, compared to skeletal muscle. Therefore, it was enough to pipette the sample up and down with a 200 µl pipett several times in 100 µl Trizol (RNA extraction) or Ripa buffer (protein extraction) supplemented with protease- and phosphatase inhibitor.

7.2.5 Cell culture

C2C12 culture

Adherent C2C12 cells were cultured in Growth medium containing DMEM (4.5 g/l glucose), 1x P/S and 10% FCS. The medium was changed at least every 3rd day and cells were split 1:10 to 1:15 before reaching 70% confluence. Therefore, the dish was washed with 1x PBS

and trypsinized (0.05% trypsin EDTA, RT, 3 min). The reaction was stopped by adding Calf and the cells were transferred into 15 ml falcons for centrifugation (3 min, 1700 rpm). The supernatant was soaked and cells resuspended in 1 ml medium and plated for maintenance or experiments.

C2C12 differentiation

Cells were seeded and grown until confluence. Then medium was switched to Differentiation medium containing DMEM (4.5 g/l glucose), 1x P/S and 2% HS. Differentiation medium was changed every day for up to 5 d (end of experiments).

Cryopreservation

To make stocks, C2C12 were cryopreserved. Cells were trypsinized as described above, resuspended in 10% DMSO in Growth medium and transferred in cryovials. The cryovials were placed in freezing boxes and incubated overnight at -80°C. Afterwards cryovials were transferred to liquid N_2 for long time storage. If needed cells were thawed quickly in a water bath set to 37°C and transferred into a dish containing Growth medium. One day after thawing medium had to be changed. Afterwards cells were cultured as described above for two passages before being used in an experiment.

Cell cycle and proliferation analysis

FACS analysis of propidium iodide (PI) stained C2C12 was used for cell cycle analysis. PI intercalates into nucleic acids proportionally to the DNA content of the cell which makes it possible to investigate the amount of cells in G1-, G2- and S-phase. First, cells had to be trypsinized and fixed in 0.5 ml 70% ice-cold Ethanol. To get rid of the Ethanol cells were centrifuged (2 min, 4000 rpm) and resuspenden in 0.5 ml PBS containing 0.25% Triton X-100. After 15 min incubation on ice samples were centrifuged (2 min, 4000 rpm), supernatant was discarded and cell pellet was resuspended in 0.5 ml PBS containing 10 µg/ml RNase A and 20 µg/ml PI. The cells were transferred in FACS tubes and incubated for 30 min in the dark at RT before FACS analysis.

Rac1, Cdc42 activity and endocytosis assays

Rac1 and CdC42 activity assays were performed according to manufacturer´s instructions (Cell Signaling, 8815S and 8819S) on subconfluent C2C12 myoblasts.

As a gold standard for endocytosis I performed a transferrin uptake assay. Therefore, I added 0.01 µg/ml Alexa Fluor 633 labelled transferrin (Life Technologies) for up to 1 h to 1h starved (Opti-MEM medium) subconfluent C2C12 cells growing on coverslips. Every 15 min a subset of cells was fixed. Later, all cells were permeabilized, blocked and stained for actin cytoskeleton using phalloidin Alexa-555. Coverslips were transferred to slides and mounted with Elvanol. Stacks of the cells were taken at Leica SP5 confocal and maximum projections were used for measuring the intensity of Alexa Fluor 633 transferrin staining per cell (cells were defined on the base of actin staining) using ImageJ. The intensity was blotted against the time to illustrate time dependent transferrin endocytosis.

To investigate internalization of Notch-receptor bound Dll4, we added 2.0 µg/ml His-tag Dll4 (Thermo Fisher Scientific) for up to 75 min to 1h starved (Opti-MEM medium) subconfluent C2C12 cells growing on coverslips. Every 15 min a subset of cells was fixed. Later, all cells were permeabilized, blocked and stained for His-tag as well as actin using phalloidin Alexa-555. Coverslips were transferred to slides and mounted with Elvanol. Stacks of the cells were taken at Leica SP5 confocal and maximum projections were used for measuring the intensity of His-tag Dll4 staining per cell (cells were defined on the base of actin staining) using ImageJ. The intensity was blotted against the time to illustrate time dependent Dll4 internalization.

Notch1 activity assay

Notch1 signaling pathway activity was detected according to manufacturer's instructions (BPS Bioscience, 60509) on C2C12 myoblasts. Instead of Lipofectamnin 2000, we performed transfection of plasmids using Neon (Invitrogen) electroporation system according to manufacturer's setup for C2C12 cells.

C2C12 differentiation efficiency

C2C12 were differentiated as described above for 5 d in IBIDI µ-24 well-plates. Afterwards, cells were fixed, permeabilized, blocked and stained for actin cytoskeleton with phalloidin Alexa-555 and DAPI. Based on Leica SP5 maximum projections of the cells, the number of nuclei within one myotube was counted using LasX software as Fusion index. On the other hand, the differentiation index was calculated as percentual fraction of nuclei that are part of a myofiber.

7.2.6 RNA biochemistry

RNA work

To avoid degradation of RNA it is crucial to work with filter tips and to clean equipment and working places with RNaseZap.

RNA isolation

Total RNA was isolated using Trizol according to manufacturer´s protocol, dissolved in ddH_2O and stored at -80°C.

Determination of the RNA concentration

The concentration of isolated RNA was measured by a NanoDrop at extinction of 260 nm. Purity of the RNA was calculated by the quotient of E_{260nm}/E_{280nm} and E_{260nm}/E_{230nm}. RNA samples with a quotient around 2.0 were stated as pure.

Reverse transcription

For the reverse transcription of RNA to cDNA 1 µg RNA was used according to manufacturer´s instructions of the Maxima First Strand cDNA synthesis kit (Thermo Fisher Scientific).

Quantitative real-time PCR (qPCR)

TaqMan qPCR was performed with 1 µl of the cDNA product, 5 µl TaqMan Fast Advanced Master Mix (Life Technologies), 3.5 µl ddH_2O and 0.5 µl TaqMan probe per reaction. All components were pipetted in the qPCR plate and the plate was sealed and centrifuged briefly. The real-time qPCR reaction was performed using the Viia7 cycler (Thermo Fisher Scientific). The C_t-values, a point of linear slope of fluorescence, were normalized among samples, transformed to linear expression values, normalized on reference genes and on the control samples.

Relative expression (gene) = $(2^{Ct\ (mean\ genes) - Ct\ (gene)})$ / $(2^{Ct\ (mean\ references) - Ct\ (reference)})$.

Normalized expression (gene) = Relative expression (gene) / Relative expression $_{control}$ (gene).

The normalized gene expression was displayed by bar graphs ± standard deviation. Significance was determined using a Student´s t-test.

7.2.7 Protein biochemistry

To avoid protein degradation, protease and phosphatase inhibitor had to be added fresh to Ripa buffer according to manufacturer's instructions. All steps had to be carried out on ice or at 4°C.

Determination of protein concentrations

Plated cells were lysed with 500 µl Ripa buffer supplemented with protease- and phosphatase inhibitor on 10 cm dishes. Dissected tissue was lyses as stated above. To ensure high protein yield, sample lysates were kelp on ice over 30 min and vortexed several times during incubation. Protein concentration was determined using Lowry assay. Therefore, 20 µl of sample were transferred to a new tube and 100 µl of 10% DOC as well as 880 µl ddH_2O were added. Lowry D was mixed fresh (Lowry A+B+C 100:1:1) and 2 ml were added per sample. After 10 min incubation, 200 µl of Folin (Folin phenol reagent + ddH_2O 1:1) were added, sample was mixed by vortexing. After 30 min incubation the absorbance was read in a NanoDrop in cuvettes at 750 nm. Absorbtion ranged from 0 to 1 IU.

Calculation of protein in µg/ml: Absorbtion [IU]/0.006x1000(sample+DOC+ddH_2O)/20(amount of sample used).

SDS-PAGE

Western Blot analysis is based on the separation of proteins according to their size. Proteins can be blotted to a membrane, specifically stained with primary and secondary horse radish peroxidase labeled antibodies and quantified.

First, SDS poly acrylamid gels were casted, separated in stacking and 10% separation gel. For 4x 10% separation gels 15.18 ml acrylamide/bisacrylamide-mixture, 11.5 ml 4x Tris/SDS buffer pH 8.8, 18.86 ml H_2O, 23 µl TEMED, 230 µl APS were mixed and poured. After 45 min polymerization the stacking gel was mixed (2.18 ml acrylamide/bisacrylamide-mixture, 4.1 ml 4x Tris/SDS buffer pH 6.8, 10.0 ml H_2O, 16.2 µl TEMED, 82 µl APS), added on top of the separation gel and a comb was used to generate pockets in the gel. The stocking gel needed another 30 min to polymerize. Second, protein lysates had to be prepared. Therefore, protein lysates were supplemented with 4x SDS loading buffer (one third of sample volume) and boiled for 10 min at 95°C. During this process proteins denaturate and get covered by negatively charged SDS. Samples were loaded on different pockets of the gel, protein ladder

for size determination was added to one pocket as well. By application of electricity, negatively charged proteins started migrating towards the positive charged anode, thereby separated by size, since large proteins migrate slower in the gel than small proteins.

Western Blot

After separation of the proteins in SDS poly acrylamide gels, proteins were transferred to nitrocellulose membranes applying electricity in a wet transfer system using 1x transfer buffer. The blots were assembled in the following order: cathode – 2x blotting paper – gel – nitrocellulose membrane – 2x blotting paper – anode. After blotting for 1 h at 80 V, the membrane was blocked in 5% milk (5% milk powder in TBS-T) for 1 h at RT to saturate unspecific binding sites of the antibodies. The primary antibody was diluted in 5% milk and the membrane was incubated in primary antibody at 4°C overnight. The membrane was washed 3x 15 min in TBS-T prior to incubation with secondary antibody diluted in 5% milk for 1 h at RT. The membrane was washed 3x 15 min in TBS-T. To develop the membranes, ECL or Femto reagent were added and the signal was detected in the developer ChemStudio SA^2 (Analytic Jena).

7.2.8 Immunostaining

Cryosections

Dissected skeletal muscle were snap-frozen in liquid N_2 cooled isopentane and stored in cryotubes at -80°C. Before cutting, the samples were chilled to -21°C in the cryostat (Leica). Muscles were fixed with a drop of tissue embedding medium (Leica) to the sample holder and 14-40 µm thick sections were cut, depending on the experiment. The sections were either transferred to SuperFrost glass slides (Thermo Scientific) or fixed in Methanol + Aceton 1:1 for NMJ staining. Sections on glass slides were stored at -80°C.

The dissected smooth and cardiac muscle tissue was fixed in 4% paraformaldehyde (PFA) for 2 hrs at RT and 2 hrs at 4°C. Afterwards the tissues were washed 3x in PBS and cryoprotected in a serial gradient of 5% (1 h), 15% (1h) and 30% (overnight) sucrose in PBS. The next day the tissue samples were incubated for 2 h in 30% sucrose + tissue embedding medium (Leica) 1:1. The tissue samples were placed in embedding molds, covered with tissue embedding medium and frozen on dry ice. For storage, the tissues were kept at -80°C. Before sectioning at -20°C the samples were chilled in the cryostat. In order to prepare cryosections, the cardiac and smooth muscle tissues were cut in 20 µm thick sections using a cryostat (Leica) and transferred to SuperFrost glass slides (Thermo Scientific). Glass slides containing samples

were stored at -80°C.

Immunostaining of cryosections

Cryosections of skeletal muscle were rehydrated with PBS for 10 min, permeabilized for 30 min in permeabilization buffer and blocked 30 min in blocking buffer (for fiber typing M.O.M. (Vector) was used for blocking). Staining with the primary antibody in blocking buffer occurred overnight at 4°C. Afterwards the sections were washed 3x with PBS before incubation with secondary antibody in blocking buffer for 1 h at RT. The sections were washed twice and stained with DAPI (1:500 in PBS) for 10 min, washed once more and mounted with Elvanol and a coverslip.

Cryosections of *HSA-MCM;ROSA26*$^{mTmG/mTmG}$ mice were washed 3x with PBS and permeabilized 45 min in 0.2% Triton and 0.1% Glycine in PBS at RT. After permeabilization, the sections were washed once and blocked in blocking buffer for 1 h at RT. Primary antibodies were diluted in blocking buffer and applied for 2 h at RT and later overnight at 4°C to the sections. The next day the sections were washed 3x with PBS and incubated with secondary antibody diluted in blocking buffer for 4 h at RT. Afterwards the sections were washed 3x and stained for 30 min with DAPI (1:500 in PBS). Washed sections were embedded with Elvanol and a coverslip.

Floating sections for staining of NMJ components were fixed in Methanol + Aceton 1:1 for 10 min directly after sectioning as described above. Sections were transferred to netwell inserts in 12-well plates for the following procedure. After washing once with PBS, sections were blocked with SuperBlock (PBS) blocking buffer for 1 h (Thermo Fisher Scientific), washed once and incubated with primary antibodies diluted in PBST at 4°C overnight. The next day sections were washed three times with PBS and secondary antibodies were applied for 2 h at RT. Bungarotoxin was added to the secondary antibody mix. Finally, the sections were washed 3x, stained with DAPI (1:500 in PBS) for 40 min, transferred to glass slides and embedded with Elvanol and a coverslip.

Immunostainings of C2C12 cells

C2C12 were grown on coverslips in 24-well plates, except cells for differentiation, which were grown, differentiated, stained and mounted in µ-24 well IBIDI plates. Cells were fixed for 10 min at 37°C with 4% PFA, washed, permeabilized with permeabilization buffer for 30 min at RT and blocked with blocking buffer for another 30 min at RT. The primary antibodies were diluted in blocking buffer and applied to the cells overnight at 4°C. The next day, C2C12 cells

were washed 3x with PBS, incubated with secondary antibodies in blocking buffer for 1 h at RT, washed 3x and stained with DAPI (1:500 in PBS) for 10 min. Finally, the coverslips were removed from the wells and sealed with Elvanol on glass slides or 300 µl Elvanol was added into the IBIDI plates per well.

Microscopy & Analysis

Images were acquired with the SP5 confocal (Leica) and analyzed using LAS AF or LasX software (Zeiss), Imaris software (Bitplane) or ImageJ (Fiji).

Oil Red-O staining

The staining was performed according to Koopman and colleagues (Koopman, Schaart, and Hesselink 2001) on 20 µm thick Gastrocnemius sections of *Bbs4* and *HSA-MCM;Ift88*$^{flox/flox}$ mice. Images were taken using Zeiss AxioScope.A1 equipped with an AxioCam MRc (Carl Zeiss AG).

7.2.9 Statistics

Results are presented as mean +/- standard deviation. Statistical significance was tested using SigmaPlot software (Systat). For single comparisons Student´s t-test was performed, for multiple comparisons one-way ANOVA. Values of $p<0.005$ were considered as statistically significant. * indicated *p*-values smaller than 0.05, ** ≤ 0.01, and *** ≤ 0.001.

8 List of Figures and Tables

8.1 List of Schematics

8.2 List of Figures

8.3 List of Tables

9 References

Abdelhamed, Z.A. et al. 2013. “Variable Expressivity of Ciliopathy Neurological Phenotypes That Encompass Meckel - Gruber Syndrome and Joubert Syndrome Is Caused by Complex de-Regulated Ciliogenesis, Shh and Wnt Signalling Defects.” *Human Molecular Genetics* 22(7): 1358–72.

Aggeler, J., and Z. Werb. 1982. “Initial Events during Phagocytosis by Macrophages Viewed from Outside and inside the Cell: Membrane-Particle Interactions and Clathrin.” *Journal of Cell Biology* 94(3): 613–23.

Ahlqvist, E. et al. 2018. “Novel Subgroups of Adult-Onset Diabetes and Their Association with Outcomes: A Data-Driven Cluster Analysis of Six Variables.” *The Lancet Diabetes and Endocrinology* 6(5): 361–69.

Albor, A. et al. 2006. “The Interaction of Piasy with Trim32, an E3-Ubiquitin Ligase Mutated in Limb-Girdle Muscular Dystrophy Type 2H, Promotes Piasy Degradation and Regulates UVB-Induced Keratinocyte Apoptosis through NFκB.” *Journal of Biological Chemistry* 281(35): 25850–66.

Altamirano, F. et al. 2014. “Whole Body Periodic Acceleration Is an Effective Therapy to Ameliorate Muscular Dystrophy in Mdx Mice.” *PLoS ONE* 9(9): e106590.

Andersen, H., M.D. Gjerstad, and J. Jakobsen. 2004. “Atrophy of Foot Muscles: A Measure of Diabetic Neuropathy.” *Diabetes Care* 27(10): 2382–85.

Badano, J.L. et al. 2003. “Identification of a Novel Bardet-Biedl Syndrome Protein, BBS7, That Shares Structural Features with BBS1 and BBS2.” *American Journal of Human Genetics* 72(3): 650–58.

Balass, M., E. Katchalski-Katzir, and S. Fuchs. 1997. “The α-Bungarotoxin Binding Site on the Nicotinic Acetylcholine Receptor: Analysis Using a Phage-Epitope Library.” *Proceedings of the National Academy of Sciences* 94(12): 6054–58.

Ballestri, S. et al. 2016. “Nonalcoholic Fatty Liver Disease Is Associated with an Almost Twofold Increased Risk of Incident Type 2 Diabetes and Metabolic Syndrome. Evidence from a Systematic Review and Meta-Analysis.” *Journal of Gastroenterology and Hepatology* 31(5): 936–44.

Bao, Z.Z., M. Lakonishok, S. Kaufman, and A.F. Horwitz. 1993. “Alpha 7 Beta 1 Integrin Is a Component of the Myotendinous Junction on Skeletal Muscle.” *Journal of Cell Science* 106(Pt 2): 579–89.

Basten, S.G., and R.H. Giles. 2013. “Functional Aspects of Primary Cilia in Signaling, Cell Cycle and Tumorigenesis.” *Cilia* 2(1): 6.

Bastiani, M. et al. 2009. “MURC/Cavin-4 and Cavin Family Members Form Tissue-Specific Caveolar Complexes.” *Journal of Cell Biology* 185(7): 1259–73.

Beales, P.L. et al. 1999. “New Criteria for Improved Diagnosis of Bardet-Biedl Syndrome: Results of a Population Survey.” *Journal of Medical Genetics* 36(6): 437–46.

———. 2003. “Genetic Interaction of BBS1 Mutations with Alleles at Other BBS Loci Can Result in Non-Mendelian Bardet-Biedl Syndrome.” *The American Journal of Human Genetics* 72(5): 1187–99.

———. 2007. “IFT80, Which Encodes a Conserved Intraflagellar Transport Protein, Is Mutated in Jeune Asphyxiating Thoracic Dystrophy.” *Nature Genetics* 39(6): 727–29.

Bell, J., and L.S. Penrose. 1958. “The Laurence-Moon Syndrome. in The Treasury of Human Inheritance.” *Cambridge University Press, Cambridge* 5(3): 51–96.

Bentzinger, C.F. et al. 2013. “Fibronectin Regulates Wnt7a Signaling and Satellite Cell Expansion.” *Cell Stem Cell* 12(1): 75–87.

Berbari, N. F., J. S. Lewis, et al. 2008. “Bardet-Biedl Syndrome Proteins Are Required for the Localization of G Protein-Coupled Receptors to Primary Cilia.” *Proceedings of the National Academy of Sciences of the United States of America* 105(11): 4242–46.

Berbari, N.F., A.D. Johnson, et al. 2008. “Identification of Ciliary Localization Sequences within the Third Intracellular Loop of G Protein-Coupled Receptors.” *Molecular Biology of the Cell* 19(4): 1540–47.

Berbari, N.F. et al. 2013. “Leptin Resistance Is a Secondary Consequence of the Obesity in Ciliopathy Mutant Mice.” *Proceedings of the National Academy of Sciences* 110(19): 7796–7801.

Beres, B.J. et al. 2011. “Numb Regulates Notch1, but Not Notch3, during Myogenesis.” *Mechanisms of Development* 128(5–6): 247–57.

Bergström, J., E. Hultman, and A.E. Roch-Norlund. 1972. “Muscle Glycogen Synthetase in Normal Subjects: Basal Values, Effect of Glycogen Depletion by Exercise and of a Carbohydrate-Rich Diet Following Exercise.” *Scandinavian Journal of Clinical and Laboratory Investigation* 29(2): 231–36.

Bi, P. et al. 2017. “Control of Muscle Formation by the Fusogenic Micropeptide Myomixer.” *Science* 356(6335): 323–27.

Biesecker, L.G. 2011. “Polydactyly: How Many Disorders and How Many Genes? 2010 Update.” *Developmental Dynamics* 240(5): 931–42.

Biressi, S., M. Molinaro, and G. Cossu. 2007. “Cellular Heterogeneity during Vertebrate Skeletal Muscle Development.” *Developmental Biology* 308(2): 281–93.

Birnbaum, M.J. 1989. “Identification of a Novel Gene Encoding an Insulin-Responsive Glucose Transporter Protein.” *Cell* 57(2): 305–15.

Bjornson, C.R.R. et al. 2012. “Notch Signaling Is Necessary to Maintain Quiescence in Adult Muscle Stem Cells.” *Stem Cells* 30(2): 232–42.

Blau, H.M. et al. 1985. “Plasticity of the Differentiated State.” *Science* 230(4727): 758–66.

Bodine, S.C. et al. 2001. “Identification of Ubiquitin Ligases Required for Skeletal Muscle Atrophy.” *Science* 294(5547): 1704–8.

Braun, B., C. Sharoff, S.R. Chipkin, and F. Beaudoin. 2004. “Effects of Insulin Resistance on Substrate Utilization during Exercise in Overweight Women.” *Journal of Applied Physiology* 97(3): 991–97.

Bren-Mattison, Y., and B.B. Olwin. 2002. “Sonic Hedgehog Inhibits the Terminal Differentiation of Limb Myoblasts Committed to the Slow Muscle Lineage.” *Developmental Biology* 242(2): 130–48.

Bricceno, K.V. et al. 2012. “Histone Deacetylase Inhibition Suppresses Myogenin-Dependent Atrogene Activation in Spinal Muscular Atrophy Mice.” *Human Molecular Genetics* 21(20): 4448–59.

Brooks-Worrell, B., and J.P. Palmer. 2011. “Is Diabetes Mellitus a Continuous Spectrum?” *Clinical Chemistry* 57(2): 158–61.

Brüning, J.C. et al. 1998. “A Muscle-Specific Insulin Receptor Knockout Exhibits Features of the Metabolic Syndrome of NIDDM without Altering Glucose Tolerance.” *Molecular Cell* 2(5): 559–69.

Buas, M.F., S. Kabak, and T. Kadesch. 2010. “The Notch Effector Hey1 Associates with Myogenic Target Genes to Repress Myogenesis.” *Journal of Biological Chemistry* 285(2): 1249–58.

Buisson, J. et al. 2013. “Intraflagellar Transport Proteins Cycle between the Flagellum and Its Base.” *Journal of Cell Science* 126(1): 327–38.

Cariou, B. et al. 2004. “Cellular and Molecular Mechanisms of Adipose Tissue Plasticity in Muscle Insulin Receptor Knockout Mice.” *Endocrinology* 145(4): 1926–32.

Castel, D. et al. 2013. “Dynamic Binding of RBPJ Is Determined by Notch Signaling Status.” *Genes and Development* 27(9): 1059–71.

Chan, D.C. et al. 2014. “Association between Skeletal Muscle Fat Content and Very-Low-Density Lipoprotein-Apolipoprotein B-100 Transport in Obesity: Effect of Weight Loss.” *Diabetes, Obesity and Metabolism* 16(10): 994–1000.

Charron, M.J., F.C. Brosius, S.L. Alper, and H.F. Lodish. 1989. “A Glucose Transport Protein Expressed Predominately in Insulin-Responsive Tissues.” *Proceedings of the National Academy of Sciences of the United States of America* 86(8): 2535–39.

Chiang, A.P. et al. 2006. “Homozygosity Mapping with SNP Arrays Identifies TRIM32, an E3 Ubiquitin Ligase, as a Bardet-Biedl Syndrome Gene (BBS11).” *Proceedings of the National Academy of Sciences of the United States of America* 103(16): 6287–92.

Chiu, T.T. et al. 2011. “Rac1 Signalling towards GLUT4/Glucose Uptake in Skeletal Muscle.” *Cellular Signalling* 23(10): 1546–54.

Christiansen, R.G., and J.M. Marshall. 1965. “A Study of Phagocytosis in the Ameba Chaos Chaos.” *The Journal of Cell Biology* 25(3): 443–57.

Clark, B.C., T.D. Law, and S. Lee Hong. 2015. “Editorial: ‘From Brain to Body: The Impact of Nervous System Declines on Muscle Performance in Aging.’” *Frontiers in Aging Neuroscience* 7: 66.

Cole, D.G. et al. 1998. “Chlamydomonas Kinesin-II-Dependent Intraflagellar Transport (IFT): IFT Particles Contain Proteins Required for Ciliary Assembly in Caenorhabditis Elegans Sensory Neurons.” *Journal of Cell Biology* 141(4): 993–1008.

Conboy, I.M., and T.A. Rando. 2002. “The Regulation of Notch Signaling Controls Satellite Cell Activation and Cell Fate Determination in Postnatal Myogenesis.” *Developmental Cell* 3(3): 397–409.

Conti, F.J. et al. 2009. “Talin 1 and 2 Are Required for Myoblast Fusion, Sarcomere Assembly and the Maintenance of Myotendinous Junctions.” *Development* 136(21): 3597–3606.

Cooper, A.J., and J.J. Cowley. 1976. “Mother-Infant Interaction in Mice Bulbectomised Early in Life.” *Physiology and Behavior* 16(4): 453–59.

Corbit, K.C. et al. 2005. “Vertebrate Smoothened Functions at the Primary Cilium.” *Nature* 437(7061): 1018–21.

Cox, K.F. et al. 2012. “Phenotypic Expression of Bardet-Biedl Syndrome in Patients Homozygous for the Common M390R Mutation in the BBS1 Gene.” *Vision Research* 75: 77–87.

Craft, J.M. et al. 2015. “Tubulin Transport by IFT Is Upregulated during Ciliary Growth by a

Cilium-Autonomous Mechanism." *Journal of Cell Biology* 208(2): 223–37.

Craige, B. et al. 2010. "CEP290 Tethers Flagellar Transition Zone Microtubules to the Membrane and Regulates Flagellar Protein Content." *Journal of Cell Biology* 190(5): 927–40.

Cruz-Jentoft, A.J. et al. 2010. "Sarcopenia: European Consensus on Definition and Diagnosis." *Age and Ageing* 39(4): 412–23.

Davenport, J.R. et al. 2007. "Disruption of Intraflagellar Transport in Adult Mice Leads to Obesity and Slow-Onset Cystic Kidney Disease." *Current Biology* 17(18): 1586–94.

Deacon, R.M.J. 2013. "Measuring the Strength of Mice." *Journal of Visualized Experiments* (76): e2610.

DeFronzo, R.A. et al. 1981. "Synergistic Interaction between Exercise and Insulin on Peripheral Glucose Uptake." *Journal of Clinical Investigation* 68(6): 1468–74.

Delaval, B., A. Bright, N.D. Lawson, and S. Doxsey. 2011. "The Cilia Protein IFT88 Is Required for Spindle Orientation in Mitosis." *Nature Cell Biology* 13(4): 461–70.

Delevoye, C. et al. 2016. "BLOC-1 Brings Together the Actin and Microtubule Cytoskeletons to Generate Recycling Endosomes." *Current Biology* 26(1): 1–13.

DeNies, M.S. et al. 2014. "Diet-Induced Obesity Alters Skeletal Muscle Fiber Types of Male but Not Female Mice." *Physiological Reports* 2(1): e00204.

Dickinson, M.E. et al. 2016. "High-Throughput Discovery of Novel Developmental Phenotypes." *Nature* 537(7621): 508–14.

Dresner, A. et al. 1999. "Effects of Free Fatty Acids on Glucose Transport and IRS-1-Associated Phosphatidylinositol 3-Kinase Activity." *The Journal of Clinical Investigation* 103(2): 253–59.

Dumont, N.A. et al. 2015. "Dystrophin Expression in Muscle Stem Cells Regulates Their Polarity and Asymmetric Division." *Nature Medicine* 21(12): 1455–63.

Egeberg, D.L. et al. 2012. "Primary Cilia and Aberrant Cell Signaling in Epithelial Ovarian Cancer." *Cilia* 1(1): 15.

Egorov, M.V. et al. 2009. "Faciogenital Dysplasia Protein (FGD1) Regulates Export of Cargo Proteins from the Golgi Complex via Cdc42 Activation." *Molecular Biology of the Cell* 20(9): 2413–27.

Eheman, C. et al. 2012. "Annual Report to the Nation on the Status of Cancer, 1975-2008, Featuring Cancers Associated with Excess Weight and Lack of Sufficient Physical Activity." *Cancer* 118(9): 2338–66.

Eichers, E.R. et al. 2006. "Phenotypic Characterization of Bbs4 Null Mice Reveals Age-Dependent Penetrance and Variable Expressivity." *Human Genetics* 120(2): 211–26.

Ervasti, J.M. et al. 1990. "Deficiency of a Glycoprotein Component of the Dystrophin Complex in Dystrophic Muscle." *Nature* 345(6273): 315–19.

Ervasti, J.M., and K.P. Campbell. 1991. "Membrane Organization of the Dystrophin-Glycoprotein Complex." *Cell* 66(6): 1121–31.

Ezratty, E.J. et al. 2011. "A Role for the Primary Cilium in Notch Signaling and Epidermal Differentiation during Skin Development." *Cell* 145(7): 1129–41.

Ezratty, E.J., H.A. Pasolli, and E. Fuchs. 2016. "A Presenilin-2-ARF4 Trafficking Axis Modulates Notch Signaling during Epidermal Differentiation." *Journal of Cell Biology*

214(1): 89–101.

Fan, Z.-C. et al. 2010. “Chlamydomonas IFT70/CrDYF-1 Is a Core Component of IFT Particle Complex B and Is Required for Flagellar Assembly.” *Molecular Biology of the Cell* 21(24): 4325–37.

Favier, B. et al. 2000. “Localisation of Members of the Notch System and the Differentiation of Vibrissa Hair Follicles: Receptors, Ligands, and Fringe Modulators.” *Developmental Dynamics* 218(3): 426–37.

Fei, D.L. et al. 2012. “Hedgehog Signaling Regulates Bladder Cancer Growth and Tumorigenicity.” *Cancer Research* 72(17): 4449–58.

Finetti, F. et al. 2009. “Intraflagellar Transport Is Required for Polarized Recycling of the TCR/CD3 Complex to the Immune Synapse.” *Nature Cell Biology* 11(11): 1332–39.

———. 2014. “Specific Recycling Receptors Are Targeted to the Immune Synapse by the Intraflagellar Transport System.” *Journal of Cell Science* 127(9): 1924–37.

Follit, J.A. et al. 2008. “The Golgin GMAP210/TRIP11 Anchors IFT20 to the Golgi Complex.” *PLoS Genetics* 4(12): e1000315.

Follit, J.A., R.A. Tuft, K.E. Fogarty, and G.J. Pazour. 2006. “The Intraflagellar Transport Protein IFT20 Is Associated with the Golgi Complex and Is Required for Cilia Assembly.” *Molecular Biology of the Cell* 17(9): 3781–92.

Fougerousse, F. et al. 2001. “The Muscle-Specific Enolase Is an Early Marker of Human Myogenesis.” *Journal of Muscle Research and Cell Motility* 22(6): 535–44.

Frosk, P. et al. 2002. “Limb-Girdle Muscular Dystrophy Type 2H Associated with Mutation in TRIM32, a Putative E3-Ubiquitin–Ligase Gene.” *The American Journal of Human Genetics* 70(3): 663–72.

Fu, W., P. Asp, B. Canter, and B.D. Dynlacht. 2014. “Primary Cilia Control Hedgehog Signaling during Muscle Differentiation and Are Deregulated in Rhabdomyosarcoma.” *Proceedings of the National Academy of Sciences* 111(25): 9151–56.

Fujimaki, S. et al. 2018. “Notch1 and Notch2 Coordinately Regulate Stem Cell Function in the Quiescent and Activated States of Muscle Satellite Cells.” *Stem Cells* 36(2): 278–85.

Fukada, S.-I. et al. 2011. “Hesr1 and Hesr3 Are Essential to Generate Undifferentiated Quiescent Satellite Cells and to Maintain Satellite Cell Numbers.” *Development* 138(21): 4609–19.

Gao, X. et al. 2014. “Effective Dystrophin Restoration by a Novel Muscle-Homing Peptide-Morpholino Conjugate in Dystrophin-Deficient Mdx Mice.” *Molecular Therapy* 22(7): 1333–41.

Gaster, M. et al. 2001. “GLUT4 Is Reduced in Slow Muscle Fibers of Type 2 Diabetic Patients: Is Insulin Resistance in Type 2 Diabetes a Slow, Type 1 Fiber Disease?” *Diabetes* 50(6): 1324–29.

Ge, X. et al. 2016. “Grip Strength Is Potentially an Early Indicator of Age-Related Decline in Mice.” *Pathobiology of Aging & Age-related Diseases* 6(1): 32981.

George, R.M. et al. 2013. “Numb-Deficient Satellite Cells Have Regeneration and Proliferation Defects.” *Proceedings of the National Academy of Sciences* 110(46): 18549–54.

Gerber, A.N., C.W. Wilson, Y.J. Li, and P.T. Chuang. 2007. “The Hedgehog Regulated Oncogenes Gli1 and Gli2 Block Myoblast Differentiation by Inhibiting MyoD-Mediated Transcriptional Activation.” *Oncogene* 26(8): 1122–36.

Gerdes, J.M. et al. 2007. “Disruption of the Basal Body Compromises Proteasomal Function and Perturbs Intracellular Wnt Response.” *Nature Genetics* 39(11): 1350–60.

———. 2014. “Ciliary Dysfunction Impairs Beta-Cell Insulin Secretion and Promotes Development of Type 2 Diabetes in Rodents.” *Nature Communications* 5: 5308.

Gerhardt, C. et al. 2015. “The Transition Zone Protein Rpgrip 1l Regulates Proteasomal Activity at the Primary Cilium.” *Journal of Cell Biology* 210(1): 115–33.

Gilda, J.E. et al. 2015. “Western Blotting Inaccuracies with Unverified Antibodies: Need for a Western Blotting Minimal Reporting Standard (WBMRS).” *PLoS ONE* 10(8): e0135392.

Gomes, M.D. et al. 2001. “Atrogin-1, a Muscle-Specific F-Box Protein Highly Expressed during Muscle Atrophy.” *Proceedings of the National Academy of Sciences of the United States of America* 98(25): 14440–45.

Goodyear, L.J. et al. 1990. “Contractile Activity Increases Plasma Membrane Glucose Transporters in Absence of Insulin.” *American Journal of Physiology* 258(4 Pt 1): 667–72.

———. 1995. “Effects of Contractile Activity on Tyrosine Phosphoproteins and PI 3-Kinase Activity in Rat Skeletal Muscle.” *American Journal of Physiology-Endocrinology and Metabolism* 268(5): 987–95.

Grace, C. et al. 2003. “Energy Metabolism in Bardet-Biedl Syndrome.” *International Journal of Obesity* 27(11): 1319–24.

Grady, R.M. et al. 1999. “Role for α-Dystrobrevin in the Pathogenesis of Dystrophin-Dependent Muscular Dystrophies.” *Nature Cell Biology* 1(4): 215–20.

———. 2000. “Maturation and Maintenance of the Neuromuscular Synapse: Genetic Evidence for Roles of the Dystrophin-Glycoprotein Complex.” *Neuron* 25(2): 279–93.

Le Grand, F. et al. 2009. “Wnt7a Activates the Planar Cell Polarity Pathway to Drive the Symmetric Expansion of Satellite Stem Cells.” *Cell Stem Cell* 4(6): 535–47.

Green, J.S. et al. 1989. “The Cardinal Manifestations of Bardet-Biedl Syndrome, a Form of Laurence-Moon-Biedl Syndrome.” *The New England Journal of Medicine* 321(15): 1002–9.

Grisanti, L., E. Revenkova, R.E. Gordon, and C. Iomini. 2016. “Primary Cilia Maintain Corneal Epithelial Homeostasis by Regulation of the Notch Signaling Pathway.” *Development* 143(12): 2160–70.

Grover, S.A. et al. 2015. “Years of Life Lost and Healthy Life-Years Lost from Diabetes and Cardiovascular Disease in Overweight and Obese People: A Modelling Study.” *The Lancet Diabetes and Endocrinology* 3(2): 114–22.

Gruenbaum-Cohen, Y. et al. 2012. “The Actin Regulator N-WASp Is Required for Muscle-Cell Fusion in Mice.” *Proceedings of the National Academy of Sciences* 109(28): 11211–16.

Guo, D.-F. et al. 2011. “Inactivation of Bardet-Biedl Syndrome Genes Causes Kidney Defects.” *Renal Physiology* 300(2): 574–80.

Guo, D.F. et al. 2016. “The BBSome Controls Energy Homeostasis by Mediating the Transport of the Leptin Receptor to the Plasma Membrane.” *PLoS Genetics* 12(2): e1005890.

Harnett, J.D. et al. 1988. “The Spectrum of Renal Disease in Laurence–Moon–Biedl Syndrome.” *New England Journal of Medicine* 319(10): 615–18.

Hawley, J.A., E.J. Schabort, T.D. Noakes, and S.C. Dennis. 1997. “Carbohydrate-Loading and

Exercise Performance." *Sports Medicine* 24(2): 73–81.

Haycraft, C.J. et al. 2001. "The C. Elegans Homolog of the Murine Cystic Kidney Disease Gene Tg737 Functions in a Ciliogenic Pathway and Is Disrupted in Osm-5 Mutant Worms." *Development* 128(9): 1493–1505.

———. 2005. "Gli2 and Gli3 Localize to Cilia and Require the Intraflagellar Transport Protein Polaris for Processing and Function." *PLoS Genetics* 1(4): e53.

———. 2007. "Intraflagellar Transport Is Essential for Endochondral Bone Formation." *Development* 134(2): 307–16.

He, Q. et al. 2014. "Primary Cilia in Stem Cells and Neural Progenitors Are Regulated by Neutral Sphingomyelinase 2 and Ceramide." *Molecular Biology of the Cell* 25(11): 1715–29.

Heath, G.W. et al. 1983. "Effects of Exercise and Lack of Exercise on Glucose Tolerance and Insulin Sensitivity." *Journal of Applied Physiology (Bethesda, Md. : 1985)* 55(2): 512–17.

Hehnly, H., K.M. Longhini, J.-L. Chen, and M. Stamnes. 2009. "Retrograde Shiga Toxin Trafficking Is Regulated by ARHGAP21 and Cdc42." *Molecular Biology of the Cell* 20(20): 4303–12.

Hernandez-Hernandez, V. et al. 2013. "Bardet-Biedl Syndrome Proteins Control the Cilia Length through Regulation of Actin Polymerization." *Human Molecular Genetics* 22(19): 3858–68.

Hickey, M.S. et al. 1995. "Skeletal Muscle Fiber Composition Is Related to Adiposity and in Vitro Glucose Transport Rate in Humans." *American Journal of Physiology-Endocrinology and Metabolism* 268(3): 453–57.

Hill, M.M. et al. 2008. "PTRF-Cavin, a Conserved Cytoplasmic Protein Required for Caveola Formation and Function." *Cell* 132(1): 113–24.

Hilton, T.N. et al. 2008. "Excessive Adipose Tissue Infiltration in Skeletal Muscle in Individuals With Obesity, Diabetes Mellitus, and Peripheral Neuropathy: Association With Performance and Function." *Physical Therapy* 88(11): 1336–44.

Van Horn, R., and M.T. Crow. 1989. "Fast Myosin Heavy Chain Expression during the Early and Late Embryonic Stages of Chicken Skeletal Muscle Development." *Developmental Biology* 134(2): 279–88.

Horst, D. et al. 2006. "Comparative Expression Analysis of Pax3 and Pax7 during Mouse Myogenesis." *International Journal of Developmental Biology* 50(1): 47–54.

Huang, P., and A.F. Schier. 2009. "Dampened Hedgehog Signaling but Normal Wnt Signaling in Zebrafish without Cilia." *Development* 136(18): 3089–98.

Huangfu, D. et al. 2003. "Hedgehog Signalling in the Mouse Requires Intraflagellar Transport Proteins." *Nature* 426(6962): 83–87.

Hutcheson, D.A. et al. 2009. "Embryonic and Fetal Limb Myogenic Cells Are Derived from Developmentally Distinct Progenitors and Have Different Requirements for β-Catenin." *Genes and Development* 23(8): 997–1013.

Huxley, A.F., and R. Niedergerke. 1954. "Structural Changes in Muscle During Contraction: Interference Microscopy of Living Muscle Fibres." *Nature* 173(4412): 971–73.

Huxley, H., and J. Hanson. 1954. "Changes in the Cross-Striations of Muscle during Contraction and Stretch and Their Structural Interpretation." *Nature* 173(4412): 973–76.

Iannaccone, A. et al. 2005. “Clinical Evidence of Decreased Olfaction in Bardet-Biedl Syndrome Caused by a Deletion in the BBS4 Gene.” *American Journal of Medical Genetics* 132 A(4): 343–46.

Ishikawa, H. et al. 2014. “TTC26/DYF13 Is an Intraflagellar Transport Protein Required for Transport of Motility-Related Proteins into Flagella.” *eLife* 2014(3): e01566.

Ivy, J.L. et al. 1988. “Muscle Glycogen Synthesis after Exercise: Effect of Time of Carbohydrate Ingestion.” *Journal of Applied Physiology* 64(4): 1480–85.

Jacobs, E. et al. 2017. “Healthcare Costs of Type 2 Diabetes in Germany.” *Diabetic Medicine* 34(6): 855–61.

James, D.E., M. Strube, and M. Muecdler. 1989. “Molecular Cloning and Characterization of an Insulin-Regulatable Glucose Transporter.” *Nature* 338(6210): 83–87.

Janich, P., and D. Corbeil. 2007. “GM1 and GM3 Gangliosides Highlight Distinct Lipid Microdomains within the Apical Domain of Epithelial Cells.” *FEBS Letters* 581(9): 1783–87.

Janssen, I., S.B. Heymsfield, Z.M. Wang, and R. Ross. 2000. “Skeletal Muscle Mass and Distribution in 468 Men and Women Aged 18–88 Yr.” *Journal of Applied Physiology* 89(1): 81–88.

Jarriault, S. et al. 1995. “Signalling Downstream of Activated Mammalian Notch.” *Nature* 377(6547): 355–58.

JeBailey, L. et al. 2004. “Skeletal Muscle Cells and Adipocytes Differ in Their Reliance on TC10 and Rac for Insulin-Induced Actin Remodeling.” *Molecular Endocrinology* 18(2): 359–72.

———. 2007. “Ceramide- and Oxidant-Induced Insulin Resistance Involve Loss of Insulin-Dependent Rac-Activation and Actin Remodeling in Muscle Cells.” *Diabetes* 56(2): 394–403.

Jensen, J. et al. 2011. “Effects of Adrenaline on Whole-Body Glucose Metabolism and Insulin-Mediated Regulation of Glycogen Synthase and PKB Phosphorylation in Human Skeletal Muscle.” *Metabolism: Clinical and Experimental* 60(2): 215–26.

Jin, H. et al. 2010. “The Conserved Bardet-Biedl Syndrome Proteins Assemble a Coat That Traffics Membrane Proteins to Cilia.” *Cell* 141(7): 1208–19.

Johnson, K.A., and J.L. Rosenbaum. 1992. “Polarity of Flagellar Assembly in Chlamydomonas.” *Journal of Cell Biology* 119(6): 1605–11.

Jonassen, J.A., J.S. Agustin, J.A. Follit, and G.J. Pazour. 2008. “Deletion of IFT20 in the Mouse Kidney Causes Misorientation of the Mitotic Spindle and Cystic Kidney Disease.” *Journal of Cell Biology* 183(3): 377–84.

Jostes, B., C. Walther, and P. Gruss. 1990. “The Murine Paired Box Gene, Pax7, Is Expressed Specifically during the Development of the Nervous and Muscular System.” *Mechanisms of Development* 33(1): 27–37.

Juneja, R. et al. 2001. “Islet Cell Antibodies and Glutamic Acid Decarboxylase Antibodies, but Not the Clinical Phenotype, Help to Identify Type 1(1/2) Diabetes in Patients Presenting with Type 2 Diabetes.” *Metabolism* 50(9): 1008–13.

Kano, S., N. Miyajima, S. Fukuda, and S. Hatakeyama. 2008. “Tripartite Motif Protein 32 Facilitates Cell Growth and Migration via Degradation of Abl-Interactor 2.” *Cancer Research* 68(14): 5572–80.

Katsanis, N. et al. 2001. “Triallelic Inheritance in Bardet-Biedl Syndrome, a Mendelian Recessive Disorder.” *Science* 293(5538): 2256–59.

———. 2004. “The Oligogenic Properties of Bardet-Biedl Syndrome.” *Human Molecular Genetics* 13(Spec No 1): R65-71.

Keller, A. et al. 1992. “Activation of the Gene Encoding the Glycolytic Enzyme Beta-Enolase During Early Myogenesis Precedes an Increased Expression During Fetal Muscle Development.” *Mechanisms of Development* 38(1): 41–54.

Kelley, D. et al. 1988. “Skeletal Muscle Glycolysis, Oxidation, and Storage of an Oral Glucose Load.” *Journal of Clinical Investigation* 81(5): 1563–71.

Kelly, R.G. et al. 1997. “Embryonic and Fetal Myogenic Programs Act through Separate Enhancers at the MLC1F/3F Locus.” *Developmental Biology* 187(2): 183–99.

Kim, J.K. et al. 2000. “Redistribution of Substrates to Adipose Tissue Promotes Obesity in Mice with Selective Insulin Resistance in Muscle.” *Journal of Clinical Investigation* 105(12): 1791–97.

Kim, M.K., G.M. Reaven, and S.H. Kim. 2017. “Dissecting the Relationship between Obesity and Hyperinsulinemia: Role of Insulin Secretion and Insulin Clearance.” *Obesity* 25(2): 378–83.

Kim, S. et al. 2011. “Nde1-Mediated Inhibition of Ciliogenesis Affects Cell Cycle Re-Entry.” *Nature Cell Biology* 13(4): 351–62.

———. 2014. “Highly Efficient RNA-Guided Genome Editing in Human Cells via Delivery of Purified Cas9 Ribonucleoproteins.” *Genome Research* 24(6): 1012–19.

Kim, S., and L. Tsiokas. 2011. “Cilia and Cell Cycle Re-Entry: More than a Coincidence.” *Cell Cycle* 10(16): 2683–90.

Kitamoto, T., and K. Hanaoka. 2010. “Notch3 Null Mutation in Mice Causes Muscle Hyperplasia by Repetitive Muscle Regeneration.” *Stem Cells* 28(12): 2205–16.

Klein, D., and F. Ammann. 1969. “The Syndrome of Laurence-Moon-Bardet-Biedl and Allied Diseases in Switzerland. Clinical, Genetic and Epidemiological Studies.” *Journal of the Neurological Sciences* 9(3): 479–513.

Klip, A., and M.R. Pâquet. 1990. “Glucose Transport and Glucose Transporters in Muscle and Their Metabolic Regulation.” *Diabetes Care* 13(3): 228–43.

Kochan, R.G. et al. 1979. “Glycogen Synthase Activation in Human Skeletal Muscle: Effects of Diet and Exercise.” *The American Journal of Physiology* 236(6): 660–66.

Kohl, L., D. Robinson, and P. Bastin. 2003. “Novel Roles for the Flagellum in Cell Morphogenesis and Cytokinesis of Trypanosomes.” *EMBO Journal* 22(20): 5336–46.

Kondoh, K., K. Sunadome, and E. Nishida. 2007. “Notch Signaling Suppresses P38 MAPK Activity via Induction of MKP-1 in Myogenesis.” *Journal of Biological Chemistry* 282(5): 3058–65.

Kondziella, W. 1964. “A New Method for the Measurement of Muscle Relaxation in White Mice.” *Archives Internationales de Pharmacodynamie et de Therapie* 152: 277–84.

Koopman, R., G. Schaart, and M.K. Hesselink. 2001. “Optimisation of Oil Red O Staining Permits Combination with Immunofluorescence and Automated Quantification of Lipids.” *Histochemistry and cell biology* 116(1): 63–68.

Kopan, R., J.S. Nye, and H. Weintraub. 1994. “The Intracellular Domain of Mouse Notch: A

Constitutively Activated Repressor of Myogenesis Directed at the Basic Helix-Loop-Helix Region of MyoD." *Development* 120(9): 2385–96.

Kopan, R., and H. Weintraub. 1993. "Mouse Notch: Expression in Hair Follicles Correlates with Cell Fate Determination." *Journal of Cell Biology* 121(3): 631–42.

Kuang, W. et al. 2009. "Cyclic Stretch Induced MiR-146a Upregulation Delays C2C12 Myogenic Differentiation through Inhibition of Numb." *Biochemical and Biophysical Research Communications* 378(2): 259–63.

Kudryashova, E., D. Kudryashov, I. Kramerova, and M.J. Spencer. 2005. "Trim32 Is a Ubiquitin Ligase Mutated in Limb Girdle Muscular Dystrophy Type 2H That Binds to Skeletal Muscle Myosin and Ubiquitinates Actin." *Journal of Molecular Biology* 354(2): 413–24.

Kulaga, H.M. et al. 2004. "Loss of BBS Proteins Causes Anosmia in Humans and Defects in Olfactory Cilia Structure and Function in the Mouse." *Nature Genetics* 36(9): 994–98.

Lai, M. et al. 2016. "Gene Editing of DNAH11 Restores Normal Cilia Motility in Primary Ciliary Dyskinesia." *Journal of Medical Genetics* 53(4): 242–49.

Lamaze, C. et al. 1996. "Regulation of Receptor-Mediated Endocytosis by Rho and Rac." *Nature* 382(6587): 177–79.

Langousis, G. et al. 2016. "Loss of the BBSome Perturbs Endocytic Trafficking and Disrupts Virulence of Trypanosoma Brucei." *Proceedings of the National Academy of Sciences* 113(3): 632–37.

Larsson, S.C., C.S. Mantzoros, and A. Wolk. 2007. "Diabetes Mellitus and Risk of Breast Cancer: A Meta-Analysis." *International Journal of Cancer* 121(4): 856–62.

Larsson, S.C., N. Orsini, and A. Wolk. 2005. "Diabetes Mellitus and Risk of Colorectal Cancer: A Meta-Analysis." *Journal of the National Cancer Institute* 97(22): 1679–87.

Laurin, M. et al. 2008. "The Atypical Rac Activator Dock180 (Dock1) Regulates Myoblast Fusion in Vivo." *Proceedings of the National Academy of Sciences* 105(40): 15446–51.

Lechtreck, K.F. et al. 2009. "The Chlamydomonas Reinhardtii BBSome Is an IFT Cargo Required for Export of Specific Signaling Proteins from Flagella." *Journal of Cell Biology* 187(7): 1117–32.

Lecker, S.H. et al. 2004. "Multiple Types of Skeletal Muscle Atrophy Involve a Common Program of Changes in Gene Expression." *The FASEB Journal* 18(1): 39–51.

Lee, A.D., P.A. Hansen, and J.O. Holloszy. 1995. "Wortmannin Inhibits Insulin-Stimulated but Not Contraction-Stimulated Glucose Transport Activity in Skeletal Muscle." *FEBS Letters* 361(1): 51–54.

Lehman, W., R. Craig, and P. Vibert. 1994. "Ca2+-Induced Tropomyosin Movement in Limulus Thin Filaments Revealed by Three-Dimensional Reconstruction." *Nature* 368(6466): 65–67.

Leitch, C.C. et al. 2014. "Basal Body Proteins Regulate Notch Signaling through Endosomal Trafficking." *Journal of Cell Science* 127(11): 2407–19.

Li, A. et al. 2011. "Ciliary Transition Zone Activation of Phosphorylated Tctex-1 Controls Ciliary Resorption, S-Phase Entry and Fate of Neural Progenitors." *Nature Cell Biology* 13(4): 402–11.

Li, Q., Y.P. Zhang, L.Y. Jia, and X.Y. Peng. 2014. "A Novel Nonsense Mutation in BBS4 Gene Identified in a Chinese Family with Bardet-Biedl Syndrome." *Chinese Medical Journal*

127(24): 4190–96.

Liang, Y. et al. 2014. “FLA8/KIF3B Phosphorylation Regulates Kinesin-II Interaction with IFT-B to Control IFT Entry and Turnaround.” *Developmental Cell* 30(5): 585–97.

Libman, I.M., K. Sun, T.P. Foley, and D.J. Becker. 2008. “Thyroid Autoimmunity in Children with Features of Both Type 1 and Type 2 Diabetes.” *Pediatric Diabetes* 9(4 Part 1): 266–71.

Liew, G.M. et al. 2014. “The Intraflagellar Transport Protein Ift27 Promotes Bbsome Exit from Cilia through the Gtpase ARL6/BBS3.” *Developmental Cell* 31(3): 265–78.

Lindsell, C.E., C.J. Shawber, J. Boulter, and G. Weinmaster. 1995. “Jagged: A Mammalian Ligand That Activates Notch1.” *Cell* 80(6): 909–17.

Liu, A., B. Wang, and L.A. Niswander. 2005. “Mouse Intraflagellar Transport Proteins Regulate Both the Activator and Repressor Functions of Gli Transcription Factors.” *Development* 132(13): 3103–11.

Liu, L. et al. 2013. “Chromatin Modifications as Determinants of Muscle Stem Cell Quiescence and Chronological Aging.” *Cell Reports* 4(1): 189–204.

Liu, Y.P. et al. 2014. “Ciliopathy Proteins Regulate Paracrine Signaling by Modulating Proteasomal Degradation of Mediators.” *Journal of Clinical Investigation* 124(5): 2059–70.

Liu, Z., C. Wang, X. Liu, and S. Kuang. 2018. “Shisa2 Regulates the Fusion of Muscle Progenitors.” *Stem Cell Research* 31: 31–41.

Locke, M., C.L. Tinsley, M.A. Benson, and D.J. Blake. 2009. “TRIM32 Is an E3 Ubiquitin Ligase for Dysbindin.” *Human Molecular Genetics* 18(13): 2344–58.

Lohmann, T. et al. 1997. “Distinct Genetic and Immunological Features in Patients with Onset of IDDM before and after Age 40.” *Diabetes Care* 20(4): 524–29.

Long, C. et al. 2016. “Postnatal Genome Editing Partially Restores Dystrophin Expression in a Mouse Model of Muscular Dystrophy.” *Science* 351(6271): 400–403.

Low, S.H., J.L. Barnes, P.S. Zammit, and J.R. Beauchamp. 2018. “Delta-Like 4 Activates Notch 3 to Regulate Self-Renewal in Skeletal Muscle Stem Cells.” *Stem Cells* 36(3): 458–66.

Luna, A. et al. 2002. “Regulation of Protein Transport from the Golgi Complex to the Endoplasmic Reticulum by CDC42 and N-WASP.” *Molecular Biology of the Cell* 13(6): 2170–79.

Lund, S., G.D. Holman, O. Schmitz, and O. Pedersen. 1995. “Contraction Stimulates Translocation of Glucose Transporter GLUT4 in Skeletal Muscle through a Mechanism Distinct from That of Insulin.” *Proceedings of the National Academy of Sciences of the United States of America* 92(13): 5817–21.

Lyons, P.R., and C.R. Slater. 1991. “Structure and Function of the Neuromuscular Junction in Young Adult Mdx Mice.” *Journal of Neurocytology* 20(12): 969–81.

M’Hamdi, O., I. Ouertani, and H. Chaabouni-Bouhamed. 2014. “Update on the Genetics of Bardet-Biedl Syndrome.” *Molecular Syndromology* 5(2): 51–56.

Ma, H. et al. 2017. “Correction of a Pathogenic Gene Mutation in Human Embryos.” *Nature* 548: 413–19.

von Maltzahn, J., A.E. Jones, R.J. Parks, and M.A. Rudnicki. 2013. “Pax7 Is Critical for the

Normal Function of Satellite Cells in Adult Skeletal Muscle." *Proceedings of the National Academy of Sciences of the United States of America* 110(41): 16474–79.

Di Marcotullio, L. et al. 2007. "Multiple Ubiquitin-Dependent Processing Pathways Regulate Hedgehog/Gli Signaling: Implications for Cell Development and Tumorigenesis." *Cell Cycle* 6(4): 390–93.

———. 2011. "Numb Activates the E3 Ligase Itch to Control Gli1 Function through a Novel Degradation Signal." *Oncogene* 30(1): 65–76.

Marican, N.H.J., S.B. Cruz-Migoni, and A.G. Borycki. 2016. "Asymmetric Distribution of Primary Cilia Allocates Satellite Cells for Self-Renewal." *Stem Cell Reports* 6(6): 798–805.

Marin, P., B. Andersson, M. Krotkiewski, and P. Bjorntorp. 1994. "Muscle Fiber Composition and Capillary Density in Women and Men With NIDDM." *Diabetes Care* 17(5): 382–86.

Marion, V. et al. 2012. "BBS-Induced Ciliary Defect Enhances Adipogenesis, Causing Paradoxical Higher-Insulin Sensitivity, Glucose Usage, and Decreased Inflammatory Response." *Cell Metabolism* 16(3): 363–77.

Marshall, J.D. et al. 2005. "New Alström Syndrome Phenotypes Based on the Evaluation of 182 Cases." *Archives of Internal Medicine* 165(6): 675–83.

Martin, P.T., S.J. Kaufman, R.H. Kramer, and J.R. Sanes. 1996. "Synaptic Integrins in Developing, Adult, and Mutant Muscle: Selective Association of A1, A7A, and A7B Integrins with the Neuromuscular Junction." *Developmental Biology* 174(1): 125–39.

Matas, O.B., S. Fritz, A. Luna, and G. Egea. 2005. "Membrane Trafficking at the ER/Golgi Interface: Functional Implications of RhoA and Rac1." *European Journal of Cell Biology* 84(8): 699–707.

Mayer-Davis, E.J. et al. 2017. "Incidence Trends of Type 1 and Type 2 Diabetes among Youths, 2002–2012." *New England Journal of Medicine* 376(15): 1419–29.

Mayer, U. et al. 2008. "Proteomic Analysis of a Membrane Preparation from Rat Olfactory Sensory Cilia." *Chemical Senses* 33(2): 145–62.

McCarthy, J.J. et al. 2012. "Inducible Cre Transgenic Mouse Strain for Skeletal Muscle-Specific Gene Targeting." *Skeletal Muscle* 2(8): 1–7.

McGill, M.A., S.E. Dho, G. Weinmaster, and C.J. McGlade. 2009. "Numb Regulates Post-Endocytic Trafficking and Degradation of Notch1." *Journal of Biological Chemistry* 284(39): 26427–38.

McGill, M.A., and C.J. McGlade. 2003. "Mammalian Numb Proteins Promote Notch1 Receptor Ubiquitination and Degradation of the Notch1 Intracellular Domain." *Journal of Biological Chemistry* 278(25): 23196–203.

McGough, I.J. et al. 2014. "Identification of Molecular Heterogeneity in SNX27-Retromer-Mediated Endosome-to-Plasma-Membrane Recycling." *Journal of Cell Science* 127(22): 4940–53.

Meehan, T.F. et al. 2017. "Disease Model Discovery from 3,328 Gene Knockouts by the International Mouse Phenotyping Consortium." *Nature Genetics* 49(8): 1231–38.

Megeney, L.A. et al. 1996. "MyoD Is Required for Myogenic Stem Cell Function in Adult Skeletal Muscle." *Genes & Development* 10(10): 1173–83.

Menzl, I. et al. 2014. "Loss of Primary Cilia Occurs Early in Breast Cancer Development." *Cilia* 3(1): 1–16.

Merrifield, C.J., D. Perrais, and D. Zenisek. 2005. “Coupling between Clathrin-Coated-Pit Invagination, Cortactin Recruitment, and Membrane Scission Observed in Live Cells.” *Cell* 121(4): 593–606.

Mikines, K.J. et al. 1988. “Effect of Physical Exercise on Sensitivity and Responsiveness to Insulin in Humans.” *American Journal of Physiology-Endocrinology and Metabolism* 254(3): 248–59.

Millay, D.P. et al. 2013. “Myomaker Is a Membrane Activator of Myoblast Fusion and Muscle Formation.” *Nature* 499(7458): 301–5.

Miosge, N. et al. 1999. “Organization of the Myotendinous Junction Is Dependent on the Presence of Alpha7beta1 Integrin.” *Laboratory Investigation* 79(12): 1591–99.

Molla-Herman, A. et al. 2010. “The Ciliary Pocket: An Endocytic Membrane Domain at the Base of Primary and Motile Cilia.” *Journal of Cell Science* 123(10): 1785–95.

Monis, W.J., V. Faundez, and G.J. Pazour. 2017. “BLOC-1 Is Required for Selective Membrane Protein Trafficking from Endosomes to Primary Cilia.” *Journal of Cell Biology* 216(7): 2131–50.

Moore, S.J. et al. 2005. “Clinical and Genetic Epidemiology of Bardet-Biedl Syndrome in Newfoundland: A 22-Year Prospective, Population-Based, Cohort Study.” *American Journal of Medical Genetics* 132 A(4): 352–60.

Mourikis, P., R. Sambasivan, et al. 2012. “A Critical Requirement for Notch Signaling in Maintenance of the Quiescent Skeletal Muscle Stem Cell State.” *Stem Cells* 30(2): 243–52.

Mourikis, P., S. Gopalakrishnan, R. Sambasivan, and S. Tajbakhsh. 2012. “Cell-Autonomous Notch Activity Maintains the Temporal Specification Potential of Skeletal Muscle Stem Cells.” *Development* 139(24): 4536–48.

Mujahid, S. et al. 2018. “The Endocrine and Metabolic Characteristics of a Large Bardet-Biedl Syndrome Clinic Population.” *Journal of Clinical Endocrinology and Metabolism* 103(5): 1834–41.

Musaro, A. et al. 2004. “Stem Cell-Mediated Muscle Regeneration Is Enhanced by Local Isoform of Insulin-like Growth Factor 1.” *Proceedings of the National Academy of Sciences* 101(5): 1206–10.

Muzumdar, M.D. et al. 2007. “A Global Double-Fluorescent Cre Reporter Mouse.” *Genesis* 45(9): 593–605.

Mykytyn, K. et al. 2001. “Identification of the Gene That, When Mutated, Causes the Human Obesity Syndrome BBS4.” *Nature Genetics* 28(2): 188–91.

———. 2002. “Identification of the Gene (BBS1) Most Commonly Involved in Bardet-Biedl Syndrome, a Complex Human Obesity Syndrome.” *Nature Genetics* 31(4): 435–38.

———. 2003. “Evaluation of Complex Inheritance Involving the Most Common Bardet-Biedl Syndrome Locus (BBS1).” *American Journal of Human Genetics* 72(2): 429–37.

———. 2004. “Bardet-Biedl Syndrome Type 4 (BBS4)-Null Mice Implicate Bbs4 in Flagella Formation but Not Global Cilia Assembly.” *Proceedings of the National Academy of Sciences of the United States of America* 101(23): 8664–69.

Nachury, M.V. et al. 2007. “A Core Complex of BBS Proteins Cooperates with the GTPase Rab8 to Promote Ciliary Membrane Biogenesis.” *Cell* 129(6): 1201–13.

Nelson, C.E. et al. 2016. “In Vivo Genome Editing Improves Muscle Function in a Mouse

Model of Duchenne Muscular Dystrophy." *Science* 351(6271): 403–7.

Nguyen, M.H., M. Cheng, and T.J. Koh. 2011. "Impaired Muscle Regeneration in Ob/Ob and Db/Db Mice." *The Scientific World Journal* 11: 1525–35.

Nielsen, J. et al. 2010. "Increased Subsarcolemmal Lipids in Type 2 Diabetes: Effect of Training on Localization of Lipids, Mitochondria, and Glycogen in Sedentary Human Skeletal Muscle." *AJP: Endocrinology and Metabolism* 298(3): 706–13.

Nowak, S.J., P.C. Nahirney, A.-K. Hadjantonakis, and M.K. Baylies. 2009. "Nap1-Mediated Actin Remodeling Is Essential for Mammalian Myoblast Fusion." *Journal of Cell Science* 122(18): 3282–93.

Nozaki, S. et al. 2012. "Role of RalA Downstream of Rac1 in Insulin-Dependent Glucose Uptake in Muscle Cells." *Cellular Signalling* 24(11): 2111–17.

Nyholm, B. et al. 1997. "Evidence of an Increased Number of Type IIb Muscle Fibers in Insulin-Resistant First-Degree Relatives of Patients with NIDDM." *Diabetes* 46(11): 1822–28.

Oberbach, A. et al. 2006. "Altered Fiber Distribution and Fiber- Specific Glycolytic and Oxidative Enzyme Activity in Skeletal Muscle of Patients With Type 2 Diabetes." *Diabetes Care* 29(4): 895–900.

Olguin, H.C., and B.B. Olwin. 2004. "Pax-7 up-Regulation Inhibits Myogenesis and Cell Cycle Progression in Satellite Cells: A Potential Mechanism for Self-Renewal." *Developmental Biology* 275(2): 375–88.

Otto, A., C. Schmidt, and K. Patel. 2006. "Pax3 and Pax7 Expression and Regulation in the Avian Embryo." *Anatomy and Embryology* 211(4): 293–310.

Ou, G. et al. 2005. "Functional Coordination of Intraflagellar Transport Motors." *Nature* 436(7050): 583–87.

Ozkan, E., H. Yu, and J. Deisenhofer. 2005. "Mechanistic Insight into the Allosteric Activation of a Ubiquitin-Conjugating Enzyme by RING-Type Ubiquitin Ligases." *Proceedings of the National Academy of Sciences* 102(52): 18890–95.

Pan, Y. et al. 2004. "γ-Secretase Functions through Notch Signaling to Maintain Skin Appendages but Is Not Required for Their Patterning or Initial Morphogenesis." *Developmental Cell* 7(5): 731–43.

Park, K.H. et al. 2012. "Ex Vivo Assessment of Contractility, Fatigability and Alternans in Isolated Skeletal Muscles." *Journal of Visualized Experiments* (69): e4198.

Park, S.W. et al. 2006. "Decreased Muscle Strength and Quality in Older Adults with Type 2 Diabetes: The Health, Aging, and Body Composition Study." *Diabetes* 55(6): 1813–18.

Pazour, G.J. et al. 2000. "Chlamydomonas IFT88 and Its Mouse Homologue, Polycystic Kidney Disease Gene Tg737, Are Required for Assembly of Cilia and Flagella." *Journal of Cell Biology* 151(3): 709–18.

Pece, S. et al. 2004. "Loss of Negative Regulation by Numb over Notch Is Relevant to Human Breast Carcinogenesis." *Journal of Cell Biology* 167(2): 215–21.

Pedersen, L.B., S. Geimer, and J.L. Rosenbaum. 2006. "Dissecting the Molecular Mechanisms of Intraflagellar Transport in Chlamydomonas." *Current Biology* 16(5): 450–59.

Pei, J., and N.V. Grishin. 2012. "Unexpected Diversity in Shisa-like Proteins Suggests the Importance of Their Roles as Transmembrane Adaptors." *Cellular Signalling* 24(3): 758–69.

Pelkmans, L., T. Bürli, M. Zerial, and A. Helenius. 2004. “Caveolin-Stabilized Membrane Domains as Multifunctional Transport and Sorting Devices in Endocytic Membrane Traffic.” *Cell* 118(6): 767–80.

Pelkmans, L., and M. Zerial. 2005. “Kinase-Regulated Quantal Assemblies and Kiss-and-Run Recycling of Caveolae.” *Nature* 436(7047): 128–33.

Peter, A.T.J. et al. 2013. “The BLOC-1 Complex Promotes Endosomal Maturation by Recruiting the Rab5 Gtpase-Activating Protein Msb3.” *Journal of Cell Biology* 201(1): 97–111.

Petersen, K.F. et al. 1998. “13C/31P NMR Studies on the Mechanism of Insulin Resistance in Obesity.” *Diabetes* 47(3): 381–86.

Pette, D., and R.S. Staron. 2000. “Myosin Isoforms, Muscle Fiber Types, and Transitions.” *Microscopy Research and Technique* 50(6): 500–509.

Piperno, G. et al. 1998. “Distinct Mutants of Retrograde Intraflagellar Transport (IFT) Share Similar Morphological and Molecular Defects.” *Journal of Cell Biology* 143(6): 1591–1601.

Piperno, G., and K. Mead. 1997. “Transport of a Novel Complex in the Cytoplasmic Matrix of Chlamydomonas Flagella.” *Proceedings of the National Academy of Sciences of the United States of America* 94(9): 4457–62.

Powell, B.C., E.A. Passmore, A. Nesci, and S.M. Dunn. 1998. “The Notch Signalling Pathway in Hair Growth.” *Mechanisms of Development* 78(1–2): 189–92.

Prieto-Echagüe, V. et al. 2017. “BBS4 Regulates the Expression and Secretion of FSTL1, a Protein That Participates in Ciliogenesis and the Differentiation of 3T3-L1.” *Scientific Reports* 7(1): 1–14.

Prior, S.J. et al. 2009. “Reduced Skeletal Muscle Capillarization and Glucose Intolerance.” *Microcirculation* 16(3): 203–12.

Putoux, A., T. Attie-Bitach, J. Martinovic, and M.C. Gubler. 2012. “Phenotypic Variability of Bardet-Biedl Syndrome: Focusing on the Kidney.” *Pediatric Nephrology* 27(1): 7–15.

Qin, H., Z. Wang, D. Diener, and J. Rosenbaum. 2007. “Intraflagellar Transport Protein 27 Is a Small G Protein Involved in Cell-Cycle Control.” *Current Biology* 17(3): 193–202.

Qiu, L. et al. 2000. “Recognition and Ubiquitination of Notch by Itch, a Hect-Type E3 Ubiquitin Ligase.” *Journal of Biological Chemistry* 275(46): 35734–37.

Quinn, M.E. et al. 2017. “Myomerger Induces Fusion of Non-Fusogenic Cells and Is Required for Skeletal Muscle Development.” *Nature Communications* 8: 15665.

Rahmouni, K. et al. 2008. “Leptin Resistance Contributes to Obesity and Hypertension in Mouse Models of Bardet-Biedl Syndrome.” *Journal of Clinical Investigation* 118(4): 1458–67.

Ramakrishna, S. et al. 2014. “Gene Disruption by Cell-Penetrating Peptide-Mediated Delivery of Cas9 Protein and Guide RNA.” *Genome Research* 24(6): 1020–27.

Rattner, J.B. et al. 2010. “Primary Cilia in Fibroblast-like Type B Synoviocytes Lie within a Cilium Pit: A Site of Endocytosis.” *Histology and Histopathology* 25(7): 865–75.

Riddle, R.D., R.L. Johnson, E. Laufer, and C. Tabin. 1993. “Sonic Hedgehog Mediates the Polarizing Activity of the ZPA.” *Cell* 75(7): 1401–16.

Riise, R. et al. 2002. “The Phenotype in Norwegian Patients with Bardet-Biedl Syndrome with

Mutations in the BBS4 Gene." *Archives of Ophthalmology* 120(10): 1364–67.

Robert, A. et al. 2007. "The Intraflagellar Transport Component IFT88/Polaris Is a Centrosomal Protein Regulating G1-S Transition in Non-Ciliated Cells." *Journal of Cell Science* 120(4): 628–37.

Roden, M. et al. 1996. "Mechanism of Free Fatty Acid-Induced Insulin Resistance in Humans." *Journal of Clinical Investigation* 97(12): 2859–65.

Rohatgi, R., L. Milenkovic, and M.P. Scott. 2007. "Patched1 Regulates Hedgehog Signaling at the Primary Cilium." *Science* 317(5836): 372–76.

Rossidis, A.C. et al. 2018. "In Utero CRISPR-Mediated Therapeutic Editing of Metabolic Genes." *Nature Medicine* 24: 1513–18.

Ryall, J.G., J.D. Schertzer, and G.S. Lynch. 2008. "Cellular and Molecular Mechanisms Underlying Age-Related Skeletal Muscle Wasting and Weakness." *Biogerontology* 9(4): 213–28.

Sacco, A. et al. 2010. "Short Telomeres and Stem Cell Exhaustion Model Duchenne Muscular Dystrophy in Mdx/MTR Mice." *Cell* 143(7): 1059–71.

Sasai, Y. et al. 1992. "Two Mammalian Helix-Loop-Helix Factors Structurally Related to Drosophila Hairy and Enhancer of Split." *Genes and Development* 6(12 Part B): 2620–34.

Scherer, P.E. et al. 1996. "Identification, Sequence, and Expression of Caveolin-2 Defines a Caveolin Gene Family." *Proceedings of the National Academy of Sciences* 93(1): 131–35.

Schmidt, A., and A. Hall. 2002. "Guanine Nucleotide Exchange Factors for Rho GTPases: Turning on the Switch." *Genes & Development* 16: 1587–1609.

Schmidt, K.N. et al. 2012. "Cep164 Mediates Vesicular Docking to the Mother Centriole during Early Steps of Ciliogenesis." *Journal of Cell Biology* 199(7): 1083–1101.

Schneider, L. et al. 2005. "PDGFRαα Signaling Is Regulated through the Primary Cilium in Fibroblasts." *Current Biology* 15(20): 1861–66.

Seale, P. et al. 2000. "Pax7 Is Required for the Specification of Myogenic Satellite Cells." *Cell* 102(6): 777–86.

Seeley, E.S. et al. 2009. "Pancreatic Cancer and Precursor Pancreatic Intraepithelial Neoplasia Lesions Are Devoid of Primary Cilia." *Cancer Research* 69(2): 422–30.

Sen, S. et al. 2011. "Upregulation of Paxillin and Focal Adhesion Signaling Follows Dystroglycan Complex Deletions and Promotes a Hypertensive State of Differentiation." *European Journal of Cell Biology* 90(2–3): 249–60.

Senetar, M.A., C.L. Moncman, and R.O. McCann. 2007. "Talin2 Is Induced during Striated Muscle Differentiation and Is Targeted to Stable Adhesion Complexes in Mature Muscle." *Cell Motility and the Cytoskeleton* 64(3): 157–73.

Seo, S. et al. 2009. "Requirement of Bardet-Biedl Syndrome Proteins for Leptin Receptor Signaling." *Human Molecular Genetics* 18(7): 1323–31.

———. 2010. "BBS6, BBS10, and BBS12 Form a Complex with CCT/TRiC Family Chaperonins and Mediate BBSome Assembly." *Proceedings of the National Academy of Sciences* 107(4): 1488–93.

———. 2011. "A Novel Protein LZTFL1 Regulates Ciliary Trafficking of the BBSome and

Smoothened.” *PLoS Genetics* 7(11): e1002358.

Setty, S.R.G. et al. 2007. “BLOC-1 Is Required for Cargo-Specific Sorting from Vacuolar Early Endosomes toward Lysosome-Related Organelles.” *Molecular Biology of the Cell* 18(3): 768–80.

———. 2008. “Cell-Specific ATP7A Transport Sustains Copper-Dependent Tyrosinase Activity in Melanosomes.” *Nature* 454(7208): 1142–46.

Shanik, M.H. et al. 2008. “Insulin Resistance and Hyperinsulinemia: Is Hyperinsulinemia the Cart or the Horse?” *Diabetes Care* 31(2): 262–68.

Sher, J., and C. Cardasis. 1976. “Skeletal Muscle Fiber Types in the Adult Mouse.” *Acta Neurologica Scandinavica* 54(1): 45–56.

Sherafat-Kazemzadeh, R. et al. 2013. “Hyperphagia among Patients with Bardet-Biedl Syndrome.” *Pediatric Obesity* 8(5): 64–67.

Shinin, V., B. Gayraud-Morel, D. Gomès, and S. Tajbakhsh. 2006. “Asymmetric Division and Cosegregation of Template DNA Strands in Adult Muscle Satellite Cells.” *Nature Cell Biology* 8(7): 677–82.

Shulman, G.I. et al. 1990. “Quantitation of Muscle Glycogen Synthesis in Normal Subjects and Subjects with Non-Insulin-Dependent Diabetes by 13 C Nuclear Magnetic Resonance Spectroscopy.” *New England Journal of Medicine* 322(4): 223–28.

Simons, D.L., S.L. Boye, W.W. Hauswirth, and S.M. Wu. 2011. “Gene Therapy Prevents Photoreceptor Death and Preserves Retinal Function in a Bardet-Biedl Syndrome Mouse Model.” *Proceedings of the National Academy of Sciences of the United States of America* 108(15): 6276–81.

Singh, P.J., and E. Tobach. 1975. “Olfactory Bulbectomy and Nursing Behavior in Rat Pups (Wistar DAB).” *Developmental Psychology* 8(2): 151–64.

Singh, P.J., A.M. Tucker, and M.A. Hofer. 1976. “Effects of Nasal ZnSO4 Irrigation and Olfactory Bulbectomy on Rat Pups.” *Physiology and Behavior* 17(3): 373–82.

Spiller, S., M. Blüher, and R. Hoffmann. 2018. “Plasma Levels of Free Fatty Acids Correlate with Type 2 Diabetes Mellitus.” *Diabetes, Obesity and Metabolism* 20(11): 2661–69.

Starks, R.D. et al. 2015. “Regulation of Insulin Receptor Trafficking by Bardet Biedl Syndrome Proteins.” *PLoS Genetics* 11(6): e1005311.

Stoetzel, C. et al. 2006. “BBS10 Encodes a Vertebrate-Specific Chaperonin-like Protein and Is a Major BBS Locus.” *Nature Genetics* 38(5): 521–24.

Su, X. et al. 2014. “Bardet-Biedl Syndrome Proteins 1 and 3 Regulate the Ciliary Trafficking of Polycystic Kidney Disease 1 Protein.” *Human Molecular Genetics* 23(20): 5441–51.

Sugiyama, N., T. Tsukiyama, T.P. Yamaguchi, and T. Yokoyama. 2011. “The Canonical Wnt Signaling Pathway Is Not Involved in Renal Cyst Development in the Kidneys of Inv Mutant Mice.” *Kidney International* 79(9): 957–65.

Swiderski, R.E. et al. 2007. “Gene Expression Analysis of Photoreceptor Cell Loss in Bbs4-Knockout Mice Reveals an Early Stress Gene Response and Photoreceptor Cell Damage.” *Investigative Ophthalmology and Visual Science* 48(7): 3329–40.

Sylow, L. et al. 2013. “Rac1 Signaling Is Required for Insulin-Stimulated Glucose Uptake and Is Dysregulated in Insulin-Resistant Murine and Human Skeletal Muscle.” *Diabetes* 62(6): 1865–75.

Szendroedi, J. et al. 2014. “Role of Diacylglycerol Activation of PKCθ in Lipid-Induced Muscle Insulin Resistance in Humans.” *Proceedings of the National Academy of Sciences* 111(26): 9597–9602.

Tabák, A.G. et al. 2009. “Trajectories of Glycemia, Insulin Sensitivity and Insulin Secretion Preceding the Diagnosis of Type 2 Diabetes: The Whitehall II Study.” *Lancet* 373(9682): 2215–21.

Tabebordbar, M. et al. 2016. “In Vivo Gene Editing in Dystrophic Mouse Muscle and Muscle Stem Cells.” *Science* 351(6271): 407–11.

Tagawa, M. et al. 2008. “MURC, a Muscle-Restricted Coiled-Coil Protein, Is Involved in the Regulation of Skeletal Myogenesis.” *American Journal of Physiology. Cell Physiology* 295(2): 490–98.

Tajbakhsh, S. 2009. “Skeletal Muscle Stem Cells in Developmental versus Regenerative Myogenesis.” *Journal of Internal Medicine* 266(4): 372–89.

Tanos, B.E. et al. 2013. “Centriole Distal Appendages Promote Membrane Docking, Leading to Cilia Initiation.” *Genes and Development* 27(2): 163–68.

Tayeh, M.K. et al. 2008. “Genetic Interaction between Bardet-Biedl Syndrome Genes and Implications for Limb Patterning.” *Human Molecular Genetics* 17(13): 1956–67.

Troy, A. et al. 2012. “Coordination of Satellite Cell Activation and Self-Renewal by Par-Complex-Dependent Asymmetric Activation of P38α/β MAPK.” *Cell Stem Cell* 11(4): 541–53.

Tsujikawa, M., and J. Malicki. 2004. “Intraflagellar Transport Genes Are Essential for Differentiation and Survival of Vertebrate Sensory Neurons.” *Neuron* 42(5): 703–16.

Tummala, P., E.J. Arnsdorf, and C.R. Jacobs. 2010. “The Role of Primary Cilia in Mesenchymal Stem Cell Differentiation: A Pivotal Switch in Guiding Lineage Commitment.” *Cellular and Molecular Bioengineering* 3(3): 207–12.

Tyler, K.M. et al. 2009. “Flagellar Membrane Localization via Association with Lipid Rafts.” *Journal of Cell Science* 122(6): 859–66.

Ueda, S., T. Kataoka, and T. Satoh. 2008. “Activation of the Small GTPase Rac1 by a Specific Guanine-Nucleotide-Exchange Factor Suffices to Induce Glucose Uptake into Skeletal-Muscle Cells.” *Biology of the Cell* 100(11): 645–61.

Vasyutina, E. et al. 2009. “The Small G-Proteins Rac1 and Cdc42 Are Essential for Myoblast Fusion in the Mouse.” *Proceedings of the National Academy of Sciences of the United States of America* 106(22): 8935–40.

Vieira, N.M. et al. 2015. “Jagged 1 Rescues the Duchenne Muscular Dystrophy Phenotype.” *Cell* 163(5): 1204–13.

Wang, X. et al. 2006. “Insulin Resistance Accelerates Muscle Protein Degradation: Activation of the Ubiquitin-Proteasome Pathway by Defects in Muscle Cell Signaling.” *Endocrinology* 147(9): 4160–68.

Wang, Z., Z.C. Fan, S.M. Williamson, and H. Qin. 2009. “Intraflagellar Transport (IFT) Protein IFT25 Is a Phosphoprotein Component of IFT Complex B and Physically Interacts with IFT27 in Chlamydomonas.” *PLoS ONE* 4(5): e5384.

Wei, Q. et al. 2012. “The BBSome Controls IFT Assembly and Turnaround in Cilia.” *Nature Cell Biology* 14(9): 950–57.

Wen, Y. et al. 2012. “Constitutive Notch Activation Upregulates Pax7 and Promotes the Self-

Renewal of Skeletal Muscle Satellite Cells." *Molecular and Cellular Biology* 32(12): 2300–2311.

White, J.D. et al. 2000. "Myotube Formation Is Delayed but Not Prevented in MyoD-Deficient Skeletal Muscle: Studies in Regenerating Whole Muscle Grafts of Adult Mice." *Journal of Histochemistry and Cytochemistry* 48(11): 1531–43.

White, R.B., A.S. Biérinx, V.F. Gnocchi, and P.S. Zammit. 2010. "Dynamics of Muscle Fibre Growth during Postnatal Mouse Development." *BMC Developmental Biology* 10: 21.

Williams, C.L. et al. 2011. "MKS and NPHP Modules Cooperate to Establish Basal Body/Transition Zone Membrane Associations and Ciliary Gate Function during Ciliogenesis." *Journal of Cell Biology* 192(6): 1023–41.

Wood, C.R. et al. 2012. "IFT Proteins Accumulate during Cell Division and Localize to the Cleavage Furrow in Chlamydomonas." *PLoS ONE* 7(2): e30729.

World Health Organization. 2016. WHO Library Cataloguing-in-Publication Data *Global Report on Diabetes 2016*.

Xu, Q. et al. 2015. "BBS4 and BBS5 Show Functional Redundancy in the BBSome to Regulate the Degradative Sorting of Ciliary Sensory Receptors." *Scientific Reports* 5(11855).

Yaffe, D., and O. Saxel. 1977. "A Myogenic Cell Line with Altered Serum Requirements for Differentiation." *Differentiation* 7(1–3): 159–66.

Yin, H. et al. 2013. "MicroRNA-133 Controls Brown Adipose Determination in Skeletal Muscle Satellite Cells by Targeting Prdm16." *Cell Metabolism* 17(2): 210–24.

———. 2016. "Therapeutic Genome Editing by Combined Viral and Non-Viral Delivery of CRISPR System Components in Vivo." *Nature Biotechnology* 34(3): 328–33.

Yoshida, M. et al. 1994. "Dissociation of the Complex of Dystrophin and Its Associated Proteins into Several Unique Groups by N-octyl B-d-glucoside." *European Journal of Biochemistry* 222(3): 1055–61.

Yoshida, M., and E. Ozawa. 1990. "Glycoprotein Complex Anchoring Dystrophin to Sarcolemma." *Journal of Biochemistry* 108(5): 748–52.

You, N. et al. 2012. "Tg737 Inhibition Results in Malignant Transformation in Fetal Liver Stem/Progenitor Cells by Promoting Cell-Cycle Progression and Differentiation Arrest." *Molecular Carcinogenesis* 51(8): 659–73.

Yu, C. et al. 2002. "Mechanism by Which Fatty Acids Inhibit Insulin Activation of Insulin Receptor Substrate-1 (IRS-1)-Associated Phosphatidylinositol 3-Kinase Activity in Muscle." *The Journal of Biological Chemistry* 277(52): 50230–36.

Yu, F., S. Sharma, A. Skowronek, and K.S. Erdmann. 2016. "The Serologically Defined Colon Cancer Antigen-3 (SDCCAG3) Is Involved in the Regulation of Ciliogenesis." *Scientific Reports* 6: 35399.

Zeng, H., J. Jia, and A. Liu. 2010. "Coordinated Translocation of Mammalian Gli Proteins and Suppressor of Fused to the Primary Cilium." *PLoS ONE* 5(12): e15900.

Zhang, Q., S. Seo, et al. 2012. "BBS Proteins Interact Genetically with the IFT Pathway to Influence SHH-Related Phenotypes." *Human Molecular Genetics* 21(9): 1945–53.

Zhang, Q., D. Yu, et al. 2012. "Intrinsic Protein-Protein Interaction-Mediated and Chaperonin-Assisted Sequential Assembly of Stable Bardet-Biedl Syndrome Protein Complex, the BBSome." *Journal of Biological Chemistry* 287(24): 20625–35.

Zhu, P. et al. 2017. “CRISPR/Cas9-Mediated Genome Editing Corrects Dystrophin Mutation in Skeletal Muscle Stem Cells in a Mouse Model of Muscle Dystrophy.” *Molecular Therapy - Nucleic Acids* 7: 31–41.

Zimmermann, K.W. 1898. “Beiträge Zur Kenntniss Einiger Drüsen Und Epithelien.” *Archiv für Mikroskopische Anatomie* 52(3): 552–706.

Zincarelli, C., S. Soltys, G. Rengo, and J.E. Rabinowitz. 2008. “Analysis of AAV Serotypes 1-9 Mediated Gene Expression and Tropism in Mice after Systemic Injection.” *Molecular Therapy* 16(6): 1073–80.

Zou, J. et al. 2011. “Whirlin Replacement Restores the Formation of the USH2 Protein Complex in Whirlin Knockout Photoreceptors.” *Investigative Ophthalmology and Visual Science* 52(5): 2343–51.

Zuris, J.A. et al. 2015. “Cationic Lipid-Mediated Delivery of Proteins Enables Efficient Protein-Based Genome Editing in Vitro and in Vivo.” *Nature Biotechnology* 33(1): 73–80.

10 Acknowledgements

First of all, this work was only accomplished because of scientific and personnel help by many people outside and inside the lab. During my PhD I learned a lot about primary cilia, but also about team spirit and mutual support.

I am very grateful to my PhD supervisor Dr. Jantje M. Gerdes for the opportunity to work on this fascinating research project, the inspiring discussions, her suggestions and scientific support. The joy and motivation she has for her scientific work is motivating and contagious.

Furthermore, I would like to thank my thesis committee members Prof. Dr. Hrabě de Angelis and Prof. Dr. Johannes Beckers for their input, motivation and helpful suggestions to improve the outcome of my project.

I would like to show my appreciation to my colleagues Dr. Julia M. Scerbo, Anett Seelig, Dr. Noah Moruzzi and Francesco Volta for their continuous discussions, suggestions and the great teamwork. I would like to deeply thank Noah Moruzzi for introducing me to many techniques in the laboratory and for sharing all his knowledge about primary cilia with me at the beginning of my PhD. Many thanks also to Donna Thomson for her overall support. Furthermore, I would like to thank the animal caretakers, the technical lab support and Dr. Lore Becker for introducing me the Grip Strength test.

I would like to acknowledge Dr. Jantje M. Gerdes, Dr. Julia M. Scerbo and Dr. Mostafa Bakhti for proofreading and correcting my thesis. I appreciated your comments and suggestions a lot.

I want to show gratitude to my friends/colleagues/collaborators in the lab for making every day in the lab special. You created a great atmosphere and I´m very thankful to made the experience in working with you. It was a pleasure to be a part of this lab and I really appreciate your friendship.

Ich möchte meiner Familie für die stete Unterstützung aus tiefstem Herzen danken. Euer Zuspruch, Verständnis und die vielen motivierenden Gespräche haben mich bei der Durchführung der Experimente und beim Schreiben der Arbeit unterstützt. Ich bin euch sehr dankbar. Bei Michael möchte ich mich bedanken für das Verständnis für die vielen Wochenenden im Labor, die Unterstützung und den entgegengebrachten Halt. Ohne euch alle wäre es mir nicht gelungen diese Arbeit zu vollenden.

11 Attachment: Scientific paper manuscript

Skeletal muscle differentiation requires ciliary inhibition of Notch-dependent signaling

Lisann Heyner[1,2,3], Jantje M. Gerdes[1,2,*]

[1]Institute of Diabetes and Regeneration Research, Helmholtz Zentrum München, D-85764 Neuherberg, Germany. [2]German Center for DiabetesResearch (DZD), D-85764 Neuherberg, Germany.[3]Technical University of Munich, TUM School of Life Sciences, 85354 Freising, Germany.

* To whom correspondence should be addressed. jantje.gerdes@helmholtz-muenchen.de

Abstract

Background

Primary cilia have been shown to be important signaling integrators during development and adult tissue homeostasis; however, their role in skeletal muscle is not very well known. Primary cilia are present on muscle satellite cells, fibro/adipogenic precursors, myoblasts and freshly formed myotubes but disassembled after time.

Methods

We combined *in vivo* magnetic resonance imaging to determine body composition of male *Bbs4*$^{-/-}$ mice at a time point when body weight is not significantly different from littermate wt animals. We tested grip strength as a read-out for muscle function independent of body weight and analyzed skeletal muscle tissues, neuro-muscular junctions and fiber type composition to characterize the muscle phenotype of *Bbs4*$^{-/-}$ mice. To better understand mechanism, we combined immunohistochemical and immunoblotting as well as luciferase-based Notch1 signaling assays in primary cells and a myoblast cell line.

Results

In male *Bbs4*$^{-/-}$ mice, lean to fat mass ratio and grip strength are significantly reduced. We did not observe atrophy or defects in neuronal input, morphology of neuro-muscular junctions or composition of metabolic fiber types. Instead, Notch signaling activity and signaling components are upregulated when ciliary/ basal body composition is impaired in muscle progenitors inhibiting myotube formation.

Conclusions

Several lines of evidence suggest that ciliary/ basal body integrity is required for skeletal muscle differentiation and the modulation of Notch1 signaling in muscle progenitor cells. This could have important implications for the treatment and management of ciliopathy patients but also potentially for those suffering from sarcopenic obesity that is more common in elderly patients.

Key words: myoblasts, Notch signaling, primary cilia, skeletal muscle differentiation

Introduction

At least a subset of ciliopathies presents with metabolic phenotypes such as obesity. While primary cilia on neurons that are part of the hypothalamic-pituitary-gonadal axis [1]–[5] and on β-cells [6; Volta et al., Nature Communications, in press] have been identified as essential regulators of metabolic function, the role of primary ciliary function in other metabolically active tissues such as skeletal muscle is not well understood. Primary cilia on muscle-resident fibro/adipogenic precursors (FAP) are involved in injury-induced adipogenesis [7] and aside from FAPs myoblasts and satellite cells are also ciliated. *Tripartite Motif-containing Protein 32* (*TRIM32*), a gene that if mutated causes Bardet-Biedl Syndrome (BBS*;* OMIM 209900) has also been linked to Limb-girdle muscular dystrophy type 2H [8], an indication that cilia/ basal body integrity is important for skeletal muscle function. *TRIM32* is a putative E3 ubiquitin ligase and several studies have shown a link between cilia-centrosomal genes and the proteasomal system [9]–[12]. Several signaling pathways rely on cilia-proteasomal processing including β-catenin dependent Wnt and NFκB signaling [11]. Notch-dependent signaling has also been linked to cilia/ basal body function [13]. Importantly, muscle progenitor self-replication and differentiation has been shown to involve Notch signaling. In muscle progenitor cells (satellite cells), Notch signaling regulates self-renewal and thus an adequate pool of progenitor cells for tissue homeostasis [14]–[16]. In differentiating cells, Notch signaling is downregulated.

Here, we report on the characterization of the muscular phenotype in *Bbs4*$^{-/-}$ mice [17]. Lean to fat mass ratio is significantly reduced in male *Bbs4*$^{-/-}$ before onset of obesity. Grip strength is also reduced in these animals compared to littermate controls. We found no obvious differences in neuronal input, neuro-muscular junctions or fiber type composition. However, we observe defects in muscle differentiation linked to increased Notch signaling in muscle

cells depleted of ciliary/ basal body components that can explain the decrease of lean mass in *Bbs4*$^{-/-}$ animals.

Material and Methods

Cell culture and differentiation

C2C12 myoblasts were cultured at 37°C and 5% CO_2 (vol/vol). Cells were grown in Growth Medium (DMEM high glucose + 10% Fetal Bovine Serum (FBS) (vol/vol)). For differentiation into myotubes cells were grown to confluence. By the day of confluence medium was switched to Differentiation Medium (DMEM high glucose + 2% Horse Serum (HS) (vol/vol)) and changed every day.

Lentiviral treatment

Stable *Ift88* knock-down C2C12 cells were generated using the Gateway System (Thermo Fisher Scientific). To silence the expression of the *Ift88* gene (NCBI Reference Sequence: NM_009376.2) short hairpin mRNA was designed (http://dharmacon.gelifesciences.com). The plasmid for shRNA delivery was generated using BLOCK.iT U6 RNAi Entry vector kit (Thermo Fisher Scientific) as manufacturer´s instruction. For recombination of the shRNA sequence from the entry clone pEntr/U6 into pLenti/Block-iT destination vector LR clonase (Thermo Fisher Scientific) was used according to manufacturer´s instruction. The virus was amplified using the ViraPower Packaging Mix and pLenti-DEST Ift88 or pLenti-DEST LacZ as a control. Virus titer determination and transduction of C2C12 cells was performed according to the ViraPower Lentivirus Expression System manual (Thermo Fisher Scientific).

Ethical approval

Lentiviral treatments regarding to biosafety level 2 were registered at the Regierung von Oberbayern (55.2-1-54-2532-187-2015). Procedures with live animals were conducted according to current animal welfare regulations with the approval of Regierung von Oberbayern (50-8791-8.1005.2021).

Induction of recombination of HSA-MCM;Ift88flox/flox and HSA-MCM;ROSA26mTmG/mTmG mice

To induce Cre-mediated recombination, mice between post-natal day 25 and day 35 were treated with 100 mg/kg bodyweight Tamoxifen dissolved in Corn Oil by sonication. Corn Oil was used as a control. The oral gavage was conducted once per day on 5 consecutive days.

Body composition and grip strength measurements

Body composition measurement by magnetic resonance analyzer (EchoMRI) and grip strength test were performed on 14 weeks old *Bbs4* mice or 4 weeks after induction on *HSA-MCM;Ift88*$^{flox/flox}$ and *HSA-MCM;ROSA26*$^{mTmG/mTmG}$ mice. Before each of the two procedures body weight of the mice was obtained. Absolute body composition values (lean and fat mass in grams) were used to calculate relative values with respect to the body weight. Absolute grip strength tests were performed with BIOSEB´s grip strength meter in grams in three measurements in a row per mouse. The relative grip strength was calculated by dividing the absolute grip strength by the body weight.

RNA isolation and quantitative rtPCR

Total RNA was isolated from subconfluent or 5d differentiated C2C12 cells, EDL and Soleus muscle as well as E12.5 limb buds using Trizol (Life Technologies) according to the

manufacturer´s instruction. Maxima First Strand cDNA synthesis kit (Thermo Fisher Scientific) was used for retro-transcription of mRNA to cDNA. TaqMan Fast Advanced Master Mix (Applied Biosystems) was used to run quantitative rtPCR. All probes (Suppl. Table 1) were normalized to Gapdh.

Ift88 Genotyping of HSA-MCM;Ift88flox/flox

Tissue samples of skeletal muscle and smooth muscle were lysed using Lysis buffer (100 mM TrisHCl pH8.5, 5 mM EDTA, 0.2% SDS and 200 mM NaCl; fill up to 500 ml with distilled water) and a tissue lyser (45 Hz, 30s). DNA was precipitated with isopropanol and washed with Ethanol before solving in water. To show Cre-activation an *Ift88*-PCR with the following primers was performed: GCCTCCTGTTTCTTGACAACAGTG (common 5´ primer), GGTCCTAACAAGTAAGCCCAGTGTT (3´ flox and wt allele primer) and CTGCACCAGCCATTTCCTCTAAGTCATGTA (3´delta allele primer). Following signals can be shown: flox allele (~370 bp), wt allele (~350 bp) and delta allele (~270 bp).

Protein isolation and Western Blot

C2C12 cells, EDL and Soleus muscle as well as E12.5 limb buds were lysed with RIPA buffer supplemented with Phosphatase- (Thermo Fisher Scientific, 88667) and Protease-Inhibitor (Thermo Fisher Scientific, 88265). Total protein content was determined by using Lowry protein assay. Standardized amounts of protein was separated on 10% polyacrylamide gels, transferred on a nitrocellulose membrane (wet transfer), blocked for 1h in 5% milk (weight/volume) and incubated with the primary antibody (Suppl. Table 2) overnight at 4°C. Membranes were incubated for 1h at RT with secondary antibodies (Suppl. Table 3), labeled with HRP and scanned with the ChemStudio SA^2 (Analytik Jena) system. For the analysis of

atrophy markers fluorescent labeled secondary antibodies were used and scanned with the Odissey Sa (Licor) system.

Cryosections

Skeletal muscle was dissected and snap-frozen in liquid-nitrogen-cooled isopentane. Snap-frozen muscles were fixed with a drop of Tissue Freezing Medium (Leica) on the sample holder. For fiber typing experiments 14 µm thick cross-sections of EDL or Soleus were cut using Cryostat and transferred on SuperFrost Plus slides (Thermo Fisher Scientific), same for Gastrocnemius sections for Oil Red-O staining. Gastrocnemius muscle of *HSA-MCM;ROSA26*$^{mTmG/mTmG}$ mice were cross-sectioned in 20 µm thick slices and transferred to Super Frost Plus slides. Longitudinal sections of 40 µm thickness were cut from *Bbs4* Gastrocnemius and transferred to ice-cold Methanol-Aceton (1:1) for 10 min. These sections were processed as floating sections in netwell-plates.

Stainings and Antibodies

Cells were fixed for 10 min in 4% PFA at 37°C, permeabilized for 30 min at RT and blocked for 30 min at RT. Cryosections on SuperFrost slides were not fixed, but permeabilized for 1 h and blocked for 1 h at RT. Samples were incubated with the primary antibody (Suppl. Table 4) diluted in Blocking Donkey Solution overnight at 4°C. After 3 times washing the sample with PBS, secondary antibody was added for 1 h at RT. Bungarotoxin and phalloidin were added to the secondary antibodies (Suppl. Table 5). Floating sections in netwell plates were fixed as described above and processed in the same procedure. DAPI was stained for 15 min at RT for cells and 30 min for skeletal muscle sections. After 3 washing steps sections were embedded in Elvanol.

Sections used for mTmG staining were permeabilized 45 min (0.1% Glycine and 0.2% Triton) at RT, washed once and blocked for 1 h at RT. Samples were incubated with the primary antibody (Suppl. Table 3) diluted in Blocking Donkey Solution for 2 h at RT plus overnight at 4°C. After 3 times washing the sample with PBS, secondary antibody (Suppl. Table 4) was added for 4 h at RT. Sections were washed 3 more times, DAPI staining was conducted for 30 min and samples were embedded in Elvanol.

For the purpose of lipid staining, Oil Red-O staining was used as previously described [18].

Notch1 activity assay

Notch1 signaling pathway activity was detected according to manufacturer's instructions (BPS Bioscience, 60509) on C2C12.

Image analysis

Calculation of the volume of Bungarotoxin Staining as well as number of Branch Points and Terminal Points was done with IMARIS Software (Bitplane). Same software was used for Fiber Type counting. Counting of Nuclei for the Fusion Index and Differentiation Index LasX (Leica) was used.

Statistical analysis

Results are presented as mean +/- standard deviation. Statistical significance was tested using SigmaPlot software (Systat). For single comparisons Student´s t-test was performed, for multiple comparisons one-way ANOVA. Values of $p<0.005$ were considered as statistically significant.

Results

Lean mass and muscle function in Bbs4$^{-/-}$ *mice*

To characterize a potential role for *Bbs4* in skeletal muscle, we determined lean mass and muscle function in *Bbs4*$^{-/-}$mice and littermate controls. *Bbs4*$^{-/-}$ mice are runted at birth and then gain weight overtime [19]. To confirm these findings, we weighed male *Bbs4*$^{-/-}$ mice and littermate controls regularly starting at three weeks. At fourteen weeks of age, there was no detectable difference in body weight (BW) between the two groups; we found that *Bbs4*$^{-/-}$ mice gained roughly five grams more compared to wt controls over this time (Fig. 1A). To understand whether the post-natal weight gain was due to an expansion of fat mass or equally distributed across all tissues, we used magnetic resonance to test body composition. We found that fat mass is more than 2.5-fold increased in *Bbs4*$^{-/-}$ mice at a time when body weight is similar in both experimental groups (WT=2.09g, KO=5.32g, $p<0.001$; Fig.1B). This is in good agreement with previous reports that found significantly elevated fat mass in both male and female adult *Bbs4*$^{-/-}$ mice (> 7 months) [19]. At the same time, and somewhat surprisingly, we also found significantly reduced lean mass in these animals (WT=24.52g, KO=21.45g, $p<0.001$, Fig. 1B). For comparison, obesity models that are unrelated to cilia/ basal body function such as *ob/ob* mice typically show no differences in lean mass [20]. Lean to fat mass ratios were three-fold reduced (WT=14.27, KO=4.76, $p<0.001$) and lean mass normalized to body weight was reduced by over 10% (WT=0.86; KO=0.77, $p<0.001$). On the other hand, fat mass normalized to body weight was more than 2.5-fold increased (WT=0.07, KO=0.18, $p<0.001$). In summary, magnetic resonance measurements revealed a misdistribution of lean and fat mass in *Bbs4*$^{-/-}$ animals that precedes obesity.

Lean mass consists of bone, ligaments and many other tissues than muscle; we tested grip strength of *Bbs4*$^{-/-}$ mice to assess the effect on muscle performance. To avoid confounding effects of body weight variability, we used an experimental set up which exerts horizontal

rather than vertical force. We found roughly 20% reduction in grip strength of *Bbs4*$^{-/-}$ animals suggesting that decreased lean mass is linked to reduced muscle mass (WT=5.6, KO=4.6, $p<0.001$, Fig.1C). As previously reported, penetrance of the obesity phenotype is roughly 40% in *Bbs4*$^{-/-}$ male mice [19]. It is not clear if the reduced penetrance also pertains to other phenotypes and therefore we used body weight to discriminate unaffected versus affected animals. We stratified the experimental cohort of *Bbs4*$^{-/-}$ male mice into likely affected (BW>35 g) and potentially unaffected (BW<35 g). 25% of the test animals were likely affected and, in this cohort, we found grip strength dramatically reduced (60%, $p<0.001$, Fig. 1C). Taken these lines of evidence together, we suggest that distribution of body weight, fat and lean mass is abnormal and this precedes the onset of obesity. Stratification by body weight reveals significantly stronger phenotypes when comparing likely affected *Bbs4*$^{-/-}$ males to littermate controls.

Bbs4 is not required for muscle composition or neuro-muscular input

Reduced grip strength in *Bbs4*$^{-/-}$ animals is likely linked to a reduction of muscle mass although we cannot exclude a role for *Bbs4* in other aspects. Muscle function is not only determined by muscle mass but also by neuronal input and fiber type composition among others. Because neurons are ciliated, we first examined neuromuscular junctions (NMJ) to understand if these contact points between motor neurons and muscle fibers might not be formed correctly (Fig. 2A). We used fluorescently labeled α-bungarotoxin which selectively binds nicotinic acetylcholine receptors that decorate NMJs in combination with antibodies raised against acetylated α-tubulin (neuronal fibers) and synaptophysin to visualize NMJs in *Bbs4*$^{-/-}$ animals. We did not observe gross morphological abnormalities; more detailed analysis showed a trend to higher volumes of α-bungarotoxin in Bbs4-deficient NMJs that is

however not statistically significant. The number of branching points and terminal points of the NMJ does not significantly differ between genotypes.

NMJ morphology alone does not determine neuromuscular input. As a functional readout for NMJs we tested atrophy markers in both experimental groups. Motor neurons do not only control voluntary movement but also muscle tone and if neuronal input is severed, muscles begin to atrophy. However, Fbox protein 32 (Fbx-32) and tripartite containing 63/ muscle ring finger protein 1 (Trim637MuRF-1), two ubiquitin ligases and atrophy markers are unchanged in absence of Bbs4 in soleus and EDL of 14 week old male mice (Fig. 2B). These observations suggest that neuronal input is unchanged in *Bbs4*$^{-/-}$ mice and that NMJs form normally.

Muscle fiber types are important determinants of muscle function. Fast- twitch fibers are important for explosive, rapid movements while slow-twitch fibers are more important for more sustained activity (such as sprint vs. long-distance running). Metabolic disease such as Type 2 *Diabetes mellitus* influences fiber type composition and affects muscle function [21]–[23]. Because body fat is abnormally high in *Bbs4*$^{-/-}$ animals at 14 wk, we investigated if *Bbs4* deficiency affected fiber type composition either directly or indirectly via fat accumulation. In soleus, a muscle type containing many slow-twitch (Type I) fibers, we did not observe significant changes of fiber type distribution upon loss of *Bbs4* function (Fig. 2C). Similarly, EDL containing predominantly fast twitch (Type II) fiber types displayed no changes in fiber type composition. In summary, we did not observe any signs of functional defects in *Bbs4*$^{-/-}$ muscle, indicating that differentiated muscle fibers perform normally.

Muscle differentiation is impaired in Bbs4$^{-/-}$ *animals*

Since muscle fibers do not display obvious morphological defects and there is no sign of atrophy, we hypothesized that muscle fibers do not differentiate normally. In skeletal muscle,

primary cilia are found on muscle FAPs which produce extracellular matrix and thus form structural support for the muscles and on satellite cells which are progenitors to skeletal muscle cells such as myoblasts [24]–[27]. Therefore we tested *Talin2* (*Tln2*) expression as a marker of muscle differentiation. In EDL and soleus, *Tln2* message is roughly 40% reduced ($p=0.008$ and $p<0.001$ respectively, Fig. 3A, B) strongly indicating defects in differentiation and tube formation. In addition, we tested *T-lymphoma invasion and metastasis 1* (*Tiam1*) expression. We have previously observed aberrant *Tiam1* expression in pancreatic islets and an insulinoma cell line (MIN6m9) [28], a GEF for *Rac family small GTPase 1* (*Rac1*) and a component of a polarity complex comprising Par3-Par6-aPKC (Mertens, Pegtel, and Collard 2006; Volta et al., Nature Communications, in press). Recently it has been shown that a switch in polarization is involved in myogenesis and thus aberrant polarization in cilia/ basal body deficient myoblasts could lead to defects in myotube fusion and myogenesis [30]. In *Bbs4*$^{-/-}$ EDL, *Tiam1* mRNA is reduced by 48% compared to littermate controls (Fig. 3A). Taken these lines of evidence together, we suggest that tube formation and muscle differentiation is impaired in *Bbs4*$^{-/-}$ mice.

Notch signaling plays a decisive role in early muscle differentiation as progenitor cells give rise to myoblasts [31], [32]. Previous studies have identified a link between primary cilia and Notch signaling in tissues other than skeletal muscle [13], [33], [34]. We tested the expression of several genes linked to Notch signaling activity in *Bbs4*$^{-/-}$ limb buds at embryonic day E12.5 when muscle differentiation starts (Fig. 3C). While *Maternally expressed gene 3* (*Meg3*) [35], *regulator of calcineurin 1* (*Rcan1*) [36] and *homeodomain interacting protein kinase 2* (*Hipk2*) [37], were expressed normally, we found 50% reduction in *γ-secretase unit* of *aph-1 homolog B* (*Aph1b*) mRNA which is involved in processing activated Notch receptor [38] ($p<0.001$; Fig. 3C). At 14 wk, *Bbs4*$^{-/-}$ EDL showed not differential expression in any of

these genes (Fig. 3D). Of note, *de novo* myogenesis is rare in adult muscle and differences might be below the detection limit.

Over all, differential gene expression in different muscle types and at different developmental stages suggests that *Bbs4*$^{-/-}$ mice show a defect in early muscle differentiation and myogenesis.

In differentiated muscle primary cilia are not required for maintenance or function

To exclude a role for primary cilia and basal body function in differentiated skeletal muscle, we ablated primary cilia specifically from differentiated myotubes. Using an inducible *Cre*-recombinase under transcriptional control of the *human skeletal actin* (*HSA*) promoter [39] we deleted *intraflagellar transport 88* (*Ift88*) (*HSA-MCM*;*Ift88*$^{loxp/loxp}$) [40]. Male *HSA-MCM*;*Ift88*$^{loxp/loxp}$ mice were treated with tamoxifen (TAM) or corn oil four weeks after birth; we detected evidence of recombination in gastrocnemius lysate but not in cardiac muscle, suggesting that skeletal muscle is targeted specifically in this model (Fig. 4A). To further test specificity as well as efficiency of recombination, *HSA-MCM*;*Rosa26*^{mTmG} mice underwent the same treatment protocol. We detected close to 100% recombination efficiency in gastrocnemius muscle of these animals. At the same time, we did not detect recombination in smooth (gut, stomach) or cardiac muscle of the animals, suggesting that recombination is specific to skeletal muscle (Fig. 4B). *HSA-MCM*;*Ift88*$^{\Delta/\Delta}$ mice weighed the same as control animals and we did not observe significant changes in lean mass (Fig. 4C). However, we observed 23% increased fat mass in TAM-treated animals (p=0.006). Consequently, the lean/ fat mass ration was significantly reduced (-20%, p=0.004) and the fat mass/ BW ratio increased (33%, p=0.005, Fig. 4C). We did not observe differences in relative grip strength in these animals (Fig. 4D), suggesting that *Ift88* and ciliary function in myofibers is not required for maintenance of lean mass or muscle function.

A recent study showed a role for primary cilia on fibro-adipogenic progenitors (FAP) in skeletal muscle [7]. Primary cilia and hedgehog signaling favor adipogenesis following injury in muscle. On the other hand, muscle fiber de-differentiation has been shown to give rise to *PR domain containing 1 with ZNF domain* (*Prdm1*) positive brown adipocytes within skeletal muscle [41]. Oil red O staining of TAM-treated *HSA-MCM*;*Ift88*$^{loxp/loxp}$ Gastrocnemius four weeks after induction revealed no differences in intra-muscular fat distribution compared to oil treated controls (Fig. 4E). Moreover, we did not detect abnormal fat distribution patterns in *Bbs4*$^{-/-}$ muscle (Fig. 4F). When determining *Prdm1* expression as a parameter of browning of intra-muscular fat depots, we also did not find changes in *Prdm1* mRNA in *Bbs4*$^{-/-}$ soleus or EDL (Fig. 4G). These lines of evidence suggest that *Ift88* and *Bbs4* do not play major roles in the maintenance of muscle identity and differentiation.

Abnormal Notch signaling in Ift88-*depleted C2C12 cells*

To better understand how loss of ciliary/ basal body integrity affects Notch signaling in differentiating myoblasts, we knocked down *Ift88* using RNA interference (*shIft88*) in C2C12 derivative clonal cell lines. Ciliation was reduced by more than 55% (25.1% vs. 11.1% ciliated C2C12 cells in controls vs. *Ift88* depleted cells, p=0.02; Fig.5A). We proceeded with these cells and tested Notch1 activity using a luciferase assay (BPS Bioscience). Firefly luciferase is expressed under the control of Notch response elements (CSL elements: CBF1/ RBPJ (recombination signal binding protein for immunoglobin kappa J), Suppressor of Hairless, Lag-1 (Lin-12 and Glp-1 phenotype)) and Renilla luciferase is used as a transfection control and internal standard. Notch signaling is induced by overexpressing Notch receptor 1 that has a deletion for the extracellular domain Notch1ΔE. γ-secretase then cleaves the intracellular domain (NICD) that is actively signaling in the nucleus. We found that *Ift88*-depleted cells show higher Notch1-transcriptional activity than control cells ($p<0.001$) and

that this activity is specific to Notch1ΔE, because the reporter construct alone does not trigger such activity (for a representative example, refer to Fig. 5B). Importantly, there is no discernible background luciferase activity in either Notch1ΔE or mock transfected controls. This is somewhat surprising when taking into account that we found a reduction in *Aph1b* expression in embryonic *Bbs4*$^{-/-}$, one of the γ-secretases that are involved in Notch signal processing. In addition to Notch1 procession, elevated signal could also be linked to increased levels of signaling molecules. Therefore, we tested expression levels of *Jagged1* (*Jag1*), a Notch1 ligand, *Notch1* and *Aph1b* in *Ift88*-depleted C2C12 cells (Fig. 5C). While we observed slightly elevated *Jag1* and slightly reduced *Aph1b* expression both trends were not statistically significant. On the other hand, *Notch1* mRNA is significantly elevated in *shIft88* C2C12 cells (158%, p=0.006). As a control, we also tested *Ift88* expression and found it reduced by 71% (p=0.017). Because protein levels do not always correlate with mRNA levels we also tested Jagged1, Notch1 and Aph1b protein levels (Fig. 5D). Again, we did not observe significant changes in Aph1b in good agreement with the mRNA levels. Notch1 protein levels were 135% higher (p=0.022), similar to the increase in mRNA levels in these cells; Jagged1 protein was increased by 45% compared to controls (p=0.02). Overall, our results show greater Notch1-dependent signaling activity upon loss of Ift88.

Ift88 is required for myotube formation

Because Notch1 dependent signaling is actively contributing to the maintenance of muscle progenitor cells and other tissues such as neuronal stem cells [32], [42], we next tested myotube formation in two different clonal *Ift88*-depleted C2C12 cell lines compared to controls. Ift88 protein was reduced by 46% and 38% compared to control (*shIft88(1)* p=0.004; *shIft88(2)* p=0.02; Fig. 6A). One measure of myoblast differentiation is the expression of *myogenic differentiation 1* (MyoD); MyoD expression rises over two days of differentiating

culture conditions (Fig. 6B). When normalized to basal levels, control cells raise MyoD expression by 71% while the two clonal *Ift88*-depleted cell lines only show increases of 43% and 35% respectively (p=0.039 and 0.020 respectively). F-actin visualization by fluorescently labeled phalloidin shows less myotubes in *shIft88* C2C12 cells compared to controls (Fig. 6C). To quantify differentiation, we determined the fusion index by calculating the number of nuclei in myotubes. Because differentiation efficiency varies considerably, we conducted three independent experiments and found that the fusion index was reduced between 20% and 41% in both *Ift88*-depleted cell lines in three independent experiments (Fig. 6D). The reduction was statistically significant in all cases.

Another measure of differentiation efficiency is the differentiation index, or the fraction of total cells incorporated into myotubes. In each experiment we found significantly less cells that were components of myotubes compared to the control cells, ranging from 23% to 56% reduction. A recent study found a role for primary cilia and sonic hedgehog signaling (Shh) in muscle differentiation [43]. We used *GLI-Kruppel family member Gli1* (*Gli1*) as a readout for Shh signaling activity and observed a decrease of *Gli1* expression after 5d of differentiation in control cells (62% reduction, p<0.001, Fig. 6E). Interestingly, we observed increased *Gli1*-expression in *Ift88*-depleted cells before starting differentiation (52% upregulation, p<0.001) but this upregulation is lost after 5d of differentiating conditions (66% reduction compared to undifferentiated controls, p<0.001, 78% compared to undifferentiated *shIft88*, p<0.001). Overall, our results suggest that loss of Ift88 function impaired myotube formation.

Discussion

While the obesity phenotype is well documented for BBS patients, little is known about skeletal muscle function in these individuals. Defects in strength might be masked by excess body weight and ataxia which often results in poor balance and incoordination [44]. Here, we

characterize *Bbs4*$^{-/-}$ mice with a specific focus on skeletal muscle function and report that lean mass is reduced in 14 wk old *Bbs4*$^{-/-}$ animals. Both lean to fat mass ration and lean mass to body weight ratio is reduced in these animals, suggesting maldistribution of lean and fat mass precedes overt obesity in these animals. Reduced lateral grip strength indicates that the reduction in lean mass translates into reduced muscular function. Importantly, *Bbs5*$^{-/-}$ animals also show reduced lean mass and grip strength [45]. This strongly suggests that the phenotype is not unique to Bbs4 function and that it might affect most Bbs mutations and possibly other cilia-centrosomal mutations.

Several lines of evidence implicate that loss of cilia/ basal body function affects myotube differentiation: A) Absence of muscle atrophy markers such as Fbx-32 and Trim63/ MuRF1 as well as NMJ morphology strongly suggest that neuronal input is normal in differentiated muscle of *Bbs4*$^{-/-}$ animals. B) We did not observe differences in fiber type composition (fast vs slow twitch fibers). C) Removal of *Ift88* in differentiated myoblasts/ myotubes does not affect lean mass or grip strength. Interestingly, we observed increased fat mass in TAM-treated *HSA-MCM*;*Ift88*$^{\Delta/\Delta}$ mice; additional experiments will have to reveal whether this is an artefact or if this might relate to metabolic defects linked to Ift88 depletion such as muscular insulin resistance. D) Expression of differentiation marker *Tln2* is reduced in *Bbs4*$^{-/-}$ soleus and EDL.

One of the main regulatory signaling pathways involved in the balance between maintenance and differentiation of stem cells/ progenitor cells is Notch signaling. Several papers have implicated a link between primary cilia and Notch signaling [13], [34], [46]. We observed increased protein levels of Notch1 receptor and Jagged1 ligand in *Ift88*-depleted C2C12 cells. In addition, a luciferase assay revealed increased Notch1-dependent transcriptional activity in these cells compared to controls. In skeletal muscle, Notch signaling is required for maintenance of the progenitor pool and inhibits myotube differentiation [31]. In good

agreement with these findings, we observed reduced myotube differentiation efficiency as marked by fusion and differentiation indices. Overall, *Bbs4* and potentially other ciliopathy disease genes are involved in myotube differentiation. Reduced muscle mass and function could contribute to documented symptoms of BBS patients such as ataxia, balance and coordination. In addition, because of the important role of skeletal muscle in post-prandial glucose uptake, it could further escalate the metabolic phenotype of the patients. Physical exercise intervention in BBS patients is severely hampered by disease manifestations such as impaired vision, cognitive disabilities and ataxia; our study suggests that reduced muscle function and impaired muscle differentiation could further limit the feasibility of physical exercise intervention in the management of BBS and potentially other metabolic ciliopathies.

Competing interests

The authors declare no competing or financial interests.

Acknowledgements

We thank Kenneth Dyar, Franziska Greulich, Maximilian Kleinert, and Noah Moruzzi, who provided expertise that greatly assisted this research and Anett Seelig for her help in the animal facility. Further we thank Lore Becker for sharing her expertise and technique of the grip strength test and Tim J. Schulz for the expertise and technique of satellite cell isolation.

Contributions

L.H. carried out the experiments, analyzed the data and edited the manuscript, J.M.G. had the idea, designed the experiments and wrote the manuscript.

Ethical guideline certification

The authors certify that they comply with the ethical guidelines for publishing in the Journal of Cachexia, Sarcopenia and Muscle: update 2017 [47].

References

[1] A. I. Koemeter-Cox *et al.*, "Primary cilia enhance kisspeptin receptor signaling on gonadotropin-releasing hormone neurons," *Proc. Natl. Acad. Sci.*, vol. 111, no. 28, pp. 10335–40, 2014.

[2] G. A. Bishop, N. F. Berbari, J. Lewis, and K. Mykytyn, "Type III adenylyl cyclase localizes to primary cilia throughout the adult mouse brain," *J. Comp. Neurol.*, vol. 505, no. 5, pp. 562–71, 2007.

[3] Z. Wang *et al.*, "Adult type 3 adenylyl cyclase-deficient mice are obese," *PLoS One*, vol. 4, no. 9, p. e6979, 2009.

[4] N. F. Berbari *et al.*, "Leptin resistance is a secondary consequence of the obesity in ciliopathy mutant mice," *Proc. Natl. Acad. Sci.*, vol. 110, no. 19, pp. 7796–7801, 2013.

[5] J. R. Davenport *et al.*, "Disruption of Intraflagellar Transport in Adult Mice Leads to Obesity and Slow-Onset Cystic Kidney Disease," *Curr. Biol.*, vol. 17, no. 18, pp. 1586–1594, 2007.

[6] J. M. Gerdes *et al.*, "Ciliary dysfunction impairs beta-cell insulin secretion and promotes development of type 2 diabetes in rodents," *Nat. Commun.*, vol. 5, p. 5308, 2014.

[7] D. Kopinke, E. C. Roberson, and J. F. Reiter, "Ciliary Hedgehog Signaling Restricts Injury-Induced Adipogenesis," *Cell*, vol. 170, no. 2, pp. 340-351.e12, 2017.

[8] P. Frosk *et al.*, "Limb-Girdle Muscular Dystrophy Type 2H Associated with Mutation in TRIM32, a Putative E3-Ubiquitin–Ligase Gene," *Am. J. Hum. Genet.*, vol. 70, no. 3,

pp. 663–672, 2002.

[9] J. M. Gerdes *et al.*, “Disruption of the basal body compromises proteasomal function and perturbs intracellular Wnt response,” *Nat. Genet.*, vol. 39, no. 11, pp. 1350–1360, 2007.

[10] C. Gerhardt, A. Wiegering, T. Leu, and U. Rüther, “Control of Hedgehog Signalling by the Cilia-Regulated Proteasome,” *J. Dev. Biol.*, vol. 4, no. 3, 2016.

[11] Y. P. Liu *et al.*, “Ciliopathy proteins regulate paracrine signaling by modulating proteasomal degradation of mediators,” *J. Clin. Invest.*, vol. 124, no. 5, pp. 2059–2070, 2014.

[12] R. P. Fabunmi, W. C. Wigley, P. J. Thomas, and G. N. DeMartino, “Activity and regulation of the centrosome-associated proteasome,” *J. Biol. Chem.*, vol. 275, no. 1, pp. 409–13, 2000.

[13] C. C. Leitch, S. Lodh, V. Prieto-Echagüe, J. L. Badano, and N. Zaghloul, “Basal body proteins regulate Notch signaling through endosomal trafficking.,” *J. Cell Sci.*, vol. 127, no. 11, pp. 2407–2419, 2014.

[14] A. Pasut *et al.*, “Notch Signaling Rescues Loss of Satellite Cells Lacking Pax7 and Promotes Brown Adipogenic Differentiation,” *Cell Rep.*, vol. 16, no. 2, pp. 333–343, 2016.

[15] P. Mourikis, R. Sambasivan, D. Castel, P. Rocheteau, V. Bizzarro, and S. Tajbakhsh, “A critical requirement for notch signaling in maintenance of the quiescent skeletal muscle stem cell state,” *Stem Cells*, vol. 30, no. 2, pp. 243–252, 2012.

[16] S. Fujimaki *et al.*, “Notch1 and Notch2 Coordinately Regulate Stem Cell Function in the Quiescent and Activated States of Muscle Satellite Cells,” *Stem Cells*, vol. 36, no. 2, pp. 278–285, 2018.

[17] H. M. Kulaga *et al.*, “Loss of BBS proteins causes anosmia in humans and defects in

olfactory cilia structure and function in the mouse," *Nat. Genet.*, vol. 36, no. 9, pp. 994–998, 2004.

[18] R. Koopman, G. Schaart, and M. K. Hesselink, "Optimisation of oil red O staining permits combination with immunofluorescence and automated quantification of lipids.," *Histochem. Cell Biol.*, vol. 116, no. 1, pp. 63–68, 2001.

[19] E. R. Eichers *et al.*, "Phenotypic characterization of Bbs4 null mice reveals age-dependent penetrance and variable expressivity," *Hum. Genet.*, vol. 120, no. 2, pp. 211–226, 2006.

[20] K. Begriche, J. Massart, A. Abbey-Toby, A. Igoudjil, P. Lettéron, and B. Fromenty, "B-aminoisobutyric acid prevents diet-induced obesity in mice with partial leptin deficiency," *Obesity*, vol. 16, no. 9, pp. 2053–67, 2008.

[21] M. Gaster, P. Staehr, H. Beck-Nielsen, H. D. Schroder, and A. Handberg, "GLUT4 is reduced in slow muscle fibers of type 2 diabetic patients: is insulin resistance in type 2 diabetes a slow, type 1 fiber disease?," *Diabetes*, vol. 50, no. 6, pp. 1324–1329, 2001.

[22] M. S. Hickey *et al.*, "Skeletal muscle fiber composition is related to adiposity and in vitro glucose transport rate in humans," *Am. J. Physiol. Metab.*, vol. 268, no. 3, pp. 453–457, 1995.

[23] A. Oberbach *et al.*, "Altered Fiber Distribution and Fiber- Specific Glycolytic and Oxidative Enzyme Activity in Skeletal Muscle of Patients With Type 2 Diabetes," *Diabetes Care*, vol. 29, no. 4, pp. 895–900, 2006.

[24] S. Sorokin, "Centrioles and the formation of rudimentary cilia by fibroblasts and smooth muscle cells.," *J. Cell Biol.*, vol. 15, pp. 363–77, 1962.

[25] U. Kühl, M. Öcalan, R. Timpl, R. Mayne, E. Hay, and K. von der Mark, "Role of muscle fibroblasts in the deposition of type-IV collagen in the basal lamina of myotubes," *Differentiation*, vol. 28, no. 2, pp. 164–72, 1984.

[26] R. D. Sanderson, J. M. Fitch, T. R. Linsenmayer, and R. Mayne, “Fibroblasts promote the formation of a continuous basal lamina during myogenesis in vitro,” *J. Cell Biol.*, vol. 2, no. 3, pp. 740–7, 1986.

[27] A. Mauro, “Satellite cell of skeletal muscle fibers.,” *J. Biophys. Biochem. Cytol.*, vol. 9, pp. 493–5, 1961.

[28] K. Minami *et al.*, “Insulin secretion and differential gene expression in glucose-responsive and -unresponsive MIN6 sublines.,” *Am. J. Physiol. Endocrinol. Metab.*, vol. 279, no. 4, pp. E773-81, 2000.

[29] A. E. E. Mertens, D. M. Pegtel, and J. G. Collard, “Tiam1 takes PARt in cell polarity,” *Trends Cell Biol.*, vol. 16, no. 6, pp. 308–16, 2006.

[30] D. Sieiro, A. C. Rios, C. E. Hirst, and C. Marcelle, “Cytoplasmic NOTCH and membrane-derived β-catenin link cell fate choice to epithelial-mesenchymal transition during myogenesis,” *Elife*, vol. 5, p. e14847, 2016.

[31] M. F. Buas, S. Kabak, and T. Kadesch, “The notch effector Hey1 associates with myogenic target genes to repress myogenesis,” *J. Biol. Chem.*, vol. 285, no. 2, pp. 1249–1258, 2010.

[32] Y. Wen, P. Bi, W. Liu, A. Asakura, C. Keller, and S. Kuang, “Constitutive Notch Activation Upregulates Pax7 and Promotes the Self-Renewal of Skeletal Muscle Satellite Cells,” *Mol. Cell. Biol.*, vol. 32, no. 12, pp. 2300–2311, 2012.

[33] L. Grisanti, E. Revenkova, R. E. Gordon, and C. Iomini, “Primary cilia maintain corneal epithelial homeostasis by regulation of the Notch signaling pathway,” *Development*, vol. 143, no. 12, pp. 2160–2170, 2016.

[34] L. Liu *et al.*, “Non-canonical Notch Signaling Regulates Actin Remodeling in Cell Migration by Activating PI3K/AKT/Cdc42 Pathway,” *Front. Pharmacol.*, vol. 10, no. 370, 2019.

[35] Q. Guo, Z. Qian, D. Yan, L. Li, and L. Huang, “LncRNA-MEG3 inhibits cell proliferation of endometrial carcinoma by repressing Notch signaling,” *Biomed. Pharmacother.*, vol. 82, pp. 589–94, 2016.

[36] C. Mammucari *et al.*, “Integration of notch 1 and calcineurin/NFAT signaling pathways in keratinocyte growth and differentiation control,” *Dev. Cell*, vol. 8, no. 5, pp. 665–676, 2005.

[37] W. Lee, B. C. Andrews, M. Faust, U. Walldorf, and E. M. Verheyen, “Hipk is an essential protein that promotes Notch signal transduction in the Drosophila eye by inhibition of the global co-repressor Groucho,” *Dev. Biol.*, vol. 325, no. 1, pp. 263–72, 2009.

[38] L. Serneels *et al.*, “Differential contribution of the three Aph1 genes to -secretase activity in vivo,” *Proc. Natl. Acad. Sci.*, vol. 102, no. 5, pp. 1719–24, 2005.

[39] J. J. McCarthy, R. Srikuea, T. J. Kirby, C. A. Peterson, and K. A. Esser, “Inducible Cre transgenic mouse strain for skeletal muscle-specific gene targeting,” *Skelet. Muscle*, vol. 2, no. 8, pp. 1–7, 2012.

[40] C. J. Haycraft *et al.*, “Intraflagellar transport is essential for endochondral bone formation,” *Development*, vol. 134, no. 2, pp. 307–316, 2007.

[41] H. Yin *et al.*, “MicroRNA-133 controls brown adipose determination in skeletal muscle satellite cells by targeting Prdm16,” *Cell Metab.*, vol. 17, no. 2, pp. 210–224, 2013.

[42] C. R. R. Bjornson, T. H. Cheung, L. Liu, P. V. Tripathi, K. M. Steeper, and T. A. Rando, “Notch signaling is necessary to maintain quiescence in adult muscle stem cells,” *Stem Cells*, vol. 30, no. 2, pp. 232–242, 2012.

[43] W. Fu, P. Asp, B. Canter, and B. D. Dynlacht, “Primary cilia control hedgehog signaling during muscle differentiation and are deregulated in rhabdomyosarcoma,” *Proc. Natl. Acad. Sci.*, vol. 111, no. 25, pp. 9151–9156, 2014.

[44] P. L. Beales, N. Elcioglu, A. S. Woolf, D. Parker, and F. A. Flinter, “New criteria for improved diagnosis of Bardet-Biedl syndrome : results of a population survey,” *J. Med. Genet.*, vol. 36, no. 6, pp. 437–446, 1999.

[45] V. Muñoz-Fuentes *et al.*, “The International Mouse Phenotyping Consortium (IMPC): a functional catalogue of the mammalian genome that informs conservation,” *Conserv. Genet.*, vol. 19, no. 4, pp. 995–1005, 2018.

[46] Y. Liu, N. Pathak, A. Kramer-Zucker, and I. A. Drummond, “Notch signaling controls the differentiation of transporting epithelia and multiciliated cells in the zebrafish pronephros,” *Development*, vol. 134, no. 6, pp. 111–22, 2007.

[47] S. von Haehling, J. E. Morley, A. J. S. Coats, and S. D. Anker, “Ethical guidelines for publishing in the journal of cachexia, sarcopenia and muscle: update 2017,” *J. Cachexia. Sarcopenia Muscle*, vol. 8, no. 6, pp. 1081–1083, 2017.

Figures

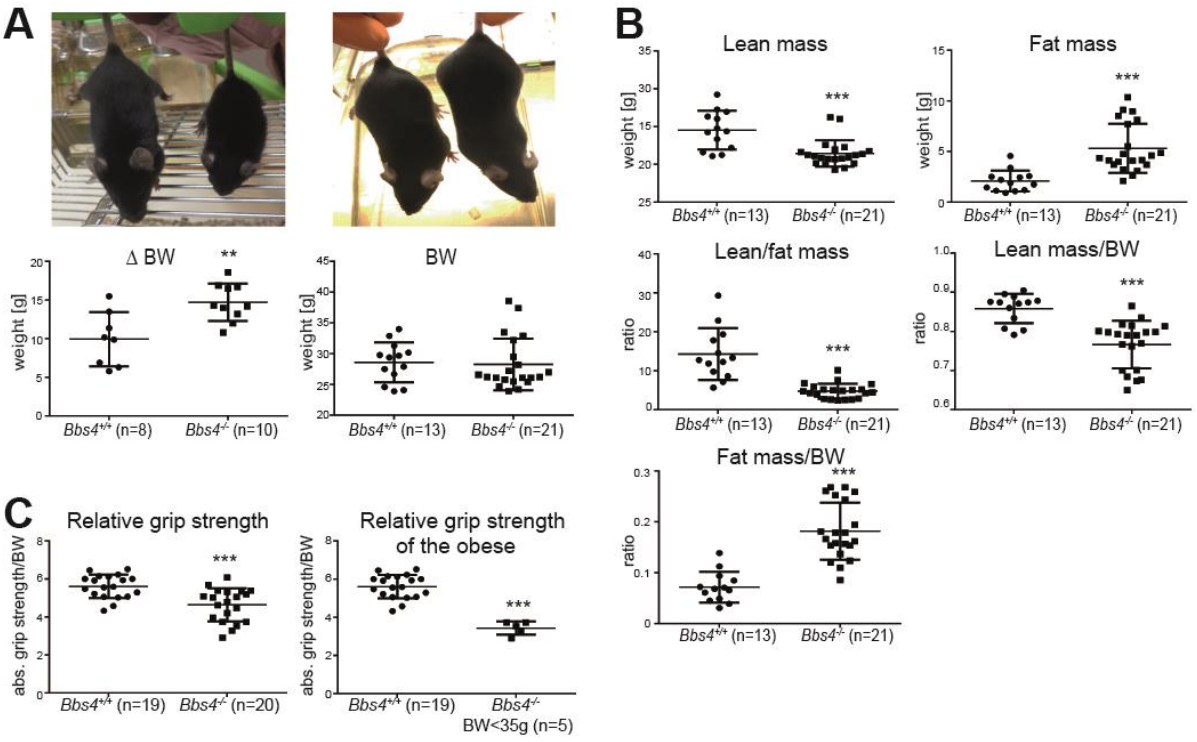

Figure 1:

Bbs4 mouse line characterization showing increased body weight gain and fat mass as well as decreased lean mass and grip strength of *Bbs4*$^{-/-}$ mice 14 weeks after birth.

(A) *Bbs4*$^{+/+}$ (left mouse on upper and lower picture) and *Bbs4*$^{-/-}$ (right mouse on upper and lower picture) littermates. Same mice 3 weeks old (left image) and 14 weeks old (right image). Increased body weight (BW) gain of *Bbs4*$^{-/-}$ between 4 and 14 weeks old mice ($p=0.003$). 14 weeks old animals exhibited the same body weight.

(B) NMR analysis results showing absolute body composition measurements and ratios of 14-week-old *Bbs4*$^{-/-}$ mice. Significant decrease of absolute lean mass ($p\leq0.001$) and increase of absolute fat mass in *Bbs4*$^{-/-}$ mice compared to *Bbs4*$^{+/+}$ controls. Ratio of lean/fat mass ($p\leq0.001$) and lean mass to body weight ($p\leq0.001$) are significantly decreased ($p\leq0.001$). Fat mass to body weight ratio is increased ($p\leq0.001$) in *Bbs4*$^{-/-}$ animals.

(C) Grip strength measurement of 14-week-old *Bbs4*$^{-/-}$ mice. Relative grip strength of *Bbs4*$^{-/-}$ mice is significantly decreased compared to *Bbs4*$^{+/+}$ controls ($p \leq 0.001$). Stratifying by severity of obesity, the effect is greater ($p \leq 0.001$).

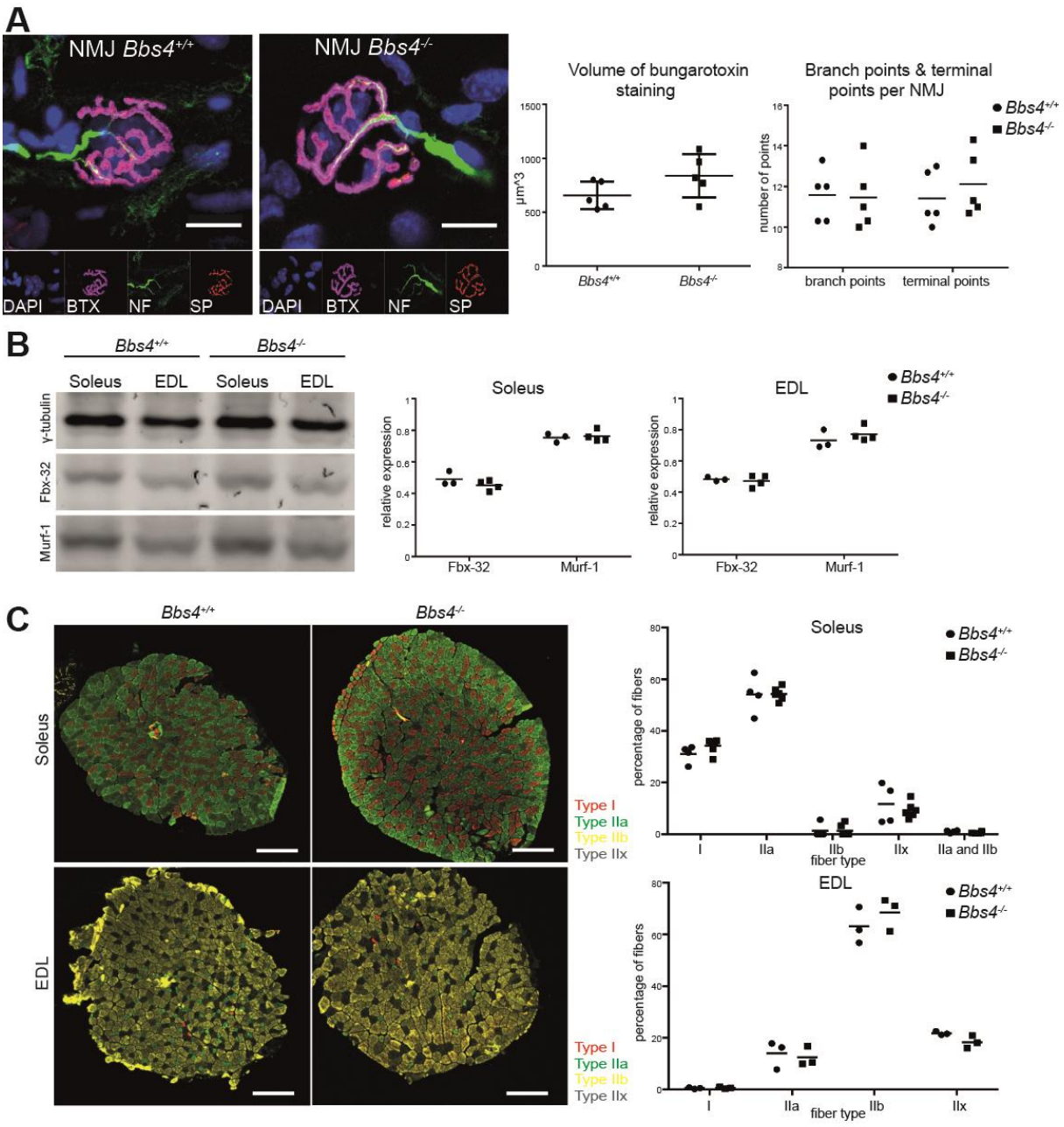

Figure 2:

Evaluation of NMJ morphology, atrophy markers and fiber types in *Bbs4*$^{-/-}$ skeletal muscles.

(A) Representative confocal maximum projections of *Bbs4* NMJ. Immunochemical staining for DAPI (blue), neurofilament (green, NF), synaptophysin (red, SP, presynaptic vesicular acetylcholine) and fluorescently labelled α-bungarotoxin (pink, BTX) are indicated. Quantification of α-bungarotoxin volume, NMJ branch points and terminal points.

(B) Western Blot and quantification of the atrophy markers Fbx-32 and Murf-1 in *Bbs4*$^{-/-}$ and *Bbs4*$^{+/+}$ Soleus and EDL.

(C) Representative image of Soleus and EDL cross sections illustrating fiber type composition of *Bbs4* Soleus and EDL. Fiber types are based on immunostaining of differentially expressed myosin heavy chains (slow fibers (Type I, red) intermediate fibers (Type IIa, green) and fast fibers (Type IIb, yellow and Type IIx, not stained)). Scale bar=300 μm. For statistics, fiber types were counted and illustrated as percentage of all fibers.

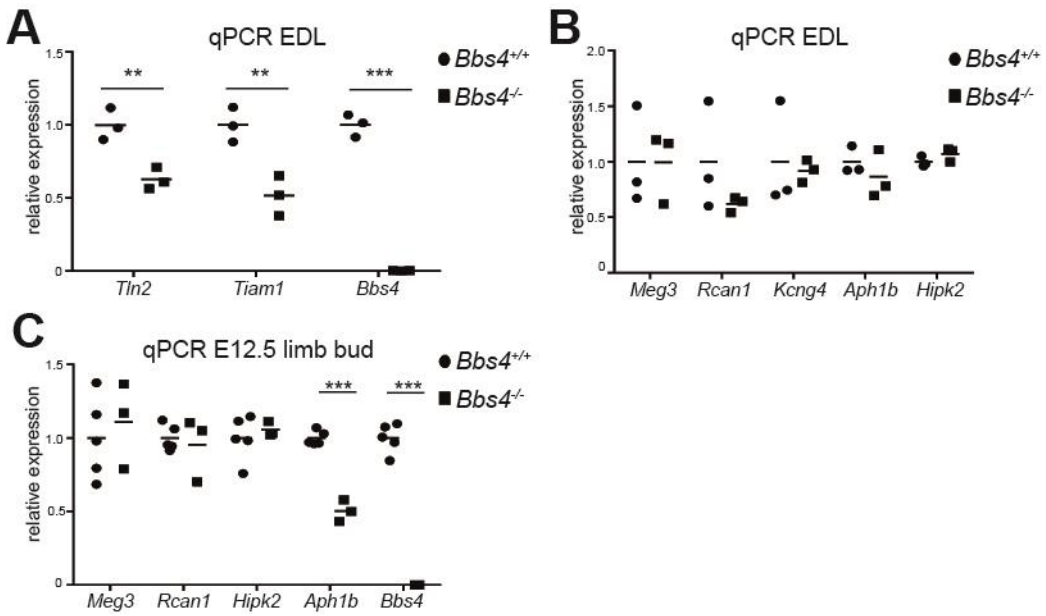

Figure 3:

Real time qPCR analysis of *Bbs4*$^{-/-}$ EDL and E12.5 limb buds.

(A) Expression level of Notch-related candidate genes *Tln2* and *Tiam1* in *Bbs4*$^{-/-}$ EDL does not significantly differ from *Bbs4*$^{+/+}$ EDL.

(B) Expression of Notch-related candidate genes is not significantly different between *Bbs4*$^{-/-}$ and *Bbs4*$^{+/+}$ muscles.

(C) Expression levels of Notch-candidate genes *Meg3*, *Rcan1* and *Hipk2* in E12.5 *Bbs4*$^{-/-}$ limb buds are similar between the genotypes. *Aph1b* is significantly downregulated ($p \leq 0.001$) in *Bbs4*$^{-/-}$ limb buds. *Bbs4* TaqMan real-time qPCR for Bbs4 added as a control ($p \leq 0.001$).

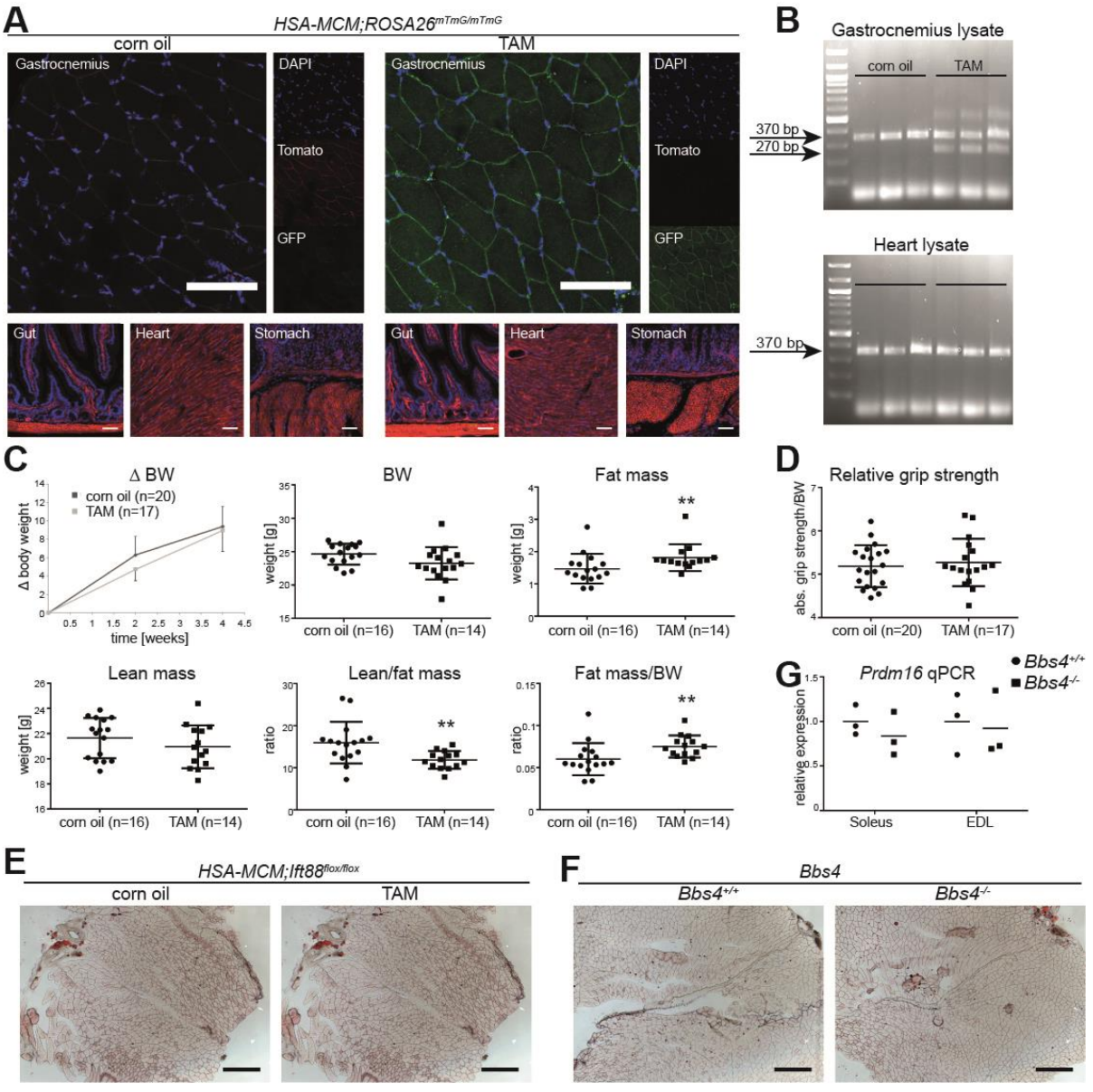

Figure 4:

Tamoxifen induced Cre expression and tissue-restriction in *HSA-MCM; ROSA26$^{mTmG/mTmG}$* reporter mice as well as phenotyping of the *HSA-MCM;Ift88$^{flox/flox}$* mouse line.

(A) Representative immunostaining images of Gastrocnemius muscle (up), cardiac and smooth muscle tissue (down: gut, heart and stomach) of *HSA-MCM;ROSA26$^{mTmG/mTmG}$* mice four weeks after induction. n=3. Scale bar=100 μm.

(B) Gastrocnemius and heart muscle lysate showing floxed wildtype (wt) alleles in both tissues (370 bp), but tamoxifen-specific induction of recombination is restricted to skeletal muscle by detection of Δ-signal (270 bp). n=3.

(C) Body composition does not indicate alterations in of *HSA-MCM;Ift88$^{flox/flox}$* skeletal muscle 4 weeks after induction, whereas absolute fat mass (p=0.006), lean/fat mass ratio (p=0.005) and fat/body mass ratio (p=0.004) differ significantly from control group.

(D) No statistically significant difference in absolute grip strength.

Histochemical Oil Red-O staining of Gastrocnemius muscle from (E) *HSA-MCM;Ift88$^{flox/flox}$* and (F) *Bbs4$^{-/-}$* mice does not initiate intramuscular adipogenesis. n=3.

(G) EDL and Soleus muscle of *Bbs4$^{+/+}$* and *Bbs4$^{-/-}$* mice do not indicate difference in *Prdm16* mRNA expression levels. n=3.

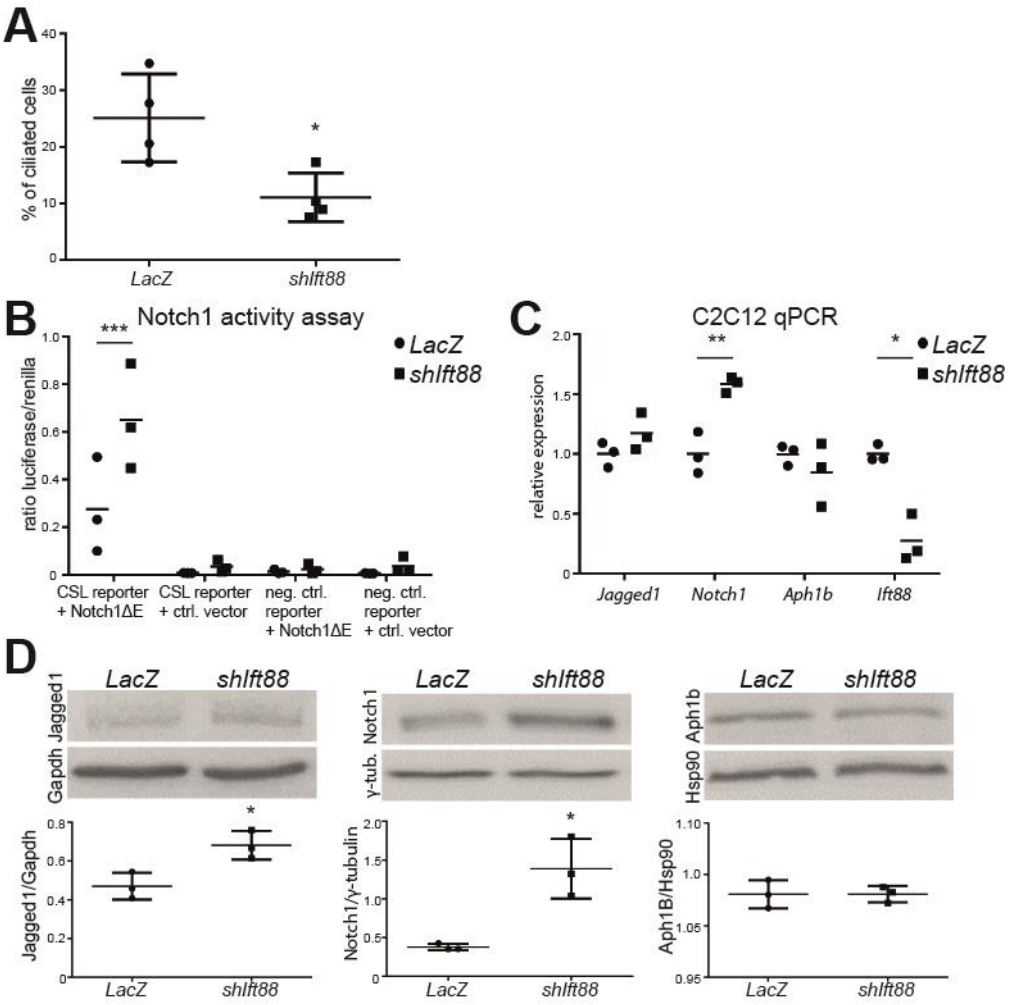

Figure 5:

Characterization of *shIft88*-expressing C2C12 myoblasts.

(A) Quantification of percentage of ciliated cells based on immunostainings. Significant reduction of cilia number in *shIft88*-expressing cells (p=0.02).

(B) Representative result of luciferase activity assay illustrating Notch1 signaling activity in C2C12 cells (p≤0.001).

(C) Real-time qPCR result showing increased *Notch1* mRNA abundance (p=0.006) and efficiency of *Ift88* knockdown (p=0.017). No aberrant expression of *Jagged1* and *Aph1b* mRNA.

(D) Confirmation of the upregulation of Notch1 (p=0.02) and Jagged1 (p=0.022) on protein level in *shIft88*-expressing C2C12 compared to *LacZ*-expressing control. Protein levels of Aph1b are not changed between the groups.

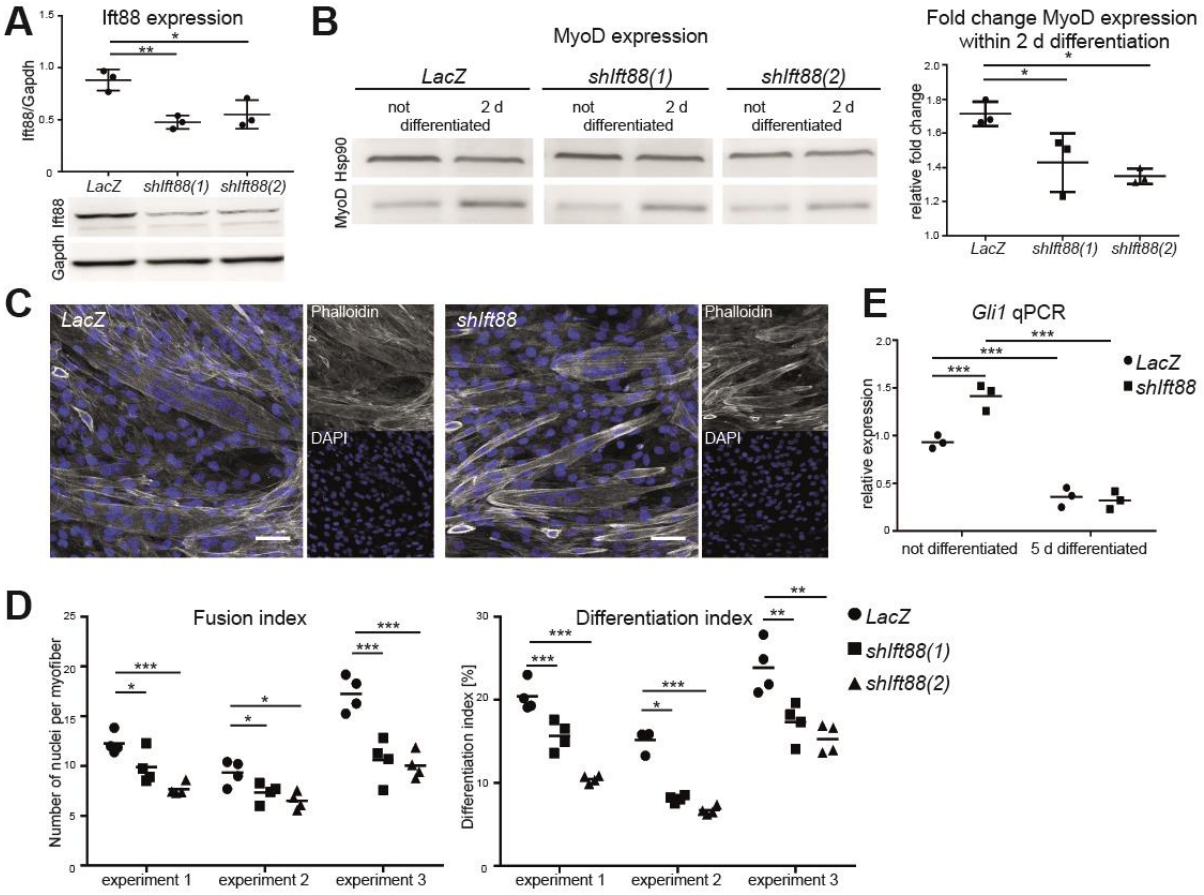

Figure 6:

Myotube formation and MyoD protein expression showing reduced differentiation capacity and altered Gli1 expression of *shIft88*-expressing C2C12 myoblasts.

(A) Western Blot analysis and quantification of Ift88 expression (*shIft88(1)* p=0.004; *shIft88(2)* p=0.02).

(B) Western Blot analysis and quantification of MyoD expression in not differentiated and 2 d differentiated *LacZ*- and *shIft88*-expressing C2C12 cells. Significant reduction in fold-change MyoD expression between *LacZ*- and *shIft88*(1)- (p=0.039) / *shIft88*(2)-expressing cells (p=0.020).

(C) Representative immunostaining images illustrating multinucleated myotubes 5 d after differentiation in *LacZ*- and *shIft88*-expressing C2C12 cells. Grey: phalloidin, blue: DAPI. (D) Fusion index indicating reduced fusion of cells in all three *Ift88* knock-down clonal cell lines. (clone 1: p(*LacZ*/*shIft88*(1))=0.041; p(*LacZ/shIft88*(2)=≤0.001; clone 2: p(*LacZ/shIft88*(1))=0.049; p(*LacZ/shIft88*(2))=0.012; clone 3: p(*LacZ/shIft88*(1))≤0.001; p(*LacZ/shIft88*(2))=0.001). Differentiation index confirming reduced differentiation efficiency of *shIft88*-expressing C2C12 myoblasts. (clone 1: p(*LacZ/shIft88*(1))=0.001; p(*LacZ/shIft88*(2))≤0.001; clone 2: p(*LacZ/shIft88*(1))=0.029; p(*LacZ/shIft88*(2))≤0.001; clone 3: p(*LacZ/shIft88*(1))=0.009; p(*LacZ/shIft88*(2)=0.002).
(E) Not differentiated *shIft88*-expressing C2C12 cells express significantly more *Gli1* mRNA compared to control. (p≤0.001). *Ift88*-depleted and *LacZ*-expressing C2C12 significantly downregulate *Gli1* during differentiation (p(*LacZ*)≤0.001; p(*shIft88*)≤0.001). Therefore, no difference in Gli1 expression after 5 d differentiation was detected.

Supplementary Material

Suppl. Table 1: TaqMan probes used for quantitative rtPCR

Probe	Catalog number	Manufacturer
Tln2	Mm00659397_m1	Thermo Fisher Scientific
Tiam1	Mm00437079_m1	Thermo Fisher Scientific
Bbs4	Mm00614565_m1	Thermo Fisher Scientific
Meg3	Mm00522599_m1	Thermo Fisher Scientific
Rcan1	Mm01213406_m1	Thermo Fisher Scientific
Hip2k	Mm00439329_m1	Thermo Fisher Scientific
Aph1b	Mm00781167_s1	Thermo Fisher Scientific
Jagged1	Mm00496902_m1	Thermo Fisher Scientific
Notch1	Mm00627185_m1	Thermo Fisher Scientific
Prdm16	Mm00712556_m1	Thermo Fisher Scientific
Ift88	Mm01313467_m1	Thermo Fisher Scientific
Gli1	Mm00494654_m1	Thermo Fisher Scientific

Suppl. Table 2: List of primary antibodies for Western Blot analysis

Primary Antibody	Catalog number	Manufacturer
Fbx-32	ab74023	Abcam
Murf-1	AF5366	R&D Systems
Tiam1	ABN1488	Millipore
Tln2	ab105458	Abcam
Jagged1	2620S	Cell Signaling
Notch1	3608S	Cell Signaling
Aph1b	PA5-69997	Thermo Fisher Scientific
MyoD	MA-12902	Thermo Fisher Scientific
Rac1	8631S	Cell Signaling
Cdc42	8747	Cell Signaling
Ift88	13967-1-AP	Proteintech
Gapdh	CB1001	Merck Biosciences
Hsp90	4874	Cell Signaling
Gamma-tubulin	T5326	Sigma
ActinA	612656	BD Biosciences

Suppl. Table 3: List of secondary antibodies for Western Blot analysis

Secondary Antibody	Label	Catalog number	Manufacturer
Anti-mouse IgG	HRP	115-036-062	Dianova
Anti-rabbit IgG	HRP	12-348	Millipore
Anti-mouse IgG (H+L)	680LT	926-68022	Licor
Anti-rabbit IgG	680LT	926-68021	Licor
Anti-goat IgG	800CW	926-32214	Licor

Suppl. Table 4: Primary antibodies for immunofluorescence

Primary Antibody	Catalog number	Manufacturer
Type I MHC	BA-D5	Developmental Studies Hybridoma Bank
Type IIa MHC	SC-71	Developmental Studies Hybridoma Bank
Type IIb MHC	BF-F3	Developmental Studies Hybridoma Bank
Neurofilament	2H3	Developmental Studies Hybridoma Bank
Synaptotagmin	ab32127	Abcam
GFP	GFP-1020	Aves Labs
RFP	ORD003515	Chromotek

Suppl. Table 5: Secondary antibodies for immunofluorescence

Secondary Antibody	Label	Catalog number	Manufacturer
Anti-chicken IgY	Cy2	703-225-155	Dianova
Anti-rat IgG (H+L)	Cy3	712-165-153	Dianova
Anti-mouse IgG1 (γ1)	488	A21121	Invitrogen
Anti-mouse IgM (μ chain)	546	A-21045	Life Technologies
Anti-mouse IgG2b (γ2b)	405	SAB4600477	Sigma
Anti-rabbit IgG	647	A31573	Invitrogen
Anti-mouse IgG2b (γ2b)	647	A-21242	Life technologies